SH
11
.A2
F53
FISH

U.S. Department
of Commerce

Volume 119
Number 2–3
April–July 2021

Fishery Bulletin

SMITHSONIAN
NOV 0 [illegible]
LIBRARIES

U.S. Department of Commerce

Gina M. Raimondo
Secretary

National Oceanic and Atmospheric Administration

Richard W. Spinrad
Administrator

National Marine Fisheries Service

Janet Coit
Assistant Administrator
for Fisheries

Fishery Bulletin

Scientific Editor
José I. Castro
National Marine Fisheries Service, NOAA
263 13th Avenue South
Saint Petersburg, Florida 33701

Managing Editor
Kathryn Dennis
Scientific Publications Office
National Marine Fisheries Service, NOAA
1845 Wasp Boulevard, Building 176
Honolulu, Hawaii 96818

Associate Editor
Cara Mayo
Scientific Publications Office
National Marine Fisheries Service, NOAA
7600 Sand Point Way NE
Seattle, Washington 98115-0070

Editorial Board

Henry L. Bart Jr.	Tulane University, New Orleans, Louisiana
Matthew D. Campbell	National Marine Fisheries Service, Pascagoula, Mississippi
Shannon L. Cass-Calay	National Marine Fisheries Service, Miami, Florida
William B. Driggers III	National Marine Fisheries Service, Pascagoula, Mississippi
Gretchen L. Grammer	South Australian Research and Development Institute, Adelaide, Australia
Richard Langton	National Marine Fisheries Service, Walpole, Maine (retired)
Richard S. McBride	National Marine Fisheries Service, Woods Hole, Massachusetts
Richard L. Merrick	National Marine Fisheries Service, Falmouth, Massachusetts (retired)
Richard D. Methot	National Marine Fisheries Service, Seattle, Washington
Lisa J. Natanson	National Marine Fisheries Service, Narragansett, Rhode Island
Mark S. Peterson	University of Southern Mississippi, Ocean Springs, Mississippi
André E. Punt	University of Washington, Seattle, Washington
Joseph M. Quattro	University of South Carolina, Columbia, South Carolina
John F. Walter III	National Marine Fisheries Service, Miami, Florida
Bruce Wright	Aleutian Pribilof Island Association, Anchorage, Alaska

***Fishery Bulletin* website: https://spo.nmfs.noaa.gov/fb.htm**

Fishery Bulletin (ISSN 0090-0656) is published quarterly by the Scientific Publications Office, National Marine Fisheries Service, NOAA, 7600 Sand Point Way NE, Seattle, WA 98115-0070.

Although the contents of this publication have not been copyrighted and may be reprinted entirely, reference to source is appreciated.

The Secretary of Commerce has determined that the publication of this periodical is necessary according to law for the transaction of public business of this Department. Use of funds for printing of this periodical has been approved by the Director of the Office of Management and Budget.

For Sale by the Superintendent of Documents, U.S. Government Publishing Office, Washington, DC 20401. Subscription price per year: $32.00 domestic and $44.80 foreign. Cost per single issue: $19.00 domestic and $26.60 foreign. **See back for order form.**

Fishery Bulletin carries original research reports on investigations in fishery science, engineering, and economics. It began as the Bulletin of the United States Fish Commission in 1881; it became the Bulletin of the Bureau of Fisheries in 1904 and the *Fishery Bulletin* of the U.S. Fish and Wildlife Service in 1941. Separates were issued as documents through volume 46; the last document was no. 1103. Beginning with volume 47 in 1931 and continuing through volume 62 in 1963, each separate appeared as a numbered bulletin. A new system began in 1963, with volume 63, in which papers are bound together in a single issue. Beginning with volume 70, number 1, January 1972, *Fishery Bulletin* became a periodical, issued quarterly. In this form, it is available by subscription from the Superintendent of Documents, U.S. Government Publishing Office, Washington, DC 20401. It is also available free in limited numbers to libraries, research institutions, and state and federal agencies and in exchange for other scientific publications.

U.S. Department of Commerce
Seattle, Washington

Volume 119
Number 2–3
April–July 2021

Fishery Bulletin

Contents

Articles

97–111 **Takahiro Kusaka, Kojiro Hara, Keisuke Furumitsu, Shinji Uehara, Yuta Yagi, Atsuko Yamaguchi, and Naoki Yagishita**

Genetic population structure of the polkadot skate (*Dipturus chinensis*) around Japan, based on mitochondrial DNA sequences and polymorphic microsatellite loci

112–122 **Yana Yu. Bolshakova, Sergei A. Evseenko, and Dmitry V. Bolshakov**

Morphology of larvae of 6 *Lampanyctus* species in the central South Pacific Ocean with notes on their occurrence

123–134 **Kevin R. Spanik, Tracey I. Smart, Marcel J. M. Reichert, and Tanya L. Darden**

Using DNA barcoding to improve taxonomic resolution of the diet of red snapper (*Lutjanus campechanus*) along the Atlantic coast of the southeastern United States

135–148 **Joshua D. Dennis, Gretchen Grammer, Tim Ward, Jonathan Smart, and Charlie Huveneers**

Using otolith chronologies to identify extrinsic drivers of growth of 2 commercially targeted small pelagic fish species

149–167 **Bai Li, Kyle W. Shertzer, Patrick D. Lynch, James N. Ianelli, Christopher M. Legault, Erik H. Williams, Richard D. Methot Jr., Elizabeth N. Brooks, Jonathan J. Deroba, Aaron M. Berger, Skyler R. Sagarese, Jon K. T. Brodziak, Ian G. Taylor, Melissa A. Karp, Chantel R. Wetzel, and Matthew Supernaw**

A comparison of 4 primary age-structured stock assessment models used in the United States

The National Marine Fisheries Service (NMFS) does not approve, recommend, or endorse any proprietary product or proprietary material mentioned in this publication. No reference shall be made to NMFS, or to this publication furnished by NMFS, in any advertising or sales promotion that would indicate or imply that NMFS approves, recommends, or endorses any proprietary product or proprietary material mentioned herein or that has as its purpose an intent to cause directly or indirectly the advertised product to be used or purchased because of this NMFS publication.

The NMFS Scientific Publications Office is not responsible for the contents of the articles.

168–183 **Peter G. Coulson and Jake A. Poad**

Biological characteristics of the primitive flatfish Indian halibut (*Psettodes erumei*) from the tropical northeastern Indian Ocean, including implications of the use of incorrect aging methods on mortality estimates

184–196 **Sarah C. Stienessen, Christopher N. Rooper, Thomas C. Weber, Darin T. Jones, Jodi L. Pirtle, and Christopher D. Wilson**

Comparison of model types for prediction of seafloor trawlability in the Gulf of Alaska by using multibeam sonar data

197–200 **Guidelines for authors**

National Marine
Fisheries Service
NOAA

Fishery Bulletin
established in 1881

Spencer F. Baird
First U.S. Commissioner
of Fisheries and founder
of *Fishery Bulletin*

Genetic population structure of the polkadot skate (*Dipturus chinensis*) around Japan, based on mitochondrial DNA sequences and polymorphic microsatellite loci

Takahiro Kusaka[1,5]
Kojiro Hara[2]
Keisuke Furumitsu[2]
Shinji Uehara[3]
Yuta Yagi[4]
Atsuko Yamaguchi[2]
Naoki Yagishita (contact author)[2]

Email address for contact author: n-yagi@nagasaki-u.ac.jp

[1] Laboratory for Aquatic Biology
Graduate School of Agriculture
Kindai University
3327-204 Nakamachi
Nara 631-8505, Japan

[2] Graduate School of Fisheries and Environmental Sciences
Nagasaki University
1-14 Bunkyo-machi
Nagasaki 852-8521, Japan

[3] Fisheries Data Sciences Division
Fisheries Stock Assessment Center
Fisheries Resources Institute
Japan Fisheries Research and Education Agency
2-12-4 Fukuura
Kanazawa, Yokohama 236-8648, Japan

[4] Niigata Field Station
Demersal Fish Resources Division
Fisheries Stock Assessment Center
Fisheries Resources Institute
Japan Fisheries Research and Education Agency
1-5939-22 Suido-cho
Chuou-ku, Niigata 951-8121, Japan

[5] Nishinihon Institute of Technology
9-30 Wakamatsu-cho
Kochi 781-0812, Japan

Abstract—The genetic population structure of the polkadot skate (*Dipturus chinensis*) around Japan was examined by using mitochondrial (mt) cytochrome (cyt) *b* gene sequences and polymorphic microsatellite (simple sequence repeat [SSR]) loci. Results of phylogenetic analysis based on mt cyt *b* gene sequences reveal 2 major lineages, clades A and B. Clade A consists of populations in the Sea of Japan and the East China Sea. Clade B contains populations in the Pacific Ocean and is divided into 2 subclades, clades B1 and B2, which correspond to the populations along the southern and northern coasts of Japan, respectively. This genetic differentiation is also supported by results from SSR analysis. The divergence of clades A and B may reflect isolation of the East China Sea from the Pacific Ocean in the Early Pleistocene. After diverging from clade A, clade B might have extended its distribution northward along the Pacific coast of Japan and divided into clades B1 and B2 in the Middle Pleistocene. The polkadot skate is clearly structured into 3 genetically discrete populations around Japan that should be treated as independent management units for management of this species in the future.

Manuscript submitted 4 February 2021.
Manuscript accepted 23 June 2021.
Fish. Bull. 119:97–111 (2021).
Online publication date: 19 July 2021.
doi: 10.7755/FB.119.2-3.1

The views and opinions expressed or implied in this article are those of the author (or authors) and do not necessarily reflect the position of the National Marine Fisheries Service, NOAA.

The polkadot skate (*Dipturus chinensis*) is distributed along the coast of Japan from Hokkaido southward to Kyushu, the East China Sea, the Korean Peninsula, and Taiwan (Fig. 1). It inhabits sandy to muddy bottoms at depths of 20–320 m, mostly shallower than 150 m (Yamada et al., 2007, 2009; Hatooka et al., 2013; Last et al., 2016). Until recently, the species had been confused with the Kwangtung skate (*D. kwangtungensis*), which occurs in the South China Sea (Last and Lim, 2010). However, Last et al. (2016) reclassified the species as *D. chinensis* on the basis of the differences in morphological characteristics.

The polkadot skate is caught mostly by bottom-trawl fishing vessels in the East China Sea (Jeong and Ishihara, 2009) and processed mainly for dried and paste products (Yamada et al., 2007). The annual catch of rajid species, including the polkadot skate, in the East China Sea peaked at 17,000 metric tons (t) in 1948 but has declined to approximately 100 t in recent years (Tokimura et al., 1998; Hara et al., 2014). Moreover, the polkadot skate was commonly found in Korean fish markets before 2000; however, presently, very few can be found in those markets (Jeong and Ishihara, 2009). The decrease in abundance of skate

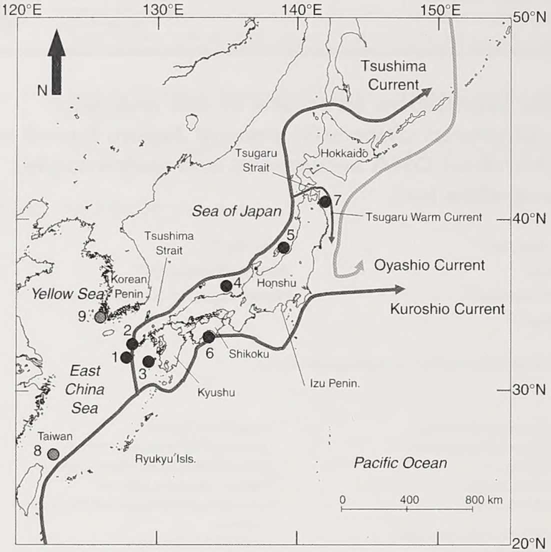

Figure 1

Map of the 7 locations (black circles) around Japan where polkadot skate (*Dipturus chinensis*) were collected during 2010–2017. Also shown are the 2 locations (gray circles) of the populations for which DNA sequences were obtained through the International Nucleotide Sequence Database Collaboration. The dark and light gray lines with arrows indicate the flow and direction of oceanic currents. The numerals next to the circles correspond to the 9 locations: (1) Danjo Islands, (2) Goto Islands, (3) Koshiki-jima Islands, (4) Kyoto Prefecture, (5) Niigata Prefecture, (6) Kochi Prefecture, (7) Aomori Prefecture, (8) Taiwan, and (9) Korean Peninsula. Isls.=Islands; Penin.=Peninsula.

species, including the polkadot skate, may result from their life history traits; as members of Elasmobranchii, they have slow growth rates, late attainment of sexual maturity, long life spans, and low fecundity (Brander, 1981; Dulvy et al., 2000; Hara et al., 2018a), making them vulnerable to exploitation.

Recently, basic life history traits, such as age, growth, and age at sexual maturity, and dietary habits of the polkadot skate were examined to establish conservation and management strategies for this species (Hara et al., 2018a, 2018b). Genetic information, such as population structure, is important for fisheries management and development of conservation policies for elasmobranch species (Domingues et al., 2018). To date, several studies on genetic population structure have been conducted for several species of Rajidae (Chevolot et al., 2006a, 2006b, 2007; Griffiths et al., 2010, 2011; Stéphan et al.[1]; Frodella et al., 2016; Im et al., 2017; Vargas-Caro et al., 2017; Ferrari et al., 2018; Weltz et al., 2018; Misawa et al., 2019a, 2019b, 2020). The results of most studies reveal significant population structuring shaped by historical, geographical, and environmental factors, indicating that Rajidae generally have low dispersal ability.

Japan is surrounded by complicated oceanic currents (Fig. 1): the Kuroshio Current flows from east of the Philippines past Taiwan and the Ryukyu Islands to the Pacific coast of Kyushu, Shikoku, and southern Honshu of Japan; the Tsushima Current, which branches off from the Kuroshio Current off southern Kyushu, flows northward along the western coast of Honshu; and the Oyashio Current originates in the Arctic Ocean and flows southward past the Bering Sea to the Pacific coast of Hokkaido and northern Honshu. The population structures of rajid species as well as of various marine animals around Japan, it has been suggested, are affected by those currents (Kojima et al., 1997, 2004; Akihito et al., 2008; Kokita and Nohara, 2011; Han et al., 2012; Hirase et al., 2012; Hirase and Ikeda, 2014). For the ocellate spot skate (*Okamejei kenojei*), the distribution of which is similar to that of the polkadot skate, the force of warm currents, the Tsushima and Kuroshio Currents, has been reported to prevent dispersal of individuals (Misawa et al., 2019b). The Tsushima Current, as a dispersal barrier, has shaped the population structure of the mottled skate (*Beringraja pulchra*), according to Misawa et al. (2019a). There is a possibility that the population structure of the polkadot skate is also affected by the currents around Japan.

In this study, we examined the genetic population structure of the polkadot skate around Japan by using partial sequences of mitochondrial (mt) cytochrome (cyt) *b* gene and polymorphic microsatellite (simple sequence repeat [SSR]) loci because those molecular markers will provide information that can help guide fishery management and

---

[1] Stéphan, E., C. Hennache, A. Delamare, N. Leblanc, V. Legrand, G. Morel, E. Meheust, and J. L. Jung. 2014. Length at maturity, conversion factors, movement patterns and population genetic structure of undulate ray (*Raja undulata*) along the French Atlantic and English Channel coasts: preliminary results, 16 p. Working paper presented at the 2014 Working Group on Elasmobranch Fishes (WGEF) meeting; Lisbon, 17–26 June. [Available from ICES Secretariat, H. C. Andersens Blvd. 44-46, 1553 Copenhagen, Denmark.]

Table 1

Sampling location, number of specimens, total length (range and mean), sampling depth, and capture date of the polkadot skate (*Dipturus chinensis*) collected during 2010–2017 from 7 locations in the East China Sea, Sea of Japan, and Pacific Ocean around Japan. For populations at 2 other locations, Taiwan and the Korean Peninsula, DNA sequences were obtained through the International Nucleotide Sequence Database Collaboration. The specific location for the sequences for Taiwan is unknown, and sequences for the Korean Peninusula are for polkadot skate from Jindo, off the southwestern coast of the peninsula, near the boundary of the East China Sea and the Yellow Sea.

Location	No. of specimens	Total length (mm)		Sampling depth (m)	Capture date
		Range	Mean		
East China Sea					
Danjo Islands	48	189–684	473	130–150	April 2010–April 2015
Goto Islands	18	370–643	523	203	January 2014
Koshiki-jima Islands	1	514	–	Unknown	November 2013
Sea of Japan					
Kyoto Prefecture	47	102–638	335	110–170	April 2014–July 2014
Niigata Prefecture	49	116–701	485	120–160	August 2013–August 2014
Pacific Ocean					
Kochi Prefecture	23	125–584	356	150–320	November 2015–January 2016
Aomori Prefecture	26	335–775	537	160–180	February 2017–March 2017
Taiwan	1	–	–	–	–
Korean Peninsula	1	–	–	–	–

conservation efforts. On the basis of mt cyt *b* sequences, we also estimated the evolutionary history of this species, information that is important for delineation of managing units that should be managed independently to ensure the viability of the species (Moritz, 1994, 2002; Palsbøll et al., 2007).

Materials and methods

Sampling and DNA extraction

A total of 212 polkadot skate (102–775 mm in total length [TL]; mean: 444 mm TL) were collected from 7 locations around Japan: 3 locations in the East China Sea, the Danjo Islands (number of samples [n]=48), Goto Islands (n=18), and Koshiki-jima Islands (n=1); 2 locations in the Sea of Japan, Kyoto Prefecture (n=47) and Niigata Prefecture (n=49); and 2 locations in the Pacific Ocean, Kochi Prefecture (n=23) and Aomori Prefecture (n=26) (Table 1, Fig. 1). In addition, individuals of 2 other species of *Dipturus*, the bigtail skate (*D. macrocaudus*) and the acutenose skate (*D. tengu*), were collected from Kochi Prefecture so that these species could serve as outgroups for phylogenetic analysis. Samples were obtained from depths of 110–320 m by using bottom or beam trawls between 2010 and 2017.

Muscle tissue was dissected from each fish and stored, either frozen at −20°C or in 99.5% ethanol, until DNA extraction. Total genomic DNA was extracted by using the DNeasy Blood & Tissue Kit[2] (QIAGEN, Hilden, Germany) following the manufacturer's protocol.

Mitochondrial DNA analyses

We used a polymerase chain reaction (PCR) to amplify approximately 1200 base pairs of the mt cyt *b* gene, with the following primers: GLU-L-*Dipturus* (5'–TCT GAA AAA CTA CCG TTG TTA–3') and CB6THR-H-Dipturus (5'–CTC CAA TCT TTG GTT TAC AAG–3'). The design of the primers was based on a primer pair, GLU-L and CB6THR-H (Palumbi et al., 2002), with reference to the cyt *b* gene sequences of skate species registered in the DNA Data Bank of Japan, which is part of the International Nucleotide Sequence Database Collaboration: the polkadot skate (registered as *D. kwangtungensis*; accession number KF318309; Jeong et al., 2015), the thorny skate (*Amblyraja radiata*) (accession number AF106038; Rasmussen and Arnason, 1999), the ocellate spot skate (accession number AY525783; Kim et al., 2005), the Korean skate (*Hongeo koreanus*) (accession number KC914433; Jeong et al., 2014), and the longnose skate (*Beringraja rhina*) (registered as *Raja rhina*; accession number KC914434; Jeong and Lee, 2015). Polymerase chain reactions were conducted by using a PCR Thermal

---

[2] Mention of trade names or commercial companies is for identification purposes only and does not imply endorsement by the National Marine Fisheries Service, NOAA.

Cycler Dice Gradient (TaKaRa Bio, Shiga, Japan), each with 10 µL of reaction solution containing 10 ng template DNA, 0.5 µM of each primer, 0.2 mM dNTP mixture, 1× PCR buffer (10 mM Tris–HCl pH 8.3, 50 mM KCl, and 1.5 mM $MgCl_2$), and 0.5 U *Ex Taq* DNA polymerase (TaKaRa Bio).

The reaction conditions were as follows: an initial denaturation at 94°C for 2 min; 30 cycles of denaturation at 94°C for 30 s, annealing at 62°C for 30 s, and extension at 72°C for 1 min; and a final extension of 72°C for 10 min. The PCR products, purified by using illustra ExoStar (Cytiva, Malborough, MA), were sequenced on an Applied Biosystems ABI Prism 3130 XL Genetic Analyzer (Thermo Fisher Scientific Inc., Waltham, MA), with the Applied Biosystems BigDye Terminator Cycle Sequencing Kit (vers. 3.1; Thermo Fisher Scientific Inc.) and the primers used in the PCR. Forward and reverse sequences were connected by using GENETYX, vers. 8 (GENETYX Corp., Tokyo, Japan). All sequences have been deposited in the DNA Data Bank of Japan under accession numbers LC547089–LC547120.

The DNA sequences and the published sequences of polkadot skate from waters around Jindo Island, off the southwestern coast of the Korean Peninsula, near the boundary of the East China Sea and the Yellow Sea (registered as *D. kwangtungensis*; accession number KF318309; Jeong et al., 2015) and from Taiwan (the specific locality is unknown; accession number EU870495; Su and Hwang, available from the DNA Data Bank of Japan at website) were aligned with CLUSTAL W, vers. 2.1 (Larkin et al., 2007). Haplotype diversity (h) (Nei, 1987) and nucleotide diversity (π) (Nei, 1987) were calculated for each *geographic population*, meaning the population at each sampling location, by using Arlequin, vers. 3.5 (Excoffier and Lischer, 2010).

Using the bigtail skate (LC547121; this study), the acutenose skate (accession number LC547122; this study), and the roughskin skate (*D. trachydermus*) (accession number KR152643; Vargas-Caro et al., 2016) as outgroups, we performed phylogenetic analysis with MEGA, vers. 6.0 (Tamura et al., 2013). The best nucleotide substitution model was determined by using Bayesian information criterion. Subsequently, the maximum likelihood tree of haplotypes was constructed from evolutionary distances calculated by using the Tamura–Nei model (Tamura and Nei, 1993) with the G parameter (ensuring heterogeneous rates across sites following the gamma distribution) (TN93+G model). Confidence values were estimated through bootstrapping analysis (Felsenstein, 1985) with 1000 replications. The time since lineage divergence (t) was estimated from net average distances between lineages (d_A) (Nei and Li, 1979; Nei and Miller, 1990) on the basis of the following relationship: $t=d_A/2\mu$, where μ is the lineage mutation rate. Values of d_A were calculated by using p-distances, the proportion (p) of nucleotide sites at which 2 sequences being compared are different, determined with MEGA. We assumed a divergence rate of 1.0–1.6% per million years, as this rate has been suggested for the mt cyt *b* gene of a species of *Raja* (Chevolot et al., 2006b). A minimum spanning network of haplotypes was constructed on the basis of the minimum sequence difference by using TCS, vers. 1.21 (Clement et al., 2000).

A hierarchical analysis of molecular variance (AMOVA) (Excoffier et al., 1992) was run in Arlequin to estimate the partitioning of genetic variation within and between populations (or groups). We assumed different groupings of locations to find the optimal grouping of locations with the highest value of molecular genetic diversity among geographic groups (Φ_{CT}). The pairwise values of molecular genetic diversity among populations (Φ_{ST}) were calculated, and their significance was tested with 10,000 permutations and adjusted with a sequential Bonferroni correction (Rice, 1989).

Analysis of mismatch distribution was performed with Arlequin to infer the recent demographic history of the samples and to test the fit of the observed distribution to that expected under the sudden expansion model. The goodness of fit between the observed and expected distributions was tested by using the sum of squared deviations (Schneider and Excoffier, 1999) and Harpending's raggedness index (Harpending, 1994). The demographic parameters of time since expansion in units of mutational time and population size before (θ_0) and after (θ_1) a rapid change in population size in units of mutational time (Rogers and Harpending, 1992; Schneider and Excoffier, 1999) were obtained by using a parametric bootstrap approach with 10,000 replications. Neutrality of the sequence variation was verified by using Tajima's D statistic (Tajima, 1989a, 1989b) and Fu's F_S test (Fu, 1997), conducted in Arlequin with 10,000 simulated samples.

We constructed a Bayesian skyline plot (BSP) (Drummond et al., 2005) with the TN93+G model to estimate past dynamics in the female effective population size (N_e) multiplied by the generation interval through time, using BEAST, vers. 2.5.0 (Bouckaert et al., 2014). Each Markov chain Monte Carlo process was based on a run of 20 million generations, and genealogies were sampled every 1000 generations. Of the sampled genealogies, 10% were discarded as burn-in. The divergence rate of 1.3% per million years was applied under the strict molecular clock model. The convergence of parameters was visually checked with effective sample sizes of estimates for all relevant parameters over 200 with TRACER, vers. 1.7.1 (Rambaut et al., 2018). The parameter sum (indicators.alltrees) that estimated the number of population change steps was used to check for the most likely numbers of demographic changes.

Microsatellite analyses

A PCR was performed to amplify each of the following 7 SSR loci: *LERI21*, *LERI26*, *LERI33*, *LERI34*, *LERI44*, *LERI50*, and *LERI63* (El Nagar et al., 2010). Polymerase chain reactions were carried out by using a PCR Thermal Cycler Dice Gradient, each with 10 µL of reaction solution containing 10 ng template DNA, 0.5 µM of each primer, 0.2 mM dNTP mixture, 1× PCR buffer (10 mM Tris–HCl pH 8.3, 50 mM KCl, and 1.5 mM $MgCl_2$), and 0.5 U

Ex Taq DNA polymerase. The reaction conditions were as follows: an initial denaturation at 94°C for 3 min; 30 cycles of denaturation at 94°C for 30 s, annealing at 53°C (*LERI26*, *LERI33*, *LERI50*, and *LERI63*) or 57°C (*LERI21*, *LERI34*, and *LERI44*) for 30 s, and extension at 72°C for 30 s; and a final extension step of 72°C for 10 min. Forward primers were labelled with the fluorescent dyes FAM, VIC, NED, or PET (Thermo Fisher Scientific Inc.). Fragments were sized on an automated DNA sequencer, the ABI Prism 3130 XL Genetic Analyzer, by using dye-labeled Applied Biosystems GeneScan 600 LIZ Size Standard (Thermo Fisher Scientific Inc.), and scored by using the Applied Biosystems software Peak Scanner, vers. 1.0 (Thermo Fisher Scientific Inc.).

Micro-Checker (vers. 2.2.3; Van Oosterhout et al., 2004) was used for identifying possible genotyping errors (i.e., stuttering, large allele dropout, and null alleles) within the SSR data set by using 1000 randomizations. Linkage disequilibrium for all loci was calculated by using GENEPOP, vers. 4.2 (Raymond and Rousset, 1995; Rousset, 2008). The observed (H_O) and expected (H_E) heterozygosities were calculated by using Arlequin. Deviations of genotypic distributions from the Hardy–Weinberg equilibrium (exact test) (Guo and Thompson, 1992) within each sampling location, by locus, were tested by using Arlequin along with a sequential Bonferroni correction (Rice, 1989), to adjust the significance level. Allelic diversity assessed as allelic richness (A_R) was calculated by using FSTAT, vers. 2.9.3.2 (Goudet, 2002). The levels of genetic diversity within and among the geographic populations were tested by hierarchical AMOVA, as implemented in Arlequin. In these microsatellite analyses, we assumed different groupings of locations to find the optimal grouping of locations with the highest value of molecular genetic diversity among geographic groups (R_{CT}), a value analogous to Φ_{CT} in the mtDNA analyses. The pairwise values of molecular genetic diversity among populations (R_{ST}), values analogous to Φ_{ST} in the mtDNA analyses, were calculated, and their significance was tested with 10,000 permutations and adjusted with a sequential Bonferroni correction (Rice, 1989).

Results

Mitochondrial DNA analyses

A 931-base-pair fragment of the mt cyt *b* gene was obtained from 214 polkadot skate from 9 locations (Table 1, Fig. 1). There were 53 polymorphic sites, and transitions and transversions were observed at 49 and 4 of these sites, respectively.

Table 2

Number of samples (n), number of haplotypes (H), haplotype diversity (h), and nucleotide diversity (π) estimated from mitochondrial cytochrome *b* gene (931 base pairs) for each population of the polkadot skate (*Dipturus chinensis*) sampled between 2010 and 2017 at 7 locations around Japan. Information is also provided for populations of Taiwan and the Korean Peninsula for which sequences were obtained through the International Nucleotide Sequence Database Collaboration. The mean values of h and π are given with standard deviations (SDs).

Locality	n	H	h (SD)	π (SD)
Clade A				
Danjo Islands	48	13	0.884 (0.028)	0.0031 (0.002)
Goto Islands	18	8	0.817 (0.073)	0.0023 (0.001)
Kyoto Prefecture	47	6	0.617 (0.072)	0.0023 (0.001)
Niigata Prefecture	49	6	0.521 (0.067)	0.0019 (0.001)
Koshiki-jima Islands	1	1	–	–
Taiwan	1	1	–	–
Korean Peninsula	1	1	–	–
Clade B1				
Kochi Prefecture	23	3	0.245 (0.113)	0.0005 (0.000)
Clade B2				
Aomori Prefecture	26	7	0.726 (0.069)	0.0014 (0.001)

Genetic variation within populations Within 6 of the 9 geographic populations, excluding those at the Koshiki-jima Islands, Taiwan, and the Korean Peninsula (each with a sample size of only 1 individual), the number of haplotypes ranged from 3 to 13 haplotypes (Table 2). The number of haplotypes within each geographic population in the Sea of Japan (6 haplotypes in the populations in both Kyoto Prefecture and Niigata Prefecture) was lower than the number in the East China Sea (13 and 8 haplotypes in the populations at the Danjo Islands and Goto Islands, respectively). Additionally, the numbers in the Pacific Ocean (3 and 7 haplotypes in the populations in Kochi and Aomori Prefectures, respectively) were lower than those in the East China Sea. The h values were high in all the geographic populations (0.521–0.884), except for in the population in Kochi Prefecture (0.245). The π values were low in all geographic populations (0.0005–0.0031), with the values in the Pacific Ocean (0.0005–0.0014) lower than those in the East China Sea and the Sea of Japan (0.0019–0.0031). The h and π values in the East China Sea and the Sea of Japan gradually decrease among populations from the Danjo Islands northward to Niigata Prefecture.

Phylogenetic relationships among haplotypes A total of 34 haplotypes were defined. Among them, 8 haplotypes were shared between populations in at least 2 different locations, accounting for 65.0% of all observations; 12 haplotypes were found in more than 1 specimen from 1 location; and the remaining 14 haplotypes were singletons (Figs. 2 and 3).

The creation of a maximum likelihood tree of haplotypes (Fig. 2) revealed 2 major lineages, clades A and

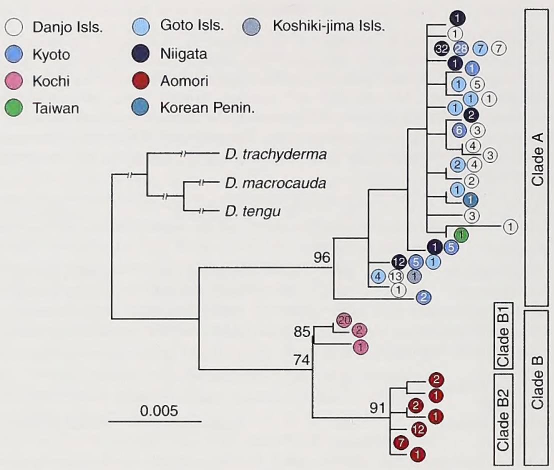

Figure 2

Maximum likelihood tree of haplotypes based on phylogenetic analysis of the mitochondrial cytochrome *b* gene sequences (931 base pairs) of 214 polkadot skate (*Dipturus chinensis*). Sequences were obtained from specimens caught at 7 locations around Japan, in the East China Sea, Sea of Japan, and Pacific Ocean, during 2010–2017 or were obtained through the International Nucleotide Sequence Database Collaboration for populations in Taiwan or off the Korean Peninsula. The evolutionary distances were calculated by using the TN93+*G* model. Numerals at nodes indicate the bootstrap probability for clades A, B, B1, and B2. Numerals in circles indicate the number of individuals sharing the same haplotype. The roughskin skate (*D. trachydermus*), bigtail skate (*D. macrocaudus*), and acutenose skate (*D. tengu*) served as outgroups for phylogenetic analysis. The bar in the bottom-left corner indicates evolutionary distance. Isls.=Islands; Penin.=Peninsula.

B, as indicated by high values of bootstrap probability (96% and 74%, respectively). Clade B is divided into 2 subclades, clades B1 and B2, with high values of bootstrap probability (85% and 91%, respectively). Clades A, B1, and B2 consist of 24, 3, and 7 haplotypes, respectively. Clade A comprises the populations in the East China Sea (populations at the Danjo Islands and Goto Islands, as well as 1 individual from the Koshiki-jima Islands), the Sea of Japan (populations in the Kyoto and Niigata Prefectures), as well as 1 individual each from Taiwan and the Korean Peninsula (*n*=165, 77.1% of all samples). Clades B1 and B2 consist of the populations along the southern (Kochi Prefecture: *n*=23, 10.7% of all samples) and northern (Aomori Prefecture: *n*=26, 12.1% of all samples) Pacific coasts of Japan, respectively. The net average distance (uncorrected *p*-distance) between clade A and clade B was 0.021. Applying the divergence rate of 1.0–1.6% per million years, we estimated that clade A and clade B diverged from each other 1.31–2.10 million years ago (MYA). The uncorrected *p*-distance between clade B1 and clade B2 was 0.008, and the divergence time was estimated to be 0.50–0.80 MYA.

The minimum spanning network of the haplotypes is given in Figure 3. Haplotypes were divided into 2 groups, group A and group B, with the latter subdivided into 2 subgroups, group B1 and group B2, which correspond to clades A, B1, and B2 in the maximum likelihood tree, respectively (Fig. 2). The 10 haplotypes of group B are separated from those of group A by a minimum of 15 mutations. The 3 haplotypes of group B1 are separated from those of group B2 by a minimum of 5 mutations. Group A consists of the most dominant haplotype, a1 (*n*=74, 44.8% of the group), 9 haplotypes that are shared with more than 2 individuals (haplotypes a2–a10), and 14 rare haplotypes that were found in only 1 or 2 individuals. Group B1 includes 1 dominant haplotype, b1, and 2 rare haplotypes that connect with haplotype b1 by 1 and 3 mutations. Group B2 consists of 2 non-rare haplotypes (b2 and b3) and of 5 rare haplotypes connected to each other by 1 or 2 mutations.

Geographic distribution of haplotypes Haplotype frequencies in the 9 locations are shown in Figure 4. The population in the Danjo Islands consists of 8 non-rare haplotypes (a1, a2, a4–a6, and a8–a10) and 5 rare haplotypes, with haplotype a2 being dominant (27.1% of samples). The population in the Goto Islands comprises 5 non-rare (a1–a3, a5, and a6) and 3 rare haplotypes, with haplotype a1 as the dominant haplotype (38.9% of samples). The population in Kyoto Prefecture includes 4 non-rare (a1, a3, a4, and a7) and 2 rare haplotypes, with the dominant haplotype being a1 (59.6% of samples). The population in Niigata Prefecture consists of 3 non-rare (a1, a3, and a7) and 3 rare haplotypes, with haplotype a1 as the dominant haplotype (65.3% of samples). In the East China Sea and the Sea of Japan, the frequency of haplotype a1 gradually increased from the Goto Islands (38.9% of samples) northward to Niigata Prefecture (65.3% of samples). The population in Kochi Prefecture includes 1 dominant (b1: 87.0% of samples) and 2 rare haplotypes. The population in Aomori Prefecture consists of 2 non-rare (b2 and b3) and 5 rare haplotypes, with haplotype b2 being the dominant haplotype (46.2% of samples).

Genetic differentiation among populations Samples from the Koshiki-jima Islands, Taiwan, and the Korean Peninsula

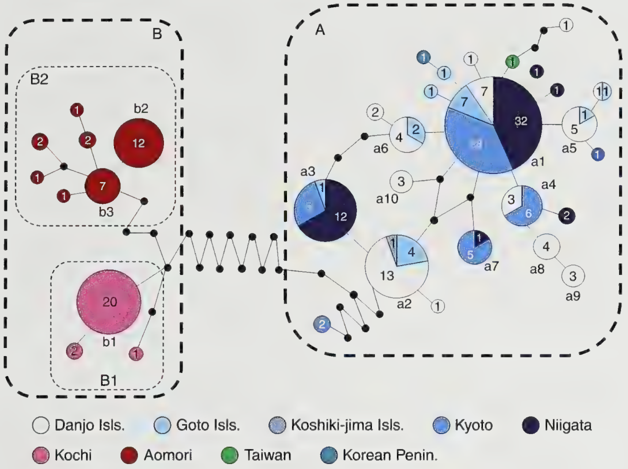

Figure 3

Minimum spanning network of haplotypes based on phylogenetic analysis of the mitochondrial cytochrome *b* gene sequences (931 base pairs) identified in 214 polkadot skate (*Dipturus chinensis*). Sequences were obtained from specimens caught at 7 locations around Japan, in the East China Sea, Sea of Japan, and Pacific Ocean, between 2010 and 2017 or were obtained through the International Nucleotide Sequence Database Collaboration for 2 other populations, in Taiwan or off the Korean Peninsula. Each circle represents a unique haplotype. Haplotypes are combined into groups A and B, and group B is further divided into subgroups B1 and B2 (all of which correspond to the clades and subclades in the maximum likelihood tree in Figure 2). Slices of the circles represent fractions of the number of individuals of a haplotype that are associated with 1 or more of the 9 locations. The size of circles is proportional to the number of individuals. Each branch equals 1 nucleotide substitution. Isls.=Islands; Penin.=Peninsula.

were excluded from analysis because the sample size for each location was only 1 individual. Results of hierarchical AMOVA (Suppl. Table 1) (online only) indicate that the Φ_{ST} value was 0.8976 (P<0.001) and that 89.76% of genetic variability was distributed among the 6 geographic populations that were included in analysis. When the 6 populations were divided into 2 groups, clade A (populations in the Danjo and Goto Islands in the East China Sea and populations in the Kyoto and Niigata Prefectures in the Sea of Japan) and clade B (populations in the Kochi and Aomori Prefectures along the southern and northern Pacific coasts of Japan, respectively), the Φ_{CT} value was 0.8529 (P=0.068), and 85.29% of genetic variability was distributed between the groups. When the 6 populations were divided into 3 groups, namely, clade A, clade B1 (population in Kochi Prefecture), and clade B2 (population in Aomori Prefecture), the Φ_{CT} value was maximized (Φ_{CT}=0.8964), and 89.64% of genetic variability was distributed between the groups. However, the P-value was barely not significant (P=0.064).

The pairwise Φ_{ST} values among the 6 geographic populations estimated from the mt cyt *b* gene sequences are shown in Table 3. The values between each of the 2 populations along the Pacific coasts (in Kochi and Aomori Prefectures) and each of the 4 populations in the East China Sea (in the Danjo and Goto Islands) and the Sea of Japan (Kyoto and Niigata Prefectures) were high (pairwise Φ_{ST}: 0.8847–0.9342) and significant after a Bonferroni correction (P<0.001). The Φ_{ST} value between the populations in the Kochi and Aomori Prefectures was also high (pairwise Φ_{ST}: 0.8507) and significant after a Bonferroni correction (P<0.001).

Demographic history The mismatch distributions for the samples in clade A (Fig. 5A) and clade B2 (Fig. 5C) follow a unimodal curve, and the distribution for the samples in clade B1 (Fig. 5B) has roughly an *L* shape. Historic demographic parameters estimated for each clade are shown in Table 4. The θ_1 in clade B1 (0.299) was an order of magnitude smaller than that in clade A (3.916) and clade B2 (6.597). The sum of squared deviations and Harpending's raggedness index values were low and not significant in any of the distributions. The negative and significant values of Tajima's *D* were detected for the samples for clade A (Tajima's *D*: −1.518, P<0.05) and clade B1 (Tajima's *D*: −1.679, P<0.05). The negative and significant values of Fu's *F*s were detected for only the samples for clade A (Fu's *F*s: −10.959, P<0.005).

The BSPs for clade A (Fig. 5D) and clade B2 (Fig. 5F) indicate that N_e increased after the Last Glacial Maximum (LGM, which occurred approximately 0.01–0.02 MYA), but such an increase of N_e with regard to LGM was not observed for clade B1 (Fig. 5E). However, the possibility of a constant population, a population that has not experienced rapid population growth or decline, could not be rejected for any clades because the 95% highest posterior density interval was not indicated to exclude zero by the parameter sum (indicators.alltrees).

Microsatellite analyses

Genetic variation within populations In the 6 geographic populations included in analysis, the mean number of alleles per locus ranged from 1.00 at locus *LERI33* to 14.00 at locus *LERI44* (Suppl. Table 2) (online only). No

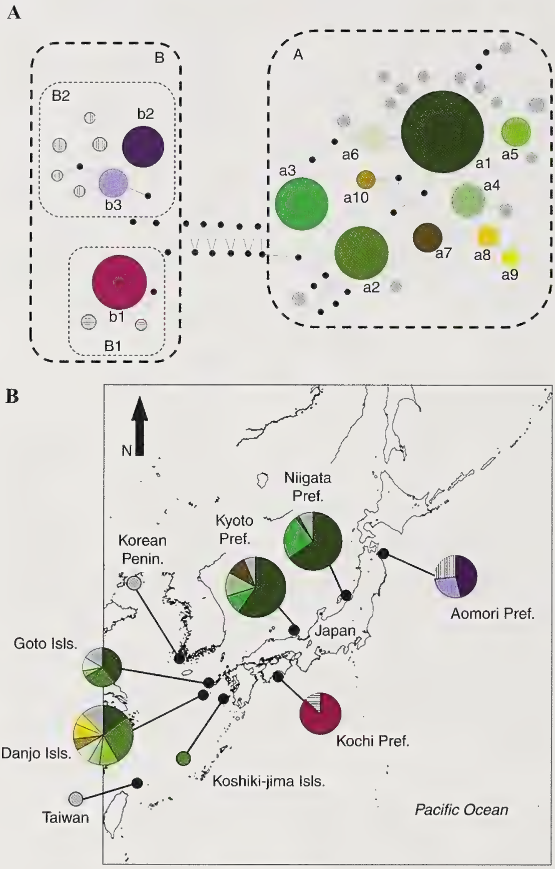

Figure 4

(**A**) A minimum spanning network of haplotypes and (**B**) a map of the geographic distribution of haplotypes based on phylogenetic analysis of the mitochondrial cytochrome *b* gene sequences (931 base pairs) of polkadot skate (*Dipturus chinensis*). Sequences were obtained from specimens caught at 7 locations around Japan during 2010–2017 or were obtained through the International Nucleotide Sequence Database Collaboration for populations in Taiwan or off the Korean Peninsula. Circles of different colors represent the 13 major haplotypes. Gray circles and circles or slices of circles with horizontal or vertical lines represent rare (observed in 1 or 2 individuals) haplotypes in groups A, B1, and B2, respectively. Isls.=Islands; Penin.=Peninsula; Pref.=Prefecture.

polymorphism was observed at locus *LERI33*; therefore, this locus was not included in further analyses. The mean number of alleles per geographic population ranged from 6.33 for the population in Kochi Prefecture to 9.83 for the population in Kyoto Prefecturue, with a mean of 8.70. The mean A_R for each geographic population varied from 6.01 for the population in Kochi Prefecture to 8.67 for the population in the Goto Islands, with a mean of 7.65. The mean H_O and H_E per locus varied from 0.484 at locus *LERI21* to 0.857 at locus *LERI44* and from 0.577 at locus *LERI21* to 0.894 at locus *LERI63*, respectively. The mean H_O per geographic population ranged from 0.476 for the population in Kochi Prefecture to 0.681 for the population in Kyoto Prefecture. The mean H_E per geographic population ranged from 0.593 for the population in Aomori Prefecture to 0.804 for the population in the Danjo Islands, with heterozygosity gradually decreasing from the Danjo Islands in the East China Sea northward to Niigata Prefecture in the Sea of Japan. Significant deviation from the Hardy–Weinberg expectations due to homozygote excess was observed at 2 loci (*LERI26* and *LERI63*). We deduced that these loci were affected by null alleles; therefore, they were also excluded from further analyses. For the 4 SSR loci (*LERI21*, *LERI34*, *LERI44*, and *LERI50*), no evidence of genotyping errors attributable to null alleles, stuttering, or large allele drop-out were observed. The results of pairwise comparisons between loci reveal no linkage disequilibrium.

Genetic differentiation among populations Results from hierarchical AMOVA (Suppl. Table 1) (online only) indicate that the R_{ST} value was 0.1409 (P<0.001) and that 14.09% of genetic variability was distributed among the 6 geographic populations included in analysis. When the 6 populations were divided into 2 groups, clade A and clade B, the R_{CT} value was 0.0868 (P=0.067), and 8.68% of genetic variability was distributed between the groups. When the 6 populations were divided into 3 groups, clade A, clade B1, and clade B2, the R_{CT} value was maximized (R_{CT}=0.1359), and 13.59% of genetic variability was distributed between the groups. However, the value was barely not significant (P=0.066).

The pairwise R_{ST} values among the 6 geographic populations estimated for 4 SSR loci are shown in Table 3. The R_{ST} values between each of the 2 populations in the Pacific Ocean (in the Kochi and Aomori Prefectures) and each of the 4 populations in the East China Sea

Table 3

Pairwise values of molecular genetic diversity among populations (Φ_{ST} and R_{ST}) estimated from mitochondrial cytochrome *b* gene (931 base pairs) (above the diagonal) and 4 microsatellite loci (below the diagonal), respectively, among 6 populations of the polkadot skate (*Dipturus chinensis*) sampled in the East China Sea, Sea of Japan, and Pacific Ocean during 2010–2017. An asterisk (*) indicates that a value is significant after a sequential Bonferroni correction ($P<0.001$).

Population location	Danjo Islands	Goto Islands	Kyoto Prefecture	Niigata Prefecture	Kochi Prefecture	Aomori Prefecture
Danjo Islands		–0.0030	0.0357	0.0269	0.8847*	0.8924*
Goto Islands	0.0002		0.0037	–0.0201	0.9342*	0.9234*
Kyoto Prefecture	0.0029	0.0194		0.0114	0.9147*	0.9156*
Niigata Prefecture	0.0093	0.0277	0.0031		0.9235*	0.9237*
Kochi Prefecture	0.0806*	0.1060*	0.0800*	0.1325*		0.8507*
Aomori Prefecture	0.1604*	0.1644*	0.1908*	0.2106*	0.1949*	

(in the Danjo and Goto Islands) and in the Sea of Japan (in the Kyoto and Niigata Prefectures) were high (pairwise R_{ST}: 0.0800–0.2106) and significant after a Bonferroni correction ($P<0.001$). The R_{ST} value between the populations in the Kochi and Aomori Prefectures was also high (pairwise R_{ST}: 0.1949) and significant after a Bonferroni correction ($P<0.001$).

Discussion

Genetic variation

The high h and low π (Table 2) in mt cyt *b* observed in each geographic population, except for the one in Kochi Prefecture, correspond to the results from previous studies in which the same genetic region as the one used for polkadot skate in our study was used for thornback skate (*Raja clavata*) in Portugal and the southwestern part of the North Sea (h=0.510–0.720, π=0.006–0.007; Chevolot et al., 2006b) and for thorny skate in Newfoundland, Iceland, the northeastern part of the North Sea, and Kattegat (h=0.719–0.916, π=0.0030–0.0071; Chevolot et al., 2007). In contrast, low h and low π observed in the population in the Kochi Prefecture are similar to the results for thornback skate in part of the Azores Islands and in the Mediterranean and Black Seas (h=0.000, π=0.000; Chevolot et al., 2006b). The mean A_R and H_E for each population from the SSR analysis in our study are higher than values reported by Griffiths et al. (2010) for the blue skate (*D. batis*) (A_R=3.65, H_E=0.349) and the flapper skate (*D. intermedius*), which was treated as the northern clade of blue skate (A_R=3.35, H_E=0.366), around the British Isles; Griffiths et al. (2010) used almost the same SSR loci as those used in our study. Among the 6 geographic populations in our study, the population in the Kochi Prefecture had the lowest A_R, and H_E was relatively lower for this population than for the others. Although factors affecting low genetic diversity of the population in Kochi Prefecture are unclear, the low diversity may be related to the demographic history of the population (see the "Evolutionary history" section).

Genetic differentiation among populations

The maximum likelihood tree (Fig. 2) and the minimum spanning network (Fig. 3) based on the haplotypes of mt cyt *b*, reveal 3 lineages, clades A, B1, and B2. Clade A consists of populations in the East China Sea (populations in the Danjo and Goto Islands and 1 individual from the Koshikijima Islands) and in the Sea of Japan (populations in the Kyoto and Niigata Prefectures). The haplotypes observed for populations in Taiwan and off the Korean Peninsula were also included in clade A; however, there was only 1 sample each from those locations. Addition of more samples in analysis is needed to improve understanding of the genetic relationships of those geographic populations to the populations around Japan. Clade B1 is the population off the southern Pacific coast of Japan (in Kochi Prefecture), and clade B2 was made up of the population from the northern Pacific coast (in Aomori Prefecture). In both mt cyt *b* and SSR analyses, the 6 geographic populations were separated into 3 groups, corresponding to the 3 clades, by using hierarchical AMOVA analyses that maximized Φ_{CT} and R_{CT} values, respectively, although the values were barely not significant (Suppl. Table 1) (online only). Genetic differentiation among the 3 groups are also indicated by both the pairwise Φ_{ST} and R_{ST} values from mt cyt *b* and SSR analyses, respectively (Table 3).

Our results indicate that the population structure of the polkadot skate is influenced by the complicated oceanic currents that surround Japan (Fig. 1). The clades A, B1, and B2 around Japan can be regarded as the Tsushima, Kuroshio, and Oyashio lineages, respectively. Similar genetic differentiations between the populations in the Sea of Japan and along the Pacific coasts have been reported for ocellate spot skate (Misawa et al., 2019b), in addition to reports for several coastal fish and invertebrate species (Kojima et al., 1997, 2004; Akihito et al., 2008; Katafuchi et al., 2011; Kokita and Nohara, 2011; Hirase et al., 2012;

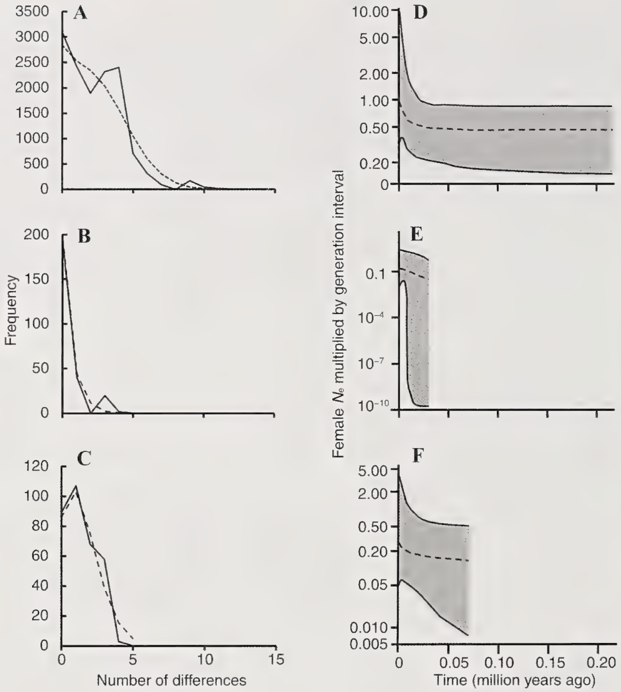

Figure 5

Mismatch distributions for (**A**) clade A, (**B**) clade B1, and (**C**) clade B2 of the polkadot skate (*Dipturus chinensis*) and Bayesian skyline plots for (**D**) clade A, (**E**) clade B1, and (**F**) clade B2, based on the mitochondrial cytochrome *b* gene sequences (931 base pairs) of 214 individuals that were obtained from 7 locations around Japan between 2010 and 2017 or were obtained through the International Nucleotide Sequence Database Collaboration for populations in Taiwan or off the Korean Peninsula. In panels A–C, solid and dashed lines represent the observed and simulated distributions under the sudden expansion model, respectively. In panels D–F, dashed lines indicate the female effective population size (N_e) multiplied by the generation interval, and the shaded area indicates the 95% highest posterior density interval.

Hirase and Ikeda, 2014). Genetic divergence between the Sea of Japan and the East China Sea has not been indicated for the polkadot skate, but Misawa et al. (2019b) suggested that populations of ocellate spot skate diverge at the boundary of those seas. They suggested that the Tsushima Strait and the Tsushima Current act as geographic barriers for dispersal that can limit distribution of ocellate spot skate and that the Kuroshio Current may have prevented dispersal of that species because of the absence of a major population of ocellate spot skate from the Pacific coast of central Japan. Different from their influence on ocellate spot skate, the Tsushima and Kuroshio Currents may have an effect on the dispersal of polkadot skate (see the "Evolutionary history" section).

The population of polkadot skate on the Pacific coast of northern Honshu (Aomori Prefecture) can be regarded as the Oyashio lineage. In contrast, for some shallow-water organisms, the Tsushima lineage is the lineage distributed on the Pacific coast of northern Honshu (Kojima et al., 2004; Akihito et al., 2008; Katafuchi et al., 2011; Kokita and Nohara, 2011; Hirase et al., 2012; Hirase and Ikeda, 2014). The Tsugaru Warm Current, one of the branches

Table 4

Results from mismatch distribution analysis and neutrality tests for 3 clades, based on phylogenetic analysis of mitochondrial cytochrome *b* gene (931 base pairs), of the polkadot skate (*Dipturus chinensis*). The demographic parameters estimated for each clade in the mismatch distribution analysis include time since expansion in units of mutational time (τ) and population size before (θ_0) and after (θ_1) a rapid change in population size in units of mutational time (Rogers and Harpending, 1992; Schneider and Excoffier, 1999). The goodness of fit between the observed and expected distributions was tested by using the sum of squared deviations (SSD) and the Harpending's raggedness index (*Hri*). The neutrality of the sequence variation was verified by using Tajima's D statistic and Fu's F_S test. P-values are provided in parentheses. DNA sequences were obtained from specimens collected around Japan, in the East China Sea, Sea of Japan, and Pacific Ocean, during 2010–2017 or were obtained through the International Nucleotide Sequence Database Collaboration for populations in Taiwan or off the Korean Peninsula.

	Mismatch distribution						Neutrality tests	
					Test of goodness of fit			
Group	τ	Mismatch observed mean	θ_0	θ_1	SSD (P)	*Hri* (P)	Tajima's D (P)	Fu's F_s (P)
Clade A	3.695	2.314	0.000	3.916	0.007 (0.686)	0.022 (0.893)	–1.518 (0.037)	–10.959 (0.002)
Clade B1	3.000	0.427	0.000	0.299	0.007 (0.334)	0.393 (0.572)	–1.679 (0.024)	–0.413 (0.248)
Clade B2	1.533	1.320	0.072	6.597	0.006 (0.578)	0.047 (0.798)	–0.858 (0.221)	–2.025 (0.089)

of the Tsushima Current, passes eastward through the Tsugaru Strait and runs into the Oyashio Current east of the Tsugaru Strait, forcing it to flow southward along the eastern coast of northern Honshu. The distribution of the Tsushima lineage of various marine animals on the Pacific coast of northern Honshu is considered to be influenced by the Tsugaru Warm Current (Kojima et al., 2004; Akihito et al., 2008; Katafuchi et al., 2011; Kokita and Nohara, 2011; Hirase et al., 2012). In contrast, a genetic differentiation between the western and eastern populations of northern Honshu has been suggested for the ocellate spot skate, the Pacific sandlance (*Ammodytes personatus*), and a zoarcid fish, *Davidijordania poecilimon* (Han et al., 2012; Kai et al., 2014; Misawa et al., 2019b), as well as for the polkadot skate as indicated by our results.

The dispersal of species is affected by many factors, including the environmental requirements and life histories of species. Kai et al. (2014) suggested that gene flow between the Sea of Japan and the Pacific populations of *D. poecilimon* is restricted by the shallow Tsugaru Strait (which has a maximum depth of approximately 150 m) because this deep-sea species is found in depths of less than 262 m (Shinohara et al., 1996). The normal habitat depths of polkadot skate (mainly 20–150 m; Hatooka et al., 2013) and ocellate spot skate (mainly 30–100 m; Last et al., 2016) are shallower than that of *D. poecilimon*, and their migrations are not as restricted by the shallow strait as that of *D. poecilimon*. The clear genetic divergence in polkadot skate and the restricted gene flow in ocellate spot skate (Misawa et al., 2019b) between the western and eastern populations of northern Honshu may be partly because of the lack of pelagic eggs and the larval stage of rajids (Ishiyama, 1967).

For polkadot skate, results of our study indicate a divergence between the southern (clade B1) and northern (clade B2) populations on the Pacific coast of Honshu. The existence of geologically discrete lineages on this coast of Honshu has been suggested for some coastal fish species (Katafuchi et al., 2011; Han et al., 2012; Hirase et al., 2012; Hirase and Ikeda, 2014). Among them, lineages of surfperch and goby species have been reported to be separated by the Izu Peninsula (Katafuchi et al., 2011; Hirase et al., 2012). Hirase et al. (2012) suggested that the shallow coastal areas in bays east and west of the Izu Peninsula, suitable for a goby species, likely disappeared owing to the sea level fall in the Pleistocene glacial periods, a change that resulted in vicariant separation.

In contrast, Han et al. (2012) detected a boundary between the lineages in the transition zone between the Kuroshio and Oyashio Currents and suggested that sea temperature is a key factor preventing the dispersal of the lineage that dominates the northern group of Pacific sandlance. The Kuroshio Current is subtropical and saline, and the Oyashio Current is subarctic and less saline (GSI, 1990). Results of the studies of the genetic population structure of mottled skate (Im et al., 2017; Misawa et al., 2019a) indicate that temperature gradients potentially affect the allopatric distributions of lineages. In thorny skate, genetic differentiation is reportedly caused by differences in salinity and temperature (Chevolot et al., 2007). The divergence between the southern (clade B1) and northern (clade B2) populations of polkadot skate on the Pacific coast of Honshu was probably due to environmental differences, such as differences in temperature and salinity between the Kuroshio and Oyashio Currents.

Evolutionary history

For polkadot skate, the divergence time between clade A and clade B was estimated to be 1.31–2.10 MYA in the Early Pleistocene. Some changes in land area with respect to glacio-eustatic sea-level fluctuation occurred in the

Quaternary period (from 2.58 MYA to present). In the Early to Middle Pleistocene (0.78–2.58 MYA), the main islands of Japan were connected to the continent of Asia, and the Ryukyu Islands were connected to the continent of Asia through Taiwan, by large land bridges, repeatedly (Kizaki and Oshiro, 1977, 1980; Ujiie, 1986; Kimura, 1996, 2000). Clade A likely became differentiated in the semi-closed environment of the East China Sea and dispersed northward when the southern straits of the Sea of Japan opened. Clade B might have extended its distribution northward along the Pacific coast after divergence from clade A and divided into clades B1 and B2 approximately 0.50–0.80 MYA in the Middle Pleistocene. The divergence of clades B1 and B2 may have been caused by changes in the dynamic of the ancient Oyashio Current, which strengthened during 0.48–0.34 MYA (Matsuzaki et al., 2014); afterward, the Kuroshio Current dominated 0.78–0.85 MYA (Kang et al., 2010; Gallagher et al., 2015). Clade B extended its distribution northward along the coast of Honshu with the Kuroshio Current but was prevented from further extension to the north by the strengthened Oyashio Current approximately 0.5 MYA, and the Kuroshio (clade B1) and the Oyashio (clade B2) lineages diverged.

Although the results of the mismatch distribution analysis, the neutrality tests (Table 4), and the combination of high h and low π values (Table 2) (Grant and Bowen, 1998) indicate a population expansion of clade A (Table 4, Fig. 5A), the possibility of a constant population could not be rejected in the BSP (Fig. 5D). However, the BSP for clade A indicates that N_e notably increased after LGM, and clade A may have expanded its distribution from the East China Sea to the Sea of Japan after LGM. The gradual decrease of genetic diversity (h in mtDNA analysis and H_E in SSR analysis) in populations of polkadot skate from the Danjo Islands in the East China Sea northward to Niigata Prefecture in the Sea of Japan (Table 2, Fig. 4, Suppl. Table 2 [online only]) may have been due to a founder event or to differences in adaptive abilities, such as tolerance to cold temperatures as frequencies of restricted haplotypes (haplotypes a1 and a3) increase with increasing latitude (Fig. 4). Similar declines in genetic diversity toward the north in the Sea of Japan have been reported for the sailfin sandfish (*Arctoscopus japonicus*) (see Shirai et al., 2006) and a rocky intertidal goby, *Chaenogobius gulosus* (see Hirase and Ikeda, 2014).

Although sum of squared deviations and the Harpending's raggedness index are not significant and Fu's *F*s does not indicate certain departures from neutrality in clade B1 (Table 4), the mismatch distributions (Fig. 5B) roughly have an *L* shape, indicating that clade B1 had experienced a population bottleneck (Rogers and Harpending, 1992). The combination of low h and low π values observed in clade B1 (Table 2) also indicates a recent population bottleneck or founder event for a single or a few mtDNA lineages (Grant and Bowen, 1998). However, no signal of population bottleneck is apparent in the BSP (Fig. 5E). In any case, N_e in clade B1 did not notably increase after LGM, and N_e in clade B1 is considerably smaller at present than N_e for the other clades, according to values for θ_1 (Table 4) and the BSP. The low genetic diversity in both mtDNA and SSR analyses for clade B1 was related to the small N_e of the clade. In clade B2, the population expansion could not be inferred by using neutrality tests (Table 4); however, results of the mismatch distribution analysis (Table 4, Fig. 5C) and the combination of high h and low π values (Table 2) indicate that the population expanded (Rogers and Harpending, 1992; Grant and Bowen, 1998). Although the possibility of a constant population could not be rejected in the BSP (Fig. 5F), the BSP for clade B2, as well as that for clade A, indicates that N_e increased after LGM (Fig. 5D).

Implications for management and conservation

The application of genetic and evolutionary measures in the conservation and management of natural resources has led to the identification of management units (MUs), which represent populations or groups of populations that are connected by low levels of gene flow and are functionally independent (Moritz, 1994, 2002). Significant population structure in the polkadot skate was observed around Japan in our study, and we suggest considering the existence of a minimum of 3 MUs for this species: the group of populations in the Sea of Japan and the East China Sea, the population along the southern Pacific coast, and the population along the northern Pacific coast. Each MU possesses unique genetic traits and, therefore, should be treated independently. Particularly, the MU for the population along the southern Pacific coast is characterized by genetic diversity that is lower than that of the other 2 MUs and should be monitored and managed more carefully. Ecological studies, such as those that focus on age, growth, reproduction, and movement patterns, for each MU are also necessary to establish appropriate conservation and management strategies.

Conclusions

We examined the genetic population structure of polkadot skate around Japan. Results of the mtDNA analysis of polkadot skate indicate that this species has 3 lineages, clades A, B1, and B2. Clade A consists of populations in the Sea of Japan and the East China Sea. Clades B1 and B2 comprise populations in the Pacific Ocean along the southern and northern coasts of Japan, respectively. This genetic differentiation is also supported by results from SSR analysis. Results of this study indicate that the divergence between clades A and B occurred because of isolation of the East China Sea in the Early Pleistocene and that the divergence between clades B1 and B2 occurred likely because of changes in the dynamics of ancient water currents in the Middle Pleistocene. Each of the 3 genetically discrete management units of polkadot skate around Japan possess unique genetic traits and evolutionary history, and each should be treated independently in management of this species in the future.

Acknowledgments

We thank H. Kanehara, T. Aoshima, G. Kume, and the staffs of the training ships *Nagasaki-Maru* (Nagasaki University) and *Kagoshima-Maru* (Kagoshima University), the staffs of the RV *Mizuho-Maru* (Japan Sea National Fisheries Research Institute) and the RV *Heian-Maru* (Kyoto Institute of Oceanic and Fishery Science), and trawl fishermen of the FV *Kosei-Maru* (Mimase, Kochi Prefecture) and FV *Kyuei-Maru* (Hachinohe, Aomori Prefecture) for collecting samples. This work was supported in part by the Japan Fisheries Agency.

Literature cited

Akihito, A. Fumihito, Y. Ikeda, M. Aizawa, T. Makino, Y. Umehara, Y. Kai, Y. Nishimoto, M. Hasegawa, T. Nakabo, et al.
2008. Evolution of Pacific Ocean and the Sea of Japan populations of the gobiid species, *Pterogobius elapoides* and *Pterogobius zonoleucus*, based on molecular and morphological analyses. Gene 427:7–18.

Bouckaert, R., J. Heled, D. Kühnert, T. Vaughan, C.-H. Wu, D. Xie, M. A. Suchard, A. Rambaut, and A. J. Drummond.
2014. BEAST 2: a software platform for Bayesian evolutionary analysis. PLoS Comput. Biol. 10(4):e1003537.

Brander, K.
1981. Disappearance of common skate *Raja batis* from Irish Sea. Nature 290:48–49.

Chevolot, M., J. R. Ellis, G. Hoarau, A. D. Rijnsdorp, W. T. Stam, and J. L. Olsen.
2006a. Population structure of the thornback ray (*Raja clavata* L.) in British waters. J. Sea Res. 56:305–316.

Chevolot, M., G. Hoarau, A. D. Rijnsdorp, W. T. Stam, and J. L. Olsen.
2006b. Phylogeography and population structure of thornback rays (*Raja clavata* L., Rajidae). Mol. Ecol. 15:3693–3705.

Chevolot, M., P. H. J. Wolfs, J. Pálsson, A. D. Rijnsdorp, W. T. Stam, and J. L. Olsen.
2007. Population structure and historical demography of the thorny skate (*Amblyraja radiata*, Rajidae) in the North Atlantic. Mar. Biol. 151:1275–1286.

Clement, M., D. Posada, and K. A. Crandall.
2000. TCS: a computer program to estimate gene genealogies. Mol. Ecol. 9:1657–1659.

Domingues, R. R. D., A. W. S. Hilsdorf, and O. B. F. Gadig.
2018. The importance of considering genetic diversity in shark and ray conservation policies. Conserv. Genet. 19:501–525.

Drummond, A. J., A. Rambaut, B. Shapiro, and O. G. Pybus.
2005. Bayesian coalescent inference of past population dynamics from molecular sequences. Mol. Biol. Evol. 22:1185–1192.

Dulvy, N. K., J. D. Metcalfe, J. Glanville, M. G. Pawson, and J. D. Reynolds.
2000. Fishery stability, local extinctions, and shifts in community structure in skates. Conserv. Biol. 14:283–293.

El Nagar, A., M. McHugh, T. Rapp, D. W. Sims, and M. J. Genner.
2010. Characterisation of polymorphic microsatellite markers for skates (Elasmobranchii: Rajidae) from expressed sequence tags. Conserv. Genet. 11:1203–1206.

Excoffier, L., and H. E. L. Lischer.
2010. Arlequin suite ver 3.5: a new series of programs to perform population genetics analyses under Linux and Windows. Mol. Ecol. Resour. 10:564–567.

Excoffier, L., P. E. Smouse, and J. M. Quattro.
1992. Analysis of molecular variance inferred from metric distances among DNA haplotypes: application to human mitochondrial DNA restriction data. Genetics 131:479–491.

Felsenstein, J.
1985. Confidence limits on phylogenies: an approach using bootstrap. Evolution 39:783–791.

Ferrari, A., F. Tinti, V. B. Maresca, A. Velonà, R. Cannas, I. Thasitis, F. O. Costa, M. C. Follesa, D. Golani, F. Hemida, et al.
2018. Natural history and molecular evolution of demersal Mediterranean sharks and skates inferred by comparative phylogeographic and demographic analyses. PeerJ 6:e5560.

Frodella, N., R. Cannas, A. Vilonà, P. Carbonara, E. D. Farrell, F. Fiorentino, M. C. Follesa, G. Garofalo, F. Hemida, C. Mancusi, et al.
2016. Population connectivity and pylogeography of the Mediterranean endemic skate *Raja polystigma* and evidence of its hybridization with the parapatric sibling *R. montagui*. Mar. Ecol. Prog. Ser. 554:99–113.

Fu, Y.-X.
1997. Statistical tests of neutrality of mutations against population growth, hitchhiking and background selection. Genetics 147:915–925.

Gallagher, S. J., A. Kitamura, Y. Iryu, T. Itaki, I. Koizumi, and P. W. Hoiles.
2015. The Pliocene to recent history of the Kuroshio and Tsushima currents: a multi-proxy approach. Prog. Earth Planet. Sci. 2:17.

Goudet, J.
2002. FSTAT: a program to estimate and test gene diversities and fixation indices, vers. 2.9.3.2. [Available from website, accessed September 2018.]

Grant, W. A. S., and B. W. Bowen.
1998. Shallow population histories in deep evolutionary lineages of marine fishes: insights from sardines and anchovies and lessons for conservation. J. Hered. 89:415–426.

Griffiths, A. M., D. W. Sims, S. P. Cotterell, A. El Nagar, J. R. Ellis, A. Lynghammar, M. McHugh, F. C. Neat, N. G. Pade, N. Queiroz, et al.
2010. Molecular markers reveal spatially segregated cryptic species in a critically endangered fish, the common skate (*Dipturus batis*). Proc. R. Soc., B 277:1497–1503.

Griffiths, A. M., D. W. Sims, A. Johnson, A. Lynghammar, M. McHugh, T. Bakken, and M. J. Genner.
2011. Levels of connectivity between longnose skate (*Dipturus oxyrinchus*) in the Mediterranean Sea and the north-eastern Atlantic Ocean. Conserv. Genet. 12:577–582.

GSI (Geographical Survey Institute).
1990. The national atlas of Japan, rev. ed., 219 p. GSI, Tokyo, Japan. [Available from website.]

Guo, S. W., and E. A. Thompson.
1992. Performing the exact test for Hardy–Weinberg proportion for multiple alleles. Biometrics 48:361–372.

Han, Z., T. Yanagimoto, Y. Zhang, and T. Gao.
2012. Phylogeography study of *Ammodytes personatus* in northwestern Pacific: Pleistocene isolation, temperature and current conducted secondary contact. PLoS ONE 7(5):e37425.

Hara, K., K. Furumitsu, and A. Yamaguchi.
2014. Record of a Korean skate, *Hongeo koreana* (Jeong and Nakabo, 1997) from off Goto islands. Rep. Jap. Soc. Elasmobranch Stud. 50:21–26. [In Japanese.]

Hara, K., K. Furumitsu, T. Aoshima, H. Kanehara, and A. Yamaguchi.
2018a. Age, growth, and age at sexual maturity of the commercially landed skate species, *Dipturus chinensis*

(Basilewsky, 1855), in the northern East China Sea. J. Appl. Ichthyol. 34:66–72.

Hara, K., K. Furumitsu, and A. Yamaguchi.
2018b. Dietary habits of the polkadot skate *Dipturus chinensis* in the East China Sea. Ichthyol. Res. 65:363–373.

Harpending, H. C.
1994. Signature of ancient population growth in a low-resolution mitochondrial DNA mismatch distribution. Hum. Biol. 66:591–600.

Hatooka, K., U. Yamada, M. Aizawa, A. Yamaguchi, and N. Yagishita.
2013. Rajidae. *In* Fishes of Japan with pictorial keys to the species, 3rd ed. (T. Nakabo, ed.), p. 205–216, 1771–1773. Tokai Univ. Press, Hadano, Japan. [In Japanese.]

Hirase, S., and M. Ikeda.
2014. Divergence of mitochondrial DNA lineage of the rocky intertidal goby *Chaenogobius gulosus* around the Japanese Archipelago: reference to multiple Pleistocene isolation events in the Sea of Japan. Mar. Biol. 161:565–574.

Hirase, S., M. Ikeda, M. Kanno, and A. Kijima.
2012. Phylogeography of the intertidal goby *Chaenogobius annularis* associated with paleoenvironmental changes around the Japanese Archipelago. Mar. Ecol. Prog. Ser. 450:167–179.

Im, Y.-J., H.-S. Jo, H.-S. Ji, S.-H. Myoung, and J.-K. Kim.
2017. Geographic variations of the mottled skate, *Beringraja pulchra* (Liu, 1932) (Rajidae) in the Yellow and East Seas based on molecular and morphometric data. J. Appl. Ichthyol. 33:950–956.

Ishiyama, R.
1967. Fauna Japonica. Rajidae (Pisces), 82 p. Biogeogr. Soc. Jap., Tokyo, Japan.

Jeong, C. H., and H. Ishihara.
2009. *Dipturus kwangtungensis*. The IUCN Red List of Threatened Species 2009. e.T161400A5415674. [Available from website, accessed January 2017.]

Jeong, D., and Y.-H. Lee.
2015. The complete mitochondrial genome of the longnose skate: *Raja rhina* (Rajiformes, Rajidae). Mitochondrial DNA 26:123–124.

Jeong, D., S. Kim, C.-G. Kim, and Y.-H. Lee.
2014. The complete mitochondrial genome of the Korean skate: *Hongeo koreana* (Rajiformes, Rajidae). Mitochondrial DNA 25:437–438.
2015. Complete mitochondrial genome of the Kwangtung skate: *Dipturus kwangtungensis* (Rajiformes, Rajidae). Mitochondrial DNA 26:873–874.

Kai, Y., Y. Ueda, K. Fujiwara, M. Itoh, A. Yamasaki, and T. Nakabo.
2014. Population structure and demographic history of *Davidijordania poecilimon* (Perciformes: Zoarcidae). Species Divers. 19:15–19.

Kang, S., D. Lim, and S.-Y. Kim.
2010. Benthic foraminiferal assemblage of Seogwipo Formation in Jeju Island, South Sea of Korea: implication for late Pliocene to early Pleistocene cold episode in the northwestern Pacific margin. Quat. Int. 225:138–146.

Katafuchi, H., Y. Kai, and T. Nakabo.
2011. Genetic divergence in *Ditrema jordani* (Perciformes: Embiotocidae) from the Pacific coast of southern Japan, as inferred from mitochondrial DNA sequences. Ichthyol. Res. 58:90–94.

Kim, I.-C., S.-O. Jung, Y.-M. Lee, C.-J. Lee, J.-K. Park, and J.-S. Lee.
2005. The complete mitochondrial genome of the rayfish *Raja porosa* (Chondrichthyes, Rajidae). DNA Sequence 16:187–194.

Kimura, M.
1996. Quaternary paleogeography of the Ryukyu Arc. J. Geogr. 105:259–285. [In Japanese.]
2000. Paleogeography of the Ryukyu Islands. Tropics 10:5–24.

Kizaki, K., and I. Oshiro.
1977. Paleogeography of the Ryukyu Islands. Mar. Sci. Mon. 9:542–549. [In Japanese.]
1980. The origin of the Ryukyu Islands. *In* Natural history of the Ryukyus (K. Kizaki, ed.), p. 8–37. Tsukiji-shokan, Tokyo, Japan. [In Japanese.]

Kojima, S., R. Segawa, and I. Hayashi.
1997. Genetic differentiation among populations of the Japanese turban shell *Turbo (Batillus) cornutus* corresponding to warm currents. Mar. Ecol. Prog. Ser. 150:149–155.

Kojima, S., I. Hayashi, D. Kim, A. Iijima, and T. Furota.
2004. Phylogeography of an intertidal direct-developing gastropod *Batillaria cumingi* around the Japanese Islands. Mar. Ecol. Prog. Ser. 276:161–172.

Kokita, T., and K. Nohara.
2011. Phylogeography and historical demography of the anadromous fish *Leucopsarion petersii* in relation to geological history and oceanography around the Japanese Archipelago. Mol. Ecol. 20:143–164.

Larkin, M. A., G. Blackshields, N. P. Brown, R. Chenna, P. A. McGettigan, H. McWilliam, F. Valentin, I. M. Wallace, A. Wilm, R. Lopez, et al.
2007. Clustal W and Clustal X version 2.0. Bioinformatics 23:2947–2948.

Last, P. R., and A. P.K. Lim.
2010. A new species of skate *Okamejei jensenae* sp. nov. (Rajoidei: Rajidae) from the seas off Borneo, with a redescription of the Kwangtung skate, *Dipturus kwangtungensis* (Chu). *In* Descriptions of new sharks and rays from Borneo (P. R. Last, W. T. White, and J. J. Pogonoski, eds.), p. 101–114. CSIRO Mar. Atmos. Res. Pap. 032.

Last, P. R., B. Séret, M. F. W. Stehmann, and S. Weigmann.
2016. Skates: family Rajidae. *In* Rays of the world (P. R. Last, W. T. White, M. R. de Carvalho, B. Séret, M. F. W. Stehmann, and G. J. P. Naylor, eds.), p. 204–363. CSIRO Publ., Clayton, Australia.

Matsuzaki, K. M., H. Nishi, N. Suzuki, G. Cortese, F. Eynaud, R. Takashima, Y. Kawate, and T. Sakai.
2014. Paleoceanographic history of the Northwest Pacific Ocean over the past 740 kyr, discerned from radiolarian fauna. Palaeogeogr. Palaeoclimatol. Palaeoecol. 396:26–40.

Misawa, R., N. Muto, T. Hamatsu, J.-K. Kim, and Y. Kai.
2019a. Genetic population structure and morphological differences in the mottled skate *Beringraja pulchra*. Jap. J. Ichthyol. 66:23–35. [In Japanese.]

Misawa, R., Y. Narimatsu, H. Endo, and Y. Kai.
2019b. Population structure of the ocellate spot skate (*Okamejei kenojei*) inferred from variations in mitochondrial DNA (mtDNA) sequences and from morphological characters of regional populations. Fish. Bull. 117:24–36.

Misawa, R., A. M. Orlov, S. Y. Orlova, I. I. Gordeev, H. Ishihara, T. Hamatsu, Y. Ueda, K. Fujiwara, H. Endo, and Y. Kai.
2020. *Bathyraja (Arctoraja) sexoculata* sp. nov., a new softnose skate (Rajiformes: Arhynchobatidae) from Simushir Island, Kuril Islands (western North Pacific), with special reference to geographic variations in *Bathyraja* (*Arctoraja*) *smirnovi*. Zootaxa 4861:515–543.

Moritz, C.
1994. Defining 'evolutionarily significant units' for conservation. Trends Ecol. Evol. 9:373–374.
2002. Strategies to protect biological diversity and the evolutionary processes that sustain it. Syst. Biol. 51:238–254.

Nei, M.
1987. Molecular evolutionary genetics, 512 p. Columbia Univ. Press, New York.

Nei, M., and W.-H. Li.
1979. Mathematical model for studying genetic variation in terms of restriction endonucleases. Proc. Natl. Acad. Sci. U.S.A. 76:5269–5273.

Nei, M., and J. C. Miller.
1990. A simple method for estimating average number of nucleotide substitutions within and between populations from restriction data. Genetics 125:873–879.

Palsbøll, P. J., M. Bérubé, and F. W. Allendorf.
2007. Identification of management units using population genetic data. Trends Ecol. Evol. 22:11–16.

Palumbi, S., A. Martin, S. Romano, W. O. McMillan, L. Stice, and G. Grabowski.
2002. The simple fool's guide to PCR, vers. 2.0, 45 p. Univ. Hawaii Press, Honolulu, HI.

Rambaut, A., A. J. Drummond, D. Xie, G. Baele, and M. A. Suchard.
2018. Posterior summarization in Bayesian phylogenetics using Tracer 1.7. Syst. Biol. 67:901–904.

Rasmussen, A.-S., and U. Arnason.
1999. Molecular studies suggest that cartilaginous fishes have a terminal position in the piscine tree. Proc. Natl. Acad. Sci. U.S.A. 96:2177–2182.

Raymond, M., and F. Rousset.
1995. GENEPOP (version 1.2): population genetics software for exact tests and ecumenicism. J. Hered. 86:248–249.

Rice, W. R.
1989. Analyzing tables of statistical tests. Evolution 43:223–225.

Rogers, A. R., and H. Harpending.
1992. Population growth makes waves in the distribution of pairwise genetic differences. Mol. Biol. Evol. 9:552–569.

Rousset, F.
2008. GENEPOP'007: a complete re-implementation of the GENEPOP software for Windows and Linux. Mol. Ecol. Resour. 8:103–106.

Schneider, S., and L. Excoffier.
1999. Estimation of past demographic parameters from the distribution of pairwise differences when the mutation rates vary among sites: application to human mitochondrial DNA. Genetics 152:1079–1089.

Shinohara, G., H. Endo, and K. Matsuura.
1996. Deep-water fishes collected from the Pacific coast of northern Honshu, Japan. Mem. Natl. Sci. Mus., Tokyo 29:153–185.

Shirai, S. M., R. Kuranaga, H. Sugiyama, and M. Higuchi.
2006. Population structure of the sailfin sandfish, *Arctoscopus japonicus* (Trichodontidae), in the Sea of Japan. Ichthyol. Res. 53:357–368.

Tajima, F.
1989a. Statistical method for testing the neutral mutation hypothesis by DNA polymorphism. Genetics 123:585–595.
1989b. The effect of change in population size on DNA polymorphism. Genetics 123:597–601.

Tamura, K., and M. Nei.
1993. Estimation of the number of nucleotide substitutions in the control region of mitochondrial DNA in humans and chimpanzees. Mol. Biol. Evol. 10:512–526.

Tamura, K., G. Stecher, D. Peterson, A. Filipski, and S. Kumar.
2013. MEGA6: molecular evolutionary genetics analysis version 6.0. Mol. Biol. Evol. 30:2725–2729.

Tokimura, M., M. Ito, and U. Yamada.
1998. New record of the rajid fish, *Raja koreana* Jeong and Nakabo (new Japanese name: Kourai-kasube) from Japan. Seikaiku Suisan Kenkyusho News 93:9–10. [In Japanese.] [Available from website.]

Ujiie, H.
1986. Beneath the Ryukyu Island Arc: sedimentology and geology, 120 p. Shinsei-tosho, Naha, Japan. [In Japanese.]

Van Oosterhout, C., W. F. Hutchinson, D. P. M. Wills, and P. Shipley.
2004. MICRO-CHECKER: software for identifying and correcting genotyping errors in microsatellite data. Mol. Ecol. Notes 4:535–538.

Vargas-Caro, C., C. Bustamante, J. Lamilla, M. B. Bennett, and J. R. Ovenden.
2016. The phylogenetic position of the roughskin skate *Dipturus trachyderma* (Krefft & Stehmann, 1975) (Rajiformes, Rajidae) inferred from the mitochondrial genome. Mitochondrial DNA, A 27:2965–2966.

Vargas-Caro, C., C. Bustamante, M. B. Bennett, and J. R. Ovenden.
2017. Towards sustainable fishery management for skates in South America: the genetic population structure of *Zearaja chilensis* and *Dipturus trachyderma* (Chondrichthyes, Rajiformes) in the south-east Pacific Ocean. PLoS ONE 12(2):e0172255.

Weltz, K., J. M. Lyle, J. M. Semmens, and J. R. Ovenden.
2018. Population genetics of the endangered Maugean skate (*Zearaja maugeana*) in Macquarie Harbour, Tasmania. Conserv. Genet. 19:1505–1512.

Yamada, U., M. Tokimura, H. Horikawa, and T. Nakabo.
2007. Fishes and fisheries of the East China and Yellow Seas, 1262 p. Tokai Univ. Press, Hadano, Japan. [In Japanese.]

Yamada, U., M. Tokimura, K. Hoshino, S. M. Deng, Y. J. Zheng, S. F. Li, Y. S. Kim, and J. K. Kim.
2009. Names and illustrations of fishes from the East China Sea and the Yellow Sea—Japanese/Chinese/Korean, new ed., 784 p. Overseas Fish. Coop. Found. Japan, Tokyo, Japan.

National Marine
Fisheries Service
NOAA

Fishery Bulletin
established in 1881

Spencer F. Baird
First U.S. Commissioner
of Fisheries and founder
of *Fishery Bulletin*

Morphology of larvae of 6 *Lampanyctus* species in the central South Pacific Ocean with notes on their occurrence

Yana Yu. Bolshakova (contact author)
Sergei A. Evseenko (deceased)
Dmitry V. Bolshakov

Email address for contact author: yanusrunaa@mail.ru

Shirshov Institute of Oceanology
Russian Academy of Sciences
36 Nakhimovsky Prospekt
Moscow 117997, Russia

Abstract—Larvae of 6 species of *Lampanyctus* (family Myctophidae) collected during the 34th cruise of RV *Dmitry Mendeleev* in 1985 in the central South Pacific Ocean (27–48°S) are described. Discussed in more detail are diagnostic characters for 4 of these species, whose morphology has been insufficiently studied: cripplefin lanternfish (*L. achirus*), southern lanternfish (*L. australis*), *L. gibbsi* or *L. wisneri*, and *Lampanyctus* sp. *D*. Additional data from larvae caught during the 16th cruise of RV *Dmitry Mendeleev* (in the southwestern Pacific Ocean) and 29th cruise of RV *Akademik Ioffe* (in the South Atlantic Ocean) are incorporated in the discussion.

Manuscript submitted 5 November 2020.
Manuscript accepted 28 June 2021.
Fish. Bull. 119:112–122 (2021).
Online publication date: 23 July 2021.
doi: 10.7755/FB.119.2-3.2

The views and opinions expressed or implied in this article are those of the author (or authors) and do not necessarily reflect the position of the National Marine Fisheries Service, NOAA.

Lampanyctus is one of the most species-rich genera of the family Myctophidae and includes more than 40 species (Fricke et al., 2020). There are 2 opinions about phylogenetic relationships within this genus based on both morphological and molecular data. One notion is that the genus *Nannobrachium* is a junior synonym of *Lampanyctus* (Becker, 1983; Moser and Ahlstrom, 1996; Olivar and Beckley, 1997; Denton, 2014; Kobyliansky, 2016; Martin et al., 2018). The other opinion is that both genera, *Nannobrachium* and *Lampanyctus*, are valid (Zahuranec, 2000). According to recent data (Martin et al., 2018), we consider the genus *Lampanyctus sensu lato*. Information of the larval development of *Lampanyctus* species is scarce. Descriptions of the early larval stages are available for only about half of the species (Tåning, 1918; Pertseva-Ostroumova, 1964; Moser and Ahlstrom, 1974; Miller et al., 1979; Olivar, 1985; Moser and Ahlstrom, 1996; Olivar and Beckley, 1997; Moser and Watson, 2001; Bolshakova and Evseenko, 2015, 2016, 2020).

Adults of at least 15 species of *Lampanyctus* have been found among Myctophidae collected in the western and central South Pacific Ocean (McGinnis, 1982; Becker, 1983; Becker and Evseenko, 1986; Zahuranec, 2000). Individuals of 5 of those species were caught during a complex expedition to the South Pacific Ocean in 1985, the 34th voyage of RV *Dmitry Mendeleev* (Becker and Evseenko, 1986). The collections made during this cruise include adults of the following 5 species: cripplefin lanternfish (*L. achirus*), southern lanternfish (*L. australis*), diamondcheek lanternfish (*L. intricarius*), rakery beaconlamp (*L. macdonaldi*), and pygmy lanternfish (*L. pusillus*). Here, we describe the morphology of larvae of the 6 lanternfish species found in open waters of the central South Pacific Ocean: *L. achirus*, *L. australis*, *L. gibbsi* or *L. wisneri*, *Lampanyctus* sp. *D*, *L. intricarius*, and *L. pusillus*. The morphology of all but the last 2 of these species has been insufficiently studied. These descriptions are the first ones of *Lampanyctus* larvae from this area and supplement the available data on the development of *Lampanyctus* species.

Materials and methods

Fish in early developmental stages sampled during the 34th expedition of RV *Dmitry Mendeleev* served as materials for the work in this study

Table 1

The stations, geographic coordinates, and depth layers at which, and the dates on which, larvae of *Lampanyctus* were captured during the 34th voyage of RV *Dmitry Mendeleev* in January–March 1985 in the central South Pacific Ocean. Larval specimens caught during this expedition were examined for this study. Ichthyoplankton and adult fish were collected as part of the expeditions of the RV *Dmitry Mendeleev* along 3 transects between 27°S and 48°S.

Station no.	Date	Coordinates	Depth layer (m)
3009	16 January 1985	46°50′S, 158°01′W	0–200
3010	17 January 1985	45°20′S, 157°33′W	0–200
3042	20–21 January 1985	45°31′S, 157°43′W	0–200
3043	22 January 1985	45°53′S, 158°09′W	0–200
3044	23 January 1985	41°32′S, 158°05′W	0–200
3049	4 February 1985	38°48′S, 157°54′W	0–200
3050	5 February 1985	37°15′S, 158°03′W	0–200
3051	6 February 1985	34°59′S, 158°06′W	0–200
3052	12–13 February 1985	37°56′S, 125°55′W	0–200
3054	14 February 1985	39°42′S, 126°01′W	0–200
3055	15 February 1985	41°43′S, 125°34′W	0–200
3056	16 February 1985	43°06′S, 125°42′W	0–50
3057	17 February 1985	44°29′S, 125°42′W	0–350
3067	25 February 1985	44°51′S, 134°41′W	0–200
3068	27 February 1985	40°47′S, 139°28′W	0–550
3069	28 February 1985	37°43′S, 143°00′W	0–500
3071	3 March 1985	17°13′S, 156°54′W	0–200

(Table 1). During January–March 1985, larval and adult fish were taken along 3 transects in the central South Pacific Ocean between 27°S and 48°S: 1) on 158°W, 2) on 126°W, and 3) between 135°W and 143°W (Figs. 1 and 2). In addition, materials from the collections of the 16th expedition of the RV *Dmitry Mendeleev* to the southwestern Pacific Ocean in 1976 and of the 29th expedition of the RV *Akademic Ioffe* to the South Atlantic Ocean in 2009 were used. The ichthyoplankton was sampled during these 3 expeditions by using an Isaacs-Kidd midwater trawl with the Samyshev-Aseev modification. The trawl net has a mouth opening of 6 m^2, a length of 25 m, 5-mm mesh without nodes, and cod end liner of 500-µm nylon mesh. The specimens were preserved and stored in 4% formaldehyde. The larvae were stained with alizarin following the standard procedure (Taylor and Van Dyke, 1985). Data on the adult meristic characters are presented in Table 2.

Information for the following features are included in the descriptions: standard body length (SL), head length (HL), body depth at pectoral fin base (BD), preanal length (PAL), predorsal length (PDL), snout length (SnL), horizontal diameter of the eye (ED), number of rays in dorsal fin (D), number of rays in anal fin (A), number of rays in pectoral fin (P_1), number of rays in pelvic fin (P_2), number of rays in caudal fin (C), number of branchiostegal rays (BrR), number of gill rakers (GR) on the upper and lower parts of the first gill arch, number of vertebrae (V), 3rd supraanal organ (SAO_3), and 2nd branchiostegal photophore (Br_2).

Results

Lampanyctus achirus (Andriashev, 1962)

Distinguishing features In addition to meristic characters, larvae of this species are easy to differentiate from those of other lanternfish species by the long, toothy rostrum, preopercular spines, pigmentation of the rostrum and postorbital region, and lack of pigment above the brain. Preopercular spines have also been found in larvae of the black lantern fish (*L. niger*) and dusky lanternfish (*L. ater*) (Moser and Watson, 2001). Characteristic differences between larval *L. achirus* and larvae of these 2 species occur in pigmentation. In *L. ater*, there is pigment in the dorsal midline behind the dorsal fin; in *L. niger*, there are melanophores at the base of pectoral fins and at the rays of pelvic fins.

Morphology In our collections, 102 larvae with sizes of 9.0–22.0 mm SL were found (Fig. 3). The head and jaws are large, taking almost half of the body length in the larvae that were 11.0–16.0 mm SL (HL 46–50% SL), with an elongated toothy rostrum (SnL 50–65% HL). The head length decreases from about 50% to 38% SL as larvae grow from a length of 16.0 mm SL to a length of 21.5 mm SL. All the larvae have 3–6 small inner preopercular spines and 3 large outer preopercular spines. The length of these spines decreases with larval size. The eyes are slightly oval and become round to a length of about 15 mm SL (ED 20–23% HL). The jaws are long and end behind the vertical of the posterior margin of the eye. Body depth increases with larval size (BD 24–27% SL). The pectoral fins are large and fan-shaped. The anus opens far behind the middle of the body. The dorsal and anal fins are displaced posteriorly (PDL 58–66% SL; PAL 67–75% SL).

Meristic characters D: 15–17, A: 18–20, P_1: 14–16, P_2: 8, C: 6+11–10+6, GR: 6+1+12–14, V: 35–36, BrR: 9. All the rays in the fins are distinguishable in the 14.5-mm-SL larva, and the definitive number of gill rakers is noticeable to a size of 16.0 mm SL.

Pigmentation Pigmentation of the head includes one melanophore at the tip of the lower jaw, a row of melanophores scattered on the dorsal side of the rostrum, and a row of 3 large melanophores on the rostrum anterior to the eye. The row of 2–5 melanophores (the number of melanophores increases with larval size) at the postorbital and opercular regions is located at the level of the middle of the eye. Minute melanophores cover the base and rays of the pectoral fin. No pigmentation occurs above the brain. Pigmentation on the body appears in larvae only up to a size of 14–15 mm SL. It includes pigment on the myosepta of the oblique myotomes of the abdomen between the pectoral fin and the anus.

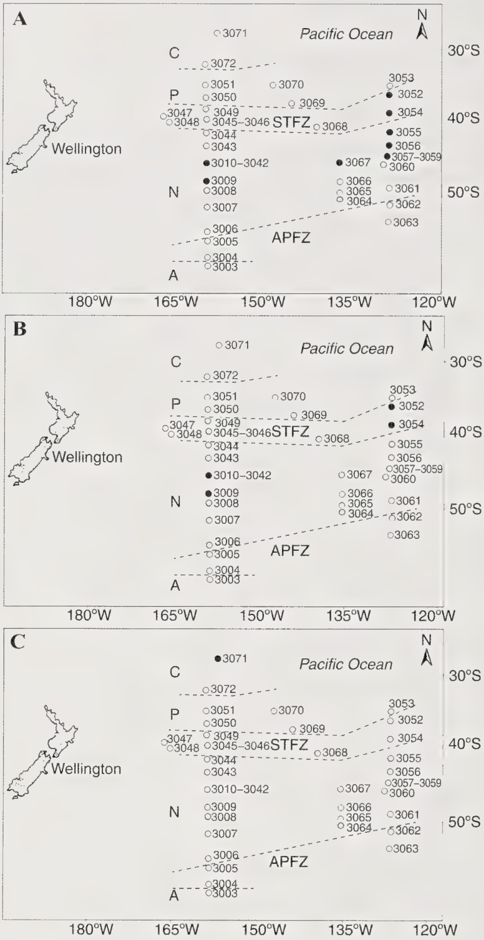

Figure 1

Schematic maps of the stations (open circles) where larvae of the following 3 species of *Lampanyctus* (black circles) were sampled during the 34th cruise of the RV *Dmitry Mendeleev* in the central South Pacific Ocean between January and March 1985: (**A**) cripple-fin lanternfish (*L. achirus*), (**B**) southern lanternfish (*L. australis*), and (**C**) *L. gibbsi* or *L. wisneri*. Dashed lines indicate the positions of biogeographic borders (Becker and Evseenko, 1986) for the central water mass (C), the periphery of the central water mass (P), subtropical frontal zone (STFZ), notal zone (N), Antarctic Polar Frontal Zone (APFZ), and Antarctic (A). Station numbers are given next to station markers. For geographic coordinates of the stations and for the dates of capture of larvae, see Table 1.

Photophore formation Br_2 are noticeable on the 9.2-mm-SL larva. No other photophores appear.

Comparative remarks A 13.4-mm-SL larva of *L. achirus* from the South Pacific Ocean has been described and illustrated (Moser and Ahlstrom, 1974; Moser et al., 1984), and a 6.0-mm-SL larva from the southwestern Indian Ocean has been described (Olivar and Beckley, 1997). The larvae of this species have such a characteristic appearance, especially a long rostrum, that it is quite easy to identify them. However, a detailed description and a series of developments is still absent in the literature. Our larvae do not differ in pigmentation from the previously described larvae of this species of a similar size (Moser and Ahlstrom, 1974; Moser et al., 1984), but they differ in the presence of preopercular spines. Spines in our larvae are noticeable in all studied individuals, starting at a length of 9.2 mm SL; therefore, it can be assumed that previous researchers did not notice this morphological feature. Further, on the 9.0-mm-SL larva from our collections taken in the South Atlantic Ocean (29th expedition of the RV *Akademik Ioffe*; station [st.] 2193; 36°56′S, 7°19′E), preopercular spines (both inner and outer) are also present.

Researchers have noted the possibility of the existence of 2 forms of this species that differ mainly in the number of gill rakers of the first gill arch (5+12–13 versus 6+13–14), in addition to the differences in the color of the body, the size of the vomerine tooth patch, and the position of the SAO_3 (Hulley, 1981; McGinnis, 1982; Zahuranec, 2000). These authors noticed that these characters were not always correlated; therefore, only one species is recognized, and these differences are explained as part of the mosaic pattern of variability. We found no differences in pigmentation or in meristic characters in the larvae we studied. In all larvae >16.0 mm SL, the number of gill rakers is 6+1+12–14.

Distribution Among *Lampanyctus* species in the investigated area, this species has the second-most abundant larvae. A total of 102 larvae of this species were collected at 8 stations (st. 3009, 3042, 3052, 3054, 3055, 3056, 3057, and 3067) in the notal zone of the South Pacific Ocean, from 45–46°S in the west of the study area to 37–48°S in the east of the study area. Single larvae of this species were found in the subtropical frontal zone in the South Pacific Ocean at 126°W (st. 3052 and 3054) (Fig. 1A). The presence of this species is an indicator of notal waters, although adults have a wider range and were found in the subtropical frontal zone (st. 3049) and in the periphery of the central water mass in the South Pacific Ocean (st. 3069) (Becker and Evseenko, 1986).

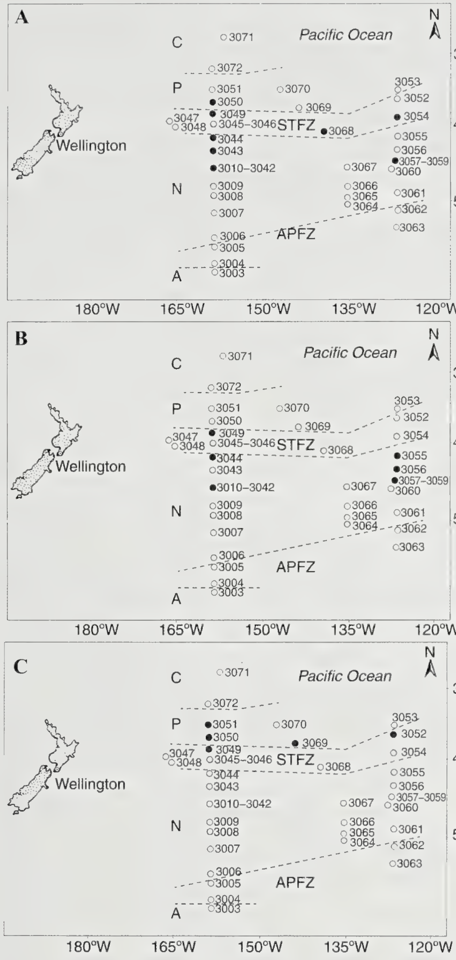

Figure 2

Schematic maps of the stations (open circles) where larvae of the following 3 species of *Lampanyctus* (black circles) were sampled during the 34th cruise of the RV *Dmitry Mendeleev* in the central South Pacific Ocean between January and March 1985: (**A**) diamondcheek lanternfish (*L. intricarius*), (**B**) *Lampanyctus* sp. *D*, and (**C**) pygmy lanternfish (*L. pusillus*). Dashed lines indicate the positions of biogeographic borders (Becker and Evseenko, 1986) for the central water mass (C), the periphery of the central water mass (P), subtropical frontal zone (STFZ), notal zone (N), Antarctic Polar Frontal Zone (APFZ), and Antarctic (A). Station numbers are given next to station markers. For geographic coordinates of the stations and for the dates of capture of larvae, see Table 1.

Lampanyctus australis Tåning, 1932

Distinguishing features Larvae of *L. australis* are intensely pigmented and characterized by the presence of a broad vertical band of pigment posterior to the pectoral fin, distinguishing it from larvae of all other known lanternfish species in the area. Among all known species of *Lampanyctus*, 2 other species have a broad stripe of pigment at the larval stage: the jewel lanternfish (*L. crocodilus*) and noble lampfish (*L. nobilis*) (Moser and Watson, 2001). Larvae of *L. australis* differ from those of *L. crocodilus* in the presence of melanophores on the cleitrum and at the tip of the lower jaw. Larvae of *L. nobilis* have no melanophores between the dorsal and adipose fins, and a row of melanophores on the isthmus is present.

Morphology In our collections, 15 larvae with sizes of 10.0–15.1 mm SL were identified, including specimens from the 34th expedition of the RV *Dmitry Mendeleev* and a 9.2-mm-SL larva from the 16th expedition of the RV *Dmitry Mendeleev* (st. 1335; 49°41′S, 148°25′E) (Fig. 4). Larvae are moderately deep bodied (BD 30–34% SL). The head length decreases from 33% to 27% SL as size increases from 9.2 mm SL to 15.1 mm SL. Larvae have a comparatively short snout (SnL 28–33% HL) and almost round eyes (EL 28–33% HL). The jaws are relatively prominent and extend behind the level of the posterior margin of the orbit. The dorsal fin originates approximately in the middle of the body (PDL 46–54% SL), and the anal fin begins under the 10–12 ray of the dorsal fin (PAL 58–66% SL). The PDL and PAL indicate the negative relationship with SL.

Meristic characters D: 13–14, A: 16–19, P_1: 13–14, P_2: 8, C: 8+10–9+8, GR: 6(7)+1+14(13), V: 36–37, BrR: 9. Fin rays are formed in all fins at 10.0 mm SL, and larvae have a definitive number of gill rakers at 10.2 mm SL. Larvae have 36–37 myomeres.

Pigmentation Larvae are intensely pigmented. Pigmentation of the head includes paired melanophores anterior to the midbrain, unpaired melanophores above the forebrain, one melanophore between the midbrain and the hindbrain, and one melanophore posterior to the hindbrain. There is one melanophore at the tip of the lower jaw. Melanophores are located on the cleithrum, on the inner surface of the base of the pectoral fins, and on its rays. One minute melanophore is located ventrally on the gut terminus. One conspicuous melanophore is on the dorsal midline between the dorsal and adipose fins. Internal melanophores are noticeable on the myosepta between the pectoral and pelvic fins and dorsally at the terminal gut section.

Table 2

Meristic characters of adults of the *Lampanyctus* species that have been found in the South Pacific Ocean. These data are from Wisner (1976), Hulley (1981), McGinnis (1982), Becker (1983), and Zahuranec (2000). A question mark (?) indicates that no data have been reported, and a dash (–) indicates that no fins have been observed. *Lampanyctus* sp. *A*, *L.* sp. *B*, *L.* sp. *C*, and *L.* sp. *D sensu* McGinnis (1982).

Species	Dorsal rays	Anal rays	Pectoral rays	Gill rakers	Vertebrae
L. achirus	14–16	16–20	–	5–6+1+11–13	35–36
L. alatus	11–13	16–18	11–13	3–4+1+9 (8)	33–35
L. ater	14–16	16–20	–	5 (4)+1+10–12	36 (35)
L. australis	12–14	17–19	13–15	6 (7)+1+13–14 (15)	35 (36–37)
L. festivus	14–15	19–21	15–17	4+1+9 (8–10)	35 (34)
L. gibbsi	13–14	18–19	13–14	3–4+1+8–10	37–38
L. intricarius	14–16	18–20	13–15	4+1+10 (9–11)	38 (37)
L. lepidolychnus	14–16	18–20	12–13	4+1+10 (8–11)	36–37
L. macdonaldi	14–16	17–18	12–13	8 (9–10)+1+17–18	34–35
L. pusillus	11–13	14–15	13–14	3+1+8 (9)	31–32
L. wisneri	14–15	17–19	–	4-5+1+10-11	36–37
L. sp. *A*	14–16	16–20	–	4+1+11–13	35–36
L. sp. *B*	15	21	17	?	?
L. sp. *C*	12–13	16–18	14–15	?	?
L. sp. *D*	12–13	16–18	14–15	?	?

Photophore formation Only Br$_2$ are formed in all individuals.

Comparative remarks Morphology of 5.5- and 6.4-mm-SL larvae of *L. australis* from the southwestern Indian Ocean (Olivar and Beckley, 1997) and of 8.3-, 9.3-, 10.1-, and 10.7-mm-SL larvae from the southeastern Atlantic Ocean (Bolshakova and Evseenko, 2016) have been described. In general, the morphology of our larvae is similar to that given previously. Larvae of a similar size from the Pacific Ocean and Atlantic Ocean do not differ in proportions. There is some variability in pigmentation between specimens from these oceans—2 larvae (8.3 and 10.1 mm SL) from the Atlantic Ocean lack the melanophore behind the dorsal fin, and all larvae from the Pacific Ocean have such a melanophore. Our description of larvae examined in our study complements the developmental series of this species.

Distribution A total of 14 larvae of this species were found in the study area (st. 3009, 3010, 3042, 3052, and 3054) between 37°S and 46°S in the subtropical frontal zone and the notal zone of the South Pacific Ocean (Fig. 1B). Adults of *L. australis* have a much broader range, with isolated specimens occurring down to 52°S (st. 3063) (Becker and Evseenko, 1986).

Lampanyctus gibbsi or *L. wisneri*

Distinguishing features Meristic characters are useful in separating the larva of either *L. gibbsi* or *L. wisneri* examined in this study from the larvae of other *Lampanyctus* species. The prominent jaw and the forward direction of teeth at the tip of the upper jaw distinguish this specimen from the larvae of *Lampanyctus* species with short rostrums. The larva is also well distinguished from the larvae of other long-rostrum species of *Lampanyctus*. These differences are clearly visible in pigmentation. In *L. ater* and the pinpoint lampfish (*L. regalis*), there is a melanophore between the dorsal and adipose fins. In *L. cuprarius* and *Nannobrachium* sp. 1 (Bolshakova and Evseenko, 2020, fig. 5), there is pigment at the midline of the body. In *L. niger*, there are melanophores at the base of pectoral fins and at the rays of pelvic fins. All these melanophores are absent in larvae of *L. gibbsi* and *L. wisneri*. The larvae of *L. lineatus* have a smaller body depth, and the larvae of *L. achirus* have a longer and more noticeable rostrum. The larva differs from larvae of *L. ater* in the absence of the preopercular spines.

Morphology A single larva was collected: 13.1 mm SL (Fig. 5). The larva has a deep body (BD 30% SL) and a large head (HL 31% SL) with long jaws extending under the vertical of the eye posterior margin. The snout is long (SnL 41% HL), and the eye is round (ED 32% HL). The dorsal fin begins at about the middle of the body (PDL 54% SL). The anal fin starts under the 9–10 ray of the dorsal fin (PAL 70% SL).

Meristic characters D: 15, A: 19, P$_1$: 13, P$_2$: 8, C: 6+10–10+5, GR: 4+1+10, V: 37, BrR: 9. Rays in all fins are fully formed.

Pigmentation Pigmentation of the head includes a melanophore at the tip of the lower jaw, a paired melanophore above the midbrain and located posterolaterally to the hindbrain. There is one melanophore on the cleithrum.

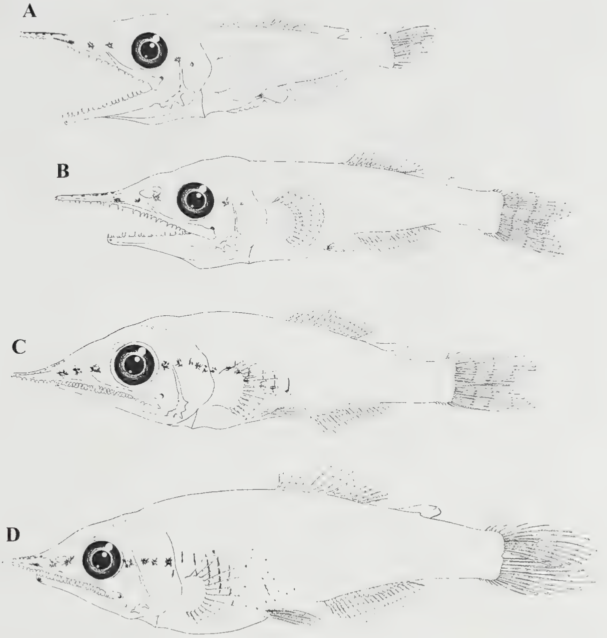

Figure 3

Illustrations of 4 early developmental stages of larval cripplefin lanternfish (*Lampanyctus achirus*) caught in the central South Pacific Ocean in 1985 (**A**) at station 3056 (9.2 mm standard body length [SL]), (**B**) at station 3056 (13.5 mm SL), (**C**) at station 3054 (15.0 mm SL), and (**D**) at station 3054 (22.0 mm SL).

Internal melanophores are visible in front of the liver, and some pigment is embedded in the peritoneal region on the myosepta between the pectoral and pelvic fins.

Photophore formation Only Br_2 are formed.

Comparative remarks On the basis of a number of characters, including elongated jaws, patch of teeth on the tip of upper jaw, long rostrum, large head, large pectoral fins, and posteriorly displaced dorsal fin (Moser et al., 1984; Zahuranec, 2000), we assign this larva to the group of long-rostrum *Lampanyctus* larvae (formerly *Nannobrachium*). Among the species that inhabit the central South Pacific Ocean, *L. macdonaldi*, *L. gibbsi*, and *L. wisneri* have not had their early stages of development described. *Lampanyctus macdonaldi* has a significantly higher number of gill rakers and lower number of vertebrae (GR: 25–28 versus 15; V: 34–35 versus 37). The meristic features of the remaining 2 types overlap (Table 2). Therefore, this larva may belong to one of these 2 species: *L. gibbsi* or *L. wisneri*.

Distribution The larva of this type was the only one with these characteristics collected in the central South Pacific Ocean. It was caught on the northernmost point of the study area (st. 3071). This station was located in the central water mass at 17°S (Fig. 1C).

Lampanuctus intricarius Tåning, 1928

Distinguishing features Larvae of this species have a highly compressed body; the larvae <14 mm SL have dorsal and ventral finfolds. The larvae are characterized by the presence of a series of prominent melanophores along the margins of dorsal and ventral finfolds and by an intensely pigmented caudal region. Among all known species of *Lampanyctus* from the Pacific Ocean, no larvae have finfolds that are so prominent at the postflexion stage. Larvae of

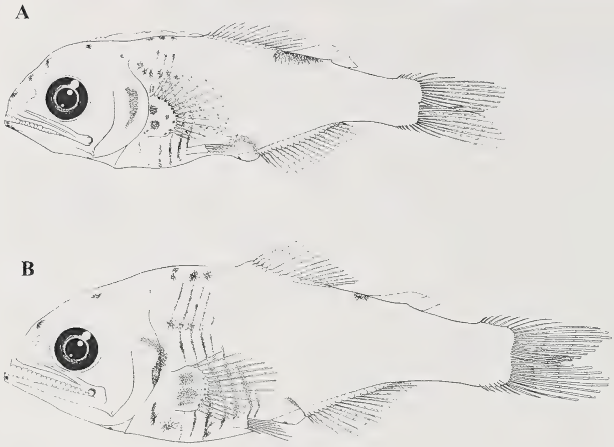

Figure 4

Illustrations of 2 early developmental stages of larval southern lanternfish (*Lampanyctus australis*) caught (**A**) during the 16th voyage of the RV *Dmitry Mendeleev* to the southwestern Pacific Ocean in 1976 at station 1335 (9.2 mm standard body length [SL]) and (**B**) during the 34th voyage of the RV *Dmitry Mendeleev* to the central South Pacific Ocean in 1985 at station 3054 (12.2 mm SL).

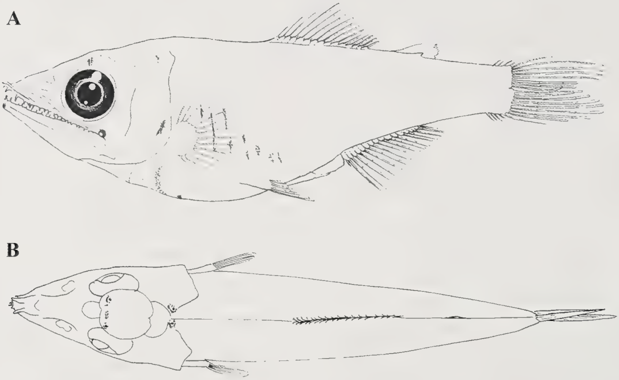

Figure 5

Illustration of one early developmental stage of larval *Lampanyctus gibbsi* or *L. wisneri*, based on a larva that could be one of those species, has a standard body length of 13.1 mm, and was caught in the central South Pacific Ocean in 1985 at station 3071.

L. intricarius are similar in pigmentation to larvae of *Lampanyctus* cf. *L. photonotus* (Moser and Watson, 2001) from the western Atlantic Ocean and differ from them in body proportions. Differences between larvae of *L intricarius* and of *Lampanyctus* cf. *L. photonotus* are found in body depth, head length, and diameter of the eye.

Morphology In our collections, 102 larvae with sizes of 6.9–20.4 mm SL were found. The larvae from the collections of the 34th expedition of RV *Dmitry Mendeleev* have been described in detail previously (Bolshakova and Evseenko, 2015).

Photophore formation All larvae 6.9–20.4 mm SL have only Br_2.

Pigmentation See Bolshakova and Evseenko (2015).

Meristic characters D: 15–16, A: 18–20, P_1: 13–14, P_2: 7–8, C: 6+10–9+6, GR: 4+1+(9)10, V: 38–39, BrR: 8.

Distribution Larvae of *L. intricarius* were collected at 9 stations (st. 3042, 3043, 3044, 3049, 3050, 3052, 3054, 3057, and 3068) between 37°S and 46°S in the notal zone and in the subtropical frontal zone of the South Pacific Ocean (Fig. 2A).

Lampanyctus sp. *D* (*sensu* McGinnis, 1982)

Distinguishing features The main feature of the larvae of this species is the almost complete absence of pigment on the body. Pigmentation is present in all larvae only in the head region above the brain and above the terminal gut section. A lack of or a small amount of pigment on the body is also noted for the larvae of *L. nobilis*, the slender lanternfish (*L. tenuiformis*), and *L. idostigma*. Larvae of *L. nobilis* have a row of melanophores on the istmus. Larvae of *L. tenuiformis* have one melanophore anterior to the anus and have a blunt snout. Larvae of *L. idostigma* have no melanophores above the brain.

Morphology In our collections, 110 larvae with sizes of 7.2–17.0 mm SL were found (Figs. 6 and 7). Larvae have relatively slender bodies (BD 24–29% SL) with large heads (HL 27–33% SL). Eyes are round and large (ED 24–34% HL) and decrease in proportion to body size during development. The jaws reach the vertical of the eye posterior margin in large larvae (SnL 26% HL), and there are teeth on both jaws. The dorsal fin originates near the middle of the body (PDL 47–56% SL). The anus opens behind the middle of the body (PAL 58–65% SL). Metamorphosis occurs at a size >17.0 mm SL.

Meristic characters D: 13–15, A: 16–17, P_1: 13–14, P_2: 8, C: 6+10–11+5, GR: 4(5)+1+10, V: 35–36, BrR: 8. All the rays in the fins are distinguishable in the 10.3-mm-SL larva, and the number of gill rakers is definitive in the 13.0-mm-SL larva.

Pigmentation The pigmentation of larvae varies considerably, even among larvae of the same size from the same sample. The pigmentation that is present in almost all studied larvae includes the following: inner melanophores

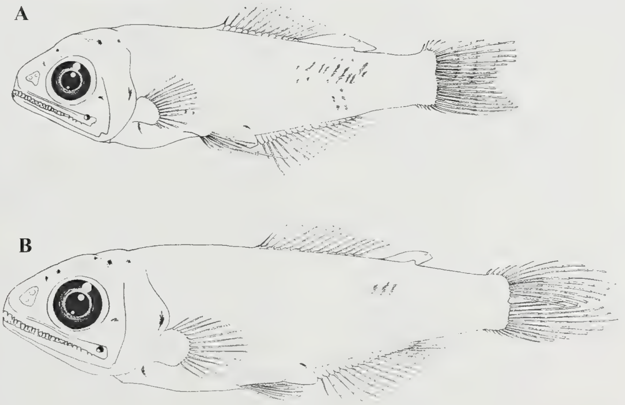

Figure 6

Illustrations of 2 early developmental stages of larval *Lampanyctus* sp. *D* caught in the central South Pacific Ocean in 1985 (**A**) at station 3042 (9.7 mm standard body length [SL]) and (**B**) at station 3049 (12.5 mm SL).

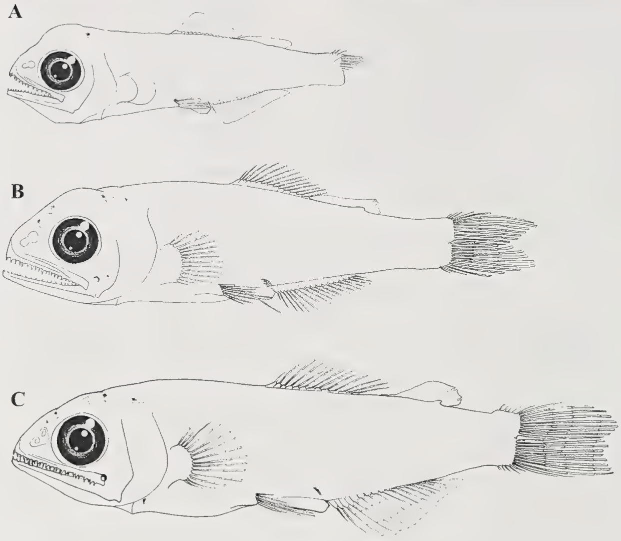

Figure 7

Illustrations of 3 early developmental stages of larval *Lampanyctus* sp. *D* caught in the central South Pacific Ocean in 1985 at station 3052: (**A**) 7.8 mm standard body length (SL), (**B**) 9.5 mm SL, and (**C**) 12.9 mm SL.

located dorsally in the intestine terminus and anterior at the liver, one unpaired melanophore anterior to the forebrain, paired melanophores between the forebrain and midbrain, one melanophore posterior to the midbrain, and one melanophore posterior to the hindbrain (Fig. 6). In addition, most larvae have 1 or 2 melanophores on the cleithrum at the level of the pectoral fin. In about half of all studied specimens, a single melanophore is visible on the inner side of the operculum at the level of the pectoral fin, and internal pigmentation occurs at the myosepta of the epaxial and hypaxial myomers in the middle part of the tail at the level of the adipose fin (Fig. 7). Less than a third of the larvae have melanophores on the tip of the lower jaw. Sometimes melanophores are present above the brain: 1 or 2 unpaired in the middle of the midbrain, on both sides or only on one side anterior to the hindbrain. The peritoneum is pigmented with large melanophores in all larvae; in some larvae, this pigment appears on the myosepta above the gut.

Photophore formation Br_2 are noticeable on the 9.5-mm-SL larva.

Comparative remarks Among the species inhabiting the study area, *L. macdonaldi*, *L. gibbsi*, and *L. wisneri* are the only species for which larvae are unknown. The meristic characters of the adults of these 3 species differ from the meristic features indicated for the larvae of *Lampanyctus* sp. *D* described here. *Lampanyctus* sp. *D* is 1 of 4 more species of *Lampanyctus* that McGinnis (1982) noted occur in the central South Pacific Ocean, with the other species being *Lampanyctus* sp. *A*, *Lampanyctus* sp. *B*, and *Lampanyctus* sp. *C*. *Lampanyctus* sp. *C* and *Lampanyctus* sp. *D* are characterized by a lower number of fin rays compared with the number for *Lampanyctus* sp. *A* and *Lampanyctus* sp. *B* (P: 14–15, D: 12–13, A: 16–18 versus P: 17, D: 14–16, A: 16–21) (Table 2). Meristic characters of *Lampanyctus* sp. *C* and *Lampanyctus* sp. *D* are similar to those described for the larvae examined in our study. Adults of these 2 species differ from each other in the relative position of unpaired fins and in the morphology of the supracaudal luminous gland; therefore, we will not be able to use these features to identify larvae examined in our study. However, McGinnis (1982) suggested that juveniles of *Lampanyctus* sp. *C* less than 30 mm SL are characterized by the presence of a large vertical band of pigment posterior to the pectoral fin. Among all the species of the southwestern Pacific Ocean whose larval development is already known, *L. australis* is the only species whose larvae have such pigmentation. Our larvae do not have such pigmentation at least up to a size of 17 mm SL; therefore, we suppose that they may belong to *Lampanyctus* sp. *D*. Adults of *Lampanyctus* sp. *D* have been found in the central South Pacific Ocean approximately between 40°S and 50°S (McGinnis, 1982), and larvae sampled between 38°S and 45°S were found in our collections.

Distribution Among the *Lampanyctus* species in the collections of the 34th expedition of the RV *Dmitry Mendeleev*, this species has the most abundant larvae. A total of 110 larvae were collected in the central South Pacific Ocean. Larvae of *Lampanyctus* sp. *D* were found at 7 stations (st. 3010, 3042, 3044, 3049, 3055, 3056, and 3057) in a narrow range between 38°S and 42°S in the subtropical frontal zone and the northern part of the notal zone in the South Pacific Ocean (Fig. 2B).

Lampanyctus pusillus (Johnson, 1890)

Distinguishing features Larvae of this species have a deep, stout body with a blunt snout. The larvae have characteristic pigmentation: the body is almost completely covered with melanophores, with a series of melanophores along the dorsum, a midlateral series on trunk and tail, and a series midventrally below the gut.

Morphology In our collections, 37 larvae with sizes of 6.8–13.0 mm SL were found. The morphology of the larvae examined in our study is significantly similar with the morphology that has been described earlier for larvae from the Atlantic Ocean (Tåning, 1918) and from the Indian Ocean (Olivar and Beckley, 1997).

Distribution Larvae of *L. pusillus* were collected at 5 stations (st. 3049, 3050, 3051, 3052, and 3069) between 34°S and 38°S in the periphery of the central water mass and in the subtropical frontal zone in the South Pacific Ocean (Fig. 2C).

Discussion

Larvae of at least 11 species of *Lampanyctus* have been found in the southwestern Pacific Ocean. These species are *L. achirus*, the winged lanternfish (*L. alatus*), *L. ater*, *L. australis*, the festive lanternfish (*L. festivus*), *L. gibbsi*, *L. intricarius*, the mermaid lanternfish (*L. lepidolychnus*), *L. macdonaldi*, *L. pusillus*, and *L. wisneri* (Wisner, 1976; Hulley, 1981; McGinnis, 1982; Becker, 1983; Zahuranec, 2000). Among these listed species, *L. macdonaldi* is the only species for which the early stages of development are unknown. The status of the larva that we identified as *L. gibbsi* or *L. wisneri* and the larvae of *L. lepidolychnus* (Olivar and Beckley, 1997) is not clear. *Lampanyctus lepidolychnus* is known to prefer coastal waters and has not been recorded in the southwestern Pacific Ocean east of 165°W. (Hulley, 1981; Becker and Evseenko, 1986), where all the larvae that we identified as *L. intricarius* were caught. At the same time, the larvae of *L. lepidolychnus* (Olivar and Beckley, 1997) and *L. intricarius* (Bolshakova and Evseenko, 2015) are similar. Adults of these 2 species differ mainly in the location of photophores, and they do not differ in meristic characters. For this reason, the species identification for larvae of *L. lepidolychnus* and *L. intricarius* is still questionable.

Although larvae of *L. lepidolychnus* and *L. intricarius* are similar, larvae of the 9 other species of *Lampanyctus* that occur in the southwestern Pacific Ocean differ well in pigmentation, body proportions and shape, morphological features (e.g., preopercular spines), length and shape of the rostrum, and time of metamorphosis. An additional factor for the identification of larvae of these species can be the region of capture. For example, *L. alatus* and *L. gibbsi* do not occur in the open waters of the southwestern Pacific Ocean south of 30°S (McGinnis, 1982; Zahuranec, 2000). The distribution of *L. achirus*, in contrast, extends as far north as 30°S, the latitude that corresponds with the southern border of the region of the Subtropical Convergence (a frontal zone between subantarctic and tropical water masses) in the Pacific Ocean. The distributions of *L. ater*, *L. australis*, *L. festivus*, *L. intricarius*, *L. lepidolychnus*, *L. macdonaldi*, and *L. pusillus* are associated with the Subtropical Convergence. In general, for the species found in the southwestern Pacific Ocean, the distribution of larvae coincides with the distribution of adults.

McGinnis (1982) noted the existence of 4 more species of *Lampanyctus* in the South Pacific Ocean: *Lampanyctus* sp. *A*, *Lampanyctus* sp. *B*, *Lampanyctus* sp. *C*, and *Lampanyctus* sp. *D*. *Lampanyctus* sp. *A* is closely related with *L. achirus*, and they have similar meristic features (Table 2). We did not find any significant differences among our larval specimens of *L. achirus* either in larval characters (i.e., pigmentation, body proportions, and formation rates for fin rays) or in the number of gill rakers of the first gill arch. *Lampanyctus* sp. *B*, in meristic features, is most similar to *L. festivus* and has high counts of pectoral-fin, dorsal-fin, and anal-fin rays (P: 17, D: 15, A: 21). *Lampanyctus* sp. *C* may be close to *L. australis* because the meristic characters of these species match; in addition, a vertical band of pigment posterior to the pectoral fin has been noted in juvenile *Lampanyctus* sp. *C*. The finding of larvae of *Lampanyctus* sp. *D* in the examination of our collections confirms the existence of an undescribed species of *Lampanyctus* in the central South Pacific Ocean.

Conclusions

Larval characters, together with the morphology of adults, may clarify the intergeneric relationships in the family Myctophidae. Comparison of the larval characters of representatives of the genus *Lampanyctus sensu lato* can confirm the possible paraphilia of this group (Denton, 2014; Martin et al., 2018). At the moment, the use of the larval characters in phylogenetic systematics are limited to a small number of species of *Lampanyctus sensu lato* for which detailed descriptions of larval stages are available (about half of them). We believe that the descriptions presented in this article will help clarify the taxonomic status of species within the genus *Lampanyctus sensu lato*.

Acknowledgments

The study was supported by the state assignment to the Shirshov Institute of Oceanology of the Russian Academy of Sciences (no. 0149-2019-0009) and financially supported by the Russian Science Foundation (no. 19-14-00026).

In memoriam

Sergei A. Evseenko was a world-renowned scientist, doctor of biological sciences, and head of the Laboratory of Oceanic Ichthyofauna of the Shirshov Institute of Oceanology, Russian Academy of Sciences. The main scientific interests of S. Evseenko included the taxonomy and ecology of the early stages of development of fish. He developed an ecological classification of flounder species, described for the first time the larvae of several dozen species of oceanic fish, and revealed the patterns of distribution of ichthyoplankton in the upwelling areas of the eastern Pacific Ocean and frontal zones of the World Ocean. He described several species and genera of marine fish. S. Evseenko described a new family of armless flounders of the Southern Ocean—the family Achiropsettidae—and clarified the morphology, anatomy, individual development, and evolution of this new family. In collaboration with N. Parin and E. Vasilyeva, he published a collective monograph, *Fish of the Russian Seas: Annotated Catalogue*. Overall, S. Evseenko published about 170 scientific works. On 15 October 2020, he died suddenly. S. Evseenko was working on this manuscript just before his death. Everyone who is fortunate enough to have known this wonderful person and outstanding scientist will keep a bright memory of him.

Literature cited

Becker, V. E.
1983. Myctophid fishes of the World Ocean, 248 p. Moscow, Russia. [In Russian.]
Becker, V. E., and S. A. Evseenko.
1986. Distribution of mesopelagic fishes and biogeographic boundaries in the southern part of the Pacific Ocean in January–February 1985. J. Ichthyol. 26:890–901. [In Russian.]
Bolshakova, Ya. Yu., and S. A. Evseenko.
2015. Larvae of the lanternfish *Lampanyctus intricarius* (Myctophidae) from the southwestern Pacific Ocean. J. Ichthyol. 55:596–600.
2016. On the species composition of ichthyoplankton of the Walvis Ridge (South Atlantic). J. Ichthyol. 56:848–860.
2020. Ichthyoplankton of the central North Atlantic Ocean: larval development of lanternfish species (Pisces: Myctophidae). Fish. Bull. 118:135–144.
Denton, J. S. S.
2014. Seven-locus molecular phylogeny of Myctophiformes (Teleostei; Scopelomorpha) highlights the utility of the order for studies of deep-sea evolution. Mol. Phylogenet. Evol. 76:270–292.
Fricke, R., W. N. Eschmeyer, and R. Van Der Laan (eds.).
2020. Eschmeyer's catalog of fishes: genera, species, references. [Available from website, accessed November 2020.]
Hulley, P. A.
1981. Results of the research cruises of FRV 'Walther Herwig' to South America: 58. Family Myctophidae (Osteichthyes, Myctophiformes). Archiv. Fischereiwiss. 31(1):1–303.
Kobyliansky, S. G.
2016. Anatomy of fishes of genus *Lampanyctus* (sensu lato), its taxonomic structure, and status in the Lampanyctini (Myctophidae) tribe system. J. Ichthyol. 56:181–199.
Martin, R. P., E. E. Olson, M. G. Girard, W. L. Smith, and M. P. Davis.
2018. Light in the darkness: new perspective on lanternfish relationships and classification using genomic and morphological data. Mol. Phylogenet. Evol. 121:71–85.
McGinnis, R. F.
1982. Biogeography of lanternfishes (Myctophidae) south of 30°S. Antarct. Res. Ser. 35, 110 p. Am. Geophys. Union, Washington D.C.
Miller, J. M., W. Watson, and J. M. Leis.
1979. An atlas of nearshore marine fish larvae of the Hawaiian Islands. Sea Grant Misc. Rep. UNIHI-Seagrant-MR-80-02, 179 p. Univ. Hawaii Sea Grant Coll. Prog., Honolulu, HI.
Moser, H. G., and E. H. Ahlstrom.
1974. Role of larval stages in systematic investigations of marine teleosts: the Myctophidae, a case study. Fish. Bull. 72:391–413.
1996. Myctophidae: lanternfishes. *In* The early stages of fishes in the California Current region (H. G. Moser, ed.), p. 387–475. CalCOFI Atlas 33.
Moser, H. G., and W. Watson.
2001. Preliminary guide to the identification of the early life history stages of Myctophiform fishes of the western central Atlantic. NOAA Tech. Memo. NMFS-SEFSC-453, 118 p.
Moser, H. G., E. H Ahlstrom, and J. R. Paxton.
1984. Myctophidae: development. *In* Ontogeny and systematics of fishes. Based on an international symposium dedicated to the memory of Elbert Halvor Ahlstrom; La Jolla, 15–18 August 1983 (H. G. Moser, W. J. Richards, D. M. Cohen, M. P. Fahay, A. W. Kendall Jr., and S. L. Richardson, eds.), p. 218–239. Am. Soc. Ichthyol. Herpetol., Spec. Publ. 1.
Olivar, M. P.
1985. Ictioplancton del Atlantico sudoriental. Ph.D. diss., 710 p. Univ. Barcelona, Barcelona, Spain. [Available from website.]
Olivar, M. P., and L. E. Beckley.
1997. Larval development of *Lampanyctus* species (Pisces: Myctophidae) from the southwestern Indian Ocean, and species groups based on larval characters. Bull. Mar. Sci. 60:47–65.
Pertseva-Ostroumova, T. A.
1918. Mediterranean Scopelidae (*Saurus*, *Aulopus*, *Cholorphthalmus*, and *Myctophum*). *In* Report of the Danish oceanographic expeditions 1908–1910 to the Mediterranean and adjacent seas, vol. 2 (Biol.) (A.7), 154 p. Høst, Copenhagen, Denmark.
1964. Some morphological characteristics of myctophid larvae (Myctophidae, Pisces). Tr. Inst. Okeanol. 73:76–92. [In Russian.]
Taylor, W. R., and G. C. Van Dyke.
1985. Revised procedures for staining and clearing small fishes and other vertebrates for bone and cartilage study. Cybium 9:107–119.
Wisner, R. L.
1976. The taxonomy and distribution of lanternfishes (family Myctophidae) of the eastern Pacific Ocean. NORDA Rep. 3, 229 p. Navy Ocean Res. Dev. Act., Bay St. Louis, MS.
Zahuranec, B. J.
2000. Zoogeography and systematics of the lanternfishes of the genus *Nannobrachium* (Myctophidae: Lampanyctini). Smithson. Contrib. Zool. 607, 69 p. [Available from website.]

National Marine
Fisheries Service
NOAA

Fishery Bulletin
established in 1881

Spencer F. Baird
First U.S. Commissioner
of Fisheries and founder
of *Fishery Bulletin*

Using DNA barcoding to improve taxonomic resolution of the diet of red snapper (*Lutjanus campechanus*) along the Atlantic coast of the southeastern United States

Kevin R. Spanik (contact author)[1,2]
Tracey I. Smart[1]
Marcel J. M. Reichert[1]
Tanya L. Darden[1]

Email address for contact author: spanikk@dnr.sc.gov

[1] South Carolina Department of Natural Resources
217 Fort Johnson Road
Charleston, South Carolina 29412

[2] Grice Marine Laboratory
College of Charleston
205 Fort Johnson Road
Charleston, South Carolina 29412

Abstract—Predator–prey interactions are a vital yet often under-studied regulator of marine fish population and community structure. However, fish prey species often cannot be identified by using morphological characters because of degradation from digestion. Consequently, diet is often poorly known for piscivorous predators. The study described here combined visual inspection and molecular diet analysis to increase taxonomic resolution for prey found in stomachs of red snapper (*Lutjanus campechanus*) (number of stomachs=105) along the Atlantic coast of the southeastern United States. Overall, the diet of red snapper from this region was diverse with 42 invertebrate and 28 vertebrate taxa identified. Broadly, shrimp were the most important prey consumed according to indices of relative importance (39.95%), followed by fish (34.38%) and crab (19.04%) species. In total, 19 fish prey species were identified by using DNA barcoding, compared with 2 species identified when visual methods alone were used. Results of the use of increased taxonomic resolution do not indicate significant predation by red snapper on other managed fish species in the snapper-grouper complex, indicating that the rebuilding stock of red snapper in the region is not affecting other managed species through direct predation.

The importance of predator–prey interactions on marine fish population and community dynamics has been recognized for decades (Sissenwine, 1984), yet it remains challenging to apply these interactions in fisheries management. Most of the world's stock assessment models focus on only the dynamics and fishing pressure of a single-species stock, but ecosystem processes significantly affect productivity of fisheries (Skern-Mauritzen et al., 2016). Multispecies population models and other ecosystem-based fisheries management approaches that consider ecological interactions have recently been implemented in several countries (Essington and Punt, 2011; Kruse et al., 2012). In the United States, for example, ecological reference points have been developed for fishery management plans for species off the Atlantic coast of the southeastern United States from North Carolina to Florida (SEDAR, 2020), and fishery management plans for species off the coasts of mid-Atlantic states from New York to North Carolina now aim to conserve vital prey resources for managed fish populations (MAFMC, 2017). Incorporation of ecological interactions in stock assessments and fishery management plans is appropriate for species in reef ecosystems off northwest Florida because many predators and their prey have high site fidelity, and high spatial overlap among multiple life stages of exploited species has been observed (Addis et al.[1]).

Diet studies are common and provide valuable ecological information on resource competition, habitat use, trophic structure, energy flow, and seasonal variability, all important factors for ecosystem-based fisheries management. Diet studies also provide estimates of natural mortality based on predation rates, and these estimates

Manuscript submitted 10 June 2020.
Manuscript accepted 29 June 2021.
Fish. Bull. 119:123–134 (2021).
Online publication date: 29 July 2021.
doi: 10.7755/FB.119.2-3.3

The views and opinions expressed or implied in this article are those of the author (or authors) and do not necessarily reflect the position of the National Marine Fisheries Service, NOAA.

---

[1] Addis, D. T., W. F. Patterson III, and M. A. Dance. 2012. Site fidelity and movement of reef fishes tagged at unreported artificial reef sites off NW Florida. Southeast Data, Assessment, and Review SEDAR31-RD33, 8 p. [Available from website.]

often exceed rates of fishing mortality (Tyrrell et al., 2011). Despite the importance of diet data to ecosystem modeling, collection and analysis of such data are fraught with challenges, and incorporation of diet data in fishery management plans and ecosystem-based fisheries management efforts has been limited.

One challenge is that prey found in stomachs can be difficult to identify because of loss of distinctive features from digestion and overlapping meristics among closely related taxa. For example, fish prey consumed by gag (*Mycteroperca microlepis*) can be 50–75% digested within 8 h of ingestion (Berens and Murie, 2008). Similarly, in other studies, species-level resolution for fish prey of red lionfish (*Pterois volitans*) (Harms and Appledoorn[2]) and gray snapper (*Lutjanus griseus*) (Longley and Hildebrand, 1941) could not be attained visually just 5 h after ingestion. Capture of predators immediately following predation is difficult; therefore, prey items are commonly in advanced stages of digestion upon examination. Calcified fish structures, such as otoliths, are less digestible than flesh and have been used to confirm species identification and even to infer prey size; however, otoliths of many species are difficult to discern, and small otoliths can be digested rapidly (Granadeiro and Silva, 2000).

For the reasons described in previous paragraphs, visual methods of diet analysis rarely provide complete taxonomic resolution and, as a result, are poor indicators of the species composition of the diets of piscivorous fish species. Poor taxonomic resolution of prey in stomachs of fish can obfuscate estimates of dietary specialization and overlap with concomitant species, which are known drivers of reef-fish community structure (Longenecker, 2007).

Results of recent studies indicate that taxonomic resolution in analysis of the diets of piscivorous predators can be improved significantly by using DNA barcoding that sequences the cytochrome oxidase I mitochondrial gene of prey items (Aguilar et al., 2017; Dahl et al., 2017). The main objective of our study was to improve resolution of diet composition for red snapper (*L. campechanus*), a commercially and recreationally valuable piscivorous predator along the Atlantic coast of the southeastern United States, by using DNA barcoding and visual methods of taxa identification. Until now, the diet of red snapper in this region has been poorly known. Although there have been similar studies in the Gulf of Mexico (e.g., Szedlmayer and Brewton, 2019), predator–prey interactions are known to be ecosystem-specific (Hanson and Chouinard, 2002) and often are not comparable across regions. Improving the resolution of diet composition for red snapper will elucidate potential effects of this species as a predator on other managed species and identify prey resources that could potentially limit population growth along the Atlantic coast of the southeastern United States.

Materials and methods

Collection of predator samples

During 2017 and 2018, samples of red snapper were collected through routine sampling of the Southeast Reef Fish Survey, a fishery-independent sampling program for which multiple organizations collaborate. The primary sampling gear used by the Southeast Reef Fish Survey during this collection period was a chevron trap (Smart et al.[3]), baited with Atlantic menhaden (*Brevoortia tyrannus*). Chevron traps were deployed for ~90 min during daylight hours in sets of 6 traps, at least 200 m apart along live bottom habitat. Samples for diet analysis were selected by using a size class (total weight: 0–2500 g, 2501–7500 g, or >7500 g) and a latitude (1° bins from 31°N to 34°N) in a stratified sampling design. The first 3 specimens in each combination of size class and latitude whose stomachs were not everted or visibly damaged and that contained prey items were retained from each trap. Similarly, additional samples were opportunistically collected with unstandardized hook-and-line gear.

Red snapper were weighed to the nearest gram and measured to the nearest millimeter in total length (TL), fork length, and standard length. Stomachs were excised at sea from the esophagus to the pyloric sphincter, individually labeled and bagged, and placed in a freezer (–20°C) to halt digestion.

Processing of stomach contents

Frozen stomachs were immersed in water to thaw uniformly. Once thawed, all contents from individual stomachs were removed, with care taken to avoid scraping cells from the stomach itself. For examination of stomach contents of all fish captured in chevron traps, Atlantic menhaden were regarded as bait and discarded. Prey items of known bait species found in stomachs of fish captured with hook-and-line gear were also discarded (usually squid species or round scad, *Decapterus punctatus*). The remaining stomach contents were examined under a dissecting microscope and identified to the lowest taxonomic level possible, counted, and weighed (by wet weight to 0.001 g) by using a Sartorius[4] CPA223S analytical balance (Sartorius AG, Goettingen, Germany). A digestion code was assigned to each fish prey item to qualitatively assess digestion level (Smith et al., 2005; Fig. 1). Invertebrate prey were identified on the basis of morphology only, and digestion level was not assessed.

---

[2] Harms, C. A., and R. S. Appeldoorn. 2013. Digestion rate analysis of fish prey items in lionfish (*Pterois volitans*). Poster presented at the 66th annual meeting of the Gulf and Caribbean Fisheries Institute; Corpus Christi, 4–8 November. Gulf Caribb. Fish. Inst., Marathon, FL.

[3] Smart, T. I., M. J. M. Reichert, J. C. Ballenger, W. J. Bubley, and D. M. Wyanski. 2015. Overview of sampling gears and standard protocols used by the Southeast Reef Fish Survey and its partners. Mar. Resour. Monit. Assess. Prect. Progr., MARAMP Tech. Rep. 2015-005, 14 p. [Available from website.]

[4] Mention of trade names or commercial companies is for identification purposes only and does not imply endorsement by the National Marine Fisheries Service, NOAA.

Molecular identification of fish prey

Muscle tissue from fish prey items that could not be morphologically identified to species level (digestion codes 2–3; Fig. 1) was retained for DNA barcoding. Tissue samples were rinsed with distilled water, preserved in a 2.5-mL vial containing 95% ethanol, and stored at −20°C. When possible, the most superficial layer was discarded to avoid contamination from the predator's stomach lining or other co-occurring prey items. Prey assigned a digestion code of 4 (Fig. 1) were not used for DNA barcoding because of predator contamination and low DNA yield in preliminary trials. Laboratory utensils were dipped in a 10% bleach solution and rinsed with distilled water between stomachs and between each prey item to prevent contamination. To isolate DNA, muscle tissue (~0.5 g) was blotted dry, placed in a microcentrifuge tube, and immersed in a 200-µL digestion solution, consisting of 145.5 µL nuclei lysis solution, 36.36 µL EDTA (0.5 M), 14.5 µL proteinase K (20 mg/mL), and 3.64 µL milli-Q water, and digested overnight at 55°C. The next morning, 180 mg of Promega Wizard SV lysis buffer (Promega Corp., Madison, WI) was added, and the sample was vortexed. Then DNA was isolated from the supernatant by using a Promega Wizard SV spin-column assembly according to the manufacturer's instructions.

A region of approximately 650 base pairs of the cytochrome oxidase I gene was amplified by using the universal fish primers Fish-F1 and Fish-R2 (Ward et al., 2005). A 25-µL polymerase chain reaction (PCR) volume consisted of 16.4 µL milli-Q water, 2.5 µL 1× 5PRIME HotMaster PCR Buffer (Qiagen Beverly Inc., Beverly, MA), 2.0 µL dNTPs, 2.0 µL $MgCl_2$, 0.3 µL each primer, 0.1 µL 5PRIME HotMaster *Taq* DNA polymerase (Qiagen Beverly Inc.), and 1.0 µL DNA template. The thermal cycler profile consisted of an initial denaturation at 94°C for 4 min, followed by 35 cycles of 94°C for 30 s, 54°C for 30 s, and 72°C for 1 min, and a final extension at 72°C for 10 min (modified procedure from Ward et al., 2005). Each PCR contained a positive and negative control.

Polymerase chain reaction products were subjected to electrophoresis on a 1.5% agarose gel stained with ethidium bromide and then examined under ultraviolet light. Products were purified by using Affymetrix ExoSAP-IT (Thermo Fisher Scientific Inc., Waltham, MA) following the manufacturer's protocol. Samples were sent to Eurofins Genomics (Louisville, KY) for bidirectional Sanger sequencing with the same primers mentioned previously. Bidirectional sequences were aligned by using Sequencher, vers. 5.4 (Gene Codes, Ann Arbor, MI) and trimmed by using default criteria. Trimmed sequences were compared to their chromatograms and edited accordingly. Edited sequences were queried within the GenBank database of the National Center for Biotechnology Information (available from website) by using the Basic Local Alignment Search Tool (Altschul et al., 1990). A species was assigned to a prey item when a query sequence (minimum 300 base pairs) and a known reference sequence shared ≥98% similarity. If a species-level identification could not be assigned by using GenBank, the sequence was submitted to the Barcode of Life Database (available from website). Our edited sequences were deposited into GenBank (accession numbers MT580050–MT580051, MT582543–MT582580).

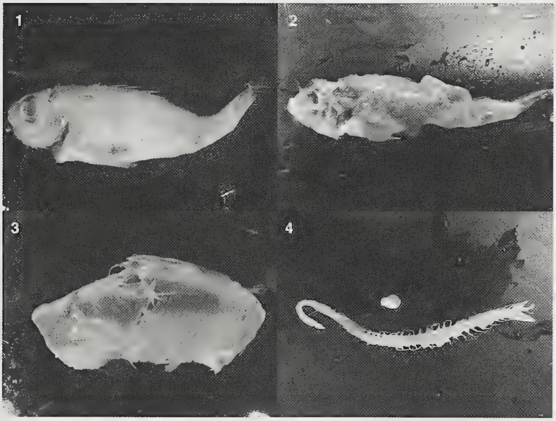

Figure 1

Images of prey items found in stomachs of red snapper (*Lutjanus campechanus*) collected along the Atlantic coast of the southeastern United States in 2017 and 2018, shown as examples of samples assigned to the 4 digestion codes used to qualitatively assess the condition of fish prey. The codes are (1) fresh, easy to identify visually; (2) partially digested: some skin or scales remain, many identifiable features remain; (3) mostly digested: most identifiable features absent, with some flesh attached to hard parts; and (4) severely digested: only hard parts (e.g., otoliths or vertebra) remain.

Data analysis

The relative contribution of prey items to the diet of red snapper examined in our study was described by using 3 traditional metrics: mean percentage by weight (%W), mean percentage by number (%N), and frequency of occurrence (%FO) (Hyslop, 1980). Because samples were collected over a large spatial and temporal range, %W and %N analyses were modified to account for the patchy distribution of marine predators and their prey in space and time (Buckel et al., 1999). In our study, a *cluster* represented a set of traps or group of hook-and-line deployments consisting of various anglers and tackle configurations at a single location (reef patch). Indices of relative importance (IRI) (Cortés, 1997) were also calculated for each individual prey item and for prey aggregated into 10 broader taxonomic categories: amphipods, bivalves, bony fish species, cephalopods, copepods, crabs, polychaetes, shrimps, stomatopods, and tunicates. Differences in diet among size classes (300–500 mm TL, 501–700 mm TL, and 701–900 mm TL) and depths of capture (0–30 m, 31–60 m, and >60 m) for red snapper were also explored by using IRI.

A species accumulation curve was generated to evaluate whether sampling intensity sufficiently characterized the diet of red snapper. A linear model was used to assess the slope of the line fit to data for the last 5 stomachs (with an asymptotic slope <0.05 indicating a saturated curve because no additional prey taxa are expected to be encountered with additional sampling; Bizzarro et al., 2009). Species richness was extrapolated by using a first-order jackknife estimator to predict the number of prey species that would completely characterize the diet (Heltshe and Forrester, 1983). The species accumulation curve and extrapolated species richness were computed in R, vers. 3.5.2 (R Core Team, 2018) by using the package vegan, vers. 2.5-2 (Oksanen et al., 2018).

Results

Red snapper (319–854 mm TL; Fig. 2) were collected throughout the sampling area of the Southeast Reef Fish Survey from 31°N to 34°N (Fig. 3) and from depths of 23–72 m. In total, 105 stomachs from red snapper were analyzed: 86 specimens of red snapper were collected by using chevron traps and 19 specimens were captured by using hook-and-line gear. Generally, fish prey items were digested well (Fig. 4) such that only ~13% were visually identifiable to at least the genus (digestion codes 1–2; Fig. 1), with the majority of fish prey items (~71%) assigned a digestion code of 3. A total of 65 fish prey items from 48 stomachs were designated as *unidentified fish* after visual examination. For the 53 prey items from 30 stomachs subjected to molecular identification, the PCR success rate was ~89%. For ~87% of these prey items, usable sequences (mean length: 540 base pairs) were produced. Most specimens for whom DNA analysis resulted in failed PCR and sequencing reactions were in a late stage of digestion (digestion code 3), and the failed reactions were likely due to low DNA yield as evidenced by faint bands on agarose gels or low peaks on chromatograms. All PCR controls performed as expected.

DNA barcoding allowed 32 fish prey items that could not be identified visually to be identified to the species level, 6 unidentified items to be identified to the genus level, and 2 items to be identified to the family level (Suppl. Table) (online only). Therefore, by using DNA barcoding, 62% of all unidentified fish prey items in our study could be identified to at least the family level, and 58% and 49% of all unidentified fish prey items could be identified to the genus and species levels, respectively. Compared with the use of visual identification methods, use of DNA barcoding reduced the amount of unidentified fish prey items in the overall diet, with amount measured both by %FO, which decreased from 45.71% to 24.76%, and by %W, which decreased from 18.75% to 9.78%. All prey identified to species shared >99% sequence similarity with reference sequences in either the GenBank or Barcode of Life Database, except for 2 items identified as Atlantic midshipman (*Porichthys plectrodon*), which shared 98% sequence similarity with a reference sequence in GenBank (accession number KF930305.1). Sequences from the 2 most closely related fish prey items that were genetically identified to the species level, both as species in the genus *Synodus*, were 19.3% dissimilar.

Several prey items could not be identified to species. Specimens of prey identified as *Ophidion* sp. were just below the a priori defined species identification threshold, with 97% similarity in GenBank to the bank cusk-eel

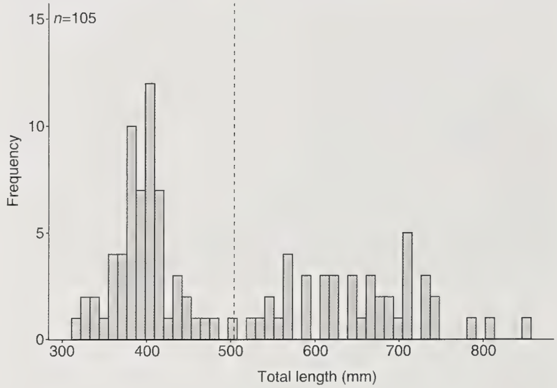

Figure 2

Size–frequency distribution of red snapper (*Lutjanus campechanus*) collected along the Atlantic coast of the southeastern United States in 2017 and 2018. The dashed line indicates the mean total length. *n*=sample size.

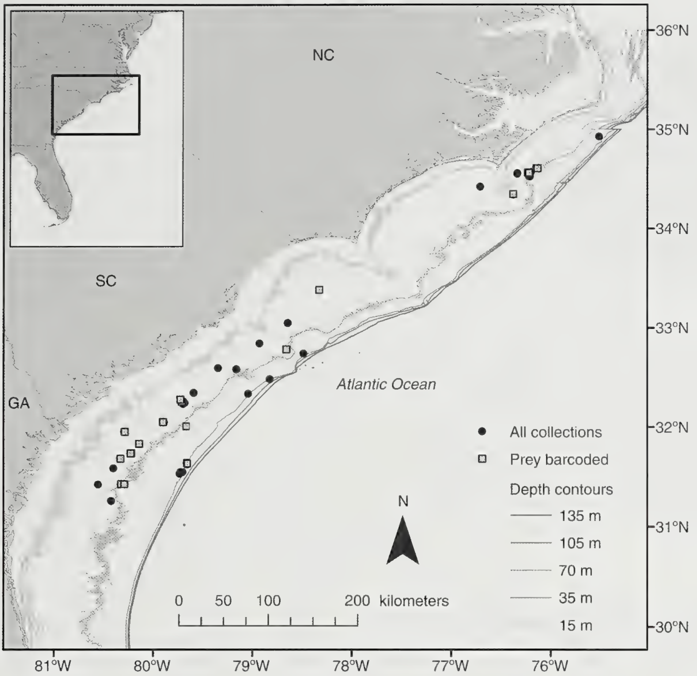

Figure 3

Map showing locations where red snapper (*Lutjanus campechanus*) were caught in 2017 and 2018 from Cape Hatteras, North Carolina (NC), to Saint Lucie, Florida. Black circles indicate capture locations for all red snapper collected. Gray squares indicate capture locations for red snapper from which prey items in stomach contents were sampled and identified with DNA barcoding. Depth contours are indicated by lines in various shades of gray. SC=South Carolina; GA=Georgia.

(*O. holbrookii*) (accession number GU702414.1). Ophidiidae is a paraphyletic family that has not been resolved well taxonomically. A neighbor-joining phylogeny generated in the Barcode of Life Database indicates that sequences from these specimens formed a monophyletic clade that includes bank cusk-eel and shorthead cusk-eel (*O. dromio*), both of which occur in the study area; therefore, we conservatively identified these specimens to genus. Specimens with sequences having top matches in GenBank to the scup (*Stenotomus chrysops*) (accession number HQ025017.1) or to the longspine porgy (*S. caprinus*) (accession number KJ012441.1) were identified conservatively as *Stenotomus* sp. because there is a difference of only one base pair (1%) between these reference sequences in GenBank and because both species occur within the study area.

Overall, the diet of red snapper captured along the Atlantic coast of the southeastern United States was diverse, with 42 invertebrate and 28 vertebrate taxa identified (Table 1). Generally, shrimp taxa composed the most important prey category consumed by red snapper in our study, on the basis of the IRI value (39.95%), followed by fish species (34.38%) and crab species (19.04%) (Fig. 5). More specifically, the most important prey taxa in the diet of red snapper, according to the IRI, were the brown rock shrimp (*Sicyonia brevirostris*), unidentified fish, portunid crabs, and the longspine swimming crab (*Achelous spinicarpus*), with IRI values of 32.58%, 28.85%, 7.14%, and 5.99%, respectively. Unidentified fish species composed the most dominant prey category by number (%N=12.97%) and occurred most frequently (%FO=24.76%), and the brown rock shrimp was the leading component of the diet by

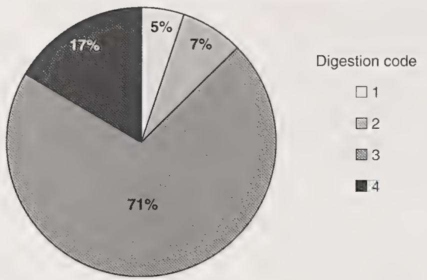

Figure 4

Proportion of fish prey found in stomachs of red snapper (*Lutjanus campechanus*) that were assigned to each of 4 digestion codes used to qualitatively assess the condition of fish prey. The codes are (1) fresh, easy to identify visually; (2) partially digested: some skin or scales remain, and many identifiable features remain; (3) mostly digested: most identifiable features absent, with flesh attached to vertebra; and (4) severely digested: only hard parts (e.g., otoliths or vertebra) remain. Red snapper were sampled along the Atlantic coast of the southeastern United States in 2017 and 2018.

weight (%W=21.25%). A total of 19 different species of fish were identified as prey. The most frequently consumed fish species were the bluespotted searobin (*Prionotus roseus*) (%FO=6.67%), snake eels (*Ophichthus* spp.) (%FO=3.81%), porgy species (*Stenotomus* spp.) (%FO=3.81%), the inshore lizardfish (*S. foetens*) (%FO=3.81%), and the tomtate (*Haemulon aurolineatum*) (%FO=2.86%).

Fish species formed the most important prey category, on the basis of IRI values across all size classes of red snapper, especially for the size classes of 300–500 mm TL (59.26%) and 701–900 mm TL (61.06%), in comparison with the size class of 501–700 mm TL (34.49%) (Fig. 6). Shrimp species composed a prey category that was more important in the diet of the size classes of 300–500 mm TL (IRI=30.14%) and 501–700 mm TL (IRI=28.85%) than in the diet of the size class of 701–900 mm TL (IRI=2.17%). Crab species were more important in the diet for the size classes of 501–700 mm TL (IRI=30.08%) and 701–900 mm TL (31.82%) than in the diet for the size class of 300–500 mm TL (IRI=8.08%). Fish species formed the most important prey category, according to the IRI, for red snapper captured at depths <30 m (74.12%) and at depths of 31–60 m (44.64%), but shrimp species were the dominate prey at depths >60 m (65.46%) (Fig. 7).

The slope of the fit of a linear model to data for the last 5 randomly sampled stomachs in the prey species accumulation curve was 0.32; therefore, the curve was not considered to reach an asymptote (Fig. 8). According to the first-order jackknife estimator, approximately 107 different prey species would be expected to have been identified, indicating that we taxonomically described ~64% of the diet of red snapper along the Atlantic coast of the southeastern United States.

Discussion

In our study, we used DNA barcoding to supplement visual identification of prey items to improve taxonomic resolution of the diet composition of red snapper along the Atlantic coast of the southeastern United States. We were able to identify a total of 19 fish prey species, using DNA barcoding. If we had relied on visual methods alone, we would have identified only 2 species and described only 10% of the total species richness of fish prey. Currently, the fishery management plan for the snapper-grouper complex in the Atlantic Ocean off the southeastern United States manages only 3 of these 19 species: the vermilion snapper (*Rhomboplites aurorubens*), the red porgy (*Pagrus pagrus*), and *Stenotomus* sp. The %W for both vermilion snapper and red porgy was <1% and for *Stenotomus* sp. was <6% in the diet of red snapper from the region in our study (Table 1).

Our findings agree with results of DNA barcoding studies done in the Gulf of Mexico that found negligible feeding on vermilion snapper (%W=1.01%), red porgy (%W=0.00%), and *Stenotomus* sp. (%W=1.31%) (Tarnecki and Patterson, 2015; Szedlmayer and Brewton, 2019). Further, feeding behavior related to ontogeny (i.e., size) of red snapper in our study was similar to observations of the diet of red snapper in the Gulf of Mexico, including that the largest fish consumed primarily fish and crab species (Wells et al., 2008). In other diet studies for red snapper in the Gulf of Mexico (McCawley and Cowan, 2007; Tarnecki and Patterson, 2015) significant consumption (>20%) of zooplankton, especially by larger fish, was observed. Such a level of consumption was not evident in our study, possibly because of under-representation of larger individuals in our study, seasonal abundance of zooplankton that did not coincide with the timing of our sampling, or other differences between ecosystems.

In our study, sequences sampled from most prey assigned to a species were >99% similar to reference sequences, exceeding the a priori sequence similarity threshold of 98% for species-level resolution. Given that Ward et al. (2005) reported average interspecific distances of 9.93% for marine fish species within the same genus and that sequences from the 2 most closely related species found in our study (both in the genus *Synodus*) were >19% dissimilar, we are confident that the 98% threshold for assigning a species in our study was appropriate and conservative for the goal of limiting false-positive species identifications. The inability to genetically distinguish between specimens in the genera *Ophidion* and *Stenotomus* in our study may be attributable to incomplete taxonomic coverage in the reference databases or to misidentification of the voucher specimens from which these reference sequences were generated (Stavrou et al., 2018).

The species accumulation curve did not achieve saturation, indicating that sampling intensity in our study

Table 1

Diet composition for red snapper (*Lutjanus campechanus*) sampled along the Atlantic coast of the southeastern United States in 2017 and 2018, based on analysis of stomach contents. For prey found in stomachs, frequency of occurrence (%FO), mean percentage by number (%N), mean percentage by weight (%W), and index of relative importance (IRI) values are provided. Taxa of prey items were identified by using visual and molecular methods combined. An asterisk (*) denotes species identifications determined by using DNA barcoding only. Prey items that could not be identified to species are designated as unidentified (unid.) members of families or other taxa.

Phylum, class or other taxa	Scientific name	Common name	%FO	%N	%W	IRI (%)
Polychaeta						
	Amphinomidae	Unid. bristle worm	2.86	0.96	0.11	0.16
	Spionidae	Unid. spionid polychaete	0.95	0.18	0.00	0.01
	Polychaeta	Unid. polychaete	0.95	0.31	0.02	0.02
Mollusca						
	Pectinidae	Unid. scallop	0.95	0.14	0.00	0.01
	Tellinidae	Unid. tellin clam	1.90	0.31	0.01	0.03
Cephalopoda						
	Illex sp.	Unid. shortfin squid	0.95	1.35	1.35	0.13
	Loligo sp.	Unid. longfin squid	0.95	0.45	1.08	0.08
	Teuthida	Unid. squid	8.57	2.81	2.75	2.46
	Octopus sp.	Unid. octopus	0.95	0.18	0.88	0.05
	Octopoda	Unid. octopus	1.90	0.76	0.20	0.09
Copepoda						
	Calanoida	Unid. calanoid copepod	1.90	1.80	0.00	0.18
Stomatopoda						
	Squillidae	Unid. mantis shrimp	5.71	2.58	3.50	1.79
Amphipoda						
	Ampeliscidae	Unid. red-eyed amphipod	0.95	0.16	0.00	0.01
	Hyperiidea	Unid. hyperiid amphipod	0.95	1.80	0.00	0.09
Decapoda						
	Leptochela papulata	Light glass shrimp	5.71	5.24	0.43	1.67
	Mesopenaeus tropicalis	Salmon shrimp	1.90	0.86	0.62	0.15
	Penaeoidea	Unid. penaeoid shrimp	9.52	3.59	1.00	2.25
	Rimapenaeus constrictus	Roughneck shrimp	2.86	1.16	0.34	0.22
	Sicyonia brevirostris	Brown rock shrimp	21.90	7.58	21.25	32.58
	Sicyonia sp.	Unid. rock shrimp	9.52	2.61	3.18	2.84
	Sicyoniidae	Unid. rock shrimp	0.95	0.31	0.02	0.02
	Solenoceridae	Solenocerid shrimp	0.95	2.76	1.53	0.21
	Stomatopoda	Unid. mantis shrimp	3.81	0.51	0.02	0.10
	Decapoda	Unid. shrimp	0.95	0.12	0.01	0.01
	Achelous ordwayi	Redhair swimming crab	4.76	2.39	2.59	1.23
	Achelous spinicarpus	Longspine swimming crab	14.29	5.02	3.11	5.99
	Achelous sp.	Swimming crab	2.86	1.84	1.45	0.48
	Portunidae	Unid. swimming crab	11.43	6.77	5.33	7.14
	Albunea catherinae	Mole crab	0.95	0.08	0.46	0.03
	Calappa flammea	Flame box crab	3.81	3.03	4.44	1.47
	Ethusa mascarone	Stalkeye sumo crab	0.95	0.12	0.03	0.01
	Hepatus epheliticus	Calico box crab	1.90	0.29	0.60	0.09
	Hepatus pudibundus	Flecked box crab	0.95	0.14	0.19	0.02
	Inachinae	Unid. spider crab	0.95	0.58	0.33	0.04
	Ovalipes stephensoni	Coarsehand lady crab	4.76	1.67	3.83	1.35
	Ovalipes sp.	Unid. lady crab	3.81	2.62	2.64	1.03
	Pilumnus sp.	Unid. hairy crap	0.95	0.14	0.08	0.01
	Pinnixa sp.	Unid. pea crab	0.95	0.31	0.02	0.02
	Ranilia muricata	Muricate frog crab	0.95	0.14	0.41	0.03
	Raninidae	Unid. frog crab	0.95	0.12	0.01	0.01
	Brachyura	Unid. true crab	1.90	0.99	0.04	0.10

(*Continued on next page*)

Table 1 (*continued*)

Phylum, class or other taxa	Scientific name	Common name	%FO	%N	%W	IRI (%)
Urochordata						
	Urochordata	Unid. tunicate	3.81	1.49	5.76	1.43
Pisces						
	Actinopterygii	Unid. ray-finned fish	24.76	12.97	9.78	28.85
	Anguilliformes	Unid. eel	0.95	0.45	0.27	0.04
	*Ariosoma balearicum**	Bandtooth conger	1.90	1.43	2.80	0.42
	*Conger oceanicus**	Conger eel	0.95	0.12	0.02	0.01
	Ophichthidae	Unid. snake eel	1.90	0.84	0.97	0.18
	*Echiophis intertinctus**	Spotted spoon-nose eel	0.95	0.31	0.52	0.04
	*Ophichthus puncticeps**	Palespotted eel	0.95	0.31	0.72	0.05
	*Saurida brasiliensis**	Largescale lizardfish	0.95	0.12	0.06	0.01
	*Synodus foetens**	Inshore lizardfish	3.81	3.02	0.19	0.63
	*Synodus poeyi**	Offshore lizardfish	0.95	0.16	0.14	0.01
	*Bregmaceros cantori**	Striped codlet	1.90	0.25	0.06	0.03
	Ophidion sp.*	Unid. cusk-eel	3.81	2.02	1.57	0.71
	*Porichthys plectrodon**	Atlantic midshipman	0.95	0.90	1.27	0.11
	Carangidae	Unid. jack	0.95	0.68	0.58	0.06
	Decapterus punctatus	Round scad	0.95	1.35	1.35	0.13
	*Citharichthys macrops**	Spotted whiff	0.95	0.18	0.00	0.01
	*Syacium papillosum**	Dusky flounder	0.95	0.14	0.15	0.01
	*Halichoeres caudalis**	Painted wrasse	0.95	0.45	0.50	0.05
	Haemulidae	Unid. grunt	0.95	0.68	1.23	0.09
	*Haemulon aurolineatum**	Tomtate	2.86	0.58	0.30	0.13
	Rhomboplites aurorubens	Vermilion snapper	0.95	0.68	0.77	0.07
	*Pagrus pagrus**	Red porgy	0.95	0.31	0.01	0.02
	Stenotomus sp.	Unid. porgy	3.81	3.28	5.96	1.82
	*Sphoeroides dorsalis**	Marbled puffer	0.95	0.58	0.08	0.03
	*Serraniculus pumilio**	Pygmy sea bass	0.95	0.31	0.22	0.03
	*Prionotus roseus**	Bluespotted searobin	6.67	1.62	0.84	0.85

may have been inadequate to completely characterize the diet of red snapper. However, because red snapper had a broad range of sizes, because the samples were collected from a large area in a range of depths, and because the species richness of the prey found in stomachs of the sampled red snapper was close to the predicted prey species richness, we are confident that the most important prey were accurately characterized. Further, the species accumulation curves used in investigations of the diets of marine fish species unlikely approach asymptote when a species-level taxonomic resolution is used for generalist predators (Preti et al., 2012). Therefore, only rare prey, which are likely opportunistically or inadvertently consumed and not considered significant diet components (Byron and Link, 2010), may be absent from this diet description. Red snapper persistently fed on few prey taxa, such as fish, portunid crab, and sicyoniid rock shrimp species, while sporadically feeding on a variety of other prey found over both reef and open sand habitats in our study, a result that is consistent with findings from a study in the Gulf of Mexico (Szedlmayer and Lee, 2004). The generalist use of resources by red snapper and our increased ability to identify prey items to the species level by using DNA barcoding likely explain the unsaturated species accumulation curve in our study.

We did not find evidence of significant predation by red snapper on other fish species managed as part of the snapper-grouper complex along the Atlantic coast of the southeastern United States, indicating that the rebuilding stock of red snapper in this region is not affecting other managed species through direct top-down control. However, competitive interactions have been identified as a major source of density-dependent mortality in marine systems (Hixon and Jones, 2005), and results from a seminal study (Pope, 1979) indicate that competitive interactions can have greater influence than direct predation on maximum sustainable yield in marine systems. Furthermore, competitive interactions may inhibit recovery of depleted stocks of marine fish species by limiting energy-rich prey necessary for reproductive success, even after fishing pressure is drastically reduced (Lambert and Dutil, 2000). Because of their broad diet, red snapper could be competing with other species. Therefore, additional studies on predator–prey interactions

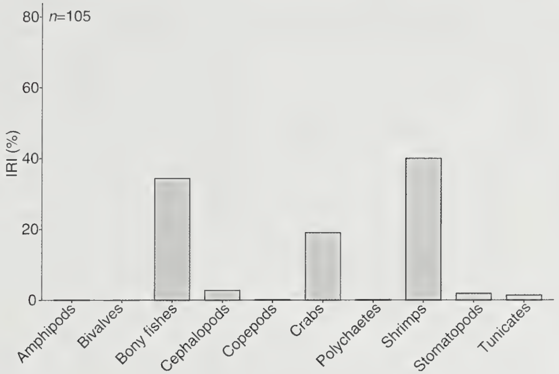

Figure 5

Generalized diet composition by prey category, according to index of relative importance (IRI) values based on examination of stomach contents of red snapper (*Lutjanus campechanus*) caught along the Atlantic coast of the southeastern United States in 2017 and 2018. Prey items were identified by using a combination of visual and DNA barcoding methods. *n*=number of stomachs analyzed.

of co-occurring predators within this ecosystem are necessary to elucidate competitive interactions between red snapper and other managed species in the region. Forage fish species, such as mackerel and anchovy species, that are extensively preyed upon by other fish species have recently been recognized as important ecosystem components and have been included in fishery management plans in the region and in bordering states (MAFMC, 2017; Federal Register, 2021). In our study, however, no specific prey emerged as strong candidates for management as potential bottom-up control mechanisms of population growth for red snapper in the region.

Conclusions

Our study addressed the critical need for detailed trophic information necessary to assess specific ecological effects of a rebuilding red snapper population along

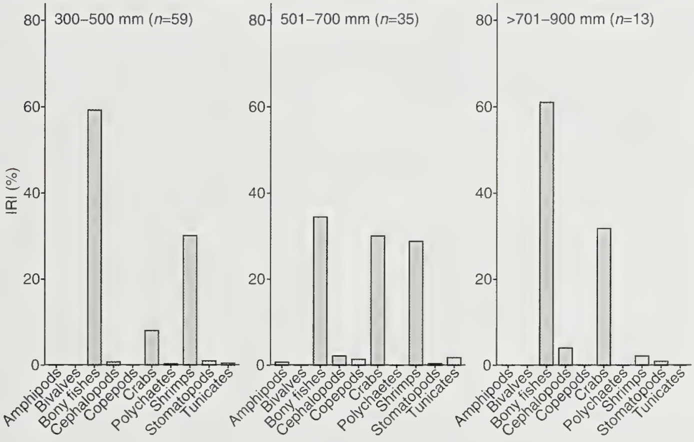

Figure 6

Generalized diet composition by size class and prey category, according to index of relative importance (IRI) values based on examination of stomach contents of red snapper (*Lutjanus campechanus*) caught along the Atlantic coast of the southeastern United States in 2017 and 2018. Prey items were identified by using a combination of visual and DNA barcoding methods. The size classes of red snapper are 300–500 mm in total length (TL), 501–700 mm TL, and 701–900 mm TL. *n*=number of stomachs analyzed.

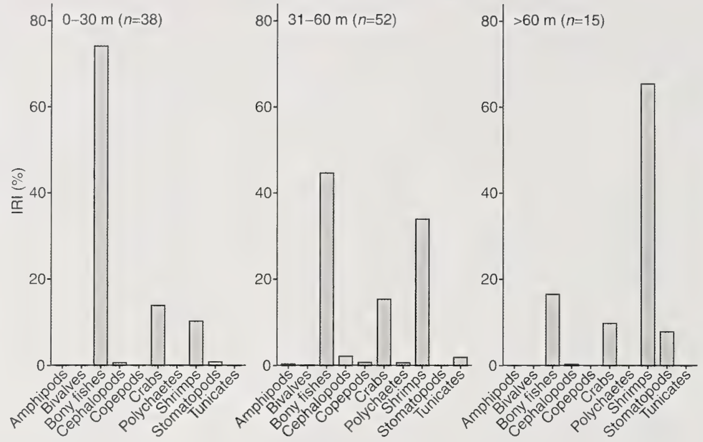

Figure 7

Generalized diet composition by depth and prey categories, according to index of relative importance (IRI) values based on examination of stomach contents of red snapper (*Lutjanus campechanus*) caught along the Atlantic coast of the southeastern United States in 2017 and 2018. Prey items were identified by using a combination of visual and DNA barcoding methods. The categories for depths at which red snapper were captured are 0–30 m, 31–60 m, and >60 m. *n*=number of stomachs analyzed.

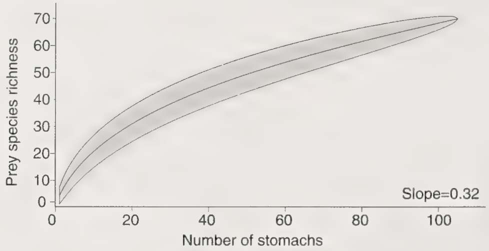

Figure 8

Species accumulation curve for prey found in stomachs of red snapper (*Lutjanus campechanus*) caught along the Atlantic coast of the southeastern United States in 2017 and 2018. Prey were identified by using a combination of visual and DNA barcoding methods. The shaded polygon represents the 95% confidence interval. The slope of a linear regression fit to data in the curve for the final 5 randomly sampled stomachs is given.

the Atlantic coast of the southeastern United States. Here, we provide results indicating that red snapper in this region are generalist predators that consume a wide range of invertebrate and vertebrate prey. Because the red snapper is a generalist predator, no individual prey species emerged as a resource that could potentially limit population growth and therefore merit management concern. Only minimal predation on other species of management concern was observed. Although we believe that the most significant prey of red snapper were documented in our study, additional sampling should be continued to further characterize the composition of prey species. Additional studies on spatial and temporal variability in the diet of red snapper and other co-occurring species would also significantly benefit the advancement of ecosystem-based fisheries management for the snapper-grouper complex in the region.

Acknowledgments

We thank K. Kanapeckas, M. Walker, and T. O'Donnell of the South Carolina Department of Natural Resources Population Genetics Lab and K. Hill-Spanik of the Molecular Core Facility at the College of Charleston for lab and data analysis assistance. Thanks to G. Sancho for input and support. Funding was provided by the Slocum-Lunz Foundation and Southeast Area Monitoring and Assessment Program South-Atlantic. This work is contribution number 824 of the South Carolina Department of

Natural Resources Marine Resources Division and contribution number 546 of the College of Charleston Grice Marine Laboratory.

Literature cited

Aguilar, R., M. B. Ogburn, A. C. Driskell, L. A. Weigt, M. C. Groves, and A. H. Hines.
2017. Gutsy genetics: identification of digested piscine prey items in the stomach contents of sympatric native and introduced warmwater catfishes via DNA barcoding. Environ. Biol. Fishes 100:325–336.

Altschul, S. F., W. Gish, W. Miller, E. W. Myers, and D. J. Lipman.
1990. Basic local alignment search tool. J. Mol. Biol. 215:403–410.

Berens, E. J., and D. J. Murie.
2008. Differential digestion and evacuation rates of prey in a warm-temperate grouper, gag *Mycteroperca microlepis*. J. Fish Biol. 72:1406–1426.

Bizzarro, J. J., W. D. Smith, J. L. Castillo-Géniz, A. Ocampo-Torres, J. F. Márquez-Farías, and R. E. Hueter.
2009. The seasonal importance of small coastal sharks and rays in the artisanal elasmobranch fishery of Sinaloa, Mexico. Pan-Am. J. Aquat. Sci. 4:513–531.

Buckel, J. A., D. O. Conover, N. D. Steinberg, and K. A. McKown.
1999. Impact of age-0 bluefish (*Pomatomus saltatrix*) predation on age-0 fishes in the Hudson River estuary: evidence for density-dependent loss of juvenile striped bass (*Morone saxatilis*). Can. J. Fish. Aquat. Sci. 56:275–287.

Byron, C. J., and J. S. Link.
2010. Stability in the feeding ecology of four demersal fish predators in the US Northeast shelf large marine ecosystem. Mar. Ecol. Prog. Ser. 406:239–250.

Cortés, E.
1997. A critical review of methods of studying fish feeding based on analysis of stomach contents: application to elasmobranch fishes. Can. J. Fish. Aquat. Sci. 54:726–738.

Dahl, K. A., W. F. Patterson, A. Robertson, and A. C. Ortmann.
2017. DNA barcoding significantly improves resolution of invasive lionfish diet in the Northern Gulf of Mexico. Biol. Invasions 19:1917–1933.

Essington, T. E., and A. E. Punt.
2011. Implementing ecosystem-based fisheries management: advantages, challenges and emerging tools. Fish Fish. 12:123–124.

Federal Register.
2021. Fisheries of the Caribbean, Gulf of Mexico, and South Atlantic; dolphin and wahoo fishery of the Atlantic; Amendment 12. Fed. Regist. 86:24742–24745. [Available from website.]

Granadeiro, J. P., and M. A. Silva.
2000. The use of otoliths and vertebrae in the identification and size-estimation of fish in predator-prey studies. Cybium 24:383–393.

Hanson, J. M., and G. A. Chouinard.
2002. Diet of Atlantic cod in the system of Gulf of St Lawrence as an index of ecosystem change, 1959–2000. J. Fish Biol. 60:902–922.

Heltshe, J. F., and N. E. Forrester.
1983. Estimating species richness using the jackknife procedure. Biometrics 39:1–11.

Hixon, M. A., and G. P. Jones.
2005. Competition, predation, and density-dependent mortality in demersal marine fishes. Ecology 86:2847–2859.

Hyslop, E. J.
1980. Stomach content analysis—a review of methods and their application. J. Fish Biol. 17:411–429.

Kruse, G. H., H. I. Browman, K. L. Cochrane, D. Evans, G. S. Jamieson, P. A. Livingston, D. Woodby, and C. I. Zhang (eds.).
2012. Global progress in ecosystem-based fisheries management. Alaska Sea Grant Coll. Prog. AK-SG-12-01, 396 p. Univ. Alaska Fairbanks, Fairbanks, AK.

Lambert, Y., and J.-D. Dutil.
2000. Energetic consequences of reproduction in Atlantic cod (*Gadus morhua*) in relation to spawning level of somatic energy reserves. Can. J. Fish. Aquat. Sci. 57:815–825.

Longenecker, K.
2007. Devil in the details: high-resolution dietary analysis contradicts a basic assumption of reef-fish diversity models. Copeia 2007:543–555.

Longley, W. H., and S. F. Hildebrand.
1941. Systematic catalogue of the fishes of Tortugas, Florida, with observations on color, habitat, and local distribution. Carnegie Inst. Wash. Publ. 535, 331 p. Carnegie Inst. Wash., Washington, DC.

MAFMC (Mid-Atlantic Fisheries Management Council).
2017. Unmanaged forage omnibus amendment, 222 p. Mid-Atl. Fish. Manage. Counc., Dover, DE. [Available from website.]

McCawley, J. R., and J. H. Cowan Jr.
2007. Seasonal and size specific diet and prey demand of red snapper on Alabama artificial reefs. Am. Fish. Soc. Symp. 60:77–104.

Oksanen, J., F. G. Blanchet, M. Friendly, R. Kindt, P. Legendre, D. McGlinn, P. R. Minchin, R. B. O'Hara, G. L. Simpson, P. Solymos, et al.
2018. vegan: community ecology package. R package, vers. 2.5-2. [Available from website, accessed December 2018.]

Pope, J. G.
1979. Stock assessment in multispecies fisheries, with special reference to the trawl fishery in the Gulf of Thailand. South China Sea Fish. Dev. Coord. Prog. SCS/DEV/79/19, 106 p.

Preti, A., C. U. Soykan, H. Dewar, R. J. D. Wells, N. Spear, and S. Kohin.
2012. Comparative feeding ecology of shortfin mako, blue and thresher sharks in the California Current. Environ. Biol. Fishes 95:127–146.

R Core Team.
2018. R: a language and environment for statistical computing. R Foundation for Statistical Computing, Vienna, Austria. [Available from website, accessed December 2018.]

SEDAR (Southeast Data, Assessment, and Review).
2020. SEDAR 69—Atlantic menhaden ecological reference points stock assessment report, 560 p. SEDAR, North Charleston, SC. [Available from website.]

Sissenwine, M. P.
1984. Why do fish populations vary? *In* Exploitation of marine communities. Dahlem Workshop Report, vol. 32 (R. M. May, ed.), p. 59–94. Springer, Berlin, Germany.

Skern-Mauritzen, M., G. Ottersen, N. O. Handegard, G. Huse, G. E. Dingsør, N. C. Stenseth, and O. S. Kjesbu.
2016. Ecosystem processes are rarely included in tactical fisheries management. Fish Fish. 17:165–175.

Smith, P. J., S. M. McVeagh, V. Allain, and C. Sanchez.
2005. DNA identification of gut contents of large pelagic fishes. J. Fish Biol. 67:1178–1183.

Stavrou, A. A., V. Mixão, T. Boekhout, and T. Gabaldón.
2018. Misidentification of genome assemblies in public databases: the case of *Naumovozyma dairenensis* and proposal of a protocol to correct misidentifications. Yeast 35:425–429.

Szedlmayer, S. T., and J. D. Lee.
2004. Diet shifts of juvenile red snapper (*Lutjanus campechanus*) with changes in habitat and fish size. Fish. Bull. 102:366–375.

Szedlmayer, S. T., and R. A. Brewton.
2019. Diet analyses of red snapper, *Lutjanus campechanus*, based on DNA barcoding from artificial reefs in the northern Gulf of Mexico. *In* Red snapper biology in a changing world (S. T. Szedlmayer and S. A. Bortone, eds.), p. 143–165. CRC Press, Boca Raton, FL.

Tarnecki, J. H., and W. F. Patterson III.
2015. Changes in red snapper diet and trophic ecology following the Deepwater Horizon oil spill. Mar. Coast. Fish. 7:135–147.

Tyrrell, M. C., J. S. Link, and H. Moustahfid.
2011. The importance of including predation in fish population models: implications for biological reference points. Fish. Res. 108:1–8.

Ward, R. D., T. S. Zemlak, B. H. Innes, P. R. Last, and P. D. N. Hebert.
2005. DNA barcoding Australia's fish species. Phil. Trans. R. Soc., B 360:1847–1857.

Wells, R. J. D., J. H. Cowan Jr., and B. Fry.
2008. Feeding ecology of red snapper *Lutjanus campechanus* in the northern Gulf of Mexico. Mar. Ecol. Prog. Ser. 361:213–225.

National Marine
Fisheries Service
NOAA

Fishery Bulletin
established in 1881

Spencer F. Baird
First U.S. Commissioner
of Fisheries and founder
of *Fishery Bulletin*

Using otolith chronologies to identify extrinsic drivers of growth of 2 commercially targeted small pelagic fish species

Joshua D. Dennis (contact author)[1]
Gretchen Grammer[2,3]
Tim Ward[2]
Jonathan Smart[2,3]
Charlie Huveneers[1]

Email address for contact author: josh.dennis@flinders.edu.au

[1] College of Science and Engineering
Flinders University
GPO Box 2100
Adelaide, South Australia 5100, Australia

[2] Aquatic Sciences Research Division
South Australian Research and Development Institute
P.O. Box 120
Henley Beach, South Australia 5022, Australia

[3] School of Biological Sciences
The University of Adelaide
Adelaide, South Australia 5005, Australia

Abstract—Climate variability is a major cause of changes in marine ecosystems, including changes in both the environment and in many fish species. Understanding the factors influencing key biological characteristics, such as growth, is important for commercially targeted species because these characteristics are used in stock assessments that inform fisheries management. In this study, otoliths were used to examine the growth rates and growth chronologies of 2 commercially targeted small pelagic fish species, the common jack mackerel (*Trachurus declivis*) and redbait (*Emmelichthys nitidus*), from 2 regions of southeastern Australia. Both species grew larger off Kangaroo Island (common jack mackerel: asymptotic length [L_∞]=299.40; redbait: L_∞=259.79) than off southern New South Wales (common jack mackerel: L_∞=249.52; redbait: L_∞=238.89). Temporal growth synchrony in both species and regions (0.17–3.50%) was low compared with that of more-site-attached benthic species. Interannual variations in growth rates of common jack mackerel off Kangaroo Island were positively correlated with sea-surface temperature (SST), with growth rates 18% higher at 18.0°C than at 16.4°C. However, growth was not correlated with SST or chlorophyll-*a* concentration for the other species and locations. Developing a more complete understanding of the environmental drivers of growth in these small pelagic fish species may require chronologies to be extended and extrinsic variables in the models to be increased.

Manuscript submitted 28 October 2020.
Manuscript accepted 8 July 2021.
Fish. Bull. 119:135–148 (2021).
Online publication date: 4 August 2021.
doi: 10.7755/FB.119.2-3.4

The views and opinions expressed or implied in this article are those of the author (or authors) and do not necessarily reflect the position of the National Marine Fisheries Service, NOAA.

Small pelagic fish species are a diverse group of marine species that form large, mobile epipelagic schools and constitute the majority of the vertebrate biomasses in most open-water ecosystems (Agenbag et al., 2003; Fréon et al., 2005). They form a pivotal link between upper and lower trophic levels, facilitating energy transfer from plankton to predators, such as marine mammals, seabirds, and large fish species (Essington et al., 2015). Disruption or alteration of this link can have broad effects on marine ecosystems (Essington et al., 2015). Small pelagic fishes also support some of the largest fisheries in the world. For example, the fishery that targets Peruvian anchoveta (*Engraulis ringens*) in the Humboldt Current is responsible for Peru having one of the largest total marine catches in the world (FAO, 2018).

Somatic growth of small pelagic fishes is highly variable and related to their reproduction, abundance, movement patterns, and mortality (Rountrey et al., 2014; Lorenzen, 2016). For example, the growth of the Atlantic horse mackerel (*Trachurus trachurus*) varies across its distribution, with growth rates and length at maturity increasing with latitude (Abaunza et al., 2008). Understanding drivers of growth variation is crucial for determining how the population dynamics of small pelagic fishes may vary over space and time (Doubleday et al., 2015; Smoliński, 2019). Predicting how populations will adapt to environmental changes and adjusting fishing strategies accordingly will help prevent overfishing (Black, 2009). For example, dominant regime shifts between sardine (*Sardinops* spp.) and anchovy (*Engraulis* spp.) species have been attributed to differences in the optimum temperature for growth (Lindegren et al., 2013), influencing future fish stocks and fisheries development (Koenigstein et al., 2016).

Age and growth are key characteristics in fisheries research and critical components of age-structured population models (Fournier et al., 1998). Growth chronologies of fish species can be constructed by examining otoliths, metabolically inert calcified structures that provide information about biological events and environmental conditions throughout a fish's life (Campana, 1999). The width of an otolith increment can be linked to the somatic growth rate of a fish (Ashworth et al., 2017). Ambient factors (e.g., temperature and food availability) influence the physiology and somatic growth rates of fishes. The width of growth increments (pairs of opaque and translucent bands) fluctuates in response to variations in growth rates (Morales-Nin, 2000; Kerr and Campana, 2014). Age and growth models have been developed to produce growth increment chronologies that can be used to investigate abiotic and biotic factors influencing growth (Black et al., 2005; Morrongiello and Thresher, 2015).

Growth chronologies have been applied to a range of fish species, including the black bream (*Acanthopagrus butcheri*) (Doubleday et al., 2015), the sand whiting (*Sillago ciliata*) (Stocks et al., 2011), species of ocean perch (*Helicolenus* spp.) (Grammer et al., 2017), the Atlantic horse mackerel (Tanner et al., 2019), the Atlantic herring (*Clupea harengus*) (Smoliński, 2019), and the snapper (*Chrysophrys auratus*) (Martino et al., 2019), to investigate the effects of climatic events, climate change, and environmental conditions on fish growth (Izzo et al., 2016; Mazloumi et al., 2017; Barrow et al., 2018). However, most studies in which this method was used have focused on benthic and estuarine species that tend to be more site-attached, with few growth chronology studies done on highly mobile, pelagic fishes (Smoliński, 2019).

In Australia, mid-water trawl and purse-seine nets are used in the Commonwealth small pelagic fishery 6–370 km (3–200 nmi) offshore between southwestern Western Australia and southern Queensland (Ward and Grammer[1]). The fishery targets spotted chub mackerel (*Scomber australasicus*); common jack mackerel (*Trachurus declivis*), also known as greenback horse mackerel; redbait (*Emmelichthys nitidus*); and Pacific sardine (*Sardinops sagax*) (Ward and Grammer[1]). The catch of the small pelagic fishery in 2018–2019 has been estimated at around 10,000 metric tons, which is approximately 5% of the annual fishery production in Australia (Steven et al.[2]). The harvest strategy for the fishery includes the use of fishery-independent surveys that follow the daily egg production method for each species, along with catch and effort data, to determine total allowable catch limits (AFMA[3]).

The common jack mackerel is a schooling pelagic species distributed across the temperate coastal waters of southern and southeastern Australia, ranging from Queensland to Western Australia (Gomon et al., 2008). The species is most commonly found over the continental shelf and outer shelf margin in depths of 20–300 m, but it can be found to depths of 500 m (Pullen and TDPIF, 1994). In Australia, the existence of 2 populations of common jack mackerel has been suggested (Ward and Grammer[1]); however, the movement patterns of common jack mackerel have been examined in no studies. The redbait is a schooling pelagic species occurring worldwide in tropical and temperate waters over continental shelfs and in association with seamounts, mid-ocean ridges, and islands (Welsford and Lyle, 2003). This species is commonly found in depths of 100–400 m but can be found to depths of 800 m (Welsford and Lyle, 2003). In no studies have the movements or stock structure of redbait in Australia been assessed (Ward and Grammer[1]). Long-term trends of abundance of common jack mackerel have changed over time with a shift in the dominant small pelagic species from common jack mackerel to redbait in the 1990s (McLeod et al., 2012). It has been suggested that this shift in abundance may be driven by environmental change in the region (McLeod et al., 2012), raising questions over how these changes may affect other aspects of their population dynamics, such as their growth.

Different oceanographic features are likely to influence the growth of small pelagic fish across their range off Australia. Along the southeastern coast of Australia, the Pacific Ocean is influenced by the El Niño–Southern Oscillation and Interdecadal Pacific Oscillation, phenomena that result in changes in rainfall, SST, and trade wind strength (Fiedler, 2002; Overland et al., 2010). In addition, the East Australian Current (EAC) is a key oceanographic feature that moves warm, nutrient-poor water south along eastern Australia (Ridgway, 2007; Ridgway and Hill[4]; Suthers et al., 2011). Originating in the Coral Sea with a southward flow, the EAC eventually forms the Tasman Front and a southward flowing eddy field (Ridgway and Hill[4]; Suthers et al., 2011). In contrast, southern Australia, bordered by the Indian Ocean, has strong coastal upwelling along the Bonney Coast, western Kangaroo Island (KI), and the southern coast of Eyre Peninsula, transporting cold, nutrient-rich waters to the surface (Kämpf et al., 2004; Middleton and Bye, 2007; Neuheimer et al., 2011).

To examine if local environmental influences may be affecting the growth patterns of small pelagic fishes, growth chronologies were produced from otolith increments of 2 commercially targeted small pelagic fish species—the common jack mackerel and redbait—from 2 regions off southeastern Australia. Using a combination of length-at-age modeling and growth chronology mixed-effects modeling, we compared the growth rates of these species and investigated potential environmental drivers of their growth. Specifically, in this study, we 1) compared growth rates of each species between KI, South Australia, and New South Wales (NSW) and 2) investigated the influence of local environmental conditions on the growth rates of both species in each region.

---

[1] Ward, T. M., and G. L. Grammer. 2018. Commonwealth small pelagic fishery: fishery assessment report 2017. Report to the Australian Fisheries Management Authority. South Aust. Res. Dev. Inst., SARDI Publ. F2010/000270-9, SARDI Res. Rep. Ser. 982, 114 p. SARDI Aquat. Sci., Adelaide, Australia. [Available from website.]

[2] Steven, A. H., D. Mobsby, and R. Curtotti. 2020. Australian fisheries and aquaculture statistics 2018, 135 p. Fish. Res. Dev. Corp. Project 2019-093. Aust. Bur. Agric. Resour. Econ. Sci., Canberra, Australia. [Available from website.]

[3] AFMA (Australian Fisheries Management Authority). 2019. Annual report 2018–19, 169 p. Aust. Fish. Manage. Auth., Canberra, Australia. [Available from website.]

[4] Ridgway, K., and K. Hill. 2009. The East Australian Current. *In* A marine climate change impacts and adaptation report card for Australia 2009 (E. S. Poloczanska, A. J. Hobday, and A. J. Richardson, eds.), Natl. Clim. Chang. Adapt. Res. Facil. Publ. 05/09, 16 p.

Materials and methods

Study sites and sample collection

Common jack mackerel and redbait were collected from 47 trawl tows at depths between 100 and 303 m off KI and from 49 trawl tows at depths between 60 and 283 m off southeast NSW throughout each year between 2014 and 2016; the samples were taken from catch of a single mid-water trawling vessel that is part of the Commonwealth small pelagic fishery (Fig. 1). From the haul of each trawl tow, 50 fish of each species were randomly selected and frozen. Fish were then subsampled (10 fish per trawl sample) for age and growth analysis, in the laboratory; fork length (FL, in millimeters), total weight (in grams), and sex were recorded, and otoliths were extracted.

Otolith preparation and increment analysis

Sagittal otoliths were removed from each fish, rinsed with water, and air-dried. Otoliths were batch embedded in clear epoxy resin and thin-sectioned (sections were ~300 μm) by using a single-blade sectioning saw (Gemmasta[5], Shell-Lap Supplies, Adelaide, Australia) through the primordium (i.e., core) (Fig. 2). Up to 3 transverse sections were taken from each otolith to ensure that a section was taken through the core. Sections were mounted on glass slides, polished, and viewed by using a stereo microscope (3.2× magnification; Olympus SZX7, Olympus Corp., Tokyo, Japan).

To ensure aging accuracy and count reproducibility prior to aging otoliths, the readers were trained with a reference library containing 100 otoliths of known ages for each species. The ages at capture of the fish caught for this study were within the age range for otoliths in the reference library. All otoliths were aged by 2 individuals with extensive experience in aging both species (coefficient of variation of <5%), providing a third reader

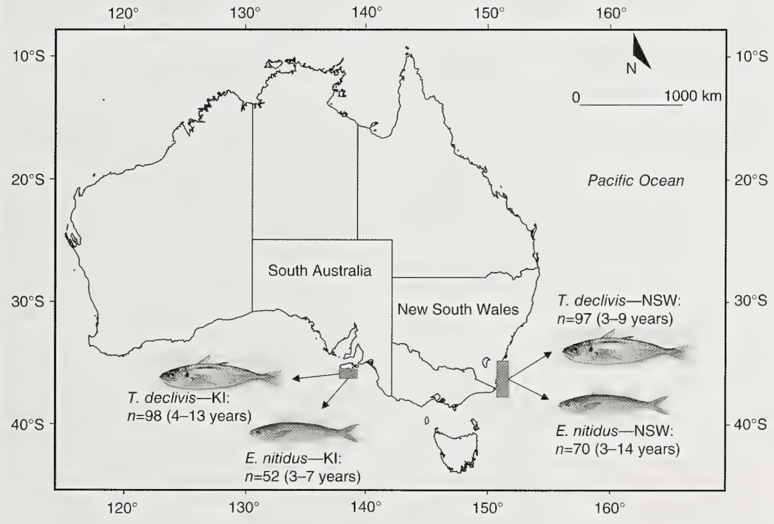

Figure 1

Map of sampling areas (indicated with gray rectangles) where common jack mackerel (*Trachurus declivis*) and redbait (*Emmelichthys nitidus*) were collected by a mid-water trawling vessel off Kangaroo Island (KI) and New South Wales (NSW) in Australia during 2014–2016. Sample sizes (*n*) and age ranges are provided for the fish sampled for each species in each region.

---

[5] Mention of trade names or commercial companies is for identification purposes only and does not imply endorsement by the National Marine Fisheries Service, NOAA.

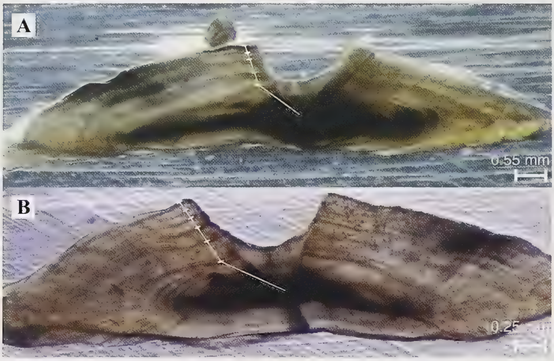

Figure 2

Photographs of thin sections of otoliths from (**A**) redbait (*Emmelichthys nitidus*) and (**B**) common jack mackerel (*Trachurus declivis*) collected off Kangaroo Island and New South Wales in Australia between 2014 and 2016. Images are shown at 3.2× magnifications under transmitted light. The white line indicates the location of measurement, and the horizontal white markings along the line indicate annual growth rings.

with a reference age for increment measurement. Otoliths were viewed under both reflected and transmitted light without focal adjustment or movement of the slide. Photographs were taken (with an Olympus DP73 digital microscope camera, Olympus Corp.) with the light sources overlaid on each other to enhance contrast and visibility of growth increments and allow increments to be accurately identified.

Annual deposition of growth bands has been validated in common jack mackerel by using bomb radiocarbon analysis (Lyle et al.[6]) and in redbait by using marginal increment analysis (Ewing and Lyle, 2009). These validations confirm that each growth increment, composed of a translucent zone and an opaque zone, represents 1 year of growth. Starting from the core, increment boundaries were delineated at the outermost edge of each opaque zone (Fig. 2), by using the image analysis software Olympus Stream (vers. 1.9.1, Olympus Corp.). The distance from the core to the first increment (which equates to growth from hatching to the first birthday; age 0) and from the final increment to the proximal edge (marginal increment) were excluded from all analysis because they did not represent a full year of growth. On the basis of the timing of spawning, a birthdate of 1 January was assigned for common jack mackerel and a birthdate of 1 October was assigned for redbait (Ewing and Lyle, 2009; Ward et al., 2016). Each increment was then assigned a calendar year of formation, back calculated from the capture date.

Growth analysis

The AquaticLifeHistory package (vers. 0.0.9000; Smart et al., 2016; Smart, 2019) was used in the statistical program R (vers. 3.4.0; R Core Team, 2017) to estimate growth parameters for all otoliths from each species and sampling location by fitting length-at-age data with the von Bertalanffy growth function (von Bertalanffy, 1938; Beverton and Holt, 1957):

$$L_t = L_0 + (L_\infty - L_0)(1 - e^{(-kt)}),$$

where t = age in years;
L_t = length at age t;
L_0 = the length at age 0 (fixed at 0);
L_∞ = asymptotic length; and
k = the growth completion parameter.

The von Bertalanffy growth function was fit by using the nls function in R. Differences in growth between sampling locations were then compared for each species by using a likelihood-ratio chi-square test (Ogle, 2016).

Chronologies and environmental variables

The growth chronology data set was truncated for years for which less than 5 increment measurements were available (Morrongiello and Thresher, 2015). A set of generalized linear mixed-effects models were fitted with a gamma error structure and a log-link function. These were used to investigate the sources of growth variation, both intrinsic and extrinsic, within species and regions (Table 1) (Morrongiello and Thresher, 2015). Sea-surface temperature and chlorophyll-*a* (Chl-*a*) concentration (used as proxy for productivity) were both included as extrinsic variables because they have been proven to influence the physiology and somatic growth of fishes (Hughes et al., 2017). Local SSTs and Chl-*a* concentrations were obtained by defining boundary coordinates around all trawl tow positions for each region in the Integrated Marine Observing System of the Australian Ocean Data Network (IMOS[7,8]). Sea-surface temperatures were obtained as 1-day composite data from polar-orbiting satellites (IMOS[7]) and then averaged to produce annual means. Chlorophyll-*a* concentrations were obtained from daily satellite images computed

---

[6] Lyle, J. M., K. Krisic-Golub, and A. K. Morison. 2000. Age and growth of jack mackerel and the age structure of the jack mackerel purse seine catch. Fish. Res. Dev. Corp. Final Rep., Proj. 1995/034, 49 p. Tasman. Aquac. Fish. Inst., Mar. Res. Lab., Univ. Tasman., Taroona, Australia. [Available from website.]

[7] IMOS (Integrated Marine Observing System). 2018. IMOS-SRS-SST-L3S-single sensor-1 day-day and night time-Australia. [Available from website, accessed December 2018.]

[8] IMOS (Integrated Marine Observing System). 2018. IMOS-SRS-MODIS-01 day-Chlorophyll-a concentration (OC3 model). [Available from website, accessed December 2018.]

Table 1

A list of the variables used in mixed-effects modeling to investigate the sources of growth variation in common jack mackerel (*Trachurus declivis*) and redbait (*Emmelichthys nitidus*) collected off Kangaroo Island and New South Wales in Australia between 2014 and 2016. Environmental data were collected for the period 2002–2016.

Variable	Description	Source
Age	Fish age (in years) when growth increment was formed	
AgeCap	Fish age (in years) when caught	
Year	Year of growth increment formation	
YearClass	Birth year of fish	
FishID	Fish identification number	
SST	Mean annual sea-surface temperature (°C)	IMOS[7]
Chl-*a*	Mean annual chlorophyll-*a* concentration inferred from relative fluorescence per unit volume of the water body (in milligrams per cubic meter)	IMOS[8]

through the OC3M algorithm (IMOS[8]), and Chl-*a* levels were also averaged to produce annual means.

All fixed effects were mean centered to assist in interpretation of interaction terms and model convergence (Morrongiello and Thresher, 2015). All fish determined to have ages ≤2 years were excluded from analysis because, with the first increment being excluded for all fish, only a single increment measurement would be available for these individuals, and a single increment is insufficient to predict growth. The Akaike information criterion corrected for bias from small sample sizes (AIC_c) was used to rank models, and AIC_c weight was used to assess model likelihood: the smaller the weight, the lower the probability the model was "true" on the basis of the included candidate models (Burnham and Anderson, 2004). Marginal and conditional coefficients of multiple determination (R^2) were used as a measure of goodness of fit, and the contribution of the fixed effects (marginal R^2) and the fixed and random effects (conditional R^2) were used to explain variance of the response variable when added to the model (Nakagawa and Schielzeth, 2013).

The optimal model explaining variation in fish growth (i.e., increment width) was determined by using a 2-step process whereby the best random-effect variables (*Year* and *YearClass*) were selected by sequentially adding them in increasing complexity to the models containing the full fixed-effect structure (i.e., the effects *Age* and *AgeCap* were included) through the use of the restricted maximum likelihood estimates of error (Zuur et al., 2009). The combination of models included *Year* and *YearClass* as random intercepts and used these same variables with *Age* included as a random slope on these variables. Random slopes of *Age* were included to allow greater flexibility in growth estimations from the model and to remove age-dependent trends during the analysis. Inclusion of *Year* as a random intercept was intended to be equivalent to the use of traditional dendrochronology, enabling annual estimates of whether growth was high or low as a result of the environmental covariates in relation to the long-term mean (Morrongiello and Thresher, 2015). Similar to the use of *Year*, *YearClass* was used as a random intercept to estimate growth conditions for a group of fish (year cohorts) over their lifetime. *FishID* with a random *Age* slope was included in all models as a random intercept to allow the growth of each fish to vary beyond the model average by inducing a correlation among increment measurements within an individual.

Estimates of the temporal similarity in growth (growth synchrony) were calculated with the interclass correlation coefficient. By using the full intrinsic effects model fit with *Year* intercept and *YearClass* intercept only, the correlation of growth increments among individuals was calculated. Growth chronologies were produced by extracting best linear unbiased predictors for each combination of species and region based on *Year* (variation in growth relative to the long-term mean) and *YearClass* (variation in growth conditions for a group of fish, i.e., year cohorts, over their lifetime relative to the long-term mean) (Morrongiello and Thresher, 2015).

The best fixed effects (*Age*, *AgeCap*, or *Age* and *AgeCap*) were then identified by sequentially adding them in increasing complexity to the selected best random-effect variables. Random-effect variables were initially selected by using maximum likelihood estimates of error, and then they were refit with restricted maximum likelihood estimates of error to produce unbiased parameter estimates (Zuur et al., 2009). Once the optimal intrinsic model was identified, environmental variables were fit as fixed effects to relate the variability in growth to the extrinsic covariates.

All analyses were performed in R, with the packages lme4 (Bates et al., 2015), effects (Fox, 2003), and AICcmodagv (Mazerolle, 2015).

Results

A total of 247 common jack mackerel and 248 redbait from trawl tows conducted south of KI were aged, and 760 common jack mackerel and 342 redbait from southeast NSW were aged. Age across both regions ranged from 1 year to 15 years for common jack mackerel and from 0+ to 14 years for redbait. From these aged samples, a subset of randomly selected otoliths was measured for growth chronology analyses (Fig. 1). A combined total of 1674 increments on otoliths from 195 common jack mackerel (KI: 662 increments, birth years 2003–2012; NSW: 425 increments, birth years 2007–2014) and on otoliths from 122 redbait (KI: 177 increments, birth years 2008–2012; NSW: 410 increments, birth years 2001–2012) were measured, with the greatest number of individuals born between 2007 and 2012 (Fig. 3). Years that corresponded to fish that had otoliths with <5 increments were removed from the

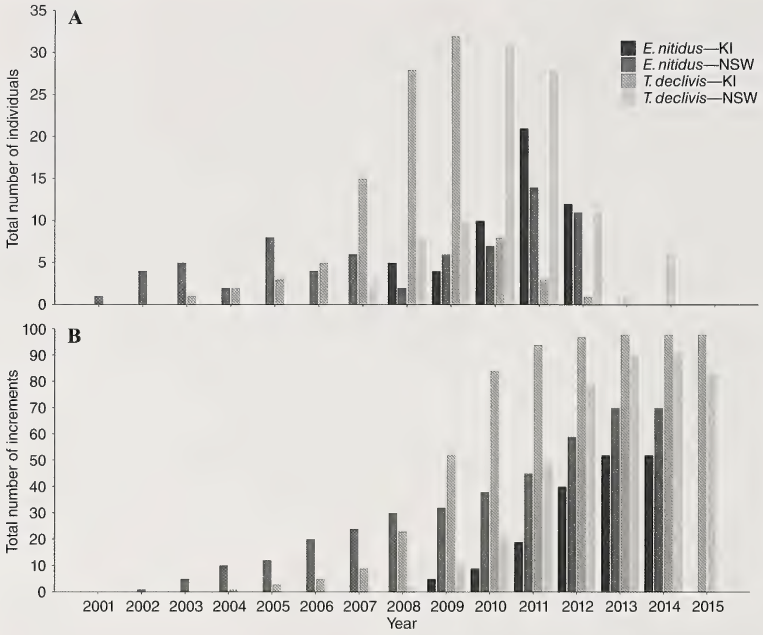

Figure 3

(**A**) Number of common jack mackerel (*Trachurus declivis*) and redbait (*Emmelichthys nitidus*) measured for each birth year and (**B**) number of otolith increments for each calendar year by species and region. These numbers indicate growth chronologies for samples collected during 2014–2016 from waters off Kangaroo Island (KI) and New South Wales (NSW) in Australia.

analyses, resulting in growth chronologies for the periods from 2005 through 2016 for common jack mackerel and from 2003 through 2015 for redbait.

Growth analysis

Estimates of von Bertalanffy growth parameters were significantly different between regions for both species (common jack mackerel: χ^2=310.46, P<0.001; redbait: χ^2=65.90, P<0.001; Fig. 4), with fish from KI (Table 2) growing slower but having a higher asymptotic length than fish caught in NSW (Table 2). Differences in growth between regions began at about 3.5 years for common jack mackerel, with the resulting difference in L_∞ by age 13 being 4 cm FL (Fig. 4A). In redbait, growth differences began at approximately the same age as common jack mackerel (3 years versus 3.5 years, respectively; Fig. 4B), but the resulting difference in L_∞ was smaller for redbait (1 cm FL; KI: L_∞=249.52 cm FL [standard error (SE) 1.6]; NSW: L_∞=238.89 cm FL [SE 1.2]) than for common jack mackerel (4 cm FL; KI: L_∞=299.40 cm FL [SE 2.5]; NSW: L_∞=259.79 cm FL [SE 1.3]). Otolith growth at age from the mixed-effects model indicates that common jack mackerel and redbait from KI had faster growth than individuals from NSW (Fig. 4, C and D).

Intrinsic predictors of growth

Overall, growth synchrony for all growth comparisons was low and varied between *Year* and *YearClass*. Common jack mackerel from both KI and NSW had greater growth synchrony within *Year* (0.94% and 3.50%, respectively) than within *YearClass* (0.08% and 0.12%, respectively). In contrast, redbait growth synchrony was greater within *YearClass* (1.40% and 1.00% for KI and NSW, respectively) than within *Year* (0.17% and 0.60%, respectively).

The best random-effect structure was different for all models; they included *FishID* as a random effect and a

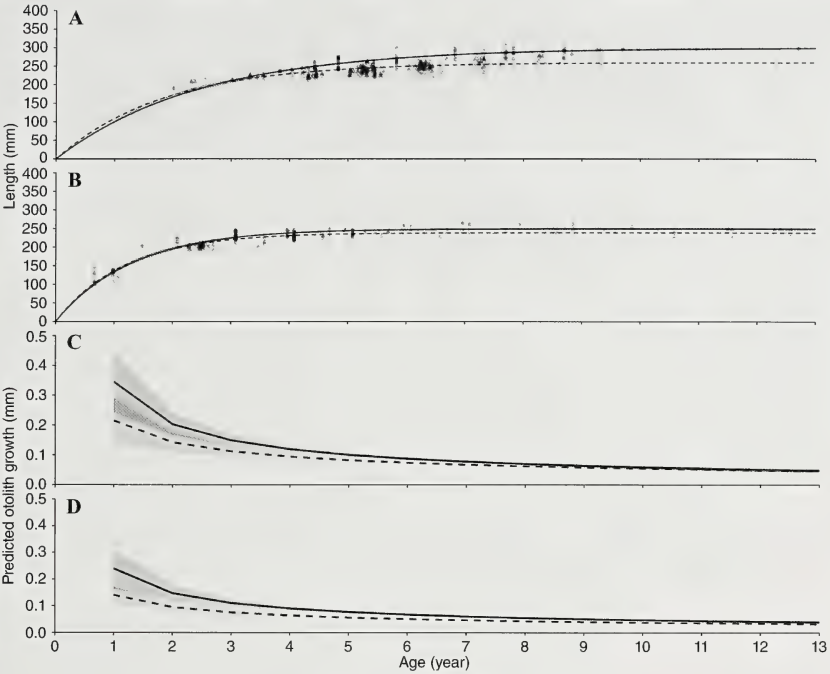

Figure 4

Von Bertalanffy growth curves for (**A**) common jack mackerel (*Trachurus declivis*) and (**B**) redbait (*Emmelichthys nitidus*) collected during 2014–2016 from waters off Kangaroo Island (KI; dark circles, solid line) and New South Wales (NSW; light triangles, dashed line) in Australia. Points indicate decimal ages based on presumed birth dates and collection dates. Also shown is predicted otolith increment growth (in millimeters) for (**C**) common jack mackerel and (**D**) redbait from KI (solid line) and NSW (dashed line). Shaded areas above and below the lines represent 95% confidence intervals.

Table 2

Estimates of von Bertalanffy growth parameters for common jack mackerel (*Trachurus declivis*) and redbait (*Emmelichthys nitidus*) collected off Kangaroo Island and New South Wales in Australia during 2014–2016. The parameters include the asymptotic length (L_∞) and the growth coefficient (k). Standard errors of the mean (SEs) are given in parentheses.

Species	Location	L_∞ (SE)	k (SE)
T. declivis	Kangaroo Island	299.40 (2.5)	0.41 (0.2)
T. declivis	New South Wales	249.52 (1.6)	0.77 (0.2)
E. nitidus	Kangaroo Island	259.79 (1.3)	0.54 (0.1)
E. nitidus	New South Wales	238.89 (1.2)	0.84 (0.2)

combination of the variables of *Year* and *YearClass*, with and without random slopes of *Age* and random intercepts (Suppl. Table 1) (online only). The best growth models that excluded environmental variables included only *Age* as a fixed effect (Suppl. Table 2) (online only). This was shown by the decrease in otolith increment growth (in millimeters per·year) as *Age* increased (Fig. 4, C and D).

Interannual variability in growth from the long-term mean ranged from –0.07 to 0.06 mm FL for common jack mackerel and from –0.02 to 0.04 mm FL for redbait. A pronounced increase in growth from the long-term mean occurred in 2013 for common jack mackerel from KI, and for both species from NSW, but not for redbait from KI (Fig. 5, A–D). Although a similar increase in growth was not observed for redbait from KI, a similar trend was observed the following year (Fig. 5C). Growth of redbait from NSW

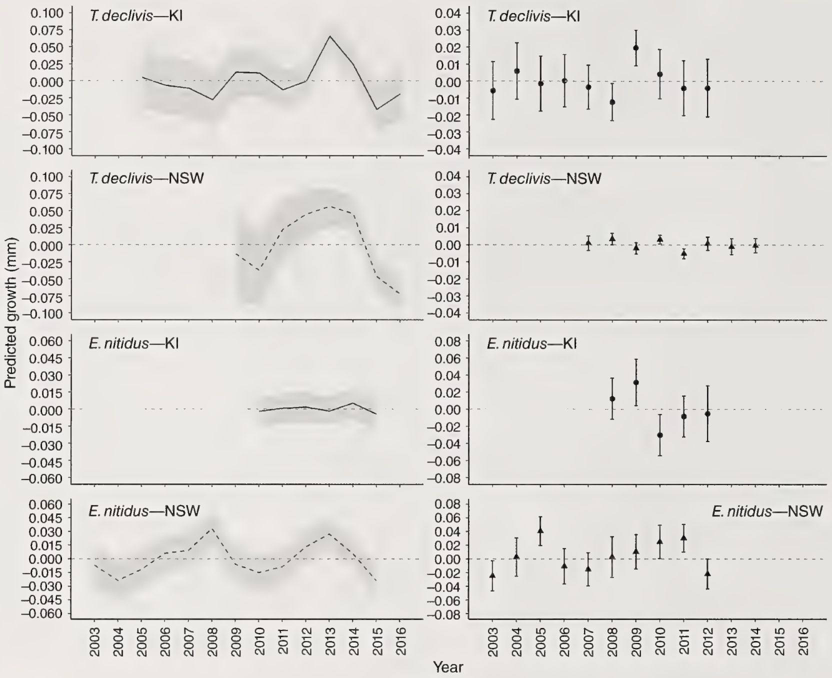

Figure 5

Panels on the left show predicted temporal variation (*Year*) in otolith increment growth relative to the long-term mean (indicated by the gray dashed line at the 0 value of the y-axis in each panel) for common jack mackerel (*Trachurus declivis*) and redbait (*Emmelichthys nitidus*) collected off Kangaroo Island (KI; black lines) and New South Wales (NSW; black dashed lines) in Australia. The shaded areas above and below the lines indicate standard errors of the mean. Panels in the right column show predicted temporal variation in otolith increment growth for common jack mackerel and redbait collected off KI (circles) and NSW (triangles) based on the birth date (*YearClass*) of fish relative to the long-term mean. Predicted variation in increment growth was produced from estimates of the *Year* and *YearClass* random effects (the best linear unbiased predictors). Error bars indicate standard errors of the mean. Note that values on the y-axis are different between species and for *Year* and *YearClass*. Common jack mackerel and redbait samples were collected between 2014 and 2016.

had higher interannual variation than that of redbait from KI, with the observed maximum predicted growth being approximately 4-fold that of fish from KI (Fig. 5, C and D). Redbait from NSW also had a pronounced increase in growth from the long-term mean in 2008, but common jack mackerel from KI had decreased growth compared with the long-term mean in the same year (Fig. 5, A and D).

YearClass variations in common jack mackerel from KI indicate that the 2009 cohort had greater growth than the long-term mean; all other cohorts had low variation between them (Fig. 5E). Conversely, the 2011 cohort of common jack mackerel from NSW had slower growth than the long-term mean (Fig. 5F). Three consecutive cohorts (2010–2012) of redbait from KI had slower growth than the long-term mean (Fig. 5G). Two *YearClass* cohorts of redbait from NSW had faster growth than the long-term mean (2005 and 2011; Fig. 5H).

Effects of environmental conditions

Chlorophyll-*a* concentrations and SSTs were both higher in NSW than off KI (0.56 mg/m^3 [SE 0.016] versus 0.22 mg/m^3 [SE 0.006] and 19.11°C [SE 0.14] versus 16.71°C [SE 0.11]). The top-ranked model assessing the effect of local environmental variables on growth for redbait from NSW and KI and for common jack mackerel from NSW was the base model, which included no environmental variables (Table 3; Suppl. Table 3) (online only). When the difference in AIC_c between the current and top models (ΔAIC_c) indicated a high degree of support for numerous models ($\Delta AIC_c < 2$), AIC_c weight was examined to determine which model had the highest likelihood (Table 3). Common jack mackerel from KI were the only fish for which growth was associated with environmental conditions. The model that included SST had the highest AIC_c weight (0.96; Table 3, Suppl. Table 3 [online only]), with predicted growth increasing 11.47% for every 1°C increase in SST in the range of 16.2–17.7°C (Fig. 6, A and B).

Discussion

In this study, the von Bertalanffy growth function and mixed-effects modeling were used to explore differences in the growth of small pelagic fishes between 2 temperate regions in southern Australia. Growth chronologies were produced from otolith increments of common jack mackerel and redbait caught off KI in South Australia and off southern NSW to explore regional differences in growth rates and to investigate the influence of local environmental conditions on the growth rates of both species in each region. This study is one of the few to apply growth chronology analyses to small pelagic fishes, and results indicate that common jack mackerel and redbait had lower growth synchrony than site-attached benthic or benthopelagic species. Consistent regional differences were also identified for both species, with fish from KI growing to greater lengths than fish from southern NSW. Age was the key intrinsic driver of growth detected across models, and each of the environmental factors selected for this study had limited influence on growth. Sea-surface temperature correlated with growth of common jack mackerel from KI, with no other correlations evident for the other species and regions.

Temporal growth synchrony (estimated with the interclass correlation coefficient) in both species and regions (0.17–3.50%) was low compared with that from other studies. For example, growth synchrony in species from similar regions has been reported as 2.0–21.6% in tiger flathead (*Platycephalus richardsoni*) (Morrongiello and Thresher, 2015), 0.4–13.7% in snapper (Martino et al., 2019), 0.1–15.0% in ocean perches (*Helicolenus* spp.) (Grammer et al., 2017), and 3.0–13.8% in black bream (Doubleday et al., 2015). The movement patterns of common jack mackerel and redbait may explain the low growth synchrony observed in our study. Results of studies on the reproductive biology of both species indicate frequent movements (Marshall et al., 1993; Welsford and Lyle, 2003; Ewing and Lyle, 2009), which expose them to a broad range of physical and biological conditions. In contrast, species that have previously been determined to have growth synchrony are mostly benthic species that tend to move over relatively small distances.

Table 3

Results from the full-fixed and intrinsic model fitted with local data for environmental variables, sea-surface temperature (SST) and chlorophyll-*a* (Chl-*a*) concentration, and used to examine growth of common jack mackerel (*Trachurus declivis*) and redbait (*Emmelichthys nitidus*) collected off Kangaroo Island (KI) and New South Wales (NSW) in Australia between 2014 and 2016. Models included the base model (full-fixed and intrinsic model), with values provided in the rows labeled *Growth*, and the base model fitted with SST or Chl-*a* concentration. Degrees of freedom (df), Akaike information criterion corrected for small sample size (AIC_c), the difference in AIC_c between the current and top models (ΔAIC_c), the proportion of the total predictive power of the model set (AIC_c weight [AIC_cWt]), log likelihood (LL), conditional coefficient of multiple determination (R^2_c), and marginal R^2 (R^2_m) are presented for each model. Values of R^2_c and R^2_m were calculated with the restricted maximum likelihood estimates of error. The top-ranked model for each species in each region is indicated with an asterisk (*).

Trachurus declivis

KI								NSW							
Model	df	AIC_c	ΔAIC_c	AIC_cWt	LL	R^2_m	R^2_c	Model	df	AIC_c	ΔAIC_c	AIC_cWt	LL	R^2_m	R^2_c
Growth	9.00	124.65	9.12	0.01	−53.19	0.50	0.72	Growth*	8.00	43.34	0.00	0.48	−13.48	0.61	0.73
+SST*	10.00	115.53	0.00	0.96	−47.59	0.54	0.73	+SST	9.00	44.00	0.66	0.35	−12.76	0.62	0.74
+Chl-*a*	10.00	122.31	6.78	0.03	−50.99	0.52	0.72	+Chl-*a*	9.00	45.43	2.09	0.17	−13.47	0.61	0.73

Emmelichthys nitidus

KI								NSW							
Model	df	AIC_c	ΔAIC_c	AIC_cWt	LL	R^2_m	R^2_c	Model	df	AIC_c	ΔAIC_c	AIC_cWt	LL	R^2_m	R^2_c
Growth*	8.00	45.84	0.00	0.52	−14.49	0.48	0.63	Growth*	9.00	250.18	0.00	0.42	−115.87	0.48	0.58
+SST	9.00	47.80	1.96	0.19	−14.36	0.48	0.63	+SST	10.00	250.44	0.26	0.37	−114.95	0.48	0.58
+Chl-*a*	9.00	47.01	1.17	0.29	−13.97	0.48	0.64	+Chl-*a*	10.00	251.53	1.35	0.21	−115.49	0.48	0.59

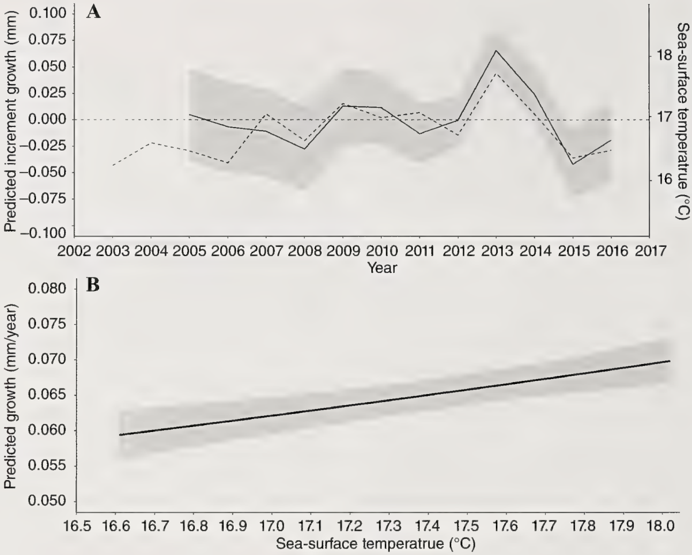

Figure 6

(**A**) Predicted temporal variation in otolith increment growth (solid line), relative to the long-term mean (gray dashed line) and to optimal local sea-surface temperature (black dashed line), and (**B**) sea-surface temperature predicted effects plot of otolith increment growth for common jack mackerel (*Trachurus declivis*) collected from waters off Kangaroo Island in Australia during 2014–2016. Predicted interannual growth variation is based on estimates for the *Year* random effect (best linear unbiased predictors). In panel A, the shaded area indicates standard error of the mean. In panel B, the shaded area indicates the 95% confidence interval.

Benthic species are more likely to be exposed to similar conditions and, therefore, have high growth synchrony among individuals, as seen in the growth synchrony of site-attached marine fishes, such as the tiger flathead (2.0–21.6%; Morrongiello and Thresher, 2015), and of sessile marine organisms, such as the Pacific geoduck (*Panopea abrupta*) (62–72%; Helser et al., 2012). In these cases, the minimal movement or lack thereof results in more consistent environmental conditions experienced across individuals, compared with the more variable and widespread movements of small pelagic fishes (Eiler and Bishop, 2016). In contrast, results of other studies in which the growth chronologies of small pelagic fishes were examined indicate synchrony in growth among individuals, and environmental effects on growth have been identified (Tanner et al., 2019). However, the species examined in other studies reside in shallow coastal waters (with depths of ~100 m); in contrast, the species investigated in our study occur at depths >100 m (Pullen and TDPIF, 1994; Welsford and Lyle, 2003; Tanner et al., 2019). As such, the low interclass correlation coefficients observed in our study may be a result of the deeper pelagic habitat of common jack mackerel and redbait causing less-defined increments compared with the habitat and increments obseved for other species (e.g., snapper or black bream) (Newman et al., 2000).

The challenges in reading growth increments on otoliths of common jack mackerel and redbait might have resulted in less precise measurements and, therefore, in artificially reduced synchrony. In the absence of cross-dating, the likelihood of errors in growth increment dating increases, possibly dampening extrinsic signals in increment data (Black et al., 2016; Smoliński et al., 2020). As a result, potential dating errors might have also contributed to the low synchrony observed (Smoliński et al., 2020).

Both species had higher growth synchrony off NSW than off KI. This finding may reflect the different oceanic processes of each region. The EAC originates in the Coral Sea and flows southward along the coast of NSW (Suthers et al., 2011). As the EAC separates from the coast, it forms a series of eddies (200–300 km in diameter) along the coastline that can persist for up to a year, and these eddies constitute a vital process for the nutrient cycling and biological productivity in this region (Ridgway and Hill[4]). The large range and timescale in which eddies exist may facilitate the high growth synchrony observed in fish from NSW. In comparison, KI is influenced by the Flinders Current, a northern boundary current, and the Leeuwin Current, a seasonal shelf-break current (Middleton and Cirano, 2002; Middleton and Bye, 2007). This region is characterized by short events (3–10 d) of summer upwelling and winter downwelling along the southern coast of Eyre Peninsula, Bonney Coast, and western KI, resulting in increased productivity in these regions (Kämpf et al., 2004; Ward et al., 2006; Middleton and Bye, 2007). In comparison with the magnitude and temporal extent of the eddies in NSW, the smaller size and shorter period of the upwelling off KI may not have the strength to drive the growth synchrony in these fishes, likely explaining the difference in growth synchrony between these regions.

Both species grew larger off KI than off southern NSW. Such regional differences have previously been documented in several temperate fish species, including the Pacific sardine (Izzo et al., 2017), Australian salmon (*Arripis trutta*) (Hughes et al., 2017), and sand whiting (Stocks et al., 2011). Variation in available resources (e.g., food and habitat) can be the driving force that alters the demographics of a population (Ruttenberg et al., 2005; Hughes et al., 2017) and results in differences across their distributions. Although the diets of both common jack mackerel and redbait are similar across their distributions, with krill being their main prey item (Ward and Grammer[1]), differences in growth across their distributions were observed in our study—between populations of common jack mackerel and within the population of redbait (Ward et al.[9,10]).

The more variable growth in both species off NSW, in comparison to that off KI, can likely be explained by the EAC and associated eddies. Upwelling and biological productivity are driven by increases in vertical mixing of the epipelagic zone due to water circulation of eddies and their interaction with the continental shelf and coastline. As a result, environmental conditions vary among years depending on the extent of the EAC southward extension and ensuing location of eddies (Tilburg et al., 2001; Ridgway and Hill[4]). Findings of studies on the larval growth of Pacific sardine (Uehara et al., 2005), white trevally (*Pseudocaranx dentex*), and jack mackerel (*Trachurus novaezelandiae*) indicate the effects of the EAC and its upwelling regions on growth and the amount of interannual variability (interannual variability in increment growth relative to the long-term mean) among species (Syahailatua et al., 2011). In comparison, the reduced temporal and spatial scale of upwelling events off KI (Middleton and Bye, 2007), in combination with the lack of basin-wide changes, has likely resulted in the lower interannual variability in growth of fishes off KI than off NSW.

Similar to differences between regions, the higher interannual variability in growth of common jack mackerel compared with that of redbait in both regions may reflect the conditions they are exposed to in their respective habitats. Although the species occur in similar habitats, redbait are also found around seamounts, mid-ocean ridges, and islands and at deeper depths than common jack mackerel (Pullen and TDPIF, 1994; Welsford and Lyle, 2003). This difference in habitat means that common jack mackerel are more likely to be influenced by the environmental conditions of surface waters, which are in turn more likely to vary between years than the deeper waters in which redbait reside (Ridgway and Dunn, 2003). Because of this increased distribution depth, SST may not be the most appropriate temperature variable for redbait; however, bottom temperature records covering the chronologies in our study areas are not available. As such, SST is currently the most suitable proxy we have for temperature changes in these regions for the chronologies in this study.

The principle factor influencing somatic growth in ectotherms is commonly thought to be environmental temperature (Hughes et al., 2017). Marine organisms require specific temperature ranges to maintain control of physiological processes and avoid thermal stress (Calosi et al., 2008). In South Australia, snapper growth declined at temperatures higher than 18–20°C, which is the likely pejus temperature for snapper in South Australia (Martino et al., 2019). Results from the linear models in our study indicate that the optimal temperature for growth of common jack mackerel at KI is approximately 16–18°C (KI actual SST range: 16.42–18.01°C), a range at which the growth rate was still increasing. However, the growth rate of common jack mackerel at 18–20°C (NSW actual SST range: 18.40–20.05°C) was lower. This result indicates that a mean temperature higher than 18°C might start to cause some thermal stress, decreasing growth rates. Within the NSW region, the growth and metabolic costs of the red moki (*Chirodactylus spectabilis*) has already been affected by the intensification of the EAC (Neuheimer et al., 2011). As such, a continued increase in water temperature may result in the decline of the growth rates of common jack mackerel off NSW; however, a specific study investigating the thermal tolerance of common jack mackerel is required to define the optimal temperature for this species.

Indirect effects, such as changes in productivity (e.g., food), structure (e.g., habitat and abundance of predators), and composition (e.g., abundance of competitors), can also affect fish growth (Brander, 2010). For example, productivity or food availability can trigger massive changes in a population (Sánchez-Garrido et al., 2019), as has been reported for populations of anchovy and sardine species

---

[9] Ward, T. M., G. L. Grammer, A. R. Ivey, J. J. Smart, and P. Keane. 2018. Spawning biomass of jack mackerel (*Trachurus declivis*) and sardine (*Sardinops sagax*) between western Kangaroo Island, South Australia and south-western Tasmania. Report to the Australian Fisheries Management Authority. South Aust. Res. Dev. Inst., SARDI Publ. F2018/000174-1, SARDI Res. Rep. Ser. 983, 51 p. SARDI Aquat. Sci., Adelaide, Australia. [Available from website.]

[10] Ward, T., G. Grammer, A. Ivey, and J. Keane. 2019. Spawning biomass of redbait (*Emmelichthys nitidus*) between western Kangaroo Island, South Australia and south-western Tasmania in October 2017. Report to the Australian Fisheries Management Authority. South Aust. Res. Dev. Inst. SARDI Publ. F2019/000053-1, SARDI Res. Rep. Ser. 1011, 38 p. SARDI Aquat. Sci., Adelaide, Australia. [Available from website.]

in response to regime shifts in the Californian (Rodríguez-Sánchez et al., 2002), Humboldt (Alheit and Niquen, 2004), Benguela (Cury and Shannon, 2004), and Canary (Sánchez-Garrido et al., 2019) current systems. However, changes in Chl-*a* concentration did not affect growth of common jack mackerel and redbait in our study, and the observed differences may be the result of other indirect effects that we did not measure. The reason for the lack of effect of SST on growth of redbait is also unclear.

Because redbait reside in deeper waters than common jack mackerel, the influence of environmental variables, such as SST, on their growth may be reduced (Welsford and Lyle, 2003; Thresher et al., 2007). This reduction in influence of environmental conditions indicates a limitation of our study: the model is limited to a small number of available local variables. In addition, the AIC_c weight does not provide overwhelming support for one candidate model for each species and region, indicating that some models are equally supported. Other factors, not included in this study, are likely driving the growth of common jack mackerel and redbait and can be an avenue for future research. Possible model extensions could include an upwelling index as a measure of the strength and productivity in upwelling events within these regions. Furthermore, inclusion of an index of EAC strength and extent would enable testing whether, and to what magnitude, the EAC may be affecting these species in NSW.

Conclusions

Here, we reveal inter-regional differences in the growth of common jack mackerel and redbait, differences we hypothesize to be linked to the EAC and associated eddies off NSW and to upwelling events off KI. The environmental variables examined (SST and Chl-*a* concentration) had little effect on growth with the exception of common jack mackerel from KI. These populations and the fisheries they support, therefore, may be more resilient to some environmental changes than has previously been assumed. However, further investigation is required to better understand the environmental drivers of growth in these populations and to assess the potential effects of climate variations over long time periods. Increasing the sample size is needed to lengthen the time series and to increase sample depth. Additional environmental factors, such as an upwelling index or intensity and extent of the EAC, should be included in future models to improve the amount of deviance explained and provide a better understanding of the factors driving growth in these small pelagic fishes. Growth chronologies, such as those that we present here, are useful for identifying the effects of environmental conditions on fish growth and can be incorporated into stock assessments to inform the management of fisheries.

Acknowledgments

Samples were collected by scientific observers employed by the Australian Fisheries Management Authority. A. Ivey and N. Navong, from the Aquatic Sciences Research Division of the South Australian Research and Development Institute (SARDI Aquatic Sciences), removed, weighed, and sectioned otoliths and assisted with aging. Salaries of T. Ward and G. Grammer were funded by SARDI Aquatic Sciences.

Literature cited

Abaunza, P., L. S. Gordo, M. T. G. Santamaría, S. A. Iversen, A. G. Murta, and E. Gallo.
2008. Life history parameters as basis for the initial recognition of stock management units in horse mackerel (*Trachurus trachurus*). Fish. Res. 89:167–180.

Agenbag, J. J., A. J. Richardson, H. Demarcq, P. Fréon, S. Weeks, and F. A. Shillington.
2003. Estimating environmental preferences of South African pelagic fish species using catch size- and remote sensing data. Prog. Oceanogr. 59:275–300.

Alheit, J., and M. Niquen.
2004. Regime shifts in the Humboldt Current ecosystem. Prog. Oceanogr. 60:201–222.

Ashworth, E. C., N. G. Hall, S. A. Hesp, P. G. Coulson, and I. C. Potter.
2017. Age and growth rate variation influence the functional relationship between somatic and otolith size. Can. J. Fish. Aquat. Sci. 74:680–692.

Barrow, J., J. Ford, R. Day, and J. Morrongiello.
2018. Environmental drivers of growth and predicted effects of climate change on a commercially important fish, *Platycephalus laevigatus*. Mar. Ecol. Prog. Ser. 598:201–212.

Bates, D., M. Maechler, B. Bolker, and S. Walker.
2015. Fitting linear mixed-effects models using lme4. J. Stat. Softw. 67:1–48.

Beverton, R., and S. Holt.
1957. On the dynamics of exploited fish populations. Fish. Invest. Ser. 2, vol. 19, 533 p. HMSO, London.

Black, B. A.
2009. Climate-driven synchrony across tree, bivalve, and rockfish growth-increment chronologies of the northeast Pacific. Mar. Ecol. Prog. Ser. 378:37–46.

Black, B. A., G. W. Boehlert, and M. M. Yoklavich.
2005. Using tree-ring crossdating techniques to validate annual growth increments in long-lived fishes. Can. J. Fish. Aquat. Sci. 62:2277–2284.

Black, B. A., D. Griffin, P. van der Sleen, A. D. Wanamaker Jr., J. H. Speer, D. C. Frank, D. W. Stahle, N. Pederson, C. A. Copenheaver, V. Trouet, et al.
2016. The value of crossdating to retain high-frequency variability, climate signals, and extreme events in environmental proxies. Global Chang. Biol. 22:2582–2595.

Brander, K.
2010. Impacts of climate change on fisheries. J. Mar. Syst. 79:389–402.

Burnham, K. P., and D. R. Anderson.
2004. Multimodel inference: understanding AIC and BIC in model selection. Social. Methods Res. 33:261–304.

Calosi, P., D. T. Bilton, and J. I. Spicer.
2008. Thermal tolerance, acclimatory capacity and vulnerability to global climate change. Biol. Lett. 4:99–102.

Campana, S. E.
1999. Chemistry and composition of fish otoliths: pathways, mechanisms and applications. Mar. Ecol. Prog. Ser. 188:263–297.

Cury, P., and L. Shannon.
2004. Regime shifts in upwelling ecosystems: observed changes and possible mechanisms in the northern and southern Benguela. Prog. Oceanogr. 60:223–243.

Doubleday, Z. A., C. Izzo, J. A. Haddy, J. M. Lyle, Q. Ye, and B. M. Gillanders.
2015. Long-term patterns in estuarine fish growth across two climatically divergent regions. Oecologia 179:1079–1090.

Eiler, J. H., and M. A. Bishop.
2016. Tagging response and postspawning movements of Pacific Herring, a small pelagic forage fish sensitive to handling. Trans. Am. Fish. Soc. 145:427–439.

Essington, T. E., P. E. Moriarty, H. E. Froehlich, E. E. Hodgson, L. E. Koehn, K. L. Oken, M. C. Siple, and C. C. Stawitz.
2015. Fishing amplifies forage fish population collapses. Proc. Natl. Acad. Sci. U.S.A. 112:6648–6652.

Ewing, G. P., and J. M. Lyle.
2009. Reproductive dynamics of redbait, *Emmelichthys nitidus* (Emmelichthyidae), from south-eastern Australia. Fish. Res. 97:206–215.

FAO.
2018. The state of world fisheries and aquaculture 2018: meeting the sustainable development goals, 210 p. FAO, Rome. [Available from website.]

Fiedler, P. C.
2002. Environmental change in the eastern tropical Pacific Ocean: review of ENSO and decadal variability. Mar. Ecol. Prog. Ser. 244:265–283.

Fournier, D. A., J. Hampton, and J. R. Sibert.
1998. MULTIFAN-CL: a length-based, age-structured model for fisheries stock assessment, with application to South Pacific albacore, *Thunnus alalunga*. Can. J. Fish. Aquat. Sci. 55:2105–2116.

Fox, J.
2003. Effect displays in R for generalised linear models. J. Stat. Softw. 8:1–27.

Fréon, P., P. Cury, L. Shannon, and C. Roy.
2005. Sustainable exploitation of small pelagic fish stocks challenged by environmental and ecosystem changes: a review. Bull. Mar. Sci. 76:385–462.

Gomon, M. F., D. J. Bray, and R. F. Kuiter.
2008. Fishes of Australia's southern coast, 928 p. Reed New Holland, Chatswood, Australia.

Grammer, G. L., J. R. Morrongiello, C. Izzo, P. J. Hawthorne, J. F. Middleton, and B. M. Gillanders.
2017. Coupling biogeochemical tracers with fish growth reveals physiological and environmental controls on otolith chemistry. Ecol. Monogr. 87:487–507.

Helser, T. E., H.-l. Lai, and B. A. Black.
2012. Bayesian hierarchical modeling of Pacific geoduck growth increment data and climate indices. Ecol. Model. 247:210–220.

Hughes, J. M., J. Stewart, J. M. Lyle, J. McAllister, J. R. Stocks, and I. M. Suthers.
2017. Influence of latitudinal variation in environmental gradients and population structure on the demography of a widespread pelagic fish, *Arripis trutta* (Forster, 1801). Environ. Biol. Fishes 100:121–135.

Izzo, C., Z. A. Doubleday, G. L. Grammer, K. L. Gilmore, H. K. Alleway, T. C. Barnes, M. C. F. Disspain, A. J. Giraldo, N. Mazloumi, and B. M. Gillanders.
2016. Fish as proxies of ecological and environmental change. Rev. Fish Biol. Fish. 26:265–286.

Izzo, C., T. M. Ward, A. R. Ivey, I. M. Suthers, J. Stewart, S. C. Sexton, and B. M. Gillanders.
2017. Integrated approach to determining stock structure: implications for fisheries management of sardine, *Sardinops sagax*, in Australian waters. Rev. Fish Biol. Fish. 27:267–284.

Kämpf, J., M. Doubell, D. Griffin, R. L. Matthews, and T. M. Ward.
2004. Evidence of a large seasonal coastal upwelling system along the southern shelf of Australia. Geophys. Res. Lett. 31:L09310.

Kerr, L. A., and S. E. Campana.
2014. Chemical composition of fish hard parts as a natural marker of fish stocks. *In* Stock identification methods: applications in fisheries science, 2nd ed. (S. X. Cadrin, L. A. Kerr, and S. Mariani, eds.), p. 205–234. Academic Press, London.

Koenigstein, S., F. C. Mark, S. Gößling-Reisemann, H. Reuter, and H.-O. Poertner.
2016. Modelling climate change impacts on marine fish populations: process-based integration of ocean warming, acidification and other environmental drivers. Fish Fish. 17:972–1004.

Lindegren, M., D. M. Checkley, T. Rouyer, A. D. MacCall, and N. C. Stenseth.
2013. Climate, fishing, and fluctuations of sardine and anchovy in the California Current. Proc. Natl. Acad. Sci. U.S.A. 110:13672–13677.

Lorenzen, K.
2016. Toward a new paradigm for growth modeling in fisheries stock assessments: embracing plasticity and its consequences. Fish. Res. 180:4–22.

Marshall, J., G. Pullen, and A. Jordan.
1993. Reproductive biology and sexual maturity of female jack mackerel, *Trachurus declivis* (Jenyns), in eastern Tasmanian waters. Mar. Freshw. Res. 44:799–809.

Martino, J. C., A. J. Fowler, Z. A. Doubleday, G. L. Grammer, and B. M. Gillanders.
2019. Using otolith chronologies to understand long-term trends and extrinsic drivers of growth in fisheries. Ecosphere 10(1):e02553.

Mazerolle, M. J.
2015. AICcmodavg: model selection and multimodel inference based on (Q)AIC (c). R package, vers. 2.0-3. [Available from website, accessed November 2018.]

Mazloumi, N., P. Burch, A. Fowler, Z. Doubleday, and B. Gillanders.
2017. Determining climate-growth relationships in a temperate fish: a sclerochronological approach. Fish. Res. 186:319–327.

McLeod, D. J., A. J. Hobday, J. M. Lyle, and D. C. Welsford.
2012. A prey-related shift in the abundance of small pelagic fish in eastern Tasmania? J. Mar. Sci. 69:953–960.

Middleton, J. F., and M. Cirano.
2002. A northern boundary current along Australia's southern shelves: the Flinders Current. J. Geophys. Res., Oceans 107(C9):3129.

Middleton, J. F., and J. A.T. Bye.
2007. A review of the shelf-slope circulation along Australia's southern shelves: Cape Leeuwin to Portland. Prog. Oceanogr. 75:1–41.

Morales-Nin, B.
2000. Review of the growth regulation processes of otolith daily increment formation. Fish. Res. 46:53–67.

Morrongiello, J. R., and R. E. Thresher.
2015. A statistical framework to explore ontogenetic growth variation among individuals and populations: a marine fish example. Ecol. Monogr. 85:93–115.

Nakagawa, S., and H. Schielzeth.
2013. A general and simple method for obtaining R^2 from generalized linear mixed-effects models. Methods Ecol. Evol. 4:133–142.

Neuheimer, A. B., R. E. Thresher, J. M. Lyle, and J. M. Semmens.
2011. Tolerance limit for fish growth exceeded by warming waters. Nat. Clim. Chang. 1:110–113.

Newman, S. J., M. Cappo, and D. M. Williams.
2000. Age, growth, mortality rates and corresponding yield estimates using otoliths of the tropical red snappers, *Lutjanus erythropterus*, *L. malabaricus* and *L. sebae*, from the central Great Barrier Reef. Fish. Res. 48:1–14.

Ogle, D. H.
2016. Introductory fisheries analyses with R, 338 p. CRC Press, Boca Raton, FL.

Overland, J. E., J. Alheit, A. Bakun, J. W. Hurrell, D. L. Mackas, and A. J. Miller.
2010. Climate controls on marine ecosystems and fish populations. J. Mar. Syst. 79:305–315.

Pullen, G., and TDPIF (Tasmanian Department of Primary Industry and Fisheries).
1994. Fishery status report: purse seine (the Tasmanian jack mackerel fishery). Internal Rep. 13, 49 p. Mar. Res. Lab., Taroona, Tasmania.

R Core Team.
2017. R: a language and environment for statistical computing. R Foundation for Statistical Computing, Vienna, Austria. [Available from website, accessed November 2018.]

Ridgway, K. R.
2007. Long-term trend and decadal variability of the southward penetration of the East Australian Current. Geophys. Res. Lett. 34:L13613.

Ridgway, K. R., and J. R. Dunn.
2003. Mesoscale structure of the mean East Australian Current system and its relationship with topography. Prog. Oceanogr. 56:189–222.

Rodríguez-Sánchez, R., D. Lluch-Belda, H. Villalobos, and S. Ortega-García.
2002. Dynamic geography of small pelagic fish populations in the California Current system on the regime time scale (1931–1997). Can. J. Fish. Aquat. Sci. 59:1980–1988.

Rountrey, A. N., P. G. Coulson, J. J. Meeuwig, and M. Meekan.
2014. Water temperature and fish growth: otoliths predict growth patterns of a marine fish in a changing climate. Global Chang. Biol. 20:2450–2458.

Ruttenberg, B. I., A. J. Haupt, A. I. Chiriboga, and R. R. Warner.
2005. Patterns, causes and consequences of regional variation in the ecology and life history of a reef fish. Oecologia 145:394–403.

Sánchez-Garrido, J., F. E. Werner, J. Fiechter, K. A. Rose, E. N. Curchitser, A. Ramos, J. G. Lafuente, J. Arístegui, S. Hernández-León, and A. R. Santana.
2019. Decadal-scale variability of sardine and anchovy simulated with an end-to-end coupled model of the Canary Current ecosystem. Prog. Oceanogr. 171:212–230.

Smart, J.
2019. AquaticLifeHistory: fisheries life history analysis using contemporary methods. R package, vers. 0.0.9000. [Available from website, accessed March 2019]

Smart, J. J., A. Chin, A. J. Tobin, and C. A. Simpfendorfer.
2016. Multimodel approaches in shark and ray growth studies: strengths, weaknesses and the future. Fish Fish. 17:955–971.

Smoliński, S.
2019. Sclerochronological approach for the identification of herring growth drivers in the Baltic Sea. Ecol. Indicators 101:420–431.

Smoliński, S., J. Morrongiello, P. van der Sleen, B. A. Black, and S. E. Campana.
2020. Potential sources of bias in the climate sensitivities of fish otolith biochronologies. Can. J. Fish. Aquat. Sci. 77:1552–1563.

Stocks, J., J. Stewart, C. A. Gray, and R. J. West.
2011. Using otolith increment widths to infer spatial, temporal and gender variation in the growth of sand whiting *Sillago ciliata*. Fish. Manage. Ecol. 18:121–131.

Suthers, I. M., J. W. Young, M. E. Baird, M. Roughan, J. D. Everett, G. B. Brassington, M. Byrne, S. A. Condie, J. R. Hartog, C. S. Hassler, et al.
2011. The strengthening East Australian Current, its eddies and biological effects—an introduction and overview. Deep-Sea Res., II 58:538–546.

Syahailatua, A., M. D. Taylor, and I. M. Suthers.
2011. Growth variability and stable isotope composition of two larval carangid fishes in the East Australian Current: the role of upwelling in the separation zone. Deep-Sea Res., II 58:691–698.

Tanner, S. E., A. R. Vieira, R. P. Vasconcelos, S. Dores, M. Azevedo, H. N. Cabral, and J. R. Morrongiello.
2019. Regional climate, primary productivity and fish biomass drive growth variation and population resilience in a small pelagic fish. Ecol. Indicators 103:530–541.

Thresher, R. E., J. A. Koslow, A. K. Morison, and D. C. Smith.
2007. Depth-mediated reversal of the effects of climate change on long-term growth rates of exploited marine fish. Proc. Natl. Acad. Sci. U.S.A. 104:7461–7465.

Tilburg, C. E., H. E. Hurlburt, J. J. O'Brien, and J. F. Shriver.
2001. The dynamics of the East Australian Current system: the Tasman Front, the East Auckland Current, and the East Cape Current. J. Phys. Oceanogr. 31:2917–2943.

Uehara, S., A. Syahailatua, and I. M. Suthers.
2005. Recent growth rate of larval pilchards *Sardinops sagax* in relation to their stable isotope composition, in an upwelling zone of the East Australian Current. Mar. Freshw. Res. 56:549–560.

von Bertalanffy, L.
1938. A quantitative theory of organic growth (Inquiries on growth laws. II). Hum. Biol. 10:181–213.

Ward, T. M., L. J. McLeay, W. F. Dimmlich, P. J. Rogers, S. McClatchie, R. Matthews, J. Kämpf, and P. D. Van Ruth.
2006. Pelagic ecology of a northern boundary current system: effects of upwelling on the production and distribution of sardine (*Sardinops sagax*), anchovy (*Engraulis australis*) and southern bluefin tuna (*Thunnus maccoyii*) in the Great Australian Bight. Fish. Oceanogr. 15:191–207.

Ward, T. M., O. W. Burnell, A. Ivey, S. C. Sexton, J. Carroll, J. Keane, and J. M. Lyle.
2016. Spawning biomass of jack mackerel (*Trachurus declivis*) off eastern Australia: critical knowledge for managing a controversial fishery. Fish. Res. 179:10–22.

Welsford, D. C., and J. M. Lyle.
2003. Redbait (*Emmelichthys nitidus*): a synopsis of fishery and biological data. Tasman. Aquac. Fish. Inst., Tech. Rep. Ser. 20, 32 p. Tasman. Aquac. Fish. Inst., Mar. Res. Lab., Univ. Tasman., Hobart, Australia.

Zuur, A., E. N. Ieno, N. Walker, A. A. Saveliev, and G. M. Smith.
2009. Mixed effects models and extensions in ecology with R, 574 p. Springer, New York.

National Marine
Fisheries Service
NOAA

Fishery Bulletin
established in 1881

Spencer F. Baird
First U.S. Commissioner
of Fisheries and founder
of *Fishery Bulletin*

A comparison of 4 primary age-structured stock assessment models used in the United States

Bai Li (contact author)[1]
Kyle W. Shertzer[2]
Patrick D. Lynch[3]
James N. Ianelli[4]
Christopher M. Legault[5]
Erik H. Williams[2]
Richard D. Methot Jr.[6]
Elizabeth N. Brooks[5]
Jonathan J. Deroba[5]
Aaron M. Berger[7]
Skyler R. Sagarese[8]
Jon K. T. Brodziak[9]
Ian G. Taylor[6]
Melissa A. Karp[10]
Chantel R. Wetzel[6]
Matthew Supernaw[11]

Email address for contact author: bai.li@noaa.gov

[1] National Research Council
1315 East-West Highway, Building SSMC3
Silver Spring, Maryland 20910

[2] Southeast Fisheries Science Center
National Marine Fisheries Service, NOAA
101 Pivers Island Road
Beaufort, North Carolina 28516-9722

[3] Office of Science and Technology
National Marine Fisheries Service, NOAA
1315 East-West Highway, Building SSMC3
Silver Spring, Maryland 20910-3282

[4] Alaska Fisheries Science Center
National Marine Fisheries Service, NOAA
7600 Sand Point Way NE, Building 4
Seattle, Washington 98115-6349

[5] Northeast Fisheries Science Center
National Marine Fisheries Service, NOAA
166 Water Street
Woods Hole, Massachusetts 02543

[6] Northwest Fisheries Science Center
National Marine Fisheries Service, NOAA
2725 Montlake Boulevard East
Seattle, Washington 98112

[7] Northwest Fisheries Science Center
National Marine Fisheries Service, NOAA
2032 SE OSU Drive
Newport, Oregon 97365-5275

[8] Southeast Fisheries Science Center
National Marine Fisheries Service, NOAA
75 Virginia Beach Drive, Building 1
Miami, Florida 33149-1003

[9] Pacific Islands Fisheries Science Center
National Marine Fisheries Service, NOAA
1845 Wasp Boulevard, Building 176
Honolulu, Hawaii 96818

[10] ECS Federal, LLC
Office of Science and Technology
1315 East-West Highway, Building SSMC3
Silver Spring, Maryland 20910-3282

[11] Office of Science and Technology
National Marine Fisheries Service, NOAA
263 13th Avenue South
St. Petersburg, Florida 33701

Abstract—The National Marine Fisheries Service conducts fishery stock assessments to provide the best scientific information available for the U.S. regional fishery management councils. The assessment models applied in the United States are often region specific, although the models share similar mathematical and statistical attributes. However, comprehensive comparison studies identifying similarities and differences among these assessment models remain scarce. We developed a multi-model comparison framework to evaluate the reliability of 4 age-structured assessment models that are commonly used in the United States: the Assessment Model for Alaska, the Age Structured Assessment Program, the Beaufort Assessment Model, and Stock Synthesis. When applied to simulated data, all 4 models produced reliable estimates of assessment quantities of interest, such as fishing mortality, spawning biomass, recruitment, and biological reference points. Although there were differences among models in the calculation of the initial population numbers at age and in the bias adjustment of recruitment, their effects on model outputs were minor when estimation models were configured similarly. In addition, we provide guidelines for converting unfished recruitment and steepness between 2 methods of bias adjustment. We recommend that next-generation stock assessment models include recruitment bias adjustment and that more research be conducted to provide guidelines for which methods might be preferred under which situations.

Fishery stock assessment models have been widely used by scientific and management communities to evaluate fish population dynamics and provide estimates of stock abundance and fishing mortality rate (F) (Hilborn and Walter, 1992; Quinn and Deriso, 1999; Maunder and Punt, 2013; Lynch et al., 2018). Over time, assessment models have become more comprehensive and more efficient to facilitate the integration of data from diverse sources and to use increasing computational power. Concurrently, the complexity of stock assessments has increased considerably, creating challenges for both analysts and reviewers of stock assessments. Given the range of stocks requiring assessments, using generic stock assessment models that are not

Manuscript submitted 29 October 2020.
Manuscript accepted 12 July 2021.
Fish. Bull. 119:149–167 (2021).
Online publication date: 30 August 2021.
doi: 10.7755/FB.119.2-3.5

The views and opinions expressed or implied in this article are those of the author (or authors) and do not necessarily reflect the position of the National Marine Fisheries Service, NOAA.

stock or region specific is common practice (NRC, 1998; Dichmont et al., 2016). Indeed, many of the age-based models used for stock assessments conducted in the United States use software developed for generic use.

In some literature reviews, the minimum data requirements, output, and projection capabilities of stock assessment models in the United States have been compared to facilitate model choice (NRC, 1998; Dichmont et al.[1]). In addition, simulation-based research has been designed to evaluate the performance of various models and their ability to meet the needs of fishery managers (Smith et al., 1993; Sampson and Yin, 1998; Cadrin and Dickey-Collas, 2015; Deroba et al., 2015). However, comparison of assessment models through both side-by-side code comparison and simulation tests remains scarce.

Four age-structured stock assessment models are used most commonly in the United States. We refer to them as models, although in reality they are software packages that may be configured to represent various forms of mathematical models. Three of the models, the Age Structured Assessment Program (ASAP) (Legault and Restrepo, 1999), the Beaufort Assessment Model (BAM) (Williams and Shertzer, 2015), and Stock Synthesis (SS) (Methot and Wetzel, 2013), are frequently used for assessments on the East Coast. On the West Coast of the continental United States, recent assessments are primarily conducted by using SS. The development trajectory for the Assessment Model for Alaska (AMAK) (AFSC, 2015) is similar to that for the ASAP. Alaska fishery scientists created simple age-structured statistical models by using a program that implements automatic differentiation, AD Model Builder (e.g., Ianelli and Fournier, 1998; Fournier et al., 2012), but they mostly tailored them for the individual stock characteristics and types of data available. From these bespoke models, a more general model, the AMAK, was developed and applied to a number of stocks, such as walleye pollock (*Gadus chalcogrammus*) in the Aleutian Islands region (Barbeaux et al., 2019). Although there are additional models and diagnostic tools that can be used to assess fish stocks (Dichmont et al.[1]), these 4 age-structured assessment models are the main approaches applied in the United States for “data-rich” stock assessments, and they share similar conceptual, mathematical, and statistical frameworks.

The varied development and preference among regions for different assessment models may be attributed to special requirements or features of a stock assessment model given the availability of observed data (data collection programs vary regionally) and length of time of commercial fishery operations (periods of hundreds of years on the East Coast versus periods that began roughly after World War II in Alaska or more recently on the West Coast) that create different states of initial depletion. Additional reasons for different software and modeling approaches include inertia and continuity with past practices (or application to similar stocks), region-specific training, and the presence of local expertise (Cadrin and Dickey-Collas, 2015). The availability of different assessment approaches may provide flexibility, but it also requires testing to determine how different assumptions affect results. A first step is to test whether various models of a given type produce similar estimates when configured similarly without introducing misspecifications to the models. Then identifying sources of any differences can inform and improve assumptions used in actual assessments (e.g., NRC, 1998).

Simulation testing provides a means to evaluate the accuracy of individual assessment models because we know the correct values used to generate the data. An *operating model* (OM) is configured to reflect hypotheses about true stock dynamics and is the basis for generating age-structured stock assessment inputs for each assessment model (which are referred to as *estimation models* [EMs]). The OM-EM framework to fit EMs to simulated data (with errors) has been used previously to assess the ability of assessment models to estimate stock conditions (Wetzel and Punt, 2011; Henríquez et al., 2016). Deroba et al. (2015) conducted both self-tests and cross-tests from a simulation-estimation framework to compare the robustness of assessment models to error. A self-test fits an assessment model to the simulated data generated from the same assessment model, and a cross-test fits an assessment model to data generated from a different model (Chang et al., 2015; Deroba et al., 2015). They highlighted that the lack of robustness in self-tests may indicate bias and that a lack of robustness in cross-tests may indicate differences in structural assumptions between assessment models. To avoid the bias introduced during the cross-test process, we attempted to develop an OM based on common features of the 4 EMs.

The aim of this study was to improve our understanding of both the similarities and differences among 4 primary age-structured stock assessment models used in the United States. To our knowledge, this evaluation is the first in which a comprehensive comparison of source codes and a simulation-estimation analysis of these models has been conducted. This study specifically addressed the following 4 primary questions: What are the key features and source code that need to be examined before developing an OM for comparing multiple EMs? Do the EMs give similar and accurate estimates under a range of cases? What are the sources of differences in estimates, if there are any? What recommendations can be drawn for future model development after examining the similarities and differences of the 4 EMs in our study? Addressing these questions is critical for improving the understanding of current models and for developing next-generation stock assessment models (Punt et al., 2020).

Materials and methods

General framework

To compare assessment models, we conducted a comparison of key features in the code from the 4 EMs as well as OM-EM simulation tests to compare estimates to true values (Fig. 1). The code comparison process helps to verify whether the code from the 4 EMs executes the intended algorithms the same way and to identify common features from the EMs to develop an OM (Table 1, Suppl. Material [online only], Suppl. Table 1 [online only]) with only those commonalities (NRC, 1998) (Table 2). The simulation-estimation process, which helps validate the accuracy of EMs, consisted of 4 main steps: 1) developing an OM to simulate annual fish population and fishery dynamics, 2) fitting the 4 EMs to the simulated data, 3) repeating the simulation-estimation 100 times with different recruitment deviations and observation errors for each iteration, and 4) comparing estimates from the EMs with the true values from the OM (Fig. 1). This process was repeated for 13 cases (Table 3). Comparisons were made among the 4 EMs within each case and across cases.

---

[1] Dichmont, C. M., A. R. Deng, A. E. Punt, and L. R. Little. 2017. Stock assessment integration: a review. Fish. Res. Dev. Corp. Rep. 2014-039, 106 p. CSIRO Publ., Hobart, Australia. [Available from website.]

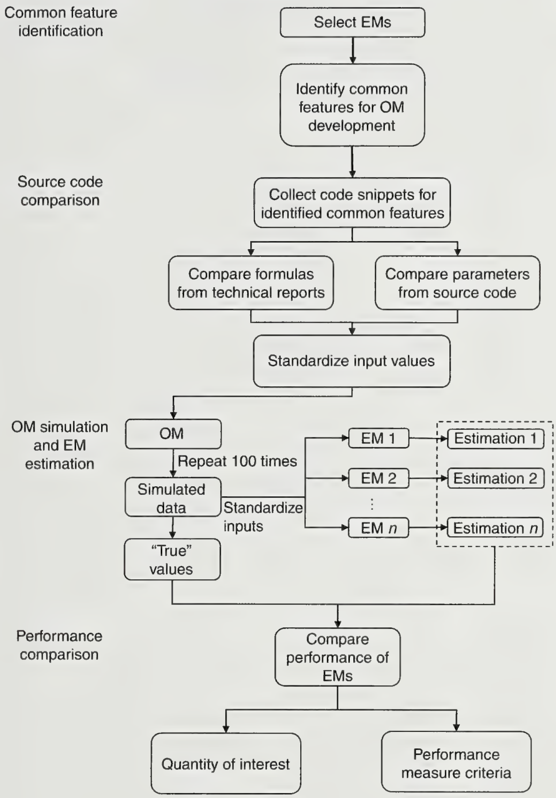
Common feature identification
Select EMs
Identify common features for OM development
Source code comparison
Collect code snippets for identified common features
Compare formulas from technical reports
Compare parameters from source code
Standardize input values
OM simulation and EM estimation
OM
Repeat 100 times
Simulated data
Standardize inputs
"True" values
EM 1
EM 2
EM *n*
Estimation 1
Estimation 2
Estimation *n*
Performance comparison
Compare performance of EMs
Quantity of interest
Performance measure criteria

Figure 1

Flow diagram of the processes used to compare 4 age-structured stock assessment models used in the United States. Steps 1 and 2, which compose the code comparison process, involve identification of common features and source code comparison of the estimation models (EMs). Steps 3 and 4, which compose the simulation-estimation process, involve operating model (OM) development, estimation with EMs, and comparison of performance between the EMs. Common features, input standardization, quantities of interest, and performance measures are described in the "Materials and methods" section and in Table 1. The "true" values include actual values used as inputs for development of the OM and simulated true values for quantities of interest.

Operating model and comparison cases

The OM developed in this study was an age-structured model, with parameter values describing life history obtained from Siegfried et al. (2016). That study simulated a population on the basis of an amalgam of life history traits common to species found in waters of the Atlantic Ocean off the southeastern United States. In our study, the OM population was simulated with an annual time step over 30 years and a maximum age of 12 years (Table 1, Suppl. Material [online only], Suppl. Table 1 [online only]). The OM null case (case 0) had one fishing fleet and one survey, with fully selected F linearly increasing with time. A time-invariant logistic selectivity function was used for both the fishing fleet and the survey in the null case. Fishery landings and survey abundance index data were simulated yearly with observation error from year 1 to year 30. The annual sample size was 200 samples for age composition data from both the fishery and survey. In all cases except case 12, the initial equilibrium recruitment was lowered from the unfished recruitment level as determined by an initial equilibrium F (spawning biomass per recruit based on F [ϕ_F] is less than unfished spawning biomass per recruit [ϕ_0], as in equation 3.4 provided in Supplementary Table 2 [online only]). The addition of case 12, for which the initial condition was equal to the unfished equilibrium population ($\phi_F=\phi_0$), as in equation 3.4 provided in Supplementary Table 2 (online only), allowed a comparison of methods for simulating the initial population. Details of parameter definitions and equations used to describe the OM under case 0 are presented in Table 1 and in the Supplementary Material (online only) (the code for creating the OM and comparing the EM results is available from website).

Eleven additional cases were explored to investigate the effects of recruitment variability, process error in F, patterns in F,

Table 1

Description and values for index variables, structural parameters, state variables, derived variables, and stochastic deviation used in the operating model to generate simulated data that served as inputs for the 4 age-structured stock assessment models evaluated in this study. Models were tested under different cases, including the null case (case 0), which has one fishing fleet and one survey, with fully selected fishing mortality rate (F) increasing linearly with time. Also provided are the value or expression in case 0 and indication of whether a parameter is estimated in the estimation model. The parameter natural mortality rate at age is assumed to be constant across years and age classes.

Symbol	Description	Case 0 value or expression	Estimated
Index variables			
y	Years	$\{1,2,\ldots,Y\}$ and $Y=30$	
a	Ages	$\{1,2,\ldots,A\}$ and $A=12+$	
Structural parameters			
l_∞	Asymptotic average length (in millimeters)	800	
K	Growth coefficient (per year)	0.18	
t_0	Age at mean length of zero (in years)	−1.36	
θ_1	Length–weight coefficient	2.50×10^{-8}	
θ_2	Length–weight exponent	3	
θ_3	Slope of maturity ogive	3	
a_{50}	Age at 50% maturity (in years)	2.25	
M_a	Natural mortality rate at age (per year)	0.2	
r_a	Proportion of females at each age	0.5	
$R0$	Median-unbiased unfished recruitment (in number)	1 million	Yes
h	Median-unbiased steepness	0.75	
x_1	Fishery selectivity slope	1	Yes
x_2	Fishery selectivity age at 50% selection (in years)	2	Yes
x_3	Survey selectivity slope	2	Yes
x_4	Survey selectivity age at 50% selection (in years)	1.5	Yes
f_y	Shape of the fully selected F in year y	Linear increase with $f_1=0.01$ and $f_Y=0.40$	Yes
φ_F	Annual sample size for age composition of fishery landings	200	
φ_I	Annual sample size for age composition of survey	200	
State variables			
R_y	Annual recruitment in year y (in number)		
SSB_y	Spawning biomass in year y (in metric tons of female biomass)		
$N_{a,y}$	Abundance at age a in year y (in number)		
A_y	Abundance in year y (in number)		
B_y	Biomass in year y (in metric tons)		
$L_{a,y}$	Landings at age a in year y (in number)		

(*Continued on next page*)

selectivity patterns, number of surveys, and bias adjustment of recruitment on performance of the EMs (Table 3). Because our goal was to demonstrate that the 4 EMs are similar at their core, we started with simple cases to compare the performance of the EMs before adding in additional complexity. It would have been harder to interpret the differences found in the results if more complicated cases had been included in the simulation. We did not implement these cases to evaluate how model misspecifications introduced in the EMs could affect the model estimates; therefore, we made the correct assumptions about parameters (e.g., fixing them at correct values) and governing processes (e.g., stock–recruit relationship and selectivity pattern).

Recruitment variability level In case 0, the standard deviation of annual recruitment variability (σ_R) in log space was 0.2. Two additional levels were explored to examine if higher recruitment variability with σ_R of 0.4 (case 1) and 0.6 (case 2) affected the performance of the EMs.

Process error in fishing mortality A comparison between case 3 and case 0 addressed the question of whether additional process error in F affected the performance of the EMs. In all cases, the standard deviation of the log fully selected F was used for generating annual deviations in fully selected F. In case 0, the same set of annual deviations was used for each iteration. In case 3, we randomly generated stochastic sets of annual deviations per iteration. Case 0 did not start with stochastic sets of annual deviations per iteration because it can be difficult to interpret differences in results if the process error in F is confounded with other settings or assumptions.

Table 1 (*continued*)

Symbol	Description	Case 0 value or expression	Estimated
L_y	Landings in year y (in metric tons)		
$I_{a,y}$	Survey abundance at age a in year y (in number)		
I_y	Survey abundance (sum across ages) in year y (in number)		
L'_y	Observed landings in year y (in metric tons) with noise		
$P_{L_{a,y}}$	Proportion at age a in year y for fishery landings		
$P'_{L_{a,y}}$	Observed proportion at age a in year y for fishery landings		
I'_y	Observed survey abundance in year y with noise (in number)		
$P_{I_{a,y}}$	Proportion at age a in year y for survey		
$P'_{I_{a,y}}$	Observed proportion at age a in year y for survey		
Derived variables			
l_a	Length at age a (in millimeters)		
w_a	Weight at age a (in metric tons)		
m_a	Proportion that reached maturity at age a		
ϕ_0	Unfished spawning biomass per recruit (in metric tons)		
$Z_{a,y}$	Total mortality rate at age a in year y		
$Fmult_y$	Fully selected F in year y (year^{-1})		
S_{F_a}	Fishery selectivity at age a		
S_{I_a}	Survey selectivity at age a		
Φ_a	Number of spawners per recruit at age		
ϕ_F	Spawning biomass per recruit given F (in metric tons)		
R_{eq}	Equilibrium recruitment (in number)		
q	Catchability coefficient for survey	3.46×10^{-7}	Yes
Stochastic deviation: process error			
σ_R	Standard deviation of log recruitment	0.2	
$Rdev_y$	Recruitment deviations in year y	$Rdev_y \sim N(0, \sigma_R^2)$	Yes
σ_F	Standard deviation of log fully selected F	0.2	
$fdev_y$	Fully selected F deviations in year y	$fdev_y \sim N(0, \sigma_F^2)$	Yes
Stochastic deviation: observation error			
CV_L	Coefficient of variation of fishery landings	0.05	
ε_{1_y}	Landings deviations in year y	$\varepsilon_{1_y} \sim N\left(0, \log\left(1 + CV_L^2\right)\right)$	
CV_I	Coefficient of variation for survey	0.2	
ε_{2_y}	Survey abundance deviations in year y	$\varepsilon_{2_y} \sim N\left(0, \log\left(1 + CV_I^2\right)\right)$	

Fishing mortality patterns In case 0, the fully selected F increased over time from a relatively low value (0.01) to a higher rate (F_{high}) (Fig. 2). Two additional trends in F were investigated on the basis of methods from Johnson et al. (2015) and Ono et al. (2015). In this study, the F either increased from a low value (0.01) to F_{high} during the first 24 years and then decreased to a lower rate (F_{low}; case 4; Fig. 2) or that F remained constant over time across 3 levels: F_{low}, the F that corresponds to maximum sustainable yield (F_{MSY}), or F_{high} (cases 5–7; Fig. 2). Values of F_{low} and F_{high} corresponded to 80% of maximum sustainable yield (MSY). Comparing cases 4–7 with case 0 allowed an evaluation of whether different fishing patterns affected the magnitude of error in estimating parameters of interest.

Selectivity patterns A comparison between case 8 and case 0 was used to examine the influence on assessment performance of using double-logistic selectivity for the fishery and the survey instead of simple logistic selectivity (case 0).

Multiple surveys Comparing case 9 (which includes 2 surveys with the same level of observation errors) with case 0 (which includes 1 survey) allowed an evaluation of whether use of an additional survey reduced error in estimating quantities of interest.

Bias adjustment of recruitment For case 10, the median-unbiased spawner-recruit parameters were used, whereas for case 11 the mean-unbiased spawner-recruit parameters were used to conduct a bias adjustment in the OM. The arithmetic mean curve of recruitment that is associated with the mean-unbiased spawner-recruit parameters is higher than the geometric mean curve of recruitment

Table 2

Comparison of features between the 4 age-structured estimation models (EMs) evaluated in this study: the Assessment Model for Alaska (AMAK), the Age Structured Assessment Program (ASAP), the Beaufort Assessment Model (BAM), and Stock Synthesis (SS). The letter *Y* indicates that the feature is implemented in the EM. *F*=fishing mortality rate.

Feature	AMAK	ASAP	BAM	SS
Age modeled	1+	1+	1+	0+/1+
Timing of spawning	Real month	Fraction	Fraction	Real month
Timing of survey	Real month	Real month	Fraction	Real month
Survey index unit	Biomass/number	Biomass/number	Biomass/number	Biomass/number
Spawner-recruit model				
Standard Beverton–Holt	Y	Y	Y	Y
Ricker	Y		Y	Y
Average recruitment	Y	Y	Y	Y
Bias adjustment of recruitment			Y	Y
Types of selectivity available				
Free parameter approach	Bound	Random walk	Logit	Random walk/logit
Simple-logistic function	Y	Y	Y	Y
Double-logistic function	Y (3 parameters)	Y (4 parameters)	Y (4 parameters)	Y (4 parameters)
Logistic-exponential function			Y	Y
Joint-logistic function			Y	Y
Double-Gaussian function			Y	Y
F in terminal year	Last year	Last year	Flexible	Last year
Definition of *F*	Flexible	Apical *F*	Apical *F*	Flexible
Likelihoods available				
Landings, lognormal	Y	Y	Y	Y
Survey index, lognormal	Y	Y	Y	Y
Age composition, standard multinomial	Y	Y	Y	Y
Age composition, Dirichlet multinomial			Y	Y
Priors				
None	Y	Y	Y	Y
Lognormal	Y	Y	Y	Y
Beta			Y	Y
Normal			Y	Y
Reference or website (see for details of other features)	website	website	Williams and Shertzer (2015)	website

that is associated with median-unbiased spanwer-recruit parameters because of lognormal deviation in recruitment residuals (Methot and Taylor, 2011).

Bias adjustment is handled differently in the 4 EMs. In the BAM, a bias adjustment is applied when median-unbiased parameters are used to compute equilibrium recruitment for the spawner-recruit model (Suppl. Table 3) (online only) (Williams and Shertzer, 2015). In contrast, in SS, mean-unbiased parameters are used for the spawner-recruit model, and then a bias adjustment is applied when computing annual recruitment (Suppl. Table 3) (online only) (Methot and Taylor, 2011). In the AMAK and ASAP, bias adjustment is not included as part of the internal machinery. Details of differences between the EMs are documented in the "Spawner-recruit parameters in bias adjustment of recruitment" subsection of the "Results" section and in Supplementary Table 3 (online only). For cases 10 and 11, σ_R was set to 0.6 to make the differences in estimates noticeable, if any were present. We also adjusted the estimates of MSY-based reference points from the AMAK and ASAP with the BAM bias adjustment method in case 10 to make estimates comparable among all 4 EMs (Suppl. Figs. 1 and 2) (online only). We adjusted the estimates of unfished recruitment (*R0*) and steepness (*h*) to mean-unbiased values and then adjusted MSY-based reference points from the AMAK and ASAP in case 11 (Suppl. Figs. 1 and 2) (online only). The estimates from cases 10 and 11 were compared with the estimates from case 2 to quantify the effect of bias adjustment methods on EM performance.

Estimation models

Four EMs were evaluated in this study. The AMAK was compiled with AD Model Builder, vers. 12.1, from source code available on GitHub (website, accessed November 2019). We used the executable file of the ASAP, vers. 3.0.16, available on the National Marine Fisheries Service Integrated Toolbox website (accessed December 2019). For the BAM, the source code is available from the authors or in the appendix of a NOAA publication (Williams and Shertzer, 2015) and was compiled by using AD Model Builder. We used the executable file of SS, vers. 3.30.15,

Table 3

Settings for recruitment variability (σ_R), deviations in fishing mortality rates (F), patterns of F, selectivity patterns, and recruitment bias adjustment in the operating model (OM) that was used to evaluate 4 age-structured stock assessment models under different cases. A dash denotes that the value or information is the same as that given for the null case (case 0). For case 0, the OM creates the same set of F deviations for a given iteration. For case 3, the OM randomly generates a unique set of F deviations per iteration. F_{low}=low F value; F_{MSY}=F that corresponds to maximum sustainable yield; F_{high}=high F value; ϕ_F=spawning biomass per recruit based on F; ϕ_0=unfished spawning biomass per recruit; $R0$=unfished recruitment; and h=steepness.

		Details						
Setting	Case	σ_R	F deviations	F patterns	Fishery and survey selectivity	No. of surveys	Bias adjustment	Initial condition
Null case	0	0.2	Same iteration	Increase	Simple-logistic	1	No	$\phi_F \neq \phi_0$
Recruitment variability	1	0.4	–	–	–	–	–	–
	2	0.6	–	–	–	–	–	–
Stochastic F	3	–	Stochastic iteration	–	–	–	–	–
F patterns	4	–	–	Roller coaster	–	–	–	–
	5	–	–	Constant F_{low}	–	–	–	–
	6	–	–	Constant F_{MSY}	–	–	–	–
	7	–	–	Constant F_{high}	–	–	–	–
Double-logistic selectivity	8	–	–	–	Double-logistic	–	–	–
Multiple surveys	9	–	–	–	–	2	–	–
Recruitment bias adjustment	10	0.6	–	–	–	–	Yes (median-unbiased $R0$ and h)	–
	11	0.6	–	–	–	–	Yes (mean-unbiased $R0$ and h)	–
Initial condition	12	–	–	–	–	–	–	$\phi_F = \phi_0$

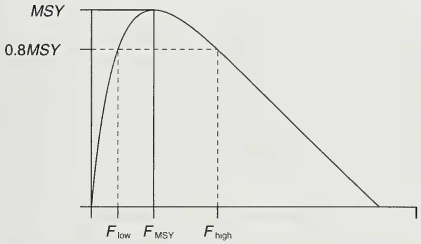

Figure 2

The curve of the relationship of yield and fishing mortality rate (F) and the definitions of the low F value (F_{low}) and the high F value (F_{high}) used in creation of various patterns of F in the operating model. The horizontal black line indicates maximum sustainable yield (MSY), and the dashed gray lines indicate 0.8*MSY*, which corresponds to F_{low} and F_{high}. The vertical black line indicates the F that corresponds to MSY (F_{MSY}).

available from the NOAA Virtual Laboratory (website, accessed November 2019).

The 4 EMs estimated time series of spawning stock biomass (SSB), recruitment, F, abundance, biomass, and landings in weight. Annual age composition of landings from the fleet and from surveys was also estimated. The annual F values used in the comparison were apical F values. The common output of biological reference points used in the comparison project included MSY, F_{MSY}, and SSB at MSY (SSB_{MSY}). The relative F (calculated as F/F_{MSY}) and relative SSB (calculated as SSB/SSB_{MSY}) for MSY-based reference points were also examined.

Performance measures

For each of the cases, performance of the EMs was evaluated by comparing estimated values against the true values from the OM. The quantities of interest included $R0$, F in the "terminal" year ($F_{terminal}$), $SSB_{terminal}$, MSY, F_{MSY}, SSB_{MSY}, relative F, and relative SSB. To evaluate performance related to a management application (e.g., stock status determination), F_{limit} was set to F_{MSY} and SSB_{limit} was set to half of SSB_{MSY} (Federal Register, 1998; Restrepo et al., 1998; Gabriel and Mace, 1999; Methot et al., 2014). The estimated values of F/F_{limit} and SSB/SSB_{limit} from the EMs were compared with the true values from the OM to verify whether the estimated stock status (i.e., overfished or overfishing) matched the true status.

The bias and variability of the bias of the EMs were determined by calculating relative error (RE) and median absolute relative error (MARE) for key parameters. The RE and MARE for each EM within a case were calculated as follows:

$$RE_{\text{i,j,t}} = (E_{\text{i,j,t}} - T_{\text{i,j,t}}) \,/\, T_{\text{i,j,t}} \text{ and} \tag{1}$$

$$MARE_{\text{i,t}} = median(\,|RE_{\text{i,j,t}}|\,), \tag{2}$$

where E = the estimated quantity of interest;
T = the true value from the OM;
i = the quantity of interest;
j = the iteration number; and
t = the year, if applicable.

For evaluating performance related to making stock status determinations (i.e., using F/F_{limit} and SSB/SSB_{limit}), the accuracy of each model under a case equals the number of correctly identified positives and negatives divided by the total number of iterations.

Results

Code comparison process

Identification of common features The structure of the OM and cases were defined on the basis of the similarities and differences found among the 4 EMs (Table 2). On the basis of the comparisons, we found that the common available spawner-recruit model among the EMs is the compensatory Beverton–Holt spawner-recruit model (Beverton and Holt, 1957) with lognormally distributed recruitment deviations. For selectivity patterns, all of the EMs have both a simple-logistic function and a double-logistic function. For the double-logistic function, the ASAP, BAM, and SS each require 4 parameters, and the AMAK requires 3 parameters. Bias adjustment of estimated mean recruitments is implemented in only the BAM and SS. For some features (e.g., available selectivity patterns), some of the EMs have more options than those listed in Table 2. We limited the options to features available in at least 2 EMs. All available options can be found in the technical manual for each EM. Differences among other features have been summarized in Dichmont et al. (2016), Dichmont et al.[1], and Punt et al. (2020).

Basic settings to ensure similar configurations Results of the comparison of formulas used in source code for key features indicate that analysts can manually adjust some basic settings to ensure that all 4 EMs are configured similarly and to ensure that a comparison study is effective. For example, in the AMAK, ASAP, and BAM, the population starts at age 1, but in SS the population routinely starts at age 0 and can be configured to start at older ages, as was done for this study. Survey index units, biomass or number of fish, can be used as input for the ASAP, BAM, and SS. In the AMAK, the default unit is biomass, but numbers could be used by setting all entries in the weight-at-age matrix to the value of 1.

Selectivity-at-age outputs can be used directly for comparison, but estimated selectivity parameters need to be further converted before being compared because they are modeled differently in EMs. The simple logistic selectivity in the AMAK and BAM share the same formula as the OM (i.e., equation 5.1 from Supplementary Table 1 [online only]). In the ASAP and SS, simple-logistic selectivity is calculated as follows:

$$S_{\text{F}_\text{a}} = \frac{1}{1 + \text{e}^{-(\text{a} - \mu_1)/\mu_2}} \text{and} \tag{3}$$

$$S_{\text{F}_\text{a}} = \frac{1}{1 + \text{e}^{-\ln(19)(\text{a} - \text{v}_1)/\text{v}_2}}, \text{ respectively,} \tag{4}$$

where S_{F_a} = fishery selectivity at age;
μ_1 = age at 50% selection parameter (equal to x_2 from equation 5.1 in Supplementary Table 1 [online only], where x_2 is age at 50% selection parameter);
μ_2 = slope parameter (equal to $1/x_1$ from equation 5.1 in Supplementary Table 1 [online only]);
a = ages;
v_1 = age at 50% selection for fishery parameter (equal to x_2 from equation 5.1 in Supplementary Table 1 [online only]); and
v_2 = slope parameter (equal to $\ln(19)/x_1$ from equation 5.1 in Supplementary Table 1 [online only]).

Similarly, the BAM and SS share the same double-logistic selectivity formula (Equation 5), and the formula from the AMAK (Equation 6) and ASAP (Equation 7) are different. Consequently, parameter values cannot be directly compared between models. However, the resultant curves and selectivity at age can be compared with the following equations:

$$S'_{\text{F}_\text{a}} = \frac{1}{1 + \text{e}^{-x_1(\text{a} - x_2)}} \left(1 - \frac{1}{1 + \text{e}^{-\beta_1(\text{a} - \beta_2)}}\right) \text{ and} \tag{5}$$

$$S_{\text{F}_\text{a}} = S'_{\text{F}_\text{a}} \,/\, \max(S'_{\text{F}_\text{a}});$$

$$\gamma_1 = p_1 + p_2, \tag{6}$$

$$\gamma_2 = p_1 + y_1 + p_3, \text{ and}$$

$$S_{\text{F}_\text{a}} = \frac{1}{1 + \text{e}^{\frac{-\ln(19)(\text{a} - \gamma_1)}{\text{p}_1}}} \left(1 - \frac{1}{1 + \text{e}^{\frac{-\ln(19)(\text{a} - \gamma_2)}{\text{p}_3}}}\right) / \, 0.95^2; \text{ and}$$

$$S'_{\text{F}_\text{a}} = \frac{1}{1 + \text{e}^{-\frac{\text{a} - \mu_1}{\mu_2}}} \left(\frac{1}{1 + \text{e}^{\frac{\text{a} - \mu_3}{\mu_4}}}\right) \text{and} \tag{7}$$

$$S_{\text{F}_\text{a}} = S'_{\text{F}_\text{a}} \,/\, \max(S'_{\text{F}_\text{a}}),$$

where S'_{F_a} = fishery selectivity at age before rescaling to ensure that it peaks at 1;

x_1 = first slope of the double-logistic selectivity function;
x_2 = first inflection point of the double-logistic selectivity function;
β_1 = second slope of the double-logistic selectivity function;
β_2 = second inflection point of the double-logistic selectivity function;
γ_1 = first inflection point of the selectivity function;
γ_2 = second inflection point of the selectivity function;
p_1 = distance between first inflection point and age at 95% selection;
p_2 = parameter to be used with p_1 to get first inflection point of the selectivity function;
p_3 = second slope of the selectivity function;
μ_1 = first inflection point of the double-logistic selectivity function;
μ_2 = first slope of the double-logistic selectivity function;
μ_3 = second inflection point of the double-logistic selectivity function; and
μ_4 = second slope of the double-logistic selectivity function.

Spawner-recruit parameters in bias adjustment of recruitment

In both the models in which a bias adjustment to recruitment was applied, the BAM and SS, the mean-unbiased relationship is used for estimating MSY-based reference points. The F_{MSY} from the OM was based on searching for the F that provides maximum equilibrium catch. The calculation started with computing equilibrium recruitment at F and involved the same equations that were used to calculate the initial equilibrium conditions (equation 3.4 in Supplementary Table 1 [online only]). That step of calculation involved $R0$ (Suppl. Table 3) (online only), and the use of $R0$ in the calculation results in differences in estimated MSY-based reference points depending on how bias adjustment of recruitment was addressed in each EM. The median-unbiased spawner-recruit parameters from the BAM correspond to the geometric mean curve of recruitment, and the mean-unbiased parameters from SS correspond to the arithmetic mean curve of recruitment (Table 4, Suppl. Table 3 [online only]).

For direct comparisons, we derived a function to convert combinations of median-unbiased $R0$ and h to mean-unbiased values, or to convert mean-unbiased values to median-unbiased values, when the Beverton–Holt spawner-recruit model was used. The derivation of the median-unbiased approach starts with calculating the median-unbiased $R0$ by using the Beverton–Holt model:

$$R0 = \frac{0.8R0hS0}{0.2\phi_0 R0\left(1-h\right)+\left(h-0.2\right)S0}, \tag{8}$$

where $S0$ = unfished spawning biomass.

Given that the bias adjustment component b equals $e^{\sigma_R^2/2}$, the mean-unbiased $R0'$ that corresponds to the arithmetic mean curve of recruitment is determined with this equation:

$$R0' = \frac{b0.8R0hS0'}{0.2\phi_0 R0\left(1-h\right)+\left(h-0.2\right)S0'}, \tag{9}$$

where $S0'$ = the mean-unbiased unfished SSB.

Then, following the derivations below, the bias-adjusted mean-unbiased $S0'$ can be obtained:

$$0.2\phi_0 R0\left(1-h\right)+\left(h-0.2\right)S0' = \frac{b0.8R0hS0'}{R0'} \tag{10}$$

$$= b0.8R0h\phi_0,$$

$$0.2R0\left(1-h\right)+\left(h-0.2\right)\frac{S0'}{\phi_0} = b0.8R0h,$$

$$\left(h-0.2\right)\frac{S0'}{\phi_0} = b0.8R0h - 0.2R0\left(1-h\right), \text{ and}$$

$$S0' = \frac{b0.8R0h\phi_0 - 0.2R0\left(1-h\right)\phi_0}{h-0.2}.$$

When converting median-unbiased values to mean-unbiased values, the bias adjustment component b equals $e^{\sigma_R^2/2}$. Inputs of the conversion function include median-unbiased $R0$, h, and ϕ_0. The outputs of the conversion include adjusted unfished SSB ($S0_b$), adjusted unfished recruitment ($R0_b$), and adjusted steepness (h_b) in mean-unbiased levels:

$$S0_b = \frac{b0.8R0h\phi_0 - 0.2\phi_0 R0(1-h)}{h-0.2}, \tag{11}$$

$$R0_b = \frac{S0_b}{\phi_0}, \tag{12}$$

$$R_{\mathrm{new}} = \frac{b0.8R0h0.2S0_b}{0.2\phi_0 R0(1-h)+(h-0.2)0.2S0_b}, \text{ and} \tag{13}$$

$$h_b = \frac{R_{\mathrm{new}}}{R0_b}, \tag{14}$$

where R_{new} = recruitment when the SSB is 20% of its unfished level.

When converting mean-unbiased values to median-unbiased values, b equals $e^{-\sigma_R^2/2}$, and the inputs from the equation (Equation 11) need to be mean-unbiased values (the outputs are median-unbiased $S0_b$, $R0_b$, and h_b). Without these conversions, the difference between mean- and median-unbiased $R0$ and the difference between mean- and median-unbiased h gradually increased when the true median-unbiased h was reduced and when σ_R was increased (Fig. 3).

Simulation-estimation process

Null case (case 0) Model parameters of $R0$ and catchability (q) were accurately estimated in all EMs with low bias.

Table 4

Methods for bias adjustment of recruitment from 2 of the age-structured stock assessment models evaluated in this study: the Beaufort Assessment Model (BAM) and Stock Synthesis (SS). MSY=maximum sustainable yield; *R0*=unfished recruitment.

Parameter	BAM method	SS method
Unfished recruitment	Median-unbiased *R0* as input Median-unbiased *R0* and mean-unbiased *R0* as output	Mean-unbiased *R0* as input and output
Unfished biomass	Based on mean-unbiased *R0*	Based on mean-unbiased *R0*
Equilibrium recruitment	Mean-unbiased	Mean-unbiased
Spawner-recruit parameters	Median-unbiased	Mean-unbiased
MSY-based reference points	Mean-unbiased	Mean-unbiased

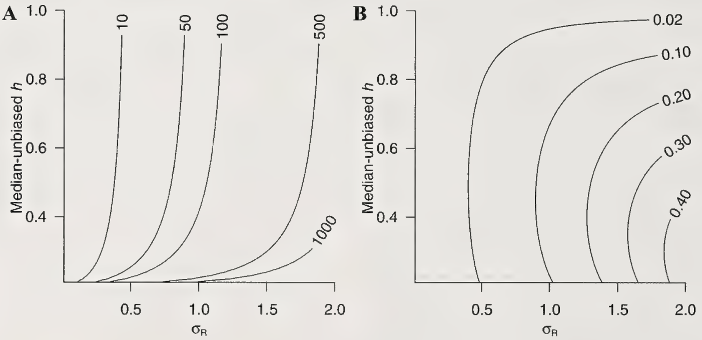

Figure 3

(**A**) Relative difference (%) in unfished recruitment (*R0*) and (**B**) difference in steepness (*h*) over possible combinations of median-unbiased *h* and standard deviation of log recruitment (σ_R), both indicated by the contour lines. The differences were determined by using the spawner-recruit parameter conversion function. Relative difference in unfished recruitment is defined as 100(mean-unbiased *R0*–median-unbiased *R0*)/median-unbiased *R0*. Relative difference in steepness is defined as mean-unbiased *h*–median-unbiased *h*.

The MAREs of *R0* and *q* were below 10% for all EMs (Table 5). The median *R0* over 100 iterations from the AMAK was generally lower compared with the estimates from the other EMs (cases 0–9), indicating that the AMAK initializes the population differently compared with the OM (Fig. 4). For case 12, in which the initial condition was simulated for an unfished equilibrium population, the estimated *R0* from the AMAK was similar to the estimates from the other EMs (Fig. 4).

Under case 0, the estimated median selectivity at age over 100 iterations from all EMs has almost identical patterns compared with the selectivity curves based on true values from fishery and survey sources (Suppl. Fig. 3) (online only). The MAREs of MSY, F_{MSY}, and SSB_{MSY} were below 10% (Table 6), and the REs indicate similar variability among all EMs (Fig. 5). The AMAK produced relatively lower MSY and SSB_{MSY}, along with a lower estimate of *R0*, compared with the true values and estimates from the other stock assessment models. The REs for SSB, *R*, *F*, relative SSB, and relative *F* centered around zero over time and had similar variability patterns (Fig. 6, Suppl. Figs. 4–8 [online only]). The accuracy of stock status determination was 100% for overfished status determination, and the accuracy of the overfishing status was 100% in most but not all years (Fig. 7).

Recruitment variability level The 4 EMs accurately estimated model parameters, but the range of RE increased when σ_R increased. The MARE in key parameters increased when σ_R increased from the null case value of 0.2 (Tables 5 and 6).

Table 5

Median absolute relative error (%) for the model parameters unfished recruitment ($R0$) and catchability of survey abundance index (q) from each simulated case used to compare the 4 age-structured stock assessment models used most commonly in the United States: the Assessment Model for Alaska (AMAK), the Age Structured Assessment Program (ASAP), the Beaufort Assessment Model (BAM), and Stock Synthesis (SS).

	$R0$				q			
Case	AMAK	ASAP	BAM	SS	AMAK	ASAP	BAM	SS
Case 0	3.05	3.87	3.86	3.88	1.60	1.67	1.68	1.63
Case 1	5.69	5.72	5.68	5.80	2.27	2.26	2.24	2.19
Case 2	8.10	8.63	8.60	8.79	2.14	2.14	2.14	2.14
Case 3	2.81	2.68	2.67	2.72	1.92	1.99	1.98	1.93
Case 4	3.25	3.20	3.18	3.18	1.77	1.87	1.87	1.83
Case 5	4.45	4.30	4.28	4.20	4.09	3.88	3.85	4.11
Case 6	3.40	3.73	3.71	3.57	1.99	1.99	2.02	2.05
Case 7	3.97	3.53	3.17	3.12	1.96	2.15	2.04	2.11
Case 8	4.15	3.94	3.84	3.72	3.56	3.44	3.88	3.42
Case 9	3.15	2.97	2.95	2.98	3.17	1.79	1.79	1.80 (survey1)
Case 9	3.15	2.97	2.95	2.98	3.28	1.61	1.62	1.73 (survey2)
Case 10	7.83	9.08	9.26	9.28	1.86	1.95	1.92	1.88
Case 11	7.13	8.77	8.74	8.81	2.06	2.04	2.06	2.01
Case 12	3.04	2.96	2.95	2.67	2.20	2.19	2.22	2.14

The range of RE in MSY-based reference points became wider when recruitment variability increased (Fig. 5). Furthermore, the increased variability in SSB_{MSY} induced a wider range of RE in relative SSB (Table 6, Fig. 6). The accuracy of determining overfishing status for all EMs was not greatly affected by changes in recruitment variability, and the same trends were retained over time compared with the accuracy trends for the null case (Fig. 7, Suppl. Figs. 7 and 8 [online only]). The accuracy of determining overfished status was 100% over time for all EMs.

Process error in fishing mortality There were no considerable differences found in key parameter estimates when examining the effect of process error in F (case 3 versus case 0 in Figures 5 and 6). For all 4 EMs, RE patterns and estimates of key parameters were almost identical. However, the accuracy of the overfishing determination from case 3 fluctuated at levels under 100% for a longer period than that from case 0, although the true F values were not always close to the true F_{MSY} (Fig. 7). This result indicates that incorporating stochastic sets of annual deviations in F induces sensitivity in the determination of overfishing, but the overall accuracy of the overfishing determination was still high with values often exceeding 94%. The accuracy of determining an overfished status was still 100% over time for all EMs.

Fishing mortality patterns The EMs produced low MARE in estimates of key parameters when patterns of F were different. The variability of RE in all 4 EMs was consistently higher than in case 0 when the F pattern was a constant F_{low}, indicating that the estimates had greater bias when there was not much contrast between initial F and the later period of constant F (case 5 versus case 0 in Table 6 and Figures 5 and 6). When there was a fair amount of contrast in F across time, the MARE among the 4 models remained similar in trends and magnitude. Although accuracy in determining an overfished status was 100% for all EMs, the accuracy in determining overfishing status was consistently lower compared with that for other cases when F fluctuated around F_{MSY} (case 6 in Figure 7).

Selectivity patterns When both the fishing fleet and survey had double-logistic selectivity, the estimated median selectivity at age over 100 iterations from all 4 EMs was close to the true selectivity at age. The estimates of key parameters from all EMs were accurate compared with the true values from the OM (Table 5). The range of RE in key estimates became wider when the fishery and survey had double-logistic selectivity (case 8 versus case 0 in Table 6, Figure 6, and Supplementary Figures 3–8 [online only]), especially in the early years. For years when fishing was not near F_{MSY}, the overfishing status determination was 100% accurate, and the overfished status determination was 100% accurate over all years.

Multiple surveys The differences in key parameter estimates between case 9 and case 0 were not considerable (Fig. 5). However, the range of RE in SSB, recruitment, F, relative SSB, and relative F became narrower after an additional survey index with the same level of observation error

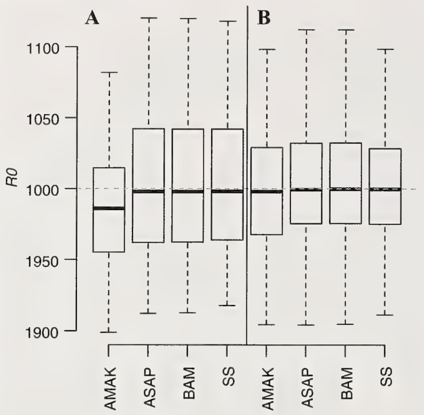

Figure 4

Box plots of true and estimated unfished recruitment (*R0*) from 4 age-structured estimation models under (**A**) case 0 and (**B**) case 12. The models, evaluated in this study for use in stock assessments, include the Assessment Model for Alaska (AMAK), the Age Structured Assessment Program (ASAP), the Beaufort Assessment Model (BAM), and Stock Synthesis (SS). The horizontal gray dashed line represents the true *R0* under the 2 cases. For case 0, which is the null case, initial equilibrium recruitment was lowered from the unfished recruitment level as determined by an initial equilibrium fishing mortality rate. For case 12, the initial condition was equal to the unfished equilibrium population. The upper and lower parts of each box represent the first and third quartiles (the 25th and 75th percentiles), and the thick horizontal line is the median. The whiskers extending above and below the box correspond to 1.5 times the interquartile range.

was included in case 9 (Table 6, Fig. 6, Suppl. Figs. 4–8 [online only]). Results were as expected, given that there was no reduction in bias but an increase in precision. The accuracy of determining overfishing and overfished status shared similar trends compared with case 0 (Fig. 7).

Bias adjustment of recruitment The accuracy of parameter estimates was high if, in the EMs, the conversion function was used before estimation when a bias adjustment of recruitment was incorporated in the OM. Median relative errors were close to zero for MSY-based reference points when the conversion function was used in the BAM and SS (Fig. 5). With ad hoc adjustment (i.e., after estimation) in the AMAK and ASAP, the median relative errors in MSY-based reference points were reduced (Fig. 5, Suppl. Figs. 1 and 2 [online only]). Estimated SSB, recruitment, and *F* remained highly accurate over time (Fig. 6). The trends in accuracy of stock status determination were similar to the trends from case 0 (Fig. 7).

Discussion

Similarity of estimates from the 4 models

In this study, the 4 stock assessment models, or EMs, produced similar estimates, an outcome that can be attributed to the fact that the models share similar mathematical and statistical attributes. Prior to our study, this supposition was expected to be true but was unverified. Under cases that are associated with different recruitment variability levels, process error in *F*, diverse patterns of *F*, various selectivity shapes, and multiple surveys, the median relative errors in key parameters remained low, and the variability of the REs were similar among the EMs. Of the 5 cases described here, the level of recruitment variability caused the most change in RE patterns. The range of REs in all 4 EMs became wider when recruitment variability increased and remained stable over other cases. Furthermore, the temporal trend in the accuracy of overfishing and overfished status determination was the same among the 4 EMs.

These findings indicate that the 4 EMs produce similar estimates when the same data are analyzed and the EMs are configured similarly. Nevertheless, the results would differ if different options of features are used for different EMs, depending on the stock-specific data and issues that assessment analysts must face. In practice, stock assessment analysts may make different configuration choices given the same data and the same model. We encourage analysts to clearly document the assumptions made in an assessment, especially when the analysis involves comparisons among multiple models. In addition, model misspecification may result from different assumptions about parameters, governing processes, and statistical properties that can have a substantial effect on stock assessment results and subsequent management advice (Piner et al., 2011; Maunder and Piner, 2015). More simulation-estimation studies could be done to quantify the effect of model misspecification on model estimates.

The fundamental differences in mathematical and statistical attributes found in this study could also serve as a starting point for diagnostics that can be used to identify the source of variation. In addition to confirming similar estimates, we identified that different approaches of computing initial numbers at age induced differences in estimates, especially those associated with *R0* and MSY-based reference points. Estimates among the 4 EMs also differed if bias adjustment of recruitment was not addressed carefully. The effects of the initial numbers at age setup and recruitment bias adjustment on EM performance are discussed in detail in subsequent sections. We also noticed that determining the overfishing status was not 100% accurate across time because, in the binary classification applied in our study, the overfishing determination was based on the maximum likelihood estimate. Use of the estimated model uncertainty interval may better capture the true overfishing determination. Aggregating this binary determination over years from one EM and using

Table 6

Median absolute relative error (%) in maximum sustainable yield (MSY), fishing mortality rate that corresponds to MSY (F_{MSY}), spawning stock biomass at MSY (SSB_{MSY}), SSB, recruitment (R), fishing mortality rate (F), relative SSB, and relative F for each case used to compare the 4 age-structured stock assessment models evaluated in this study: the Assessment Model for Alaska (AMAK), the Age Structured Assessment Program (ASAP), the Beaufort Assessment Model (BAM), and Stock Synthesis (SS).

	MSY				F_{MSY}				SSB_{MSY}			
Case	AMAK	ASAP	BAM	SS	AMAK	ASAP	BAM	SS	AMAK	ASAP	BAM	SS
Case 0	3.25	4.10	4.07	3.84	1.04	1.04	1.04	1.04	3.13	3.91	3.95	3.92
Case 1	5.47	5.83	5.80	5.77	1.04	1.04	1.04	1.04	5.69	5.68	5.62	5.67
Case 2	7.90	9.02	8.97	9.08	1.04	1.04	1.04	1.04	8.17	8.48	8.42	8.78
Case 3	3.06	2.76	2.74	2.81	1.04	1.04	1.04	1.04	3.03	2.67	2.76	2.65
Case 4	3.41	3.17	3.12	3.20	1.04	1.04	1.04	1.04	3.33	3.28	3.16	3.30
Case 5	4.57	4.43	4.42	4.09	1.04	1.04	1.04	1.04	4.63	4.28	4.37	4.08
Case 6	3.13	3.39	3.36	3.44	1.04	1.04	1.04	1.04	3.32	3.66	3.63	3.51
Case 7	4.06	3.55	3.40	3.28	1.04	1.04	1.04	1.04	4.08	3.32	3.26	3.10
Case 8	4.07	4.02	3.98	3.62	1.22	1.22	1.22	1.22	3.96	3.78	3.79	3.75
Case 9	3.22	3.24	3.23	3.24	1.04	1.04	1.04	1.04	3.14	3.00	2.88	2.92
Case 10	7.68	9.70	9.75	9.50	0.98	0.98	0.98	0.98	7.99	9.52	9.50	9.27
Case 11	7.19	9.10	9.12	9.17	0.98	0.98	0.98	0.98	6.83	8.55	8.56	8.77
Case 12	3.09	3.01	2.97	2.57	1.04	1.04	1.04	1.04	3.13	2.92	3.05	2.59

	SSB				R				F			
Case	AMAK	ASAP	BAM	SS	AMAK	ASAP	BAM	SS	AMAK	ASAP	BAM	SS
Case 0	2.11	2.11	2.12	2.07	3.82	3.80	3.80	3.81	2.74	2.67	2.67	2.63
Case 1	1.93	2.03	2.03	2.00	3.87	3.94	3.93	3.92	2.46	2.50	2.49	2.49
Case 2	2.08	2.07	2.07	2.06	4.17	4.17	4.17	4.17	2.58	2.63	2.63	2.58
Case 3	2.01	2.09	2.09	2.07	3.72	3.75	3.74	3.75	2.42	2.44	2.45	2.40
Case 4	1.75	1.77	1.76	1.76	3.83	3.82	3.82	3.80	2.34	2.35	2.35	2.27
Case 5	4.00	3.92	3.94	3.95	4.78	4.79	4.77	4.71	4.21	4.23	4.25	4.22
Case 6	2.07	2.13	2.13	2.13	3.87	3.90	3.92	3.91	2.49	2.61	2.62	2.60
Case 7	1.73	1.98	1.79	1.77	3.72	3.85	3.64	3.62	2.37	2.72	2.50	2.48
Case 8	3.62	4.93	5.95	4.18	4.15	4.20	4.25	4.15	3.45	4.66	4.92	4.04
Case 9	1.68	1.53	1.54	1.51	3.19	3.20	3.21	3.19	2.01	1.87	1.87	1.84
Case 10	2.01	2.04	2.04	2.03	4.25	4.26	4.23	4.27	2.65	2.68	2.64	2.64
Case 11	2.02	2.02	2.02	2.00	4.17	4.13	4.13	4.15	2.59	2.58	2.58	2.55
Case 12	2.01	2.05	2.05	1.95	3.81	3.79	3.79	3.86	2.61	2.61	2.63	2.47

	Relative SSB				Relative F			
Case	AMAK	ASAP	BAM	SS	AMAK	ASAP	BAM	SS
Case 0	3.73	4.29	4.31	4.30	2.06	2.10	2.03	2.01
Case 1	5.99	6.39	6.39	6.51	2.06	2.04	2.01	2.02
Case 2	8.19	9.83	9.75	9.95	2.16	2.22	2.12	2.17
Case 3	3.67	3.28	3.25	3.19	2.08	2.17	2.14	2.13
Case 4	3.80	3.80	3.80	3.69	1.85	1.90	1.86	1.87
Case 5	3.40	3.24	3.20	3.18	3.98	4.00	3.92	3.96
Case 6	3.68	4.44	4.45	4.31	2.21	2.38	2.26	2.27
Case 7	4.44	4.50	4.14	4.13	1.96	2.26	2.00	1.98
Case 8	3.98	5.50	5.97	4.99	3.29	4.40	4.96	3.81
Case 9	3.43	3.46	3.45	3.46	1.76	1.74	1.68	1.69
Case 10	8.25	9.73	9.71	10.14	2.06	2.06	2.06	2.09
Case 11	7.83	9.43	9.41	9.77	2.08	2.06	2.07	2.09
Case 12	3.49	3.51	3.52	3.04	2.13	2.08	2.08	2.01

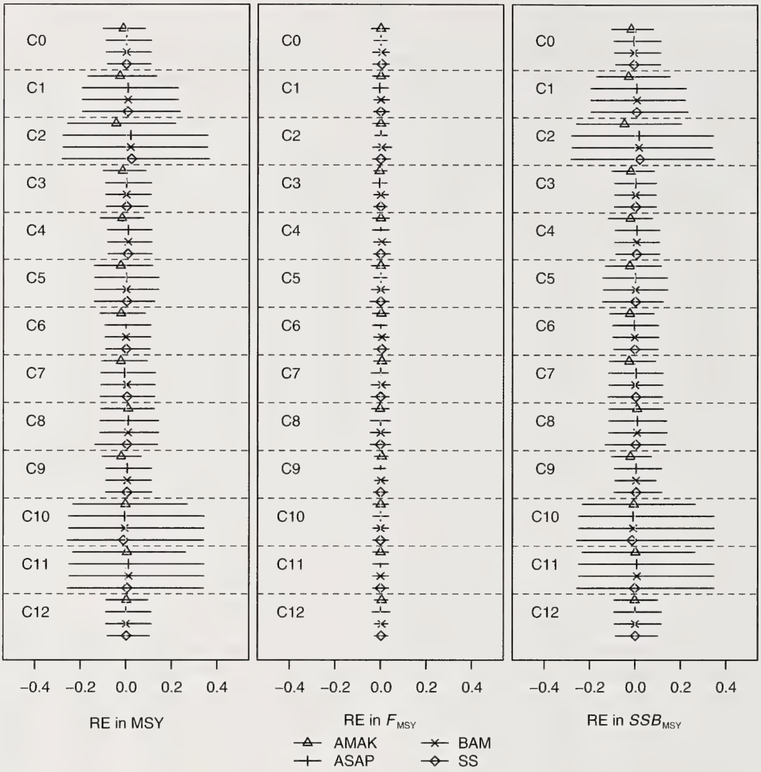

Figure 5

Relative error (RE) in maximum sustainable yield (MSY), fishing mortality rate that corresponds to MSY (F_{MSY}), and spawning stock biomass at MSY (SSB_{MSY}) for 4 age-structured estimation models under cases 0–12 (C0–C12). The models, evaluated in this study for use in stock assessments, include the Assessment Model for Alaska (AMAK), the Age Structured Assessment Program (ASAP), the Beaufort Assessment Model (BAM), and Stock Synthesis (SS). The bar is equivalent to the whisker of a box plot. The left bar represents the smallest value larger than 1.5 times the interquartile range below the first quartile. The right bar represents the largest value smaller than 1.5 times the interquartile range above the third quartile. The symbols in the center represent median RE.

receiver operating characteristic curves may also help summarize the overall degree of agreement (e.g., true positive and false negative classifications, accuracy rate, error rate, and sensitivity) between estimates and true status (Connors and Cooper, 2014; Cortés and Brooks, 2018).

Examination of the value of the code comparison process

This study is unique among other model comparison studies because a code comparison process was included before the simulation-estimation process. Identifying common features among the EMs and comparing source code can reduce contamination by parameter misspecification or analyst effect if the parameters are fixed in a comparison study. Although we estimated selectivity in this comparison study, during the early stage of the study, we fixed the selectivity at the true values. It is important to carefully apply fixed values because, in the 4 models, simple logistic selectivity was defined with parameters that had the same name (e.g., slope) but different interpretations. Otherwise,

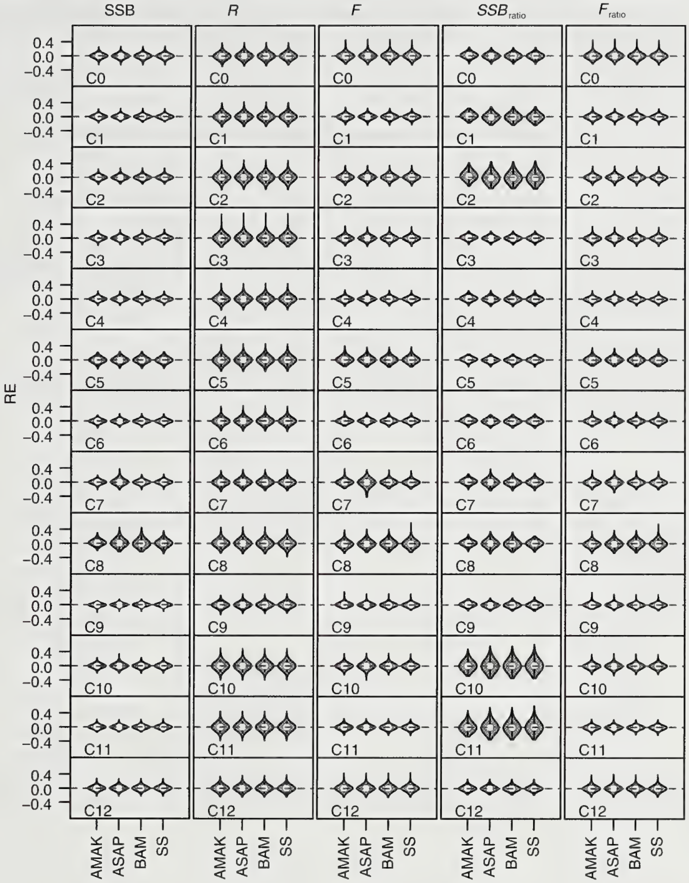

Figure 6

Violin plot of relative error (RE) across years and iterations for spawning stock biomass (SSB), recruitment (R), fishing mortality rate (F), SSB_{ratio} (ratio of SSB to SSB at maximum sustainable yield [MSY]), and F_{ratio} (ratio of F to F at MSY) for each of 4 estimation models under cases 0–12 (C0–12). The models, evaluated in this study for use in stock assessments, include the Assessment Model for Alaska (AMAK), the Age Structured Assessment Program (ASAP), the Beaufort Assessment Model (BAM), and Stock Synthesis (SS).

differences in estimates might have been forced unwittingly, because of parameter misspecification.

In addition to differences in selectivity parameterization, we also identified differences in how age is modeled in the EMs. If ages modeled in SS start with age 0 (the default) and not age 1, a mismatch between SS and the other EMs would have been induced. In this case, the mismatch would manifest only in scaling of recruitment to account for natural mortality at age 0. Therefore, identification of common features and comparison of source codes are particularly important in cross-testing a set of assessment models. The comparison framework developed (Fig. 1) and the approach

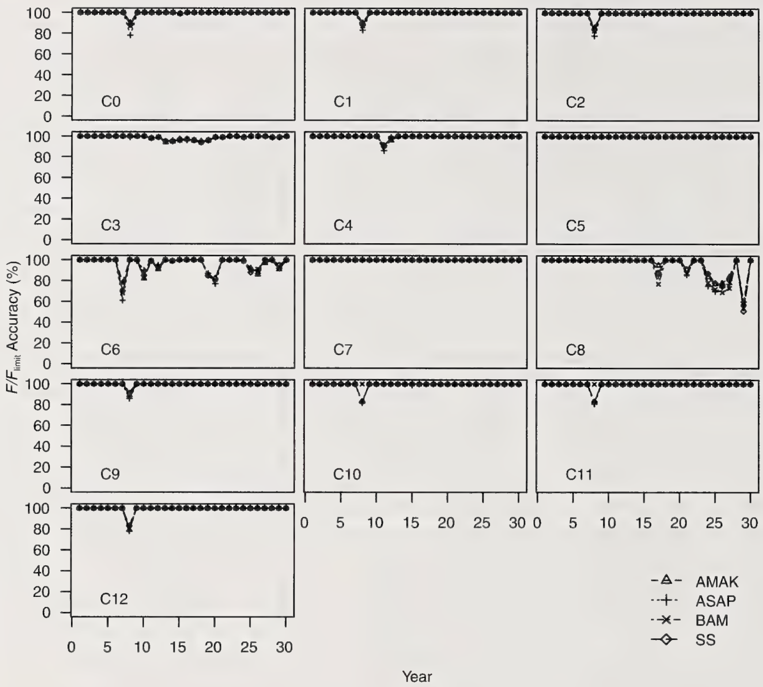

Figure 7

Accuracy (%) of determining overfishing status over time for each of 4 estimation models under cases 0–12 (C0–C12). Overfishing status is determined by dividing fishing mortality rate (F) by F_{limit}, which was set to the F that corresponds to maximum sustainable yield. The models, evaluated in this study for use in stock assessments, include the Assessment Model for Alaska (AMAK), the Age Structured Assessment Program (ASAP), the Beaufort Assessment Model (BAM), and Stock Synthesis (SS).

to identification of common features used (Table 2) in this study could be applied to multi-model comparisons in other studies. They might also prove useful in ensemble modeling, which is now gaining traction in fisheries science as a means to combine the estimates from multiple stock assessment methods (Brodziak and Legault, 2005; Brodziak and Piner, 2010). Ensemble modeling loosens the assumptions associated with selecting a single "best" assessment model (Rosenberg et al., 2018). Stewart and Martell (2015) proved that ensemble modeling benefits from guidelines for developing sets of candidate models. The steps developed in this study to identify common features across alternative models may facilitate selection of plausible models and identification of the sources of differences among estimates before constructing an ensemble.

Examination of similarity in initial numbers at age

The approach used in each EM to estimate the initial numbers at age depends on 3 factors: the selected initial year; the level of fishing, if any, that typically occurred prior to that initial year; and the availability of age data beginning with the initial year, such that the initial non-equilibrium age composition can be estimated. In principle, if informative age data are available across years, the EM results should not be dependent on the choice of the initial year because the estimated age composition in the initial year could have been alternatively estimated by starting the model at an earlier year and estimating the age composition for that year as projected from earlier recruitments. Also, when age composition data from the fleet and survey are available in the first year, the numbers at age for the population can be estimated directly as parameters. In all 4 EMs, this feature of estimating the initial numbers at age is implemented by estimating the initial age composition as deviations from an equilibrium age composition. The level of recruitment that anchors the equilibrium age composition is calculated by using the spawner–recruit relationship. In other words, the initial equilibrium recruitment is lowered from the unfished recruitment level by an initial equilibrium *F*. However, in the AMAK, the initial equilibrium stock size is treated independently of historical fishing *F* because it typically is used in situations where this value would be negligible.

In this study, results from the comparison between case 0 and case 12 indicate that the AMAK, which does not specify the initial *F*, will scale the *R0* downwards to match the numbers at age 1 in the initial year and, consequently, the EM will produce lower MSY and SSB_{MSY} compared with the true values. The magnitude of RE will increase when initial *F* becomes higher.

This study was not designed to compare the performance of EMs under different initial population conditions, and the initial *F* and recruitment variability were fixed at low levels in cases 0 and 12. The initial numbers at age in year 1 may be quite different from those for the unfished equilibrium populations, especially when fishing occurred many years prior to the first year of data or with large variability in recruitment. When fishery or survey composition data are available near the start of commercial fishing, the estimates of unfished condition or stock status may accurately reflect the true conditions when initial equilibrium stock size is treated independently of historical fishing *F* in an EM. In addition to having this configuration option, the ASAP, BAM, and SS allow the initial numbers at age to be controlled through different processes (Legault and Restrepo, 1999; Methot and Wetzel, 2013; Williams and Shertzer, 2015). Future work on assessment model development should consider which options are most accurate and efficient for computing initial numbers at age.

Spawner-recruit parameters: median-unbiased or mean-unbiased

The results from cases 10 and 11 have clear implications for bias adjustment of recruitment. First, we identified the fundamental differences between 2 bias adjustment methods (Table 4, Suppl. Table 3 [online only]). In the BAM, median-unbiased spawner-recruit parameters are used, and in SS mean-unbiased parameters are used. Therefore, the inputs and outputs of *R0* and *h* from the 2 models are comparable only after conversion, for example, by using the function introduced here (Equations 11–14). These findings highlight the importance of clarifying in assessment reports and meta-analyses whether estimates of spawner-recruit parameters correspond to geometric mean or arithmetic mean curves of recruitment and the significance of the need for developing functions for conversion of mean-unbiased parameters to median-unbiased parameters (and vice versa) for other spawner-recruit models (e.g., Ricker spawner-recruit model; Hilborn, 1985). In various studies, bias adjustment of recruitment has been implemented differently, but no study has clearly demonstrated the strengths and weaknesses of different bias adjustment methods (Walters, 1990; Chen, 2004; Yin and Sampson, 2004; Methot and Taylor, 2011; Subbey et al., 2014). We recommend further work on bias adjustment to derive conversion functions for other spawner-recruit models and to provide clear guidance on which estimation process (mean-unbiased or median-unbiased) might be preferred under different situations.

Second, we established that ad hoc bias adjustment of recruitment can be implemented in EMs that do not have the bias adjustment feature (Suppl. Fig. 2) (online only). The ad hoc adjustment affects recruitment and fishery management parameters, such as MSY-based reference points. In this study, we found that the AMAK and ASAP produced estimates of *R0* and MSY-based reference points that are similar to the true values, if the estimates from those models were adjusted from a median-unbiased relationship to a mean-unbiased relationship.

Limits and future research

In addition to the specific recommendations coming from the issues found in this study, we think the comparison design could be extended to address other specific needs, such as quantifying the value of estimation of time-varying parameters as random effects (e.g., numbers at age, selectivity, and *F*), estimation of spawner-recruit parameters, data weighting, spatial structure, and other attributes to the performance of EMs. Growth was assumed to be known in this study because not all EMs have the capability to estimate growth. We can further compare EMs with more complicated cases, such as those that involve estimating growth within the assessments or using lower quality weight-at-age data. It would also be useful to conduct comparisons across life history patterns (e.g., patterns of long-lived versus short-lived species or patterns of demersal versus pelagic species), but further work on development of more complex OMs for simulation testing would be required. Punt et al. (2020) outlined essential features that should be considered for the next-generation stock assessment model, and they highlighted the importance of simulation testing in evaluation of estimation performance. Continued development of the OM used in this study through addition of essential features would result in an OM that can serve as an independent test bed to validate existing models as well as next-generation stock assessment models.

The comparison framework used in our study focused on age-structured models. Other age-structured stock assessment models that were not included in this study can be evaluated by using the comparison framework and creating connection files that automatically write input files, run the model, and save standard outputs. In addition, the comparison framework can be further applied to include other types of stock assessment models (e.g., surplus production, length-based, and catch-only models).

Having more comparison practices that involve both next-generation stock assessment models and existing models (inside and outside the United States) will enhance the communication among model developers and users, facilitate the interpretation of comparison results among models, and improve future assessments.

Conclusions

This study was designed to verify if the assessment models developed in different regions of the United States can produce similar estimates when given the same input data and configured similarly. However, it had a secondary objective of informing development of next-generation models (Punt et al., 2020). It is clear that all 4 models tested in this study provide similar and accurate estimates of quantities of interest under the tested cases. This outcome was expected given that the 4 EMs share similar mathematical and statistical attributes and that the simulated data were very informative. Nevertheless, it was expected also because we carefully evaluated the conversions among models to ensure that model configurations were similar to each other and model outputs were comparable. For future model comparison work or ensemble work, we recommend comparison of key features in source code before any multi-model analysis is done in order to identify differences in parameterization that could be misleading when results are compared (e.g., selectivity function parameters). We also recommend minimizing the variations of parameterizations for the same feature during development of next-generation stock assessment models. Standardized inputs and outputs for common parameters would allow easy comparisons of results from different models.

In this study, we have identified the sources of slight differences among model estimates under different cases. The differences are associated with computation of initial numbers at age and bias adjustment of recruitment. Improved insights on these key differences should help the development of next-generation stock assessment models. Key potential areas for future improvements include better clarification of terminology used in assessment reports, use of the conversion function developed in this study to convert between median-unbiased and mean-unbiased spawner-recruit parameters in stock assessment, use of the conversion function in other meta-analyses to ensure the inputs of meta-analysis are comparable, and development of guidance on which bias adjustment method is preferable under which situations.

Acknowledgments

This research was performed while the senior author held a National Research Council Research Associateship award at the Office of Science and Technology, National Marine Fisheries Service. We thank K. Doering, C. Stawitz, E. Dick, M. Masi, K. Johnson, and C. Bassin for their comments and suggestions for improving the development of the operating model in this study and this paper.

Literature cited

AFSC (Alaska Fisheries Science Center).
2015. Assessment Model for Alaska description of GUI and instructions, 50 p. [Available from website.]

Barbeaux, S. J., J. Ianelli, and W. Palsson.
2019. Assessment of the pollock stock in the Aleutian Islands, 3 p. *In* Stock assessment and fishery evaluation report for the groundfish resources of the Bering Sea/Aleutian Islands regions. North Pac. Fish. Manage. Counc., Anchorage, AK. [Available from website.]

Beverton, R. J. H., and S. J. Holt.
1957. On the dynamics of exploited fish populations. Fish. Investig. (G.B. Minist. Agric. Fish. Food), Ser. 2, vol. 19, 533 p. HMSO, London.

Brodziak, J., and C. M. Legault.
2005. Model averaging to estimate rebuilding targets for overfished stocks. Can. J. Fish. Aquat. Sci. 62:544–562.

Brodziak, J., and K. Piner.
2010. Model averaging and probable status of North Pacific striped marlin, *Tetrapturus audax*. Can. J. Fish. Aquat. Sci. 67:793–805.

Cadrin, S. X., and M. Dickey-Collas.
2015. Stock assessment methods for sustainable fisheries. ICES J. Mar. Sci. 72:1–6.

Chang, Y.-J., J. Brodziak, J. O'Malley, H.-H. Lee, G. DiNardo, and C.-L. Sun.
2015. Model selection and multi-model inference for Bayesian surplus production models: a case study for Pacific blue and striped marlin. Fish. Res. 166:129–139.

Chen, D. G.
2004. Bias and bias correction in fish recruitment prediction. North Am. J. Fish. Manage. 24:724–730.

Connors, B. M., and A. B. Cooper.
2014. Determining decision thresholds and evaluating indicators when conservation status is measured as a continuum. Conserv. Biol. 28:1626–1635.

Cortés, E., and E. N. Brooks.
2018. Stock status and reference points for sharks using data-limited methods and life history. Fish Fish. 19:1110–1129.

Deroba, J. J., D. S. Butterworth, R. D. Methot Jr., J. A. A. De Oliveira, C. Fernandez, A. Nielsen, S. X. Cadrin, M. Dickey-Collas, C. M. Legault, J. Ianelli, et al.
2015. Simulation testing the robustness of stock assessment models to error: some results from the ICES strategic initiative on stock assessment methods. ICES J. Mar. Sci. 72:19–30.

Dichmont, C. M., R. A. Deng, A. E. Punt, J. Brodziak, Y.-J. Chang, J. M. Cope, J. N. Ianelli, C. M. Legault, R. D. Methot Jr., C. E. Porch, et al.
2016. A review of stock assessment packages in the United States. Fish. Res. 183:447–460.

Federal Register.
1998. Magnuson-Stevens Act provisions; national standard guidelines. Fed. Regist. 63:24212–24237.

Fournier, D. A., H. J. Skaug, J. Ancheta, J. Ianelli, A. Magnusson, M. N. Maunder, A. Nielsen, and J. Sibert.
2012. AD Model Builder: using automatic differentiation for statistical inference of highly parameterized complex nonlinear models. Optim. Methods Softw. 27:233–249.

Gabriel, W. L., and P. M. Mace.
1999. A review of biological reference points in the context of the precautionary approach. *In* Proceedings of the 5th annual NMFS National Stock Assessment Workshop, p. 34–45. NOAA Tech. Memo. NMFS-F/SPO-40.

Henríquez, V., R. Licandeo, L. A. Cubillos, and S. P. Cox.
2016. Interactions between ageing error and selectivity in statistical catch-at-age models: simulations and implications for assessment of the Chilean Patagonian toothfish fishery. ICES J. Mar. Sci. 73:1074–1090.

Hilborn, R.
1985. Simplified calculation of optimum spawning stock size from Ricker's stock recruitment curve. Can. J. Fish. Aquat. Sci. 42:1833–1834.

Hilborn, R., and C. J. Walters.
1992. Quantitative fisheries stock assessment, choice, dynamics and uncertainty, 570 p. Routledge, Chapman and Hall, London.

Ianelli, J. N., and D. A. Fournier.
1998. Alternative age-structured analyses of the NRC simulated stock assessment data. *In* Analyses of simulated data sets in support of the NRC study on stock assessment methods (V. R. Restrepo, ed.), p. 81–96. NOAA Tech. Memo. NMFS-F/SPO-30.

Johnson, K. F., C. C. Monnahan, C. R. McGilliard, K. A. Vert-pre, S. C. Anderson, C. J. Cunningham, F. Hurtado-Ferro, R. R. Licandeo, M. L. Muradian, K. Ono, et al.
2015. Time-varying natural mortality in fisheries stock assessment models: identifying a default approach. ICES J. Mar. Sci. 72:137–150.

Legault, C. M., and V. R. Restrepo.
1999. A flexible forward age-structured assessment program. ICCAT Collect. Vol. Sci. Pap. 49(2):246–253. SCRS/98/058. [Available from website.]

Lynch, P. D., R. D. Methot, and J. S. Link (eds.).
2018. Implementing a next generation stock assessment enterprise. An update to the NOAA Fisheries stock assessment improvement plan. NOAA Tech. Memo. NMFS-F/SPO-183, 127 p.

Maunder, M. N., and A. E. Punt.
2013. A review of integrated analysis in fisheries stock assessment. Fish. Res. 142:61–74.

Maunder, M. N., and K. R. Piner.
2015. Contemporary fisheries stock assessment: many issues still remain. ICES J. Mar. Sci. 72:7–18.

Methot, R. D., Jr., and I. G. Taylor.
2011. Adjusting for bias due to variability of estimated recruitments in fishery assessment models. Can. J. Fish. Aquat. Sci. 68:1744–1760.

Methot, R. D., Jr., and C. R. Wetzel.
2013. Stock synthesis: a biological and statistical framework for fish stock assessment and fishery management. Fish. Res. 142:86–99.

Methot, R. D., Jr., G. R. Tromble, D. M. Lambert, and K. E. Greene.
2014. Implementing a science-based system for preventing overfishing and guiding sustainable fisheries in the United States. ICES J. Mar. Sci. 71:183–194.

NRC (National Research Council).
1998. Improving fish stock assessments, 188 p. National Academies Press, Washington, D.C.

Ono, K., R. Licandeo, M. L. Muradian, C. J. Cunningham, S. C. Anderson, F. Hurtado-Ferro, K. F. Johnson, C. R. McGilliard, C. C. Monnahan, C. S. Szuwalski, et al.
2015. The importance of length and age composition data in statistical age-structured models for marine species. ICES J. Mar. Sci. 72:31–43.

Piner, K. R., H.-H. Lee, M. N. Maunder, and R. D. Methot.
2011. A simulation-based method to determine model misspecification: examples using natural mortality and population dynamics models. Mar. Coast. Fish. 3:336–343.

Punt, A. E., A. Dunn, B. Þ. Elvarsson, J. Hampton, S. D. Hoyle, M. N. Maunder, R. D. Methot, and A. Nielsen.
2020. Essential features of the next-generation integrated fisheries stock assessment package: a perspective. Fish. Res. 229:105617.

Quinn, T. J., II, and R. B. Deriso.
1999. Quantitative fish dynamics, 540 p. Oxford Univ. Press, Oxford, UK.

Restrepo, V. R., G. G. Thompson, P. M. Mace, W. L. Gabriel, L. L. Low, A. D. MacCall, R. D. Methot, J. E. Powers, B. L. Taylor, P. R. Wade, et al.
1998. Technical guidance on the use of precautionary approaches to implementing National Standard 1 of the Magnuson-Stevens Fishery Conservation and Management Act. NOAA Tech Memo NMFS-F/SPO-31, 48 p.

Rosenberg, A. A., K. M. Kleisner, J. Afflerbach, S. C. Anderson, M. Dickey-Collas, A. B. Cooper, M. J. Fogarty, E. A. Fulton, N. L. Gutiérrez, K. J. W. Hyde, et al.
2018. Applying a new ensemble approach to estimating stock status of marine fisheries around the world. Conserv. Lett. 11:e12363.

Sampson, D. B., and Y. Yin.
1998. A Monte Carlo evaluation of the Stock Synthesis assessment program. *In* Fishery stock assessment models. Alaska Sea Grant Rep. 98-01 (D. Sampson and Y. Yin, eds.), p. 315–338. Alaska Sea Grant College Prog., Univ. Alaska Fairbanks, Fairbanks, AK.

Siegfried, K. I., E. H. Williams, K. W. Shertzer, and L. G. Coggins.
2016. Improving stock assessments through data prioritization. Can. J. Fish. Aquat. Sci. 73:1703–1711.

Smith, S. J., J. J. Hunt, and D. Rivard (eds.).
1993. Risk evaluation and biological reference points for fisheries management. Can. Spec. Publ. Fish. Aquat. Sci. 120, 442 p.

Stewart, I. J., and S. J. D. Martell.
2015. Reconciling stock assessment paradigms to better inform fisheries management. ICES J. Mar. Sci. 72:2187–2196.

Subbey, S., J. A. Devine, U. Schaarschmidt, and R. D. M. Nash.
2014. Modelling and forecasting stock–recruitment: current and future perspectives. ICES J. Mar. Sci. 71:2307–2322.

Walters, C. J.
1990. A partial bias correction factor for stock–recruitment parameter estimation in the presence of autocorrelated environmental effects. Can. J. Fish. Aquat. Sci. 47:516–519.

Wetzel, C. R., and A. E. Punt.
2011. Performance of a fisheries catch-at-age model (Stock Synthesis) in data-limited situations. Mar. Freshw. Res. 62:927–936.

Williams, E. H., and K. W. Shertzer.
2015. Technical documentation of the Beaufort Assessment Model (BAM). NOAA Tech. Memo. NMFS-SEFSC-671, 43 p.

Yin, Y., and D. B. Sampson.
2004. Bias and precision of estimates from an age-structured stock assessment program in relation to stock and data characteristics. North Am. J. Fish. Manage. 24:865–879.

National Marine
Fisheries Service
NOAA

Fishery Bulletin
established in 1881

Spencer F. Baird
First U.S. Commissioner
of Fisheries and founder
of *Fishery Bulletin*

Biological characteristics of the primitive flatfish Indian halibut (*Psettodes erumei*) from the tropical northeastern Indian Ocean, including implications of the use of incorrect aging methods on mortality estimates

Peter G. Coulson (contact author)
Jake A. Poad

Email address for contact author: peter.coulson@dpird.wa.gov.au

Centre for Sustainable Aquatic Ecosystems
Murdoch University
90 South Street
Murdoch, Western Australia 6150, Australia
Present address for contact author: Department of Primary Industries and Regional Development
Western Australian Fisheries and Marine Research Laboratories
P.O. Box 20
North Beach, Western Australia 6920, Australia

Abstract—The Indian halibut (*Psettodes erumei*) is an important flatfish species in tropical and subtropical waters of the northern Indian Ocean. However, inappropriate aging methods used in previous studies of Indian halibut limited the use of age and growth data from those studies. This study highlights the importance of correct aging methods and identification of sexually dimorphic growth, particularly if growth characteristics are used to estimate mortality rates. Counts of opaque zones in whole otoliths of Indian halibut were almost always fewer than those in their corresponding sections, particularly for older individuals. Multiple validation methods have been used to demonstrate that opaque zones form annually in otoliths of Indian halibut. Although the frequency of females increased with size, because of sexually dimorphic growth, males attained a greater maximum age (16 versus 11 years). Because of the greater ages and rapid early growth of Indian halibut described in this study, natural mortality estimates calculated by using the Pauly equation, particularly for males, were higher than estimates derived from the same equation in previous studies, which employed growth parameter estimates based on ages derived from whole otoliths, vertebrae, or monthly length–frequency trends and, typically, did not account for sexually dimorphic growth. In northwestern Australia, spawning in Indian halibut commences when water temperature and day length begin to increase and occurs between early spring and late summer.

Manuscript submitted 22 December 2020.
Manuscript accepted 20 July 2021.
Fish. Bull. 119:168–183 (2021).
Online publication date: 30 August 2021.
doi: 10.7755/FB.119.2-3.6

The views and opinions expressed or implied in this article are those of the author (or authors) and do not necessarily reflect the position of the National Marine Fisheries Service, NOAA.

Globally, flatfish species (flounders, halibuts, and soles) are an important group of fish species, contributing over 1 million metric tons (t) to world fisheries production in 2014 (FAO[1]; Nelson et al., 2016). The Indian halibut (*Psettodes erumei*) is a moderate-sized flatfish distributed in tropical and subtropical waters of the Indian and western Pacific Oceans, where it is an important component of trawl fisheries (Mathew et al., 1992; Vivekanandan et al., 2003). The annual catch of Indian halibut from 3 of the tropical fishing regions designated by the Food and Agricultural Organization of the United Nations ranged from ~15,000 to ~30,000 t between 2000 and 2011 (Gibson et al., 2015). In waters of India, where the majority of previous research on Indian halibut has been carried out (e.g., Pradhan, 1962; Hussain, 1990; Mathew et al., 1992; Gilanshahi et al., 2012), this species constituted ~1300 t of the total flatfish catch in 2012 (Nair and Gopalakrishnan, 2014). Although most flatfish have eyes on the right-hand (dextral) or left-hand side (sinistral) of the mouth (Nelson et al., 2016), a few species, including the Indian halibut and its 2 congeners, have varying proportions of dextral to sinistral polymorphism (Hubbs and Hubbs, 1945; Policansky, 1982). In addition, spiny dorsal and pelvic fin rays, vertebrae number, mouth structure, and upright swimming behavior are characteristics that separate *Psettodes* species from other flatfishes and why they are considered the most primitive form of flatfish (Hubbs and Hubbs, 1945; Platt, 1983).

The importance of choosing the appropriate aging structure and then validating the periodicity of growth increments has been made clear (Beamish and McFarlane, 1983; Campana, 2001), as have the implications of not doing so (c.f. Mace et al., 1990; Smith et al., 1995). Previous age estimates for Indian halibut have been derived from counting growth rings in vertebrae (Edwards and Shaher, 1991), scales (Druzhinin and Petrova, 1980), and whole otoliths (Das and Mishra, 1990), and none of those methods were validated; ages also have been estimated by examining trends displayed by monthly length frequencies (Silvestre and Garces, 2004; Gilanshahi et al., 2012). The use of vertebrae to age fish has been associated with large discrepancies in age estimates between readers (e.g., Esteves et al., 1995; Filmalter et al., 2009) and interpretation difficulties (e.g., Baker and Timmons, 1991; Marriott and Cappo, 2000; Khemiri et al., 2005). Although scales have been shown to be a useful aging structure for which removal is not lethal (e.g., Robillard and Marsden, 1996; Khan and Khan, 2009), the accuracy of ages derived from counts of growth zones on scales is questionable (Beamish and McFarlane, 1983). Even though whole otoliths are suitable to age short-lived species (e.g., Fairclough et al., 2000; Kornis et al., 2017), for many fishes, including a number of flatfishes, it has been acknowledged that ages based on whole otoliths are often underestimated (e.g., Campana, 1984; Forsberg[2]; Stevens et al., 2005; Albert et al., 2009).

---

[1] FAO (Food and Agriculture Organization of the United Nations). 2016. FAO yearbook. Fishery and aquaculture statistics 2014, 76 p. FAO, Rome. [Available from website.]

Previous estimates of the instantaneous rate of natural mortality (M) for Indian halibut, calculated by using the Pauly (1980) empirical equation, range from 0.51 to 0.76 year^{-1} (Edwards and Shaher, 1991; Silvestre and Garces, 2004; Gilanshahi et al., 2012) and are higher than the median value of 0.41 year^{-1} for members of the Pleuronectidae (Froese and Pauly[3]). The fact that the landings of Indian halibut in waters of India have declined by ~70% over the past 30 years, even as the overall catch of flatfishes has increased over the same period (Nair and Gopalakrishnan, 2014), indicates that the level of fishing pressure on this species may have been too high, possibly as a result of management advice based on unreliable age estimates.

This study was undertaken to determine the biological characteristics, including age, growth trends, timing and duration of spawning, and lengths and ages at maturity, of Indian halibut in waters off northwestern Australia. Because of the now known unreliability of the aging structures or methods that have previously been used to age Indian halibut in other regions, this study aimed to provide sound age estimates based on proven and validated aging methods, thereby facilitating accurate estimates of growth and of both natural and total mortality. The data were also used to test the hypothesis that, as reported for many other flatfishes (e.g., Stevens et al., 2005; Félix et al., 2011; Black et al., 2013), male Indian halibut grow faster than females, and females grow to a larger size. Furthermore, it has been hypothesized that the beginning of the spawning period for Indian halibut, like that of other subtropical species, is associated with increasing day length and water temperatures (Lam, 1983).

Materials and methods

Sample collection and fish measurements

Large (>250 mm in total length [TL]) Indian halibut were purchased whole from a wholesale market in Perth, Australia, in each month between February 2014 and December 2015, such that 20–50 fish were collected for each calendar month. These fish were taken as bycatch by commercial bottom trawlers that deployed standard stern trawling gear (a single net with extension sweeps) at depths of 50–200 m in the eastern Indian Ocean off the Pilbara coast in northwestern Australia (approximately between 19°S, 120°E and 20°S, 116°E), where the catch is largely composed of lutjanid and lethrinid species (Wakefield et al.[4]; Newman et al.[5]). Additional smaller individuals, 35–215 mm TL), caught in August 2015 and September 2017, were provided by the Western Australian Department of Primary Industry and Regional Development. These fish were caught during research surveys off the Pilbara coast, by using an otter trawl with net mesh sizes of 229 mm (9 in) in the wings and 110 mm (4.3 in) in the pocket.

The TL and total body mass of each Indian halibut was measured to the nearest 1 mm and 0.1 g, respectively. The eye side (i.e., right or left) of each fish was recorded, and the sagittal otoliths of each fish were removed, cleaned, dried, and stored in envelopes.

Mean monthly sea-surface temperatures in waters off the Pilbara coast, for the 1° grid block of 19–20°S, 117–118°E, were calculated from monthly values in 2010–2015 obtained from the Koninklijk Nederlands Meteorologisch Instituut Climate Explorer (available from website), which employs data from Reynolds optimum interpolation analysis of sea-surface temperatures (Reynolds et al., 2007). Daily lengths of days for the town of Karratha (~22°S, 117°E), on the Pilbara coast, obtained from timeanddate.com (day length data available from website), were employed to generate mean monthly day lengths for 2014 and 2015.

---

[2] Forsberg, J. E. 2001. Aging manual for Pacific halibut: procedures and methods used by the International Pacific Halibut Commission. Tech. Rep. 46, 50 p. [Available from website.]

[3] Froese, R., and D. Pauly (eds.). 2017. FishBase, vers. 12/2017. World Wide Web electronic publication. [Available from website, accessed January 2018.]

[4] Wakefield, C. B., S. Blight, S. R. Dorman, A. Denham, S. J. Newman, J. Wakeford, B. W. Molony, A. W. Thomson, C. Syers, and S. O'Donoghue. 2014. Independent observations of catches and subsurface mitigation efficiencies of modified trawl nets for endangered, threatened and protected megafauna bycatch in the Pilbara fish trawl fishery. Fish. Res. Rep. 244, 33 p. West. Aust. Dep. Fish., North Beach, Australia. [Available from website.]

[5] Newman, S., C. Wakefield, C. Skepper, D. Boddington, R. Jones, and P. Dobson. 2017. North coast demersal resource status report 2016. *In* Status reports of the fisheries and aquatic resources of Western Australia 2015/16: the state of the fisheries (W. J. Fletcher, M. D. Mumme, and F. J. Webster, eds.), p. 144–152. West. Aust. Dep. Fish., Perth, Australia. [Available from website.]

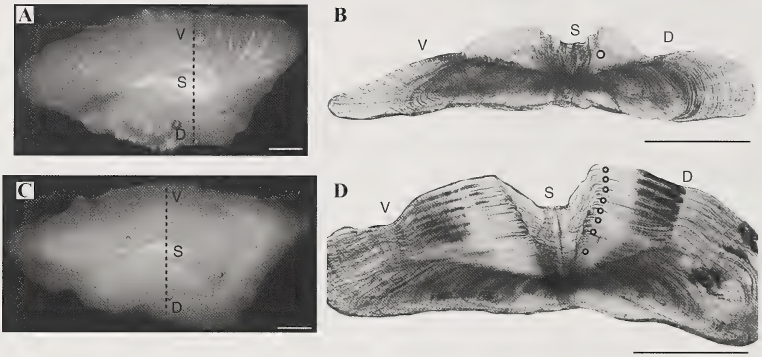

Figure 1

Photographs of the (**A** and **C**) whole otoliths and (**B** and **D**) corresponding transverse sections of the blind side of otoliths of 2 Indian halibut (*Psettodes erumei*) caught in the Indian Ocean off the Pilbara coast in northwestern Australia during February and July 2014. Each photograph shows the dorsal edge (D), ventral edge (V), sulcus (S), and nucleus (N) of the otolith. The horizontal dashed line across each whole otolith indicates the position of the corresponding transverse section taken from each otolith. Panels C and D show 1 and 8 opaque zones (white circles), respectively. The location of the white circles reflects the axis along which opaque zones were counted. All scale bars are equal to 1 mm.

Otolith preparation and age determination

The otolith corresponding to the *blind side* of each Indian halibut (i.e., the side of the fish facing downward and therefore having no eyes) was selected for aging purposes because it has been proven that the blind-side otolith in some flatfishes provides a clearer interpretation of growth zones than the eye-side otolith (Lear and Pitt, 1975; Forsberg[2]; Armsworthy and Campana, 2010). The whole blind-side otoliths of 272 fish were each placed in a black dish with low viscosity immersion oil, with the ventral side facing upward, and photographed under reflected light by using a Leica DFC 425 camera (Leica Microsystems Inc.[6], Buffalo Grove, IL) mounted on a Leica MZ7.5 dissecting microscope (Leica Microsystems Inc.). Captured images were viewed by using Leica Application Suite, vers. 4.3 (Leica Microsystems Inc.), enabling opaque zones in each otolith to be marked and counted. The number of opaque zones in the whole blind-side otoliths were counted on a single occasion by the primary reader (senior author).

Those same otoliths were cleaned, dried, and embedded in a clear epoxy resin, along with the blind-side otoliths from another 265 individuals, and cut transversely through the primordium into sections of ~250–300 µm with a low-speed diamond saw (IsoMet Low Speed Precision Cutter, Buehler Ltd., Lake Bluff, IL). Otolith sections were then mounted on microscope slides by using DePeX mounting adhesive (VWR International LLC, Radnor, PA) and a coverslip. Digital images of each sectioned otolith were taken, by using a 12-MP Olympus DP70 camera (Olympus Corp., Tokyo, Japan) mounted on an Olympus BX51 compound microscope (Olympus Corp.) and by employing transmitted light.

Counting of opaque zones on the digital images of sectioned otoliths was facilitated by the use of Leica Application Suite, which enabled such zones to be marked and readily counted and the distances required for marginal increment analysis to be measured with confidence (Coulson et al., 2021). Opaque zones on the edge of the dorsal side of the otolith section, closest to the sulcus, were counted (Fig. 1). Measurements for marginal increment analysis were recorded to the nearest 0.01 mm and taken on an axis perpendicular to the opaque zones on the dorsal side.

To validate that a single opaque zone is formed annually in the otoliths of Indian halibut, we analyzed trends observed throughout the year by using the mean monthly marginal increments (MI) on sectioned otoliths (i.e., the distance between the outer edge of the single or outermost opaque zone and the otolith periphery). When one opaque zone is present, the MI was expressed as a proportion of the distance between the primordium and the outer edge of the single opaque zone. When 2 or more opaque zones were present, the MI was expressed as a proportion of the distance between the outer edges of the 2 outermost opaque zones. An approach based on the methods of Okamura and Semba (2009) was applied to determine the periodicity of occurrence of otoliths of Indian halibut with marginal increments falling within the lower 30th percentile of values for each category of zone counts (Coulson et al., 2016, 2017). For this analysis, binomial models linked with von Mises circular distributions were fitted by assuming 1) no cycle, 2) an annual cycle, or 3) a biannual (twice yearly) cycle. When compared by using the Akaike information criterion (AIC), the model with the lowest value was deemed to best represent the data (Burnham and Anderson, 2002).

---

[6] Mention of trade names or commercial companies is for identification purposes only and does not imply endorsement by the National Marine Fisheries Service, NOAA.

The number of opaque zones in all sectioned otoliths were counted twice by the primary reader, with the counts from the second read considered the most accurate. The level of precision between the primary reader's second counts and those of a second experienced reader (J. Poad) for a subsample of 280 otoliths was assessed by calculating the coefficient of variation (CV) (Chang, 1982; Campana, 2001):

$$CV_j = 100\% \times \frac{\sqrt{\sum_{i=1}^{R}\left(X_{ij} - X_j\right)^2 / \left(R - 1\right)}}{X_j}, \qquad (1)$$

where CV_j = the age precision estimate for the *j*th fish;
X_{ij} = the *i*th age determination for the *j*th fish;
X_j = the mean age estimate for the *j*th fish; and
R = the number of times each fish is aged.

Growth and sex ratio

Each Indian halibut was assigned an age, on the basis of the number of opaque zones in sectioned otoliths, the date of capture of the fish, the "average" birth date (i.e., the approximate midpoint of the spawning period; see the "Reproductive biology" subsection in the "Results" section) of 1 December, and the time of year when the outermost opaque zone typically becomes delineated in the otoliths. Growth was described by fitting von Bertalanffy growth curves to the lengths at age of the females and males, with estimates of von Bertalanffy growth function (VBGF) parameters, and their 95% confidence limits, obtained by using a nonlinear function in R, vers. 3.4.1 (R Core Team, 2017). The VBGF used was as follows:

$$L = L_\infty\left(1 - e\left(-k(t - t_0)\right)\right), \qquad (2)$$

where L = the total length (in millimeters) at age t (in years),
L_∞ = the estimated asymptotic total length (in millimeters);
k = the growth coefficient (year^{-1}); and
t_0 = the hypothetical age (in years) at which fish have zero length.

A likelihood-ratio chi-square test was used to compare the growth curves from the VBGF for female and male Indian halibut. The test statistic was twice the difference between the log-likelihoods obtained by fitting growth curves to the lengths at age for each sex, separately, and by fitting a common growth curve to all lengths at age regardless of sex (Cerrato, 1990). The hypothesis that the growth of the 2 groups could be represented by a single growth curve was rejected at the level of significance (α) of 0.05 if the previously mentioned test statistic exceeded $\chi^2_\alpha(q)$, where q is the difference between the numbers of parameters in the 2 approaches, for example, a difference of 3 numbers (Cerrato, 1990). The log-likelihood (λ) for each curve, ignoring constants, was calculated as follows:

$$\lambda = (-n/2)\ \ln(ss/n), \qquad (3)$$

where n = sample size; and
ss = the sum of the squared residuals between the observed and expected lengths at age.

Chi-square tests were used to determine whether the ratio of females to males in each of the main TL and age classes, as well as the sex ratio for all TLs and ages collectively, differed significantly from parity.

Spawning time and maturation

When identifiable as ovaries or testes, the mass of the gonads of each Indian halibut was weighed to the nearest 0.01 g. On the basis of its macroscopic characteristics, each ovary was allocated to one of the following 4 groups of maturity stages adapted from the criteria used by Laevastu (1965): virgin and immature or resting (stages 1 and 2); developing and maturing (stages 3 and 4); prespawning and spawning (stages 5 and 6); and spent and recovering (stages 7 and 8). Ovaries at stages 3–7 in each year were considered likely to become mature (stages 3–5) or to have matured (stages 6–7) during that year; therefore, for convenience, ovaries at these stages are referred to as *mature*. The prevalence of females and males with gonads at each developmental stage in each month was determined.

Because all female Indian halibut >300 mm TL collected during the spawning period possessed mature gonads, the mean monthly gonadosomatic indices (GSIs) for females were determined by using all individuals greater than this length. For males, the mean monthly GSIs were determined by using individuals with lengths greater than or equal to the TLs at which 50% of the males attained maturity (L_{50}) (see the "Lengths and ages at maturity" subsection in the "Results" section). For both sexes, the mean monthly GSI was determined by using this equation:

$$GSI = (GM\ /\ TM)\ /\ TM \times 100, \qquad (4)$$

where GM = wet gonad mass, and
TM = wet total body mass.

To confirm the macroscopic gonoad staging, histological sections were prepared from the gonads of a subsample of the Indian halibut collected in each month; the subsample of fish had a wide range of lengths, and their gonads were at all maturity stages found in fish in that month. Depending on the size of the gonads, they were placed in Bouin's fixative for 24–48 h, prior to being dehydrated in a series of increasing concentrations of ethanol. The mid-region of each gonad was next embedded in paraffin wax, cut into 6-µm transverse sections, and stained with Mallory's trichrome.

The TLs at which 50% and 95% of males reached maturity, together with their 95% confidence limits, were determined by using logistic regression analysis, as has been done in similar studies for other species (Coulson et al., 2005, 2009). Fish were considered mature (i.e., about to spawn, spawning, or just spawned) if they possessed gonads at a maturity level between stage 3 and stage 8. The spawning period is defined as the consecutive months in which ≥50% of fish possessed gonads at stage 5 or 6, together with elevated mean monthly GSIs. Logistic regression analysis was restricted to males obtained during the spawning period, from September through February (see the "Reproductive biology" subsection in the "Results" section). The form of the logistic model relating the probability that a male Indian halibut is mature to its TL is as follows:

$$P = \{1 + e[-\ln(19)\,(L - L_{50})/(L_{95} - L_{50})]\}^{-1}, \qquad (5)$$

where P = proportion mature;
L = total length in millimeters;
L_{50} = total lengths in millimeters at which 50% of fish were mature; and
L_{95} = total lengths in millimeters at which 95% of fish were mature.

Mortality estimates

In northwestern Australia, the Indian halibut is considered a bycatch species and is caught in very low numbers in a fishery that targets larger bodied, more valuable lutjanids, lethrinids, and serranids (WADF[7]). This low level of catch is indicated, for example, by the total weight of Indian halibut available on market days at the wholesale market in Perth typically ranging only between 5 and 15 kg (senior author, personal observ.), with all fish available on a particular day, in some instances, being purchased for this study. Therefore, the sizes and ages of fish collected for this study are assumed to be representative of the population of this species in northwestern Australia.

Estimates of the M of females and males were calculated from their maximum individual ages, by using both the Hoenig (1983) and Hoenig$_{\mathrm{NLS}}$ (Then et al., 2015) equations, with the estimates from the latter equation recognized as the more reliable (Maunder and Piner, 2015). The estimates of M, derived with the Hoenig (1983) equation, are provided to make comparisons possible because this equation has been widely used in previous studies. To further enable comparisons with previous studies (Edwards and Shaher, 1991; Silvestre and Garces, 2004; Gilanshahi et al., 2012), M was also estimated by using the Pauly (1980) empirical equation for length and by using a water temperature of 27°C (i.e., the mean annual sea-surface temperature for waters off the Pilbara coast).

For catch curve analysis, only those age classes consisting of individuals 1 year older than the age at full recruitment for each sex (i.e., 4 years) were used (Ricker, 1975), with the remaining age classes assigned an age relative to the age at full recruitment (i.e., the first fully recruited age was assigned the age of zero). Total mortality (Z) for fully recruited fish was estimated by using the Chapman and Robson (1960) approach, as implemented in the chapmanRobson function of the FSA package (vers. 0.8.6; Ogle, 2016) in R.

Results

Whole versus sectioned otoliths

Although a single opaque zone was visible in all of the whole otoliths whose sections also possessed a single opaque zone, the level of agreement between the opaque zone counts for whole otoliths and for their corresponding sections decreased rapidly (Fig. 2). For example, the same number of opaque zones were visible in only 4 of the 41 otoliths in which 5 opaque zones were visible in their sections. There was no agreement in opaque counts when the number of opaque zones in sections was ≥7. In the most severe case, only 4 opaque zones were clearly visible in a whole otolith whose corresponding section revealed 16 opaque zones (Fig. 2).

Validation of aging methods

The mean monthly MIs on sectioned otoliths of Indian halibut with 2–4 opaque zones remained ≤0.41 between January and March before increasing to 0.49 in May and to a maximum of 0.57 in July (Fig. 3). The mean monthly MI remained at elevated levels in August and September, before declining rapidly to a minimum in December. The mean monthly MIs for otoliths with ≥5 opaque zones in other months of the year followed a similar trend, increasing from low levels in January to a maximum in September, before declining to lower levels in December (Fig. 3). The single pronounced decline and then progressive increase of the mean monthly MIs during the year for otoliths with different numbers of opaque zones indicates that a single opaque zone is formed annually in the otoliths of Indian halibut. The validity of the notion that the mean monthly MIs followed a single cycle during the year is substantiated by the results in this study from circular distribution models (Okamura and Semba, 2009; Coulson et al., 2016). For otoliths with 2–4 opaque zones and ≥5 opaque zones, the accompanying AIC values of 302 and 169, respectively, for an annual cycle were less than the AIC values of 309 and 183 for no cycle and 312 and 182 for a biannual cycle; in addition, the difference between the former value and the AIC values of the latter 2 cycles exceeded 2, the number required to

---

[7] WADF (Western Australia Department of Fisheries). 2010. A bycatch action plan for the Pilbara fish trawl interim managed fishery. Fish. Manage. Pap. 244, 24 p. West. Aust. Dep. Fish., Perth, Australia. [Available from website.]

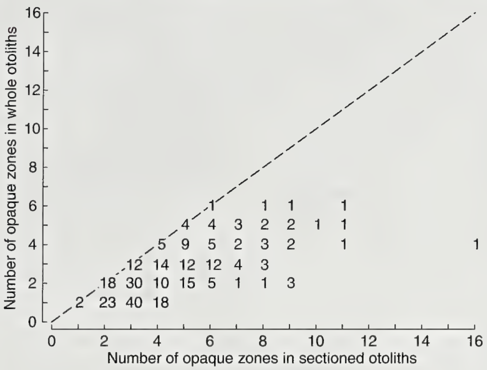

Figure 2

Bias plot of opaque zone counts showing the level of agreement between the counts of the number of opaque zones in whole otoliths and their corresponding sections from Indian halibut (*Psettodes erumei*) caught as bycatch by commercial trawlers between February 2014 and December 2015 and with an otter trawl during research surveys between August 2015 and September 2017 off the Pilbara coast in northwestern Australia. Values represent the number of individual otoliths. The diagonal dashed line represents perfect agreement between counts of the 2 readers.

identify definitively the best model in terms of the Kullback–Leibler distance for the 2 groups of otoliths (Burnham and Anderson, 2002). The number of opaque zones in sectioned otoliths can, therefore, be used for aging individual Indian halibut.

The sectioned otoliths of 5 small Indian halibut (135–196 mm TL) caught in August (late winter) contained a large, central opaque region and a surrounding wide translucent area, and, in 2 cases, an opaque edge. The sectioned otoliths of several similarly sized fish (151–211 mm TL) and of larger individuals (272–310 mm TL), caught in the same month, possessed the same characteristics but, in addition, contained 1 and 2 recently formed and diffuse opaque zones, respectively, that had become delineated from the otolith edge through the presence of a narrow, translucent zone at the otolith margin. The patterns of opacity within the otoliths of several small Indian halibut provide strong evidence that the first opaque zone is formed during the first winter of life, when Indian halibut are on average ~8 months old. Therefore, those Indian halibut caught in August with a wide translucent zone surrounding the nucleus and with an opaque zone on, or just delineated from, the edge of the otolith were ~9 months old. Those fish with 2 opaque zones in their otoliths, the second being recently deposited, were therefore ~21 months old.

The resultant CV of 1.85% indicates a high level of agreement between the counts of opaque zones for each otolith by each reader, falling well below the reference level of 5% for correspondence recommended by Campana (2001).

Length and age compositions and growth

The numbers of female and male Indian halibut <250 mm TL, all of which were largely collected in trawl nets during research surveys, were very similar (Fig. 4). Although males were far more abundant in the length classes of 250–299 mm TL and 300–349 mm TL, caught by commercial trawlers, females were considerably more abundant than males in the length class of 350–399 mm TL. The 2 largest length classes were composed of females exclusively (Fig. 4). The ratios of females to males in the 3 length classes of the commercially caught fish that contained both sexes, 250–299 mm TL, 300–349 mm TL, and 350–399 mm TL, were 0.2:1.0, 0.8:1.0, and 12.8:1.0, respectively. For all 3 of these length classes, the sex ratio was significantly different from parity (the χ^2 statistic for each class was 53.0, 4.1, and 56.8, respectively, with $P>0.05$ for all of them). The TLs of the largest female and male were 469 and 380 mm TL, respectively, with these fish also having the greatest total body mass for their sex, 1773 and 752 g, respectively.

Male Indian halibut were more abundant in the youngest and 3 oldest age classes in which both sexes were present, but females were more abundant in the age class of 4–5 years (Fig. 3). A single male constituted the oldest age class of 16–17 years. The ratio of females to males in each age class that contained ≥20 individuals varied from 0.6:1.0 in the age classes of 6–7 years and 8–9 years to 1.3:1.0 in the age class of 4–5 years. However, for no age class was the sex ratio significantly different from parity (χ^2=0.6–3.1, $P>0.05$). The maximum ages recorded for female and male Indian halibut were 11 and 16 years, respectively.

The length–mass relationships for the female and male Indian halibut were not significantly different (P=0.24); therefore, the length–mass data for both sexes were pooled and described by using this equation:

$$\ln TM = 3.17(\ln L) - 12.20 \qquad (6)$$

(coefficient of determination [r^2]=0.99, sample size [n]=544). The von Bertalanffy growth curves for female and male Indian halibut provide good fits to the lengths at ages for the individuals of each sex (Fig. 5), as indicated by the high values for the r^2 for each sex (Table 1). The von Bertalanffy growth curves for females and males, which were significantly different ($P<0.001$), increasingly diverged with increasing age, a pattern that is reflected in the values for L_∞ and k (Table 1). On the basis of estimates from the VBGF, females attained lengths of 196, 322, 379, and 392 mm TL at 1, 3, 6, and 9 years of age compared with

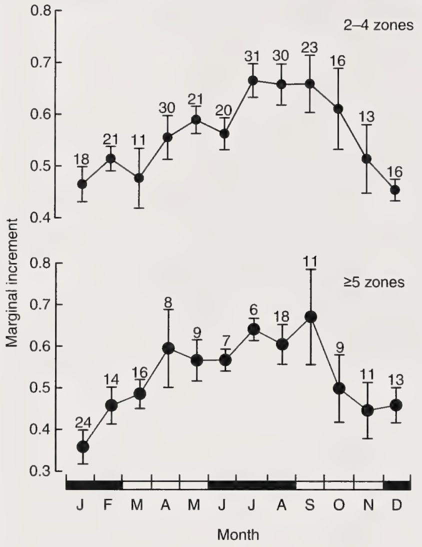

Figure 3

Mean monthly marginal increments of sectioned otoliths, with 2–4 opaque zones and with ≥5 opaque zones, from Indian halibut (*Psettodes erumei*) caught by commercial trawlers between February 2014 and December 2015 and during research surveys between August 2015 and September 2017) off the Pilbara coast in northwestern Australia. Error bars indicate standard errors of the mean. Sample sizes are given above error bars. Black bars on the *x*-axis indicate summer and winter months, and open bars indicate autumn and spring months.

the lengths of 201, 287, 314, and 318 mm TL, respectively, attained by males at the same ages.

Reproductive biology

Mean monthly temperatures in offshore waters, adjacent to the Pilbara coast, increased steadily from a minimum of 24.4°C in August (late winter) to a maximum of 30.0°C in March (mid-autumn) before declining to 25.6°C in June (early winter) (Fig. 6). Day length was shortest in June (early winter) and longest in December (early summer) (Fig. 6).

The mean monthly GSI for female Indian halibut rose sharply from 0.6 in July to a well-defined maximum of 6.6 in October. Although it declined to 4.0 and 4.7 in December and January, respectively, the mean monthly GSI for females remained at levels >4.0 until February, after which it declined precipitously to 1.2 in April and to a minimum of 0.6 in June (Fig. 6). The mean monthly GSI for male Indian halibut followed the same trend.

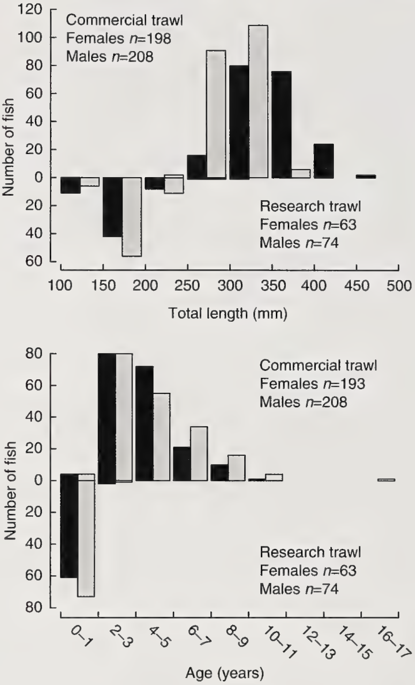

Figure 4

Length–frequency and age–frequency distributions for female (black bars) and male (gray bars) Indian halibut (*Psettodes erumei*) caught as bycatch by commercial trawlers between February 2014 and December 2015 and with an otter trawl during research surveys between August 2015 and September 2017 in the Indian Ocean off the Pilbara coast in northwestern Australia. n=sample size.

All female Indian halibut sampled from May through July possessed ovaries that were either immature or resting (stage 2) or spent and recovering (stages 7 and 8). The frequency of females with ovaries at such stages declined in August, when those with mature or spawning ovaries (stages 5 and 6) were first present (Fig. 7). The vast majority of females sampled between September and February had ovaries in stages 5 and 6. Although ~45% of females in March also possessed ovaries in those stages, a similar proportion of females had ovaries in stages 7 and 8. The frequency of females with such ovaries increased to ~92% in April (Fig. 7). The trends in the frequency of occurrence of male Indian halibut with testes at different stages of development followed closely that of the females, in that males with mature or spawning

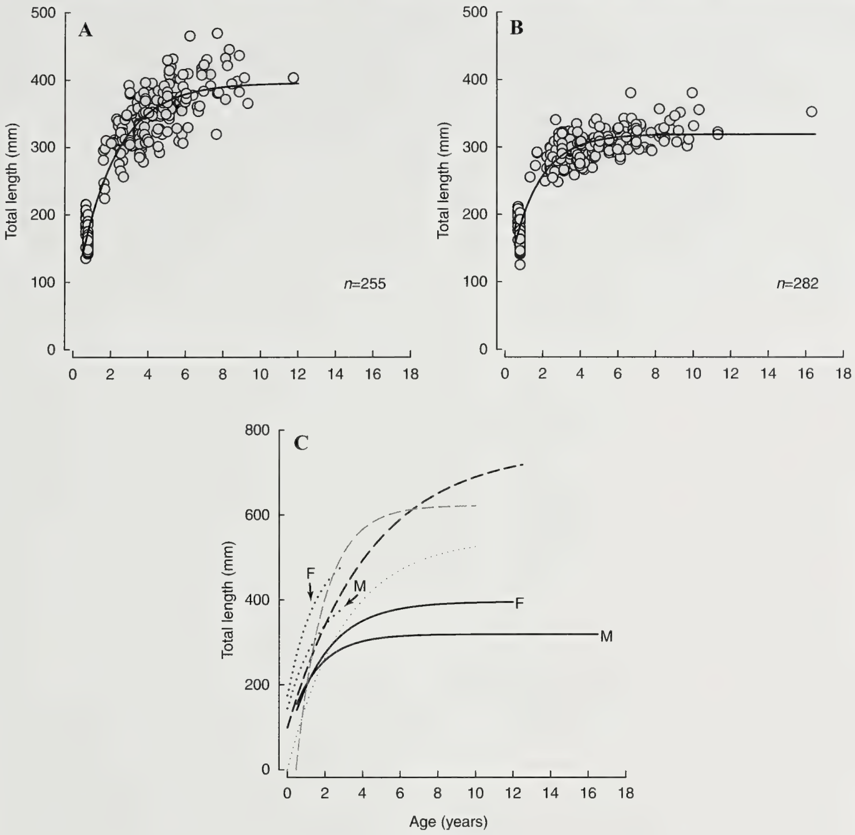

Figure 5

von Bertalanffy growth curves fit to total lengths at age for (**A**) female and (**B**) male Indian halibut (*Psettodes erumei*) caught by commercial trawlers in February 2014–December 2015 and during research surveys in August 2015–September 2017 off the Pilbara coast in northwestern Australia. Samples sizes (*n*) are given for each graph. (**C**) Comparisons of growth curves fit to the lengths at age of female (F) and male (M) Indian halibut from northwestern Australia (solid black lines) and from the northwestern Bay of Bengal (dotted black lines) (Das and Mishra, 1990) and of growth curves fit to the lengths at age of females and males combined from Brunei (dotted gray line) (Silvestre and Garces, 2004), the Gulf of Aden (dashed gray line) (Edwards and Shaher, 1997), and the Persian Gulf (dashed black line) (Gilanshahi et al., 2012). Growth curves from Gilanshahi et al. (2012) and Silvestre and Garces (2004) were derived from trends in monthly length frequencies, and curves from Das and Mishra (1990) and Edwards and Shaher (1997) are based on individual fish aged by using whole otoliths and vertebrate, respectively.

testes (stages 5 and 6) largely dominated samples collected between September and February.

Although the prevalence of female and male Indian halibut with gonads at stages 5–8 between September and February increased, the abundance of individuals with gonads at stages 3 and 4 declined markedly or were not even present. Still, female and male Indian halibut with gonads at stages 3 and 4 more than likely become mature during the spawning season. Therefore, fish with gonads at stages 3 and 4 and at stages 5–8 were collectively regarded as mature for the purposes of estimating length and age at maturity. Trends in the GSIs and prevalences of females and males

Table 1

Estimates of parameters of the von Bertalanffy growth function (VBGF) for female (F) and male (M) Indian halibut (*Psettodes erumei*) caught in the Indian Ocean off the Pilbara coast in northwestern Australia by commercial trawlers as bycatch between February 2014 and December 2015 and during research surveys with an otter trawl between August 2015 and September 2017. The parameters are the asymptotic length (L_∞) in total length, growth coefficient (k), and hypothetical age at which fish have zero length (t_0). The upper and lower 95% confidence limits, coefficient of determination (r^2), and sample size (n) are provided for each estimate. Values were derived from the total lengths at age of individuals. The VBGF parameters obtained for Indian halibut in other studies are provided for comparison. The values for L_∞ and k from Gilanshahi et al. (2012) and Silvestre and Garces (2004) were derived from trends in monthly length frequencies, and those from Edwards and Shaher (1997) and Das and Mishra (1990) are based on individual fish aged by using vertebrae and whole otoliths, respectively.

			VBGF parameter				
Source	Sex	Value	L_∞ (mm)	k (year^{-1})	t_0 (years)	r^2	n
This study	F	Estimate	395	0.49	−0.38	0.88	255
		Upper	407	0.57	−0.22		
		Lower	384	0.42	−0.55		
	M	Estimate	319	0.66	−0.51	0.88	282
		Upper	324	0.76	−0.33		
		Lower	313	0.56	−0.69		
Edwards and Shaher (1997)	Both		622	0.68	0.46		
Silvestre and Garces (2004)	Both		545	0.33			
Gilanshahi et al. (2012)	Both		745	0.23	−0.61		
Das and Mishra (1990)	F		535	0.64	−0.61		
	M		436	0.56	−0.72		

with mature or spawning gonads (stages 5 and 6) indicate that the spawning period for Indian halibut in northwestern Australia extends from September through February.

Lengths and ages at maturity

Because all female Indian halibut with TLs <225 mm that were caught during the spawning period were immature and all those with TLs >300 mm had mature gonads (stages 3–8), no attempt was made to determine an L_{50} for this sex (Fig. 8). All male Indian halibut <250 mm TL that were caught during the spawning period, except 2 individuals (163 and 164 mm TL), were immature (Fig. 7). The percentage of mature males increased sharply to 50% and 85% in the length classes of 250–274 and 275–299 mm TL, with all males ≥300 mm TL being mature. The L_{50} and L_{95}, and their upper and lower 95% confidence intervals (CIs), for male Indian halibut were estimated to be 268 mm TL (95% CI: 250–288 mm TL) and 284 mm TL (95% CI: 255–325 mm TL), respectively.

All females and most males that were ≤1 year old and caught during the spawning period were immature (Fig. 7). In contrast, all females that were 2–9 years old and most males that were 2–10 years old, and caught during the spawning period, were mature. This result indicates that, generally, female and male Indian halibut do not mature until they are almost 2 years old.

Mortality

Estimates for M of female and male Indian halibut, derived by using the Pauly (1980) equation and the respective VBGF parameters, were far higher than those derived by using either the Hoenig (1983) equation or the Then et al. (2015) equation, both of which use the maximum age of each sex (Table 2). In addition, the M values estimated by using the equation of Then et al. (2015) were slightly greater than those derived by using the Hoenig (1983) equation, noting that, through cross validation, Then et al. (2015) established that their equation provided a better estimate of published values of M than other equations that they tested. The catch curve estimates of Z for both sexes were slightly less than the corresponding estimates of M derived from use of the Then et al. (2015) equation (Table 2).

Discussion

Method of aging

The results of the comparison between the number of opaque zones in whole otoliths and the number in their corresponding sections indicate that ages of Indian halibut estimated from counts of opaque zones in whole otoliths, even when the numbers of such zones are few, are

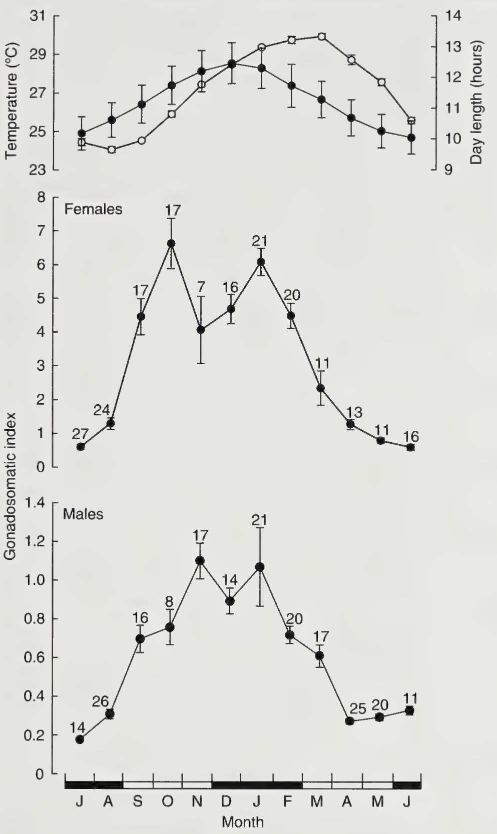

Figure 6

Mean monthly sea-surface temperatures (gray circles) in offshore waters along the Pilbara coast off northwestern Australia during 2010–2015 and mean monthly day lengths (black circles) in the same region during 2014 and 2015. Also shown are mean monthly gonadosomatic indices for female and male Indian halibut (*Psettodes erumei*) greater than the total length of sex at maturity (i.e., 286 mm). Fish were caught by commercial trawlers in February 2014–December 2015 and during research surveys in August 2015–September 2017 off the Pilbara coast. Error bars indicate standard errors of the mean. Sample sizes are given above error bars. Black bars on the *x*-axis indicate summer and winter months, and open bars indicate autumn and spring months

considerably underestimated. Although this species is not long-lived, the thickness, and therefore the opacity, of otoliths prevent annuli from being readily detected when otoliths are read whole; similar results have been reported for other flatfish species, such as the starry flounder (*Platichthys stellatus*) (Campana, 1984), New Zealand brill (*Colistium guntheri*) and *C. nudipinnis* (Stevens et al., 2005), marbled flounder (*Pseudopleuronectes yokohamae*) (Lee et al., 2009), and turbot (*Scophthalmus maximus*) (Yoneda et al., 2007). The finding of a maximum age of 16 years for Indian halibut from northwestern Australia, from use of sectioned otoliths in this study, indicates that this species is much longer lived than the maximum age of 3 years that has been obtained for this species in waters of northeastern India by using whole otoliths (Das and Mishra, 1990). The maximum age determined in our study also is slightly older than the age of 12.4 years that has been obtained for this species in the Persian Gulf by analyzing trends in monthly length frequencies (Gilanshahi et al., 2012).

In other regions, Indian halibut have been caught as large as 640 and 705 mm TL (Hussain, 1990; Gilanshahi et al., 2012) and, because of the sexually dimorphic growth of this species, are most likely to be females. Considering that the oldest female (11 years old) collected in this study was only 403 mm TL, it is not unreasonable to expect that Indian halibut may attain ages ≥20 years. However, in those regions where Indian halibut is an important component of the commercial catch, regions such as those in the Arabian Sea, Persian Gulf, Gulf of Oman, and Bay of Bengal, fish ages have been determined by counts of growth zones in vertebrae or whole otoliths (Das and Mishra, 1990; Hussain, 1990; Edwards and Shaher, 1991). These apparently unvalidated aging methods have led to estimates of a maximum age of only 3 years that, if employed in mortality estimates when developing management plans for this species, would grossly overestimate the resilience of this species to fishing pressure (see the "Mortality" subsection later in this section). Therefore, we recommend that, for those regions where Indian halibut account for an important component of the fishery, age estimates be determine from sectioned otoliths. Although analysis of trends in monthly length–frequency data by Gilanshahi et al. (2012) has provided a more realistic estimate of maximum age, for a species in which growth is negligible for a large proportion of their adult life, this method of aging is not recommended (e.g., Morales-Nin, 1989).

Growth

Results from comparisons of the von Bertalanffy growth curves indicate that female and male Indian halibut have different growth patterns, with females attaining a larger size at age than males. This pattern of sexually dimorphic growth is a common feature of many flatfishes, including those of the Paralichthyidae and Pleuronectidae

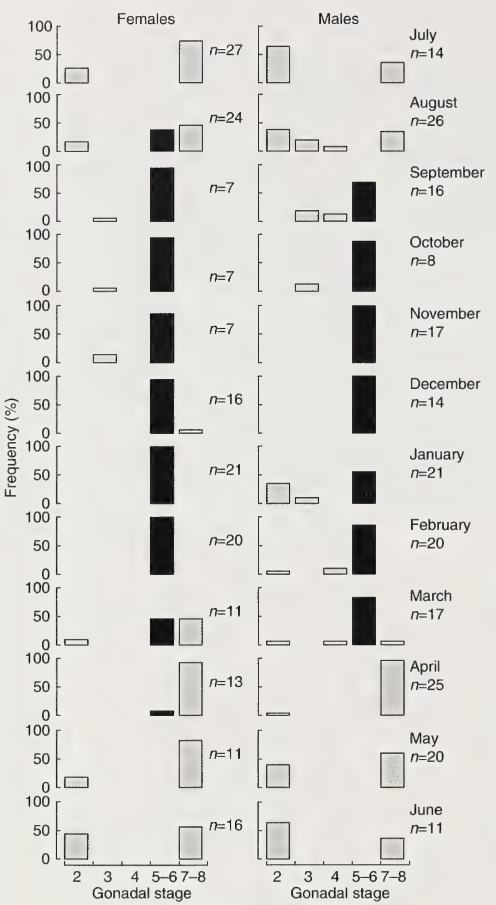

Figure 7

Monthly frequencies of occurrence of sequential stages in the gonadal development and sample sizes (n) of female and male Indian halibut (*Psettodes erumei*) greater than the total length of that sex at maturity (i.e., 286 mm in total length) and caught by commercial trawler between February 2014 and December 2015 and during research surveys between August 2015 and September 2017 off the Pilbara coast in northwestern Australia. Stages include virgin (1), immature or resting (2), developing (3), maturing (4), prespawning (5), spawning (6), spent (7), and recovering (8). Black bars highlight values for fish with gonads at stages 5–6.

(e.g., MacNair et al., 2001; Fischer and Thompson, 2004; Pearson and McNally, 2005; Yoneda et al., 2007). Das and Mishra (1990) identified a difference in length at age of the 2 sexes (Fig. 4), but in the other previous studies of Indian halibut no difference was assumed, and growth curves were fit to data for females and males combined (Fig. 4; Hussain, 1990; Edwards and Shaher, 1991; Gilanshahi et al., 2012).

The results of this study indicate that the early growth of females and males is similarly rapid, with the majority of growth occurring in the first 3–4 years of life. Although findings from previous growth studies indicate rapid early growth as well, they also indicate that growth is sustained, with little or no asymptote (Table 1, Fig. 5). The discrete length modes of individual age groups identified in monthly length–frequency data of fast growing, short-lived species enable programs, such as the systems of methods known as electronic length–frequency analysis (ELEFAN) and multiple length–frequency analysis (MULTIFAN), to be valuable alternatives for determining fish growth (e.g., Morales-Nin and Aldebert, 1997; Bellido et al., 2000; Campana, 2001). If applied to long-lived, slow-growing species, however, these tools involve the use of the well-defined length modes of the youngest cohorts of a species to fit a growth model to all fish (Campana, 2001). Species that have a broad spawning period are also not suitable for such analysis because the long spawning period results in age cohorts with a wide length distribution that obscures the distinction between those cohorts (Morales-Nin and Ralston, 1990).

Spawning

Latitude, and therefore water temperature, influences the timing and duration of the spawning period of fishes (e.g., Gray et al., 2012; Wakefield et al., 2015). The commencement of the spawning period for Indian halibut in late winter or early spring is typical of temperate species (e.g., Hyndes and Potter, 1997; Morato et al., 2007; Gray and Barnes, 2015; Coulson et al., 2017), in which an increasing photoperiod or rising temperatures stimulate gonadal recrudescence (Lam, 1983). However, the timing of the spawning period of Indian halibut through spring and summer is also similar to that of a range of teleost species in tropical and subtropical waters (e.g., Mackie, 2000; Sumpton and Brown, 2004; Grandcourt et al., 2006; Russell and McDougall, 2008).

Results from reproductive studies of Indian halibut in the Arabian Sea by Hussain (1990), at a latitude (~24–25°N) higher than that considered in this study, indicate that the spawning period for Indian halibut occurred early and was far more restricted, from March (boreal early spring) through May (boreal late spring), than the spawning period observed in this study. However, Ramanathan and Natarajan (1979) determined that, at the far lower latitude of ~11°N in the Arabian Sea, Indian halibut had a more extended spawning period, from May through

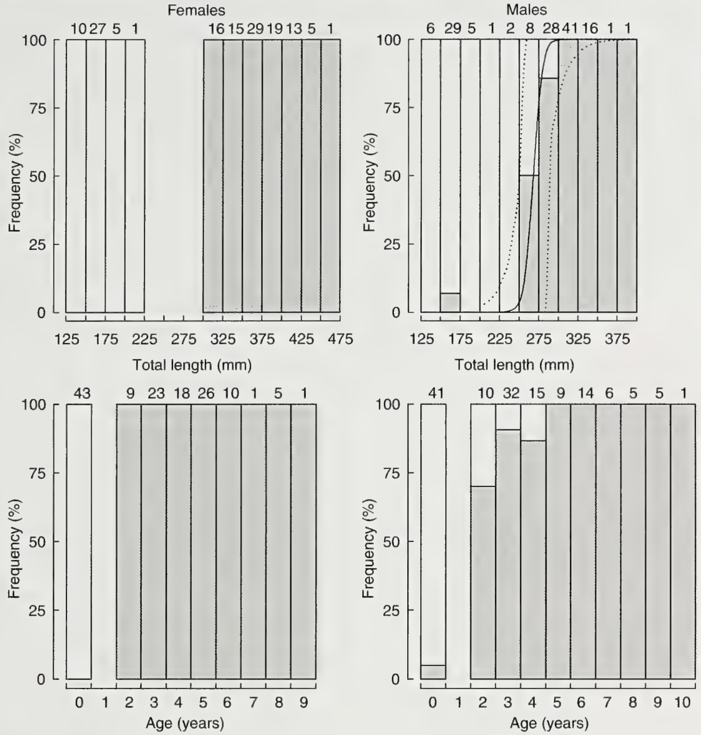

Figure 8

Frequencies of occurrence of female and male Indian halibut (*Psettodes erumei*) with mature gonads (gray bars) in sequential length classes (in 25-mm intervals of total length [TL]) and age classes. Samples were caught during the peak spawning period (September–February) off the Pilbara coast in northwestern Australia. The logistic curve (solid line) and its 95% confidence limits (dotted lines) for males by length class were derived from the probability that a fish at a given TL is mature. The numeral at the top of each bar indicates the sample size for that class.

September (boreal mid-autumn), a period that is similar in terms of timing and duration to that found in this study for fish from northwestern Australia at ~19–20°S. In contrast, in the Bay of Bengal at latitudes of 19–20°N, Indian halibut spawn from August (boreal late summer) through December (boreal early winter) (Pradhan, 1962; Das and Mishra, 1990), similar to the spawning time of other teleosts in that region (Rao, 1983). The difference in the timing and duration of the spawning period of Indian halibut in the Bay of Bengal, compared with those of fish in similar latitudes off northwestern Australia and in the Arabian Sea may be related to the influence of the monsoons and freshwater input into coastal waters in the region of Bay of Bengal.

During the summer monsoon season, the Bay of Bengal becomes highly stratified, with a surface layer of freshwater because weaker winds prevent vertical mixing (Prasanna Kumar et al., 2002; Sengupta et al., 2006). In contrast, coastal upwelling along the southern part of the west coast of India and upwelling, wind-driven mixing, and lateral advection in open-ocean waters (Bauer et al., 1991; Lee et al., 2000; Prasanna Kumar et al., 2001; Krishnakumar and Bhat, 2008) make the Arabian Sea more productive. Off northwestern Australia, where the nutrient-deficient Leeuwin Current is the dominant oceanographic feature (Cresswell and Golding, 1980; Koslow et al., 2008), rainfall and terrestrial input from rivers is limited (Molony et al., 2011). Although in other regions, the increase in water

Table 2

Maximum age, natural mortality (*M*), and total mortality (*Z*) for female (F) and male (M) Indian halibut (*Psettodes erumei*) caught by commercial trawlers between February 2014 and December 2015 and during research surveys between August 2015 and September 2017 in northwestern Australia. Estimates of *M* were calculated by using the Pauly (1980), Hoenig (1983), and Then et al. (2015) equations, and estimates of *Z* (provided with standard errors in parentheses) were calculated by using the catch curve method of Chapman and Robson (1960). Estimates of *M* from Gilanshahi et al. (2012) and Silvestre and Garces (2004) were based on estimates of von Bertalanffy growth function parameters, asymptotic length and growth coefficient, derived from trends in monthly length frequencies, and those from Edwards and Shaher (1997) are based on individual fish aged by using vertebrae. Estimates of *Z* from Gilanshahi et al. (2012) and Silvestre and Garces (2004) were derived from length-converted catch curves.

			M			*Z*
Source	Sex	Max. age	Pauly (1980)	Hoenig (1983)	Then et al. (2015)	Chapman and Robson (1960)
This study	F	11	1.02	0.40	0.55	0.39 (0.09)
This study	M	16	1.31	0.28	0.39	0.32 (0.07)
Edwards and Shaher (1997)	Both		0.76			
Silvestre and Garces (2004)	Both		0.73			0.85
Gilanshahi et al. (2012)	Both		0.51			1.20

temperature from its winter minimum may provide a cue for the onset of gonadal development for Indian halibut, in the Bay of Bengal, it appears that spawning may be delayed until the post-monsoon period, when primary productivity is greatest (Choudhury and Pal, 2010) and when suitable prey for recently spawned larvae is abundant.

Mortality

The estimates of *M* for females, and particularly for males, derived in this study by using the Pauly (1980) equation were far higher than the values derived by using the same method in previous studies (Table 2). Because *k* is used for the Pauly (1980) equation, the resultant value for *M* reflects the accuracy of the estimates of that parameter. The results of the studies carried out by Silvestre and Garces (2004) and Gilanshahi et al. (2012) indicate that the growth of Indian halibut is slow and does not reach an asymptote (Fig. 4C), as reflected by lower values for *k* from those studies: 0.33 year^{-1} and 0.23 year^{-1}, respectively, in comparison with *k* values from our study. In the cases of those studies, the use of *k* to estimate *M* for Indian halibut is not suitable, firstly because *k* is not reliably estimated (i.e., monthly length–frequency data) and secondly because the estimated *k* values reflect a species that never reaches its asymptotic length (Kenchington, 2014). Although in our study *k* was estimated reliably by using individual length at (validated) ages, the fact that females and males grew rapidly in the first 2–3 years, after which growth slowed appreciably, also prohibits those *k* values for each sex from being employed to estimate *M* (Kenchington, 2014).

Direct estimates of *Z* should always exceed the true *M* value. Results from this study indicate that indirect estimates of *M* for female and male Indian halibut, derived from the $\text{Hoenig}_{\text{NLS}}$ equation of Then et al. (2015), exceed the estimates of *Z* and are therefore considered overestimates (Coulson et al., 2017). However, indirect estimates of *M* for each sex derived by using the equation of Hoenig (1983) are more consistent with those of *Z*. The similarity in values of *Z* and *M*, from the Hoenig (1983) equation, is consistent with the fact that, in northwestern Australia, the Indian halibut is a bycatch species. This similarity in mortality values parallels the mortality estimates for 4 of 5 platycephalid species from southwestern Australia that are caught as bycatch in commercial fisheries that target other species, as part of the catch in multispecies commercial fisheries, or as catch in low numbers in a recreational fishery (Coulson et al., 2017).

The use of mortality estimates that supposedly reflect a species that has high natural mortality, when those estimates are based on underestimates of age, may lead fisheries managers to set catch limits higher than is suitable for a species that actually has far lower natural mortality rates. It is, therefore, imperative that the management of Indian halibut in those regions where this species accounts for a significant proportion of catch, and the management of species that have similar life history characteristics (i.e., sexually dimorphic growth, rapid initial growth, and medium longevity), is based on a sound understanding of their biology, determined by using proven and validated techniques.

Conclusions

This study is the first comprehensive investigation of the biological characteristics of Indian halibut. The greater number of opaque zones visible in sectioned otoliths compared with the number visible in the corresponding whole otolith indicates the importance of identifying the correct aging structure and preparation methods to enable the provision of reliable fish ages. The maximum age of 16 years observed in this study was much greater than the previous estimate of 3 years from whole otoliths. In addition, this study found that Indian halibut have sexually dimorphic growth, a finding that has implications for the use of growth characteristics to estimate natural mortality. Although the Indian halibut is a bycatch species in the trawl fishery in northwestern Australia, in other regions of the northern Indian Ocean, this species is far more important. In those regions, the information provided in this study, in particular the ages, growth characteristics, and mortality estimates, will be important to fisheries agencies for developing appropriate management plans for Indian halibut.

Acknowledgments

Many thanks to T. Abbot and G. Buscombe from Kailis Bros. for their assistance in obtaining whole Indian halibut and to G. Mitsopoulos, G. Davis, and C. Skepper from the Department of Primary Industry and Development, Western Australia, for kindly providing small individuals. Comments by N. Hall on an earlier version of this manuscript and his assistance with mortality calculations are greatly appreciated. Comments by 4 anonymous reviewers greatly improved the manuscript. Financial support was provided by Murdoch University.

Literature cited

Albert, O. T., M. Kvalsund, T. Vollen, and A.-B. Salberg.
2009. Towards accurate age determination of Greenland halibut. J. Northwest Atl. Fish. Sci. 40:81–95.

Armsworthy, S. L., and S. E. Campana.
2010. Age determination, bomb-radiocarbon validation and growth of Atlantic halibut (*Hippoglossus hippoglossus*) from the Northwest Atlantic. Environ. Biol. Fishes 89:279–295.

Baker, T. T., and L. S. Timmons.
1991. Precision of ages estimated from five bony structures of Arctic char (*Salvelinus alpinus*) from the Wood River system, Alaska. Can. J. Fish. Aquat. Sci. 48:1007–1014.

Bauer, S., G. L. Hitchcock, and D. B. Olson.
1991. Influence of monsoonally-forced Ekman dynamics upon surface layer depth and plankton biomass distribution in the Arabian Sea. Deep-Sea Res. Oceanogr., A 38:531–553.

Beamish, R. J., and G. A. McFarlane.
1983. The forgotten requirement for age validation in fisheries biology. Trans. Am. Fish. Soc. 112:735–743.

Bellido, J. M., G. J. Pierce, J. L. Romero, and M. Millán.
2000. Use of frequency analysis methods to estimate growth of anchovy (*Engraulis encrasicolus* L. 1758) in the Gulf of Cádiz (SW Spain). Fish. Res. 48:107–115.

Black, B. A., M. E. Matta, T. E. Helser, and T. K. Wilderbuer.
2013. Otolith biochronologies as multidecadal indicators of body size anomalies in yellowfin sole (*Limanda aspera*). Fish. Oceanogr. 22:523–532.

Burnham, K. P., and D. R. Anderson.
2002. Model selection and multimodel inference: a practical information-theoretic approach, 2nd ed., 488 p. Springer-Verlag, New York.

Campana, S. E.
1984. Comparison of age determination methods for the starry flounder. Trans. Am. Fish. Soc. 113:365–369.
2001. Accuracy, precision and quality control in age determination, including a review of the use and abuse of age validation methods. J. Fish Biol. 59:197–242.

Cerrato, R. M.
1990. Interpretable statistical tests for growth comparisons using parameters in the von Bertalanffy equation. Can. J. Fish. Aquat. Sci. 47:1416–1426.

Chang, W. Y. B.
1982. A statistical method for evaluating the reproducibility of age determination. Can. J. Fish. Aquat. Sci. 39:1208–1210.

Chapman, D. G., and D. S. Robson.
1960. The analysis of a catch curve. Biometrics 16:354–368.

Choudhury, A. K., and R. Pal.
2010. Phytoplankton and nutrient dynamics of shallow coastal stations at Bay of Bengal, Eastern Indian coast. Aquat. Ecol. 44:55–71.

Coulson, P. G., S. A. Hesp, I. C. Potter, and N. G. Hall.
2005. Comparisons between the biology of two co-occurring species of whiting (Sillaginidae) in a large marine embayment. Environ. Biol. Fishes 73:125–139.

Coulson, P. G., S. A. Hesp, N. G. Hall, and I. C. Potter.
2009. The western blue groper (*Achoerodus gouldii*), a protogynous hermaphroditic labrid with exceptional longevity, late maturity, slow growth, and both late maturation and sex change. Fish. Bull. 107:57–75.

Coulson, P. G., N. G. Hall, and I. C. Potter
2016. Biological characteristics of three co-occurring species of armorhead from different genera vary markedly from previous results for the Pentacerotidae. J. Fish Biol. 89:1393–1418.

Coulson, P. G., N. G. Hall, and I. C. Potter.
2017. Variations in biological characteristics of temperate gonochoristic species of Platycephalidae and their implications: a review. Estuar. Coast. Shelf Sci. 190:50–68.

Coulson, P. G., D. J. Hodgkinson, and L. E. Beckley.
2021. Age validation and growth of the small-tooth flounder *Pseudorhombus jenynsii* from estuaries and coastal waters in south-western Australia. Ichthyol. Res. 68:249–262.

Cresswell, G. R., and T. J. Golding.
1980. Observations of a south-flowing current in the southeastern Indian Ocean. Deep-Sea Res. Oceanogr., A 27:449–466.

Das, M., and B. Mishra.
1990. On the biology of *Psettodes erumei* (Bloch and Schn.), an Indian halibut. Indian J. Fish. 37:79–92.

Druzhinin, A. D., and Y. G. Petrova.
1980. Some data on the ecology and growth of *Psettodes erumei* (Family Psettodidae, Order Pleuronectiformes) of the Gulf of Aden. J. Ichthyol. 20:143–147.

Edwards, R. R. C., and S. Shaher.
1991. The biometrics of marine fishes from the Gulf of Aden. Fishbyte 9(2):27–29.

Esteves, E., P. Simões, H. M. da Silva, and J. P. Andrade.
1995. Ageing of swordfish, *Xiphias gladius* Linnaeus, 1758, from the Azores, using sagittae, anal-fin spines and vertebrae. Life Mar. Sci. 13A:39–51.

Fairclough, D. V., W. F. Dimmlich, and I. C. Potter.
2000. Length and age compositions and growth rates of the Australian herring *Arripis georgiana* in different regions. Mar. Freshw. Res. 51:631–640.

Félix, P. M., C. Vinagre, and H. N. Cabral.
2011. Life-history traits of flatfish in the Northeast Atlantic and Mediterranean Sea. J. Appl. Ichthyol. 27:100–111.

Filmalter, J. D., O. L.F. Weyl, and W. Sauer.
2009. Otoliths and vertebrae as potential hard structures for ageing South African yellowfin tuna *Thunnus albacares*. Afr. J. Mar. Sci. 31:271–276.

Fischer, A. J., and B. A. Thompson.
2004. The age and growth of southern flounder, *Paralichthys lethostigma*, from Louisiana estuarine and offshore waters. Bull. Mar. Sci. 75:63–77.

Gibson, R. N., R. D. M. Nash, A. J. Geffen, and H. W. Van der Veer (eds.).
2015. Flatfishes: biology and exploitation, 2nd ed., 576 p. Wiley-Blackwell, West Sussex, UK.

Gilanshahi, R., S. A. Taghavimotlagh, F. Kaymaram, S. M. R. Fatemi, and G. H. Vosooghi.
2012. Estimatin of growth parameters and mortality rates of *Psettodes* (*erumei* in the Persian Gulf and Oman sea) Hormozgan province. Int. J. Mar. Sci. Eng. 2:197–202.

Grandcourt, E. M., T. Z. Al Abdessalaam, and F. Francis.
2006. Age, growth, mortality and reproduction of the blackspot snapper, *Lutjanus fulviflamma* (Forsskål, 1775), in the southern Arabian Gulf. Fish. Res. 78:203–210.

Gray, C. A., and L. M. Barnes.
2015. Spawning, maturity, growth and movement of *Platycephalus fuscus* (Cuvier, 1829) (Platycephalidae): fishery management considerations. J. Appl. Ichthyol. 31:442–450.

Gray, C. A., J. A. Haddy, J. Fearman, L. M. Barnes, W. G. Macbeth, and B. W. Kendall.
2012. Reproduction, growth and connectivity among populations of *Girella tricuspidata* (Pisces: Girellidae). Aquat. Biol. 16:53–68.

Hoenig, J.
1983. Empirical use of longevity data to estimate mortality rates. Fish. Bull. 82:898–902.

Hubbs, C. L., and L. C. Hubbs.
1945. Bilateral asymmetry and bilateral variation in fishes. Pap. Mich. Acad. Sci. Arts Lett. 30:229–310.

Hussain, S. M.
1990. Biology of *Psettodes erumei* (Schneider, 1801) and *Pseudorhombus arsius* (Hamilton, 1822) from the northern Arabian Sea. Indian J. Fish. 37:63–66.

Hyndes, G. A., and I. C. Potter.
1997. Age, growth and reproduction of *Sillago schomburgkii* in south-western Australian, nearshore waters and comparisons of life history styles of a suite of *Sillago* species. Environ. Biol. Fishes 49:435–447.

Kenchington, T. J.
2014. Natural mortality estimators for information-limited fisheries. Fish Fish. 15:533–562.

Khan, M. A., and S. Khan.
2009. Comparison of age estimates from scale, opercular bone, otolith, vertebrae and dorsal fin ray in *Labeo rohita* (Hamilton), *Catla catla* (Hamilton) and *Channa marulius* (Hamilton). Fish. Res. 100:255–259.

Khemiri, S., A. Gaamour, L. Zylberberg, F. Meunier, and M. S. Romdhane.
2005. Age and growth of bogue, *Boops boops*, in Tunisian waters. Acta Adriat. 46:159–175.

Kornis, M. S., B. C. Weidel, and M. J. Vander Zanden.
2017. Divergent life histories of invasive round gobies (*Neogobius melanostomus*) in Lake Michigan and its tributaries. Ecol. Freshw. Fish 26:563–574.

Koslow, J. A., S. Pesant, M. Feng, A. Pearce, P. Fearns, T. Moore, R. Matear, and A. Waite.
2008. The effect of the Leeuwin Current on phytoplankton biomass and production off southwestern Australia. J. Geophys. Res. Oceans 113:C07050.

Krishnakumar, P. K., and G. S. Bhat.
2008. Seasonal and interannual variations of oceanographic conditions off Mangalore coast (Karnataka, India) in the Malabar upwelling system during 1995–2004 and their influences on the pelagic fishery. Fish. Oceanogr. 17:45–60.

Laevastu, T.
1965. Manual of methods in fisheries biology, 51 p. FAO, Rome.

Lam, T. J.
1983. Environmental influences on gonadal activity in fish. *In* Fish physiology, vol. 9, part B (W. S. Hoar, D. J. Randall, and E. M. Donaldson, eds.), p. 65–116. Academic Press, London.

Lear, W. H., and T. K. Pitt.
1975. Otolith age validation of Greenland halibut (*Reinhardtius hippoglossoides*). J. Fish. Res. Board Can. 32:289–292.

Lee, C. M., B. H. Jones, K. H. Brink, and A. S. Fischer.
2000. The upper-ocean response to monsoonal forcing in the Arabian Sea: seasonal and spatial variability. Deep-Sea Res., II 47:1177–1226.

Lee, J.-H., K. Kodama, G. Kume, M. Oyama, S. Katayama, Y. Takao, and T. Horiguchi.
2009. Comparison between surface-reading and cross-section methods using sagittal otolith for age determination of the marbled sole *Pseudopleuronectes yokohamae*. Fish. Sci. 75:379–385.

Mace, P. M., J. M. Fenaughty, R. P. Coburn, and I. J. Doonan.
1990. Growth and productivity of orange roughy (*Hoplostethus atlanticus*) on the north Chatham Rise. N.Z. J. Mar. Freshw. Res. 24:105–119.

Mackie, M.
2000. Reproductive biology of the halfmoon grouper, *Epinephelus rivulatus*, at Ningaloo Reef, Western Australia. Environ. Biol. Fishes 57:363–376.

MacNair, L. S., M. L. Domeier, and C. S. Y. Chun.
2001. Age, growth, and mortality of California halibut, *Paralichthys californicus*, along southern and central California. Fish. Bull. 99:588–600.

Marriott, R., and M. Cappo.
2000. Comparative precision and bias of five different ageing methods for the large tropical snapper *Lutjanus johnii*. Asian Fish. Sci. 13:149–160.

Mathew, G., M. F. Khan, and K. Nandakumaran.
1992. Present status of exploitation of fish and shellfish resources: flatfishes and flatheads. Bull. Cent. Mar. Fish. Res. Inst. 45:197–204.

Maunder, M. N., and K. R. Piner.
2015. Contemporary fisheries stock assessment: many issues still remain. ICES J. Mar. Sci. 72:7–18.

Molony, B. W., S. J. Newman, L. Joll, R. C. J. Lenanton, and B. Wise.
2011. Are Western Australian waters the least productive waters for finfish across two oceans? A review with a focus on finfish resources in the Kimberley region and North Coast Bioregion. J. R. Soc. West. Aust. 94:323–332.

Morales-Nin, B.
1989. Growth determination of tropical marine fishes by means of otolith interpretation and length frequency analysis. Aquat. Living Resour. 2:241–253.

Morales-Nin, B., and S. Ralston.
1990. Age and growth of *Lutjanus kasmira* (Forskål) in Hawaiian waters. J. Fish Biol. 36:191–203.

Morales-Nin, B., and Y. Aldebert.
1997. Growth of juvenile *Merluccius merluccius* in the Gulf of Lions (NW Mediterranean) based on otolith microstructure and length-frequency analysis. Fish. Res. 30:77–85.

Morato, T., P. Afonso, N. Carvalho, P. Lourinho, R. S. Santos, H. M. Krug, and R. D. M. Nash.
2007. Growth, reproduction and recruitment patterns of the wide-eyed flounder, *Bothus podas* Delaroche (Pisces: Bothidae), from the Azores. Mar. Biol. Res. 3:403–411.

Nair, R. J., and A. Gopalakrishnan.
2014. A review on the fisheries, taxonomy, and status of the flatfishes in tropical waters. Rev. Fish. Sci. Aquac. 22:175–183.

Nelson, J. S., T. C. Grande, and M. V. H. Wilson.
2016. Fishes of the world, 5th ed., 752 p. John Wiley and Sons, Hoboken, NJ.

Ogle, D. H.
2016. FSA: fisheries stock analysis. R package, vers. 0.8.6. [Available from website, accessed July 2017.]

Okamura, H., and Y. Semba.
2009. A novel statistical method for validating the periodicity of vertebral growth band formation in elasmobranch fishes. Can. J. Fish. Aquat. Sci. 66:771–780.

Pauly, D.
1980. On the interrelationships between natural mortality, growth parameters, and mean environmental temperature in 175 fish stocks. ICES J. Mar. Sci. 39:175–192.

Pearson, D. E., and S. V.G. McNally.
2005. Age, growth, life history, and fisheries of the sand sole, *Psettichthys melanostictus*. Mar. Fish. Rev. 67(4):9–18.

Platt, C.
1983. Retention of generalized hair cell patterns in the inner ear of the primitive flatfish *Psettodes*. Anat. Rec. 207:503–508.

Policansky, D.
1982. The asymmetry of flounders. Sci. Am. 246(5):116–123.

Pradhan, M. J.
1962. Observations on the maturity and spawning of *Psettodes erumei* (Schneider). Indian J. Fish. 9:580–589.

Prasanna Kumar, S., M. Madhupratap, M. D. Kumar, P. M. Muraleedharan, S. N. de Souza, M. Gauns, and V. V. S. S. Sarma.
2001. High biological productivity in the central Arabian Sea during the summer monsoon driven by Ekman pumping and lateral advection. Curr. Sci. 81:1633–1638.

Prasanna Kumar, S., P. M. Muraleedharan, T. G. Prasad, M. Gauns, N. Ramaiah, S. N. de Souza, S. Sardesai, and M. Madhupratap.
2002. Why is the Bay of Bengal less productive during summer monsoon compared to the Arabian Sea? Geophys. Res. Lett. 29(24):2235.

R Core Team.
2017. R: a language and environment for statistical computing. R Foundation for Statistical Computing, Vienna, Austria. [Available from website, accessed July 2017]

Ramanathan, N., and R. Natarajan.
1979. Breeding biology of *Psettodes erumei* (Bloch and Schn.) and *Pseudorhombus arsius* (Ham. Buch.) Pisces: Pleuronectiformes along Porto Novo coast (S. India). Aquaculture 18:269–282.

Rao, K. V. S.
1983. Maturation and spawning of lizard fishes (*Saurida* spp.) from northwestern part of Bay of Bengal. Indian J. Fish. 30:27–45.

Reynolds, R. W., T. M. Smith, C. Liu, D. B. Chelton, K. S. Casey, and M. G. Schlax.
2007. Daily high-resolution-blended analyses for sea surface temperature. J. Clim. 20:5473–5496.

Ricker, W. E.
1975. Computation and interpretation of biological statistics of fish populations. Bull. Fish. Res. Board Can. 191, 382 p.

Robillard, S. R., and J. E. Marsden.
1996. Comparison of otolith and scale ages for yellow perch from Lake Michigan. J. Gt. Lakes Res. 22:429–435.

Russell, D. J., and A. J. McDougall.
2008. Reproductive biology of mangrove jack (*Lutjanus argentimacuiatus*) in northeastern Queensland, Australia. N.Z. J. Mar. Freshw. Res. 42:219–232.

Sengupta, D., G. N. B. Raj, and S. S. C. Shenoi.
2006. Surface freshwater from Bay of Bengal runoff and Indonesian throughflow in the tropical Indian Ocean. Geophys. Res. Lett. 33:L22609.

Silvestre, G. T., and L. R. Garces.
2004. Population parameters and exploitation rate of demersal fishes in Brunei Darussalam (1989–1990). Fish. Res. 69:73–90.

Smith, D. C., S. G. Robertson, G. E. Fenton, and S. A. Short.
1995. Age determination and growth of orange roughy (*Hoplostethus atlanticus*): a comparison of annulus counts with radiometric ageing. Can. J. Fish. Aquat. Sci. 52:391–401.

Stevens, D. W., M. P. Francis, P. C. Shearer, R. P. McPhee, R. W. Hickman, and M. J. Tait.
2005. Age and growth of two endemic flatfish (*Colistium guntheri* and *C. nudipinnis*) in central New Zealand waters. Mar. Freshw. Res. 56:143–151.

Sumpton, W., and I. Brown.
2004. Reproductive biology of the red throat emperor *Lethrinus miniatus* (Pisces: Lethrinidae) from the southern Great Barrier Reef, Australia. Bull. Mar. Sci. 74:423–432.

Then, A. Y., J. M. Hoenig, N. G. Hall, and D. W. Hewitt.
2015. Evaluating the predictive performance of empirical estimators of natural mortality rate using information on over 200 fish species. ICES J. Mar. Sci. 72:82–92.

Vivekanandan, E., P. U. Zacharia, M. F. Khan, and R. J. Nari.
2003. Flatfishes. *In* Status of exploited marine fisheries resources of India (M. M. Joseph and A. A. Jayaprakash, eds.), p. 164–170. Cent. Mar. Fish. Res. Inst., Kochi, India.

Wakefield, C. B., I. C. Potter, N. G. Hall, R. C. J. Lenanton, and S. A. Hesp.
2015. Marked variations in reproductive characteristics of snapper (*Chrysophrys auratus*, Sparidae) and their relationship with temperature over a wide latitudinal range. ICES J. Mar. Sci. 72:2341–2349.

Yoneda, M., Y. Kurita, D. Kitagawa, M. Ito, T. Tomiyama, T. Goto, and K. Takahashi.
2007. Age validation and growth variability of Japanese flounder *Paralichthys olivaceus* off the Pacific coast of northern Japan. Fish. Sci. 73:585–592.

National Marine
Fisheries Service
NOAA

Fishery Bulletin
established in 1881

Spencer F. Baird
First U.S. Commissioner
of Fisheries and founder
of *Fishery Bulletin*

Comparison of model types for prediction of seafloor trawlability in the Gulf of Alaska by using multibeam sonar data

Sarah C. Stienessen (contact author)[1]
Christopher N. Rooper[2]
Thomas C. Weber[3]
Darin T. Jones[1]
Jodi L. Pirtle[4]
Christopher D. Wilson[1]

Email address for contact author: sarah.stienessen@noaa.gov

[1] Alaska Fisheries Science Center
National Marine Fisheries Service, NOAA
7600 Sand Point Way NE
Seattle, Washington 98115

[2] Stock Assessment and Research Division
Pacific Biological Station
Fisheries and Oceans Canada
3190 Hammond Bay Road
Nanaimo, V9T 6N7 Canada

[3] Center for Coastal and Ocean Mapping
University of New Hampshire
24 Colovos Road
Durham, New Hampshire 03824

[4] Alaska Regional Office
National Marine Fisheries Service, NOAA
P.O. Box 21668
Juneau, Alaska 99802

Abstract—Many rockfishes (*Sebastes* spp.) inhabit rugged areas of seafloor that are inaccessible to survey trawl gear. Their utilization of such habitat makes estimation of their abundance difficult. Furthermore, it is often difficult to assess whether habitat is trawlable or untrawlable and to estimate the spatial extent of both habitat types. To help determine trawlability for the continental shelf in the Gulf of Alaska, we used multibeam sonar data collected in the area during 2011, 2013, and 2015. These data were used to derive 3 characteristics of the seafloor: oblique incidence backscatter strength (S_b oblique), seafloor ruggedness, and bathymetric position index. Habitat type was categorized as trawlable or untrawlable through analysis of video from deployed drift cameras. We tested the effectiveness of the use of these seafloor characteristics in prediction of habitat trawlability with 4 types of models: generalized linear model, generalized additive model, boosted regression tree, and random forest. All 4 models perform moderately well at predicting trawlability across the shelf, and results from all of them indicate that S_b oblique is the most important characteristic in discriminating between trawlable and untrawlable habitat. These results indicate that multibeam sonar data can help determine habitat type, information that in turn can help improve habitat-specific estimates of biomass of marine fish species.

Manuscript submitted 11 September 2020.
Manuscript accepted 18 August 2021.
Fish. Bull. 119:184–196 (2021).
Online publication date: 13 September 2021.
doi: 10.7755/FB.119.2-3.7

The views and opinions expressed or implied in this article are those of the author (or authors) and do not necessarily reflect the position of the National Marine Fisheries Service, NOAA.

The bottom-trawl surveys conducted by the Alaska Fisheries Science Center (AFSC) provide estimates of biomass of numerous rockfishes (*Sebastes* spp.) in the Gulf of Alaska (GOA) (Aydin et al., 2019). An area-swept method is used for the bottom-trawl surveys conducted over trawlable areas within the GOA (von Szalay and Raring, 2018). Results (e.g., biomass and numbers of various fish species) obtained from surveys in trawlable areas are expanded to the entire GOA, including untrawlable areas (i.e., those locations where the structure of the seafloor prevents survey gear from being properly or successfully deployed according to survey protocols). The biomass estimates from bottom-trawl surveys are essential input for stock assessment efforts and data-based fisheries management. However, many rockfish species prefer rocky and rugged habitat that is often inaccessible to bottom-trawl gear; in other words, many rockfish species reside at higher densities in untrawlable habitats (Jagielo et al., 2003). Acoustic backscatter attributed to individual rockfish in untrawlable areas is estimated to be 3 times that of backscatter attributed to individuals in trawlable areas (Jones et al., 2021).

By not sampling the preferred (untrawlable) habitat of some rockfish species, the biomass of these species in the GOA can be underestimated. Similarly, by sampling only the preferred (trawlable) habitat for other rockfish species, the biomass of these species can be overestimated. Survey efforts targeting only one of the habitat types occupied by a species can add non-random error to biomass estimates (Cordue, 2007). Consequently, reliable assessments of rockfish species are needed for both trawlable and untrawlable habitat types in the surveyed area. Acoustic methods, with complementary direct sampling tools, are being used to assess semi-pelagic rockfish populations that cannot be successfully sampled with trawl nets (Williams et al., 2010; Jones et al., 2012; Rooper et al., 2012; Jones et al., 2021).

During the AFSC bottom-trawl surveys, trawl tows are conducted at stations selected by using a stratified random sampling design (von Szalay and Raring, 2018). Historically, 25-km^2 grid cells have been designated as either trawlable or untrawlable; however, the initial classification of a grid cell is often uncertain. The trawlablilty of the seafloor in grid cells has been determined by a vessel skipper searching for a minimum of 2 h to locate trawlable ground with a multibeam echo sounder. Realistically, knowledge of seafloor trawability is not complete across each grid cell, and most grid cells include both trawlable and untrawlable bottom types. For an entire grid cell to be designated as trawlable, a trawlable path of only 1.5 km along the seafloor is necessary (1.5 km is the trawl length of a standard 15-min bottom-trawl tow). Trawling in an untrawlable area within a grid cell classified as trawlable can result in substantial gear damage, lost survey time, habitat damage, and the cell may end up being reclassified as untrawlable. More accurate knowledge of the actual extent of trawlable and untrawlable areas within the grid cells of a bottom-trawl survey can help to improve biomass estimates and survey productivity.

Research efforts have used the combination of acoustic backscatter data and analysis of underwater camera video to improve estimates of availability of rockfish species in the GOA, in part by using video images to determine the extent of seafloor trawlability (e.g., Jones et al., 2012; Rooper et al., 2012; Jones et al., 2021). These studies are limited by the time it takes to deploy a camera and the area that can be covered by a single camera. Multibeam sonar systems collect high-resolution acoustic bathymetry and backscatter data. These data can be used to generate comprehensive images of the seafloor, describe features of seafloor morphology, and discriminate among substrate types (e.g., Jagielo et al., 2003; Goff et al., 2004; Wilson et al., 2007; Brown and Blondel, 2009; Weber et al., 2013). If multibeam sonar data can be used to successfully categorize seafloor trawlability, large areas of seafloor can be classified as trawlable or untrawlable quickly and efficiently.

Researchers with the AFSC and the Center for Coastal and Ocean Mapping at the University of New Hampshire began collaborating in 2008 to optimize standard operating procedures for seafloor mapping with a Simrad ME70[1] multibeam echo sounder (Kongsberg Maritime AS, Kongsberg, Norway). The Simrad ME70 was designed specifically for fishery research applications as a calibrated, user-configurable multibeam sonar system intended to collect quantitative data on acoustic targets in the water column (Trenkel et al., 2008; Stienessen et al., 2019). However, the Simrad ME70 can also be used to simultaneously collect bathymetry and seafloor backscatter data (Cutter et al., 2010). Customized software can be used to extract bottom detections that characterize the seafloor from data collected with a Simrad ME70 (Weber et al., 2013).

A case study at Snakehead Bank, off Kodiak Island in Alaska, used seafloor characteristics extracted from the multibeam data collected with a Simrad ME70 in tandem with analysis of video images to distinguish trawlable from untrawlable habitat in the GOA (Weber et al., 2013). In a subsequent study, more areas in the GOA were included, several characteristics of benthic terrain derived from multibeam sonar data at various scales were considered, and optical technology was used to validate seafloor classification derived from mutlibeam sonar data (Pirtle et al., 2015). The authors of the latter study reported that the 2 best generalized linear models (GLMs) described 54% of the variation between trawlable and untrawlable seafloor types. These quantitative models were developed by using data collected with a Simrad ME70, at stations where video data were also recorded, and combined either oblique incidence backscatter strength (S_b oblique) or mosaic seafloor backscatter strength with vector ruggedness measure (VRM) and bathymetric position index (BPI) to predict seafloor trawlability.

Each of the predictors identified by Pirtle et al. (2015) describe a component of seafloor morphology. Backscatter strength is dependent on incidence angle of the acoustic signal with the seafloor. At normal incidence, there is not much difference in S_b between strong scatterers (e.g., hard rock and boulders) and weak ones (e.g., fine sand). However, S_b is higher from strong scatterers than from weak scatterers when the incidence angle is oblique (Jackson and Richardson, 2007; Lamarche et al., 2011; Weber et al., 2013). Values of S_b oblique can therefore help differentiate between substrate types. Vector ruggedness measure is a measure of seafloor rugosity (i.e., seafloor complexity), and values of VRM account for variability in both seafloor slope and aspect. This predictor describes the variation in terrain and should differentiate smooth and rugged substrates (Sappington et al., 2007; Grohmann et al., 2011). Finally, BPI is a measure of elevation relative to surrounding locations (Guisan et al., 1999). Values of BPI can be used to highlight topographic features, such as seafloor valleys or knolls, which are shallower or deeper than neighboring areas. Prior to our study, it was unclear whether the model that includes these 3 predictors, or seafloor characteristics, could be used to effectively classify seafloor trawlability outside of the study area utilized by Pirtle et al. (2015) or whether application of this model to other areas in the GOA would result in high misclassification.

The primary objective of our study was to use a combination of seafloor characteristics derived from multibeam sonar data and from analysis of underwater video images to determine whether the GLM that combines S_b oblique values with VRM and BPI values can continue to correctly classify seafloor trawlability over a larger extent of the GOA than the area classified by Pirtle et al. (2015). Secondarily, we wanted to determine whether nonlinear models are better at predicting seafloor trawlability; therefore, we tested the effectiveness of 3 other model types (generalized additive models [GAMs], boosted regression trees [BRTs], and random forests [RFs]) in predicting seafloor trawlability in the GOA, using the same 3 seafloor characteristics used in the GLM. Finally, on the basis of the performances of the 4 models, we identified which of the 3 seafloor characteristics determined with multibeam sonar data are the most consistently useful to discriminate between trawlable and untrawlable seafloor.

---

[1] Mention of trade names or commercial companies is for identification purposes only and does not imply endorsement by the National Marine Fisheries Service, NOAA.

Materials and methods

Field methods

Large-scale acoustic trawl surveys that assess the stock of walleye pollock (*Gadus chalcogrammus*) in the GOA are conducted biennially aboard the NOAA Ship *Oscar Dyson* during the summer (e.g., Jones et al.[2,3,4]). Fine-scale multibeam surveys were conducted with a Simrad ME70 opportunistically during the evening hours in 2011, 2013, and 2015. The multibeam surveys followed parallel transects spaced 2 km (1 nmi) apart, within nearby 25-km^2 grid cells. Only one fine-scale multibeam survey was conducted within each grid cell. Immediately after the multibeam survey, video data were also collected at 1–5 locations (i.e., camera stations) to characterize the extent of trawlable and untrawlable seafloor at areas covered during each fine-scale multibeam survey (Fig. 1). Selection of the locations of camera stations was often dependent on wind and current direction, sea state, and placement of other camera stations within the same grid. Fine-scale multibeam surveys were conducted in similar numbers of trawlable and untrawlable 25-km^2 grid cells. However, the extent of actual trawlable and untrawlable areas within a grid cell was unknown a priori, ultimately resulting in an unbalanced number of trawlable versus untrawlable camera stations.

Multibeam surveys The Simrad ME70 was configured with 31 symmetrical split beams, with the middle beam vertically oriented (i.e., steered at 0°). The beams in this configuration ranged from the spherical 2.8° nadir beam (0°) operating at 117 kHz to the 2 ellipsoidal 4.5°-alongship-by-11.0°-athwartship beams steered from −66° to 66° and operating at 75 kHz (Weber et al., 2013; Stienessen et al., 2019). A pulse duration of 1.5-ms was used for each beam. The sampling rate was synchronized with that of the ship's downward-looking Simrad EK60 scientific echo sounder (Kongsberg Maritime AS) to eliminate interference between the 2 instruments, resulting in an effective sampling interval of 1.35 s. A 25-mm tungsten carbide sphere was used to calibrate each beam by using the standard sphere calibration method (Demer et al.[5]).

A POS MV V4 system (Applanix, Richmond Hill, Canada) was used to compensate beam steering for pitch and roll of the vessel by exporting dynamic motion and position data directly into the Simrad ME70. It was also used to georeference the multibeam sonar data. A C-Nav MBX-4 system (Oceaneering International Inc., Houston, TX) was used to apply differential correction data to the POS MV to improve position accuracy. Expendable bathythermograph probes and casts of a conductivity, temperature, and depth instrument (SBE 911plus CTD, Sea-Bird Scientific, Bellevue, WA) were used to collect water temperature and salinity profile data at selected locations throughout the study area (Jones et al.[2,3,4]). Conductivity and water temperature data at transducer depth (5 m) were continuously transmitted to the Simrad ME70 sonar system from the ship's sensors.

Camera stations Camera stations were sampled during nighttime hours for all years, with one camera deployment conducted at each station. During camera deployments, the ship and camera were allowed to drift over the seafloor at a speed of approximately 1 kt (0.53 m/s). The depths of camera stations ranged between 75 and 300 m. A camera station is defined as the entire area over which a camera drifted during a particular deployment, and the location of a camera station is the location of the initial deployment. Selection of the locations of camera stations was often limited by current and wind speed and direction.

Video images were collected at camera stations by using either a single digital camera or a stereo digital camera (SDC) system in 2011 and by using only an SDC system in 2013 and 2015. The digital camera was equipped with one digital video recorder and 2 lights placed above the camera housing (Pirtle et al., 2015). The version of the SDC system used in 2011 had 2 Sony TRD-900 progressive scan camcorders (Sony Corp., Tokyo, Japan), both with a resolution of 1280 by 720 pixels, and 2 lights placed above the camera housing (Williams et al., 2010). Both video cameras resided in an aluminum cage. The version of the SDC system used in 2013 and 2015 is described in Rooper et al. (2016). It comprised paired machine-vision cameras that were spaced approximately 30 cm apart in underwater housing and were used to collect synchronized still images at a rate of 1 Hz. Lighting for this camera system was provided by 4 LED strobe lights. Each deployment of the

---

[2] Jones, D. T., P. H. Ressler, S. C. Stienessen, A. L. McCarthy, and K. A. Simonsen. 2014. Results of the acoustic-trawl survey of walleye pollock (*Gadus chalcogrammus*) in the Gulf of Alaska, June–August 2013 (DY2013-07). AFSC Process. Rep. 2014-16, 95 p. Alaska Fish. Sci. Cent., Natl. Mar. Fish. Serv., Seattle, WA. [Available from website.]

[3] Jones, D. T., S. Stienessen, K. A. Simonsen, and M. A. Guttormsen. 2015. Results of the acoustic-trawl survey of walleye pollock (*Gadus chalcogrammus*) in the western/central Gulf of Alaska, June–August 2011 (DY2011-03). AFSC Process. Rep. 2015-04, 74 p. Alaska Fish. Sci. Cent., Natl. Mar. Fish. Serv., Seattle, WA. [Available from website.]

[4] Jones, D. T., S. Stienessen, and N. Lauffenburger. 2017. Results of the acoustic-trawl survey of walleye pollock (*Gadus chalcogrammus*) in the Gulf of Alaska, June–August 2015 (DY2015-06). AFSC Process. Rep. 2017-03, 102 p. Alaska Fish. Sci. Cent., Natl. Mar. Fish. Serv., Seattle, WA. [Available from website.]

[5] Demer, D. A., L. Berger, M. Bernasconi, E. Bethke, K. Boswell, D. Chu, R. Domokos, A. Dunford, S. Fässler, S. Gauthier, et al. 2015. Calibration of acoustic instruments. ICES Coop. Res. Rep. 326, 133 p. [Available from website.]

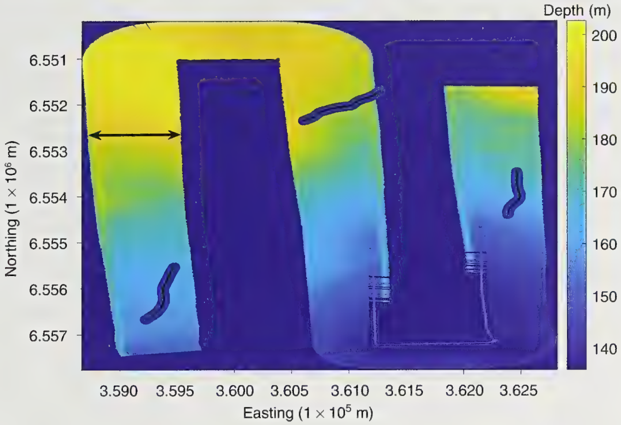

Figure 1

An example of bathymetry from a fine-scale multibeam survey conducted with a Simrad ME70 echo sounder and examples of the positions of associated camera stations deployed in the summers of 2011, 2013, and 2015 in the Gulf of Alaska. Data from multibeam surveys and camera deployments were used in models to characterize the extent of trawlability of habitat utilized by rockfishes (*Sebastes* spp.). The double-headed arrow indicates the depth-dependent width of the swath of seafloor insonified (i.e., area targeted) with the Simrad ME70. The black sinuate lines depict the track of the camera as it drifted along the seafloor (i.e., camera stations). The blue shading around each of the black lines indicates the area within 20 m of a camera station, and the data collected within this shaded area with the Simrad ME70 were used to calculate the seafloor characteristics used in the models. This image shows the north–south transects of 1 fine-scale multibeam survey and tracks at 3 camera stations.

single digital camera included 5 min on the seafloor, and each deployment of the SDC system included 15–30 min on the seafloor in 2011 or 30 min just above the seafloor in 2013 and 2015. The SDC system had a real-time video feed to the surface and a winch that allowed the camera position to be adjusted vertically in the water column as the camera drifted over rough terrain.

Data extraction and analysis

Multibeam data Bathymetry and backscatter data were extracted from the raw files retrieved from the Simrad ME70. More specifically, acoustic power associated with each detection of the seafloor was converted to backscatter following protocols established by Weber et al. (2013) in which system gains, calibration offsets, water column spherical spreading and absorption, and the area targeted by the beam are considered. Detections of the bottom were further used to calculate values for 3 seafloor characteristics identified by Pirtle et al. (2015) as among the best metrics with the best scale of analysis to predict seafloor trawlability in the GOA. The characteristics were S_b oblique, VRM, and BPI. The S_b oblique data were limited to the angle-dependent S_b data collected at incidence angles between 35° and 50°.

On the basis of results of Pirtle et al. (2015), VRM was calculated with data from a 21-by-21 array of 6-m^2 grid cells by using the bathymetry of each cell and 8 surrounding neighbor cells, and BPI was calculated with data from analysis windows, each with a radius of 200 6-m^2 grid cells. In our study, VRM was calculated by using only metric units (i.e., positions in meters of x and y coordinates in the Universal Transverse Mercator system and depth in centimeters). In contrast, Pirtle et al. (2015) used 2 different types of units for VRM calculations (i.e., positions in degrees of x and y coordinates in a geographic coordinate system and depth in meters).

Only seafloor characteristics calculated for the area within 20 m of a given camera station (i.e., within 20 m of the path of the camera as it drifted over the seafloor) were associated with that particular station. Specifically, if the bottom detection was within 20 m of the camera station, VRM and BPI were calculated, even if part or all of the array of 6-m^2 grid cells (VRM) or of the radius of the analysis window (BPI) was outside of the 20 m. Single S_b oblique, VRM, and BPI values were derived for each camera station by taking an average of each value collected along the camera path.

Video data Seafloor substrate was classified as either trawlable or untrawlable during review of video images by an experienced AFSC analyst. Designation of trawlability was based on whether the standard 4-seam Poly-Nor'Eastern bottom trawl used by AFSC in biennial bottom-trawl surveys (Stauffer, 2004) could successfully trawl in a given area. Specifically, analysts defined untrawlable areas in video images as any substrate containing boulders higher than 20 cm off bottom, an elevation that corresponds to the height of the roller gear on the footrope of the Poly-Nor'Eastern trawl (Rooper et al., 2012). They also classified areas in video images as untrawlable if the seafloor contained bedrock with vertical relief or ruggedness greater than 20 cm that would likely prevent the bottom trawl from passing over it without damage to the net from seafloor contact.

Modeling seafloor trawlability

Ultimately, each camera station was classified as either trawlable or untrawlable and was characterized by S_b oblique, VRM, and BPI. The analyses done with models included only the stations for which data for all 3 variables were produced. Occasionally it was not possible to calculate S_b oblique at a camera station. Although the camera deployment paths fell within the area covered during a fine-scale multibeam survey (Fig. 1), the positions of the camera deployments did not always overlap with the portion of the survey swath for which a Simrad ME70 collected data at 35–50° incidence angles. The effectiveness of using the seafloor characteristics derived from multibeam sonar data to discriminate between trawlable and untrawlable habitat was tested with 4 different kinds of predictive models: GLMs, GAMs, BRTs, and RFs. The GLMs were used to build upon, and allow direct comparisons to, the work of Pirtle et al. (2015). The GAMs are similar to the GLMs but allow any nonlinear relationships between the seafloor characteristics to be expressed. The BRTs and RFs have machine learning strength for classification and allow inclusion of nonlinear components.

Generalized linear models Seafloor trawlability was modeled with logistic regression by using the GLM:

$$\begin{aligned} trawlability = B_0 + (B_1 \times S_b\, oblique) + (B_2 \times VRM) \\ + (B_3 \times BPI) + E, \end{aligned} \tag{1}$$

where $B_{0,1,2,3}$ = the parameters estimated by the model, and

E = error;

in the GLM, the logit link function $p(Y)=e(Y)/1+e(Y)$ is used for binary response data (McCullagh and Nelder, 1983). The logit link function maps probability values (p) between 0 and 1 for any given real number Y between negative and positive infinity. Seafloor characteristics were standardized prior to analysis by subtracting the mean and dividing by the standard deviation.

We ran a GLM with all 3 years (2011, 2013, and 2015) of data. Backward variable selection was then performed on the data from all 3 years by fitting the model and dropping terms on the basis of an insignificant P-value for the model term (i.e., $P \geq 0.05$) and the Akaike information criterion (AIC). The predicted responses of models with AIC values within 2 digits are not considered different (Burnham and Anderson, 2002). Deviance explained (D^2), an analysis of deviance test comparing the model results to a null model (level of significance=0.05), and the area under the receiver operating characteristic curve (AUC) were also calculated for comparison with the 3 other types of predictive models. In general, an AUC value of 0.5 indicates that the model cannot discriminate between trawlable and untrawlable seafloor; AUC values of 0.7–0.8 are acceptable, values of 0.8–0.9 are good, and values >0.9 are excellent (Hosmer and Lemeshow, 2000). To evaluate the performance of the GLMs, we fit a GLM to two-thirds of the data (randomly drawn without replacement) and used the remaining one-third of the data for testing. Closer agreement between the area under the receiver operating characteristic curve for the test data set containing out-of-sample data (test AUC) and the area under the receiver operating curve for the training data set (training AUC) indicates better predictive performance by the model.

Generalized additive models Seafloor trawlability was also modeled with GAMs by using the mgcv package, vers. 1.8-28 (Wood, 2017), in RStudio, vers. 1.2.5019-6 (RStudio, Boston, MA). These models assume that the effects of trawlability are additive and can use smooth functions (penalized regression splines) to model each predictor on the response variable (Wood and Augustin, 2002). Best-fitting models were determined in a backward stepwise fashion beginning with the GAM model:

$$trawlability = s(S_b\, oblique) + s(VRM) + s(BPI) + E, \tag{2}$$

where the function $s(x)$ indicates a smooth effect of each predictor. In the GAM, the logit link function is used for binary response data. Terms were dropped on the basis of a nonsignificant test for the F-term in the nonparametric effects, and terms were made into a linear function instead of a smooth function on the basis of a significant test for the F-term in the parametric effects. Model results were compared on the basis of values for D^2, AIC, and training AUC. To evaluate the performance of the GAMs, we fit a GAM to two-thirds of the data and used the remaining one-third of the data for testing (the same training and testing data sets used in the work with the GLMs).

Boosted regression trees Seafloor trawlability was modeled with BRTs by using the dismo package, vers. 1.1-4 (Hijmans et al., 2017), in RStudio. Unlike traditional regression tree methods, BRT boosting is used to combine large numbers of simple tree models adaptively to display nonlinear relationships between the response and its predictors and to optimize predictive performance (e.g., Elith et al., 2006, 2008). That is, the input data are weighted in subsequent trees rather than allowing each occurrence to have an equal probability of being selected. Boosted regression trees require the specification of 3 parameters: learning rate, tree complexity (the number of nodes in the tree), and bag fraction (Elith et al., 2006, 2008). We ran the BRT model,

$$trawlability = S_b\ oblique + VRM + BPI, \qquad (3)$$

following the guidelines discussed in Elith et al. (2008) by using the Bernoulli family for binary response data and reducing the learning rate to aim for over 1000 trees. For example, we used a learning rate of 0.001 shrinkage applied per tree, a tree complexity of 5, and bag fraction of 0.5. We assessed the value in simplifying the model by using the gbm.simplify procedure in the dismo package. Two-thirds of the data were selected to be part of the training set, and the remaining one-third of the data were used as the test set (the same training and testing data sets used in the work with GLMs and GAMs). Model results were evaluated on the basis of values for D^2, AUC, and the influence of the predictors.

Random forests Seafloor trawlability was modeled with RFs by using the randomForest package, vers. 4.6-14 (Liaw and Wiener, 2002), and caret package, vers. 6.0-84 (Kuhn, 2019), in RStudio. In the RFs, random samples of predictor variables are used to generate many individual decision trees (forests) where each decision tree is constructed by an individual bootstrap with replacement sample drawn from the original data. That is, the split determination at each node is based on the best-splitting variable from a randomly selected subset of variables. For classification, a weighted vote of the decision trees is used (Breiman, 2001). Data not in the bootstrap sample are out-of-bag data and are used as samples to be classified in each decision tree. Random forests require the specification of 2 parameters: number of classification trees (number of bootstrap iterations) and the number of input variables to be used at each node. An RF has reliable predictive performance even when most predictive variables are noisy; therefore, it does not require preselection of predictors (Díaz-Uriarte and Alvarez de Andres, 2006; Okun and Priisalu, 2007).

On the basis of the results of a sensitivity analysis, we found that the caret package defaults (number of trees set at 500, and number of input variables set at 1) are appropriate for our data and used them in the RF model:

$$trawlability = S_b\ oblique + VRM + BPI. \qquad (4)$$

Two-thirds of the data were selected to be part of the training set, and the remaining one-third of the data were used as the test set (the same training and testing data sets used in the work with the GLMs, GAMs, and BRTs). Model results were evaluated on the basis of values for the out-of-bag error estimate, AUC, and mean decrease in the accuracy of the predictors.

Ensemble model An ensemble model was produced for estimation of seafloor trawlability by averaging predictions of the best GLM, GAM, BRT, and RF at each raster cell (i.e., for each camera station). Two-thirds of the data were selected to be part of the training set, and the remaining one-third of the data were used as the test set (the same training and testing data sets used in the GLM, GAM, BRT, and RF) to compare the ensemble model fit to the individual models.

Results

A total of 47, 64, and 92 camera stations were sampled during the fine-scale surveys conducted with a Simrad ME70 during 2011, 2013, and 2015, respectively. Of these, only 38 (21 trawlable and 17 untrawlable) camera stations in 2011, 36 (22 trawlable and 14 untrawlable) camera stations in 2013, and 56 (29 trawlable and 27 untrawlable) camera stations in 2015 produced data that could be used to estimate all 3 seafloor characteristics (Fig. 2). This was largely due to the fact that the video data were collected outside of the portion of the swath surveyed with a Simrad ME70 that was characterized by 35–50° incidence angles (i.e., there were no overlapping measures for S_b oblique) at a number of camera stations. This effect, coupled with the unknown extent of trawlable and untrawlable areas within a grid cell a priori, produced an unbalanced final number of trawlable and untrawlable camera stations.

The seafloor characteristic S_b oblique had a low correlation with the other 2 characteristics (VRM: coefficient of correlation [r]=0.15; BPI: r=0.05), and VRM and BPI also had a low correlation with one another (r=0.09). Values of S_b oblique associated with trawlable seafloor were significantly lower than those associated with untrawlable seafloor when all 3 years of data were used (Fig. 3A). Values of VRM and BPI associated with trawlable seafloor were also lower than those associated with untrawlable seafloor when all 3 years of data were used, although the differences were not significant (Fig. 3, B and C).

Generalized linear model

The best-fit GLM was a single-variable model in which S_b oblique is used. Only S_b oblique was significant in the full model (P=0.0001). The variables VRM (P=0.11) and BPI (P=0.22) were not. Additionally, the AIC value for the single-variable model in which only S_b oblique (AIC=151.5) is used was slightly less than that for the full model (AIC=153.4) (Table 1).

Generalized additive model

The best-fit GAM included a smoothed VRM term and a linearized S_b oblique term. The BPI seafloor characteristic was not significant for the model. In the best model, the remaining terms were significant, linearized S_b oblique was significant, AIC (147.5) was minimized, and D^2 (0.31) was relatively high (Table 2). Compared with this model, a

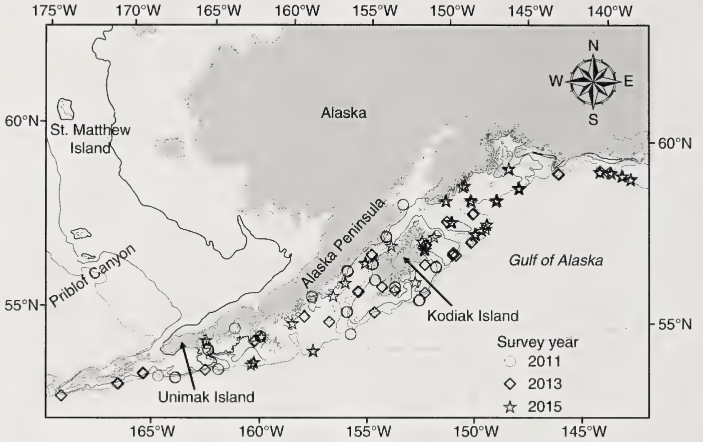

Figure 2

Map of the locations of camera stations where fine-scale multibeam surveys were conducted in the Gulf of Alaska during the summers of 2011 (circles), 2013 (diamonds), and 2015 (stars). The collected multibeam sonar data were used to derive seafloor characteristics used in models to predict trawlability of habitat utilized by rockfishes (*Sebastes* spp.).

model that included a smooth function for S_b oblique had a higher AIC (150.5), although the D^2 (0.31) was the same. A model that included all 3 seafloor characteristics and assigned a smooth function to them had an even higher AIC (154.4), and the D^2 (0.25) was lower.

Boosted regression tree

Results from the use of the gbm.simplify procedure indicate that the full BRT model (with all 3 variables) could be simplified to a 2-variable model by dropping VRM. This simplification resulted in a more parsimonious model without degradation of model fit. That is, the removal of VRM did not adversely affect model predictive performance. Deviance explained (0.31) was the same for the 2 models, and test AUC increased by 0.01 (to 0.65) in the simplified model. The predictor S_b oblique influenced both models the most (68% in the simplified model and 59% in the full model), followed by BPI (simplified: 32%; full: 28%). The VRM influenced the full model by only 13% (Table 3).

Random forest

The global accuracy (proportion of correct classification of trawlability) for this model was 0.655. Restated, the RF incorrectly classified trawlability 34.5% of the time (out-of-bag error estimate=0.345). The seafloor characteristic S_b oblique contributed the most to the model's prediction performance (mean decrease accuracy=0.180), but permuting VRM (mean decrease accuracy=0.013) and BPI (mean decrease accuracy=0.006) did not obstruct the model substantially. That is, VRM and BPI were not helpful predictors. When either VRM or BPI was permuted in a way that allowed its distribution to remain the same but assigned its specific observations randomly to the data, there was minimal loss of accuracy in classification.

Model evaluation

Results from all full models indicate a strong relationship between seafloor trawlability and S_b oblique. Additionally, S_b oblique was the most important predictor in all models. The seafloor characteristic VRM was significant in the GAM, and BPI contributed to the performance of the BRT. The GLM and GAM produced smooth or linear responses, but the significance of VRM was not consistent in these 2 models (Fig. 4). The response curves for the BRT and RF were similar to each other, indicating that the use of these 2 models revealed the same relationships in the data (Fig. 4), although the different learning methods between the 2 models resulted in different associations. In the RF, the initial variable is selected at random, and over many iterations the choice typically becomes obvious (e.g., S_b oblique). However, when similar predictions result from

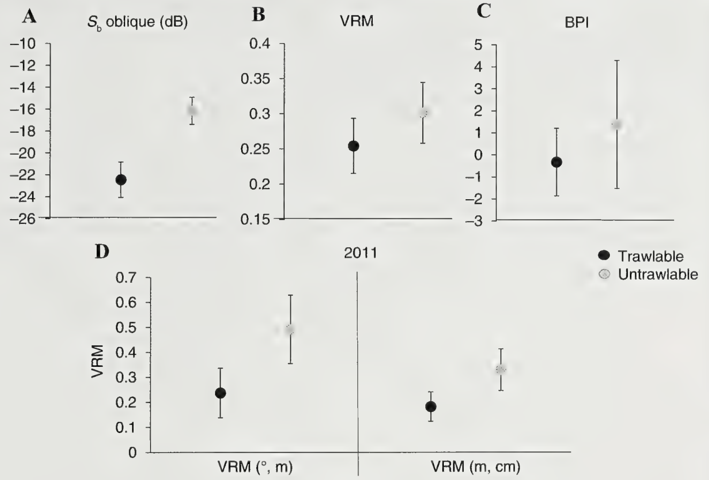

Figure 3

Mean values of seafloor characteristics derived from multibeam sonar data and used in models to classify habitat utilized by rockfishes (*Sebastes* spp.) as trawlable (black circles) or untrawlable (gray circles). Data were collected during fine-scale multibeam surveys conducted in 2011, 2013, and 2015 in the Gulf of Alaska. Plots show the effect of trawlability on 3 seafloor characteristics, (**A**) oblique incidence backscatter strength (S_b oblique), (**B**) vector ruggedness measure (VRM), and (**C**) bathymetric position index (BPI), over all years combined and (**D**) show the effect of units on VRM in 2011. In this study, VRM was calculated by using meters for coordinates in the Universal Transverse Mercator system and depth in centimeters (right half of the plot in panel D), but Pirtle et al. (2015) used degrees for coordinates in a geographic coordinate system and depth in meters (left half of the plot). Error bars indicate 95% confidence intervals.

Table 1

Comparison of results from generalized linear models used to predict seafloor trawlability of habitat utilized by rockfishes (*Sebastes* spp.) at locations of camera stations surveyed during 2011, 2013, and 2015 in the Gulf of Alaska. Predictor variables are seafloor characteristics derived from multibeam sonar data: oblique incidence backscatter strength (S_b oblique), vector ruggedness measure (VRM), and bathymetric position index (BPI). Values of Akaike information criterion (AIC), deviance explained (D^2), area under the receiver operating curve for the training data set (training AUC), and area under the receiver operating curve for the test data set containing out-of-sample data (test AUC) are provided for each model.

Year range	Model	AIC	D^2	Model significance	Training AUC	Test AUC
2011–2015	S_b oblique	151.5	0.17	2.34×10^{-8}	0.77	0.75
2011–2015	S_b oblique + VRM + BPI	153.4	0.19	2.78×10^{-7}	0.81	0.73

models with 2 different variables (e.g., models with VRM or BPI), the randomness of the RF becomes more apparent.

Model fits were reasonable for each best model (test AUC values range from 0.63 to 0.75), with the best GLM and GAM having higher test AUC scores (0.75 and 0.70, respectively) than the simplified BRT model and RF (0.65 and 0.63, respectively) (Tables 1–3). However, both the best GAM and simplified BRT accounted for more D^2 (0.31; Tables 2–3) than the best GLM (0.17; Table 1).

Ensemble model

The ensemble model was produced by averaging the predictions of the best models (i.e., the single-variable GLM in which S_b oblique was used, the GAM that included a smoothed VRM term and a linearized S_b oblique term, the simplified BRT, and the full RF) for each camera station. The fit for the ensemble model indicates that the model was reasonably effective in separating trawlable and untrawlable habitat (test AUC=0.70). The ensemble model's performance in predicting trawlability with the test data was better than the performance of the simple BRT (AUC=0.65; Table 3) and RF (AUC=0.63), it was equal to the performance of the best GAM (AUC=0.70; Table 2), and it was slightly lower than the performance of the best GLM (AUC=0.75; Table 1).

Table 2

Comparison of results from generalized additive models used to predict seafloor trawlability of habitat utilized by rockfishes (*Sebastes* spp.) at locations of camera stations surveyed during 2011, 2013, and 2015 in the Gulf of Alaska. In the models, $s(x)$ indicates a smooth effect of the predictor. Models are listed in order of decreasing accuracy of the predictions of trawlability. Predictor variables are seafloor characteristics derived from multibeam sonar data: oblique incidence backscatter strength (S_b oblique), vector ruggedness measure (VRM), and bathymetric position index (BPI). Values of Akaike information criterion (AIC), deviance explained (D^2), area under the receiver operating curve for the training data set (training AUC), and area under the receiver operating curve for the test data set containing out-of-sample data (test AUC) are provided for each model.

Model	AIC	D^2	Training AUC	Test AUC
S_b oblique + s(VRM)	147.5	0.31	0.86	0.70
s(S_b oblique) + s(VRM)	150.5	0.31	0.87	0.70
s(S_b oblique) + s(VRM) + s(BPI)	154.4	0.25	0.88	0.68

Discussion

All 4 types of predictive models produced similar overall results: S_b oblique was the most significant predictor to discriminate between seafloor designated as trawlable or untrawlable through analysis of video images, and all tested models were moderately effective in predicting trawlability at camera stations across the shelf in the GOA (D^2 range from 0.17 to 0.31, and test AUC values range from 0.63 to 0.73). Results from the GAM and BRT indicate that one predictor can be omitted, but they disagree as to whether the predictor should be BPI (GAM) or VRM (BRT). Results from the GLM and RF indicate that both BPI and VRM could be omitted without much loss in the accuracy of the classification of trawlable versus untrawlable habitat.

The prominence of S_b oblique in predicting trawlability corroborates the results of previous work (Jagielo et al., 2003), specifically those studies on trawlability in the GOA (Weber et al., 2013; Pirtle et al., 2015), but over a much larger geographic extent. Additionally, the lower values of S_b oblique associated with trawlable areas compared with those associated with untrawlable areas indicate a lack of strong scatterers, like hard rock and boulders, in trawlable habitat (Jackson and Richardson, 2007; Lamarche et al., 2011). Weber et al. (2013) found that trawlable areas had lower S_b oblique values than untrawlable areas at Snakehead Bank in the GOA. Furthermore, of the measured seafloor characteristics, S_b oblique had the best performance in predicting trawlability at the Snakehead Bank study site (Weber et al., 2013). Pirtle et al. (2015) also found that untrawlable areas had higher S_b oblique values than trawlable areas at many locations between Akutan Island (53°43′N, 164°58′W) and the eastern side of Kodiak Island (57°18′W, 151°30′N). In their

Table 3

Comparison of results from boosted regression trees, with 2 or 3 variables, used to predict seafloor trawlability of habitat utilized by rockfishes (*Sebastes* spp.) at locations of camera stations surveyed during 2011, 2013, and 2015 in the Gulf of Alaska. Predictor variables are seafloor characteristics derived from multibeam sonar data: oblique incidence backscatter strength (S_b oblique), vector ruggedness measure (VRM), and bathymetric position index (BPI). Values of deviance explained (D^2), area under the receiver operating curve for the training data set (training AUC), and area under the receiver operating curve for the test data set containing out-of-sample data (test AUC) are provided for each model. The dash in the table signifies that the corresponding predictor variable (VRM) was not used in the associated model.

Model	D^2	S_b oblique influence	VRM influence	BPI influence	Training AUC	Test AUC
S_b oblique + BPI	0.31	68.2	–	31.8	0.86	0.65
S_b oblique + VRM + BPI	0.31	59.3	13.1	27.6	0.88	0.64

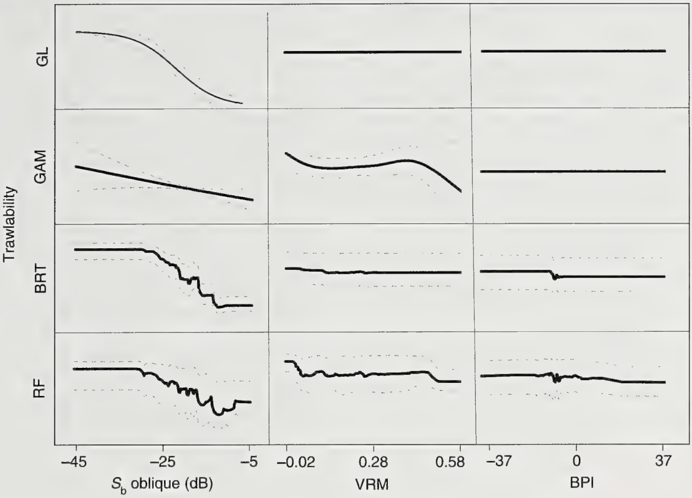

Figure 4

Relationships between explanatory variables of models—oblique incidence backscatter (S_b oblique), vector ruggedness measure (VRM), and bathymetric position index (BPI)—and trawlability of habitat utilized by rockfishes (*Sebastes* spp.). The generalized linear model (GLM) depicts the single-variable model in which S_b oblique was used, the generalized additive model (GAM) includes a smoothed VRM term and a linearized S_b oblique term, the boosted regression tree (BRT) is the full model, and the random forest (RF) is the full model. Response curves that are horizontal lines for the entire extent of variables in the GLM and GAM models indicate that these variables were not significant in the model. Gray dashed lines indicate 95% confidence intervals. Data used in models were collected during fine-scale multibeam surveys in 2011, 2013, and 2015 in the Gulf of Alaska.

study, characteristics derived from multibeam sonar data were used to predict seafloor trawlability for both locations of camera stations and for historic locations of trawl tows of the AFSC bottom-trawl survey. The latter was defined as areas where a bottom-trawl survey had previously been conducted, either successfully with little or no gear damage (trawlable) or unsuccessfully with extensive gear damage (untrawlable). For both camera station and trawl tow locations, Pirtle et al. (2015) found that a model in which only S_b oblique is used to be among the most discriminating single-variable models for predicting trawlability. Furthermore, the addition of other variables did not improve predictive discrimination for data from tow locations.

The relevance of VRM and BPI in predicting trawlability is less clear. Results of our study indicate that the addition of VRM and BPI does not improve on the effectiveness of a single-variable linear model in which only S_b oblique is used to predict trawlability. Similarly, in other studies, seafloor rugosity was a poor discriminator between trawlable and untrawlable seafloor at Snakehead Bank (Weber et al., 2013), and neither VRM nor BPI improved on the performance of the single-variable linear model in predicting trawlability at tow locations over larger portions of the GOA (Pirtle et al., 2015). However, the addition of both VRM and BPI improved the effectiveness of the single-variable linear model in predicting trawlability at camera stations in the study of Pirtle et al. (2015). They found that including S_b oblique, VRM, and BPI resulted in 1 of the 2 most discriminating GLMs for explaining trawlability in the GOA (AIC=32.1, D^2=0.55). They calculated VRM slightly differently than we did, but that difference does not appear to explain the discrepancy in results. When we updated the data from 2011 used in the Pirtle et al. (2015) study with VRM calculated with consistent units (i.e., updated with positions in meters of *x* and *y* coordinates in the Universal Transverse Mercator system and depth in centimeters), the relationship between trawlable and untrawlable areas determined by using VRM values did not change. The VRM values for trawlable areas were still significantly lower than values for untrawlable areas (Fig. 3D), although the performance of the model decreased slightly (AIC=33.4, D^2=0.45).

When 2 more years of data (i.e., data from 2013 and 2015) were added to the model, performance decreased further (AIC=153.4; D^2=0.19; Table 1).

Pirtle et al. (2015) postulated that VRM and BPI were important in predicting trawlability at locations of camera stations but not at trawl tow locations because at camera stations the range of seafloor types that was sampled (i.e., both trawlable and untrawlable) was broader than the range sampled at tow locations where surveys were designed to target trawlable seafloor. However, with the addition of the data from 2013 and 2015 to the linear model that incorporates a broader range of seafloor types, VRM and BPI were no longer necessary predictors. The portions of the GOA where data were collected from camera stations were larger in 2013 and 2015 than in 2011 (Fig. 1). That is, they were collected farther west (i.e., west of Umnak Island: 52°38′N, 169°14′W) and farther east (i.e., east of Kodiak Island) (Fig. 2). This difference indicates that VRM and BPI are not as effective in GLM predictive discrimination of trawlability beyond the geographic area sampled in 2011.

The power of the use of seafloor characteristics derived from multibeam sonar data to predict seafloor structures is dependent on spatial scale (Wilson et al., 2007). That is, the predictive power of the seafloor characteristics is dependent on the areal extent used to initially create the model. The predictive power of the characteristics is also more pronounced when they have a greater range of values. The ranges of BPI values extracted in 2013 and 2015 were not as large as the range of those extracted in 2011 (Fig. 5). The VRM and BPI may be more useful as predictors when more "extreme" bottom types are encountered, and they may not have as much predictive power when their extracted values are closer to the overall mean. The areal extent of the study site used by Pirtle et al. (2015) to create the model likely affects the applicability of the model over a larger extent of the GOA.

Even though VRM and BPI can be omitted from the GLMs and RFs without much loss in effectiveness at defining trawlable versus untrawlable seafloor in the GOA, they were independently useful for predictive discrimination of trawlability in the GAMs and BRTs. That is, VRM was included in the most parsimonious GAM, and BPI was included in the most parsimonious (i.e., simplified) BRT. It is unclear why predictive performance with VRM and BPI is not consistent among the GAMs and BRTs, because these characteristics are not strongly correlated. They measure different seafloor properties; therefore, there should be no confusion about which characteristic should be dropped from the model. The addition of either VRM or BPI to the respective nonlinear models results in reasonable test AUC scores for the out-of-sample sites.

Our results indicate that all the models identify S_b oblique as the primary driver for predictive discrimination

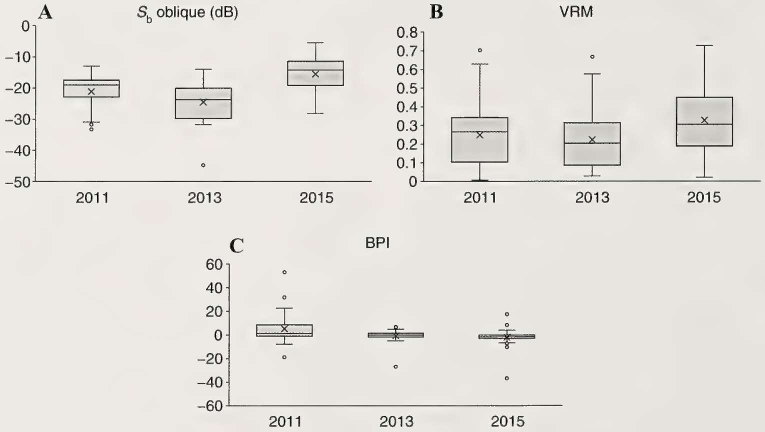

Figure 5

Box plots for the seafloor characteristics, (**A**) oblique incidence backscatter (S_b oblique), (**B**) vector ruggedness measure (VRM), and (**C**) bathymetric position index (BPI), derived from data collected with a Simrad ME70 multibeam echo sounder in 2011, 2013, and 2015 in the Gulf of Alaska. Seafloor characteristics were used to predict trawlability of habitat utilized by rockfishes (*Sebastes* spp.). The boxes show the first quartile (lower line), median (middle line), and third quartile (upper line). The whiskers extend to the minimum and maximum values. Gray circles represent outliers, and the x in the middle of each box indicates the mean.

of seafloor trawlability. This finding may encourage steering a scientific echo sounder's single beam between 35° and 50° to collect the necessary data. Single-beam echo sounders are fairly ubiquitous on both scientific and fishing vessels. Research results indicate that, when added to models that help explain distribution of benthic animals relative to their habitat, data collected with echo sounders increase the percentage of explained variance (McConnaughey and Syrjala, 2009; Somerton et al., 2017). However, S_b oblique is an incidence angle measurement, and is not dependent on steering angle. Theoretically, steering a single-beam echo sounder at 35–50° over flat terrain would yield the appropriate incidence angles. Yet as soon as there was any change in seafloor bathymetry, the incidence angles would also change, likely outside of the range of the steered single beam. Therefore, multibeam echo sounders are well-suited to collecting S_b oblique data. Having beams steered at a range of angles (from −66° to 66° in our study) increases the odds that at any given time one or more of the beams will insonify the seafloor at angles between 35° and 50°.

A limitation to using seafloor characteristics derived from multibeam sonar data to predict trawlability is that such data are restricted to the area within the width of the swath of the sonar and not necessarily applicable to the area outside of the swath. Additionally, seafloor characteristics cannot be calculated near the boundary of the swath, because of the prerequisite spatial scale of the analysis window needed to calculate them. The effect of this limitation is less for multibeam surveys with 100% bottom coverage (Pirtle et al., 2015). However, the "effective area" for extracting data on seafloor characteristics is further reduced by the inclusion of S_b oblique. This predictor can be derived from only small areas of the sonar swath (i.e., incidence angles of 35–50°), effectively prohibiting full bottom coverage. That is, data collected at incidence angles <35° and >50° are not useful in predicting seafloor trawlability.

Conclusions

The GLM that combines S_b oblique values with VRM and BPI values produces reliable classification (on the basis of AUC results) of seafloor trawlability, even when applied to a larger geographic extent than that in previous work on seafloor trawlability in the GOA (Weber et al., 2013; Pirtle et al., 2015). However, VRM and BPI are not always critical predictors to the GLM—they are only beneficial in specific areas within the GOA (e.g., over the extent of the area sampled by Pirtle et al., 2015). The nonlinear models are not better at predicting seafloor trawlability, but the inclusion of VRM or BPI is more beneficial to these models and requires minimal computation effort.

These results indicate that, to predict seafloor trawlability in the GOA, it is important to use a model that has been developed with data from the entire extent of the area to which the model is being applied. Although results indicate that S_b oblique is a robust predictor of trawlability over both small and large extents of the GOA, the usefulness of the other seafloor characteristics may be limited to specific areas of the GOA. Consequentially, the use of seafloor characteristics derived from multibeam sonar data in models to predict seafloor trawlability is essential because the models are dependent on spatial representation across the specific area of interest within the GOA.

The strength of the case for using models, rather than analysis of video images from camera deployments, to predict seafloor trawlaiblity is the fact that multibeam sonar data can be collected relatively quickly and efficiently. A camera deployment on bottom for 30 min collects data only over an area that is approximately 1 m wide and 0.9 km long on the seafloor, whereas the Simrad ME70 echo sounder collects multibeam data across a swath width of 335–1345 m (which corresponds to the range of camera stations at depths between 75–300 m) and along a track of 10.2 km (assuming the ship is moving at 11 kt) during the same time period (i.e., 30 min). Reliable estimates of the extent of trawlable and untrawlable seafloor can be used to improve the accuracy of acoustic backscatter attributed to rockfishes in grid cells for areas classified as untrawlable (Jones et al., 2021), in turn improving the accuracy of stock assessments for these species.

Acknowledgments

We thank the scientists and crew of the NOAA Ship *Oscar Dyson* for their hard work in helping with the data collection. We thank T. Honkalehto and C. O'Leary for valuable comments and remarks on earlier drafts of this paper.

Literature cited

Aydin, K., S. Barbeaux, M. Bryan, S. Cleaver, C. Cunningham, O. Davis, M. Dorn, A. Dreary, K. Echave, C. Faunce, et al.
2019. Stock assessment and fishery evaluation report for the groundfish resources of the Gulf of Alaska, 43 p. North Pac. Fish. Manage. Counc., Anchorage, AK. [Available from website.]

Breiman, L.
2001. Random forests. Mach. Learn. 45:5–32.

Brown, C. J., and P. Blondel.
2009. Developments in the application of multibeam sonar backscatter for seafloor habitat mapping. Appl. Acoust. 70:1242–1247.

Burnham, K. P., and D. R. Anderson.
2002. Model selection and multi-model inference: a practical information-theoretic approach, 2nd ed., 488 p. Springer, New York.

Cordue, P. L.
2007. A note on non-random error structure in trawl survey abundance indices. ICES J. Mar. Sci. 64:1333–1337.

Cutter, G. R., Jr., L. Berger, and D. A. Demer.
2010. A comparison of bathymetry mapped with the Simrad ME70 multibeam echosounder operated in bathymetric and fisheries modes. ICES J. Mar. Sci. 67:1301–1309.

Díaz-Uriarte, R., and S. Alvarez de Andrés.
2006. Gene selection and classification of microarray data using random forest. BMC Bioinf. 7:3.

Elith, J., C. H. Graham, R. P. Anderson, M. Dudík, S. Ferrier, A. Guisan, R. J. Hijmans, F. Huettmann, J. R. Leathwick, A. Lehmann, et al.
2006. Novel methods improve prediction of species' distributions from occurrence data. Ecography 29:129–151.

Elith, J., J. R. Leathwick, and T. Hastie.
2008. A working guide to boosted regression trees. J. Anim. Ecol. 77:802–813.

Goff, J. A., B. J. Kraft, L. A. Mayer, S. G. Schock, C. K. Sommerfield, H. C. Olsen, S. P. S. Gulick, and S. Nordfjord.
2004. Seabed characterization on the New Jersey middle and outer shelf: correlatability and spatial variability of seafloor sediment properties. Mar. Geol. 209:147–172.

Grohmann, C. H., M. J. Smith, and C. Riccomini.
2011. Multiscale analysis of topographic surface roughness in the midland valley, Scotland. IEEE Trans. Geosci. Remote Sens. 49:1200–1213.

Guisan, A., S. B. Weiss, and A. D. Weiss.
1999. GLM versus CCA spatial modeling of plant species distribution. Plant Ecol. 143:107–122.

Hijmans, R. J., S. Phillips, J. Leathwick, and J. Elith.
2017. dismo: species distribution modeling. R package, vers. 1.1-4. [Available from website, accessed October 2019.]

Hosmer, D. W., and S. Lemeshow.
2000. Applied logistic regression, 2nd ed., 392 p. John Wiley and Sons, New York.

Jackson, D. R., and M. D. Richardson.
2007. High-frequency seafloor acoustics, 616 p. Springer, New York.

Jagielo, T., A. Hoffmann, J. Tagart, and M. Zimmermann.
2003. Demersal groundfish densities in trawlable and untrawlable habitats off Washington: implications for the estimation of habitat bias in trawl surveys. Fish. Bull. 101:545–565.

Jones, D. T., C. D. Wilson, A. De Robertis, C. N. Rooper, T. C. Weber, and J. L. Butler.
2012. Evaluation of rockfish abundance in untrawlable habitat: combining acoustic and complementary sampling tools. Fish. Bull. 110:332–343.

Jones, D. T., C. N. Rooper, C. D. Wilson, P. D. Spencer, D. H. Hanselman, and R. E. Wilborn.
2021. Estimates of availability and catchability for select rockfish species based on acoustic-optic surveys in the Gulf of Alaska. Fish. Res. 236:105848.

Kuhn, M.
2019. caret: classification and regression training. R package, vers. 6.0-84. [Available from website, accessed January 2020.]

Lamarche, G., X. Lurton, A.-L. Verdier, and J.-M. Augustin.
2011. Quantitative characterisation of seafloor substrate and bedforms using advanced processing of multibeam backscatter—application to Cook Strait, New Zealand. Cont. Shelf Res. 31(Suppl. 2):S93–S109.

Liaw, A., and M. Wiener.
2002. Classification and regression by randomForest. R News 2(3):18–22.

McConnaughey, R. A., and S. E. Syrjala.
2009. Statistical relationships between the distributions of groundfish and crabs in the eastern Bering Sea and processed returns from a single-beam echosounder. ICES J. Mar. Sci. 66:1425–1432.

McCullagh, P., and J. A. Nelder.
1983. Generalized linear models, 261 p. Chapman and Hall, New York.

Okun, O., and H. Priisalu.
2007. Random forest for gene expression based cancer classification: overlooked issues. *In* Pattern recognition and image analysis. IbPRIA 2007. Lecture notes in computer science, vol. 4478 (J. Martí, J. M. Benedí, A. M. Mendonça, and J. Serrat, eds.), p. 438–490. Springer, Berlin, Germany.

Pirtle, J. L., T. C. Weber, C. D. Wilson, and C. N. Rooper.
2015. Assessment of trawlable and untrawlable seafloor using multibeam-derived metrics. Methods Oceanogr. 12:18–35.

Rooper, C. N., M. H. Martin, J. L. Butler, D. T. Jones, and M. Zimmermann.
2012. Estimating species and size composition of rockfishes to verify targets in acoustic surveys of untrawlable areas. Fish. Bull. 110:317–331.

Rooper, C. N., M. F. Sigler, P. Goddard, P. Malecha, R. Towler, K. Williams, R. Wilborn, and M. Zimmerman.
2016. Validation and improvement of species distribution models for structure-forming invertebrates in the eastern Bering Sea with an independent survey. Mar. Ecol. Prog. Ser. 551:117–130.

Sappington, J. M., K. M. Longshore, and D. B. Thompson.
2007. Quantifying landscape ruggedness for animal habitat analysis: a case study using bighorn sheep in the Mojave Desert. J. Wildl. Manage. 71:1419–1426.

Somerton, D. A., R. A. McConnaughey, and S. S. Intelmann.
2017. Evaluating the use of acoustic bottom typing to inform models of bottom trawl sampling efficiency. Fish. Res. 185:14–16.

Stauffer, G.
2004. NOAA protocols for groundfish bottom trawl surveys of the nation's fishery resources. NOAA Tech. Memo. NMFS-F/SPO-65, 205 p.

Stienessen, S. C., C. D. Wilson, T. C. Weber, and J. K. Parrish.
2019. External and internal grouping characteristics of juvenile walleye pollock in the eastern Bering Sea. Aquat. Living Resour. 32:19.

Trenkel, V. M., V. Mazauric, and L. Berger.
2008. The new fisheries multibeam echosounder ME70: description and expected contribution to fisheries research. ICES J. Mar. Sci. 65:645–655.

von Szalay, P. G., and N. W. Raring.
2018. Data report: 2017 Gulf of Alaska bottom trawl survey. NOAA Tech. Memo. NMFS-AFSC-374, 260 p.

Weber, T. C., C. Rooper, J. Butler, D. Jones, and C. Wilson.
2013. Seabed classification for trawlability determined with a multibeam echo sounder on Snakehead Bank in the Gulf of Alaska. Fish. Bull. 111:68–77.

Williams, K., C. N. Rooper, and R. Towler.
2010. Use of stereo camera systems for assessment of rockfish abundance in untrawlable areas and for recording pollock behavior during midwater trawls. Fish. Bull. 108:352–362.

Wilson, M. F. J., B. O'Connell, C. Brown, J. C. Guinan, and A. J. Grehan.
2007. Multiscale terrain analysis of multibeam bathymetry data for habitat mapping on the continental slope. Mar. Geod. 30:3–35.

Wood, S. N.
2017. Generalized additive models: an introduction with R, 2nd ed., 496 p. CRC Press, Boca Raton, FL.

Wood, S. N., and N. H. Augustin.
2002. GAMs with integrated model selection using penalized regression splines and applications to environmental modelling. Ecol. Model. 157:157–177.

Fishery Bulletin

Guidelines for authors

Contributions published in *Fishery Bulletin* describe original research in marine fishery science, fishery engineering and economics, and marine environmental and ecological sciences (including modeling). Preference will be given to manuscripts that examine processes and underlying patterns. Descriptive reports, surveys, and observational papers may occasionally be published but should appeal to an audience outside the locale in which the study was conducted.

Although all contributions are subject to peer review, responsibility for the contents of papers rests upon the authors and not on the editor or publisher. *Submission of an article implies that the article is original and is not being considered for publication elsewhere.*

All submissions are subject to a double-blind review to remove the identity of author and reviewer during the review process.

Plagiarism and double publication are considered serious breaches of publication ethics. To verify the originality of the research in papers and to identify possible previous publication, manuscripts may be screened with plagiarism-detection software.

Manuscripts must be written in English; authors whose native language is not English are strongly advised to have their manuscripts checked by English-speaking colleagues before submission.

Once a paper has been accepted for publication, online publication takes approximately 2 weeks.

There is no cost for publication in *Fishery Bulletin*.

Types of manuscripts accepted by the journal

Articles generally range from 20 to 30 double-spaced typed pages (12-point font) and describe an original contribution to fisheries science, engineering, or economics. Tables and figures are not included in this page count, but the number of figures should not exceed 1 figure for every 4 pages of text. Articles contain the following divisions: abstract, introduction, methods, results, discussion, and conclusions.

Notes are generally less than 10 double-spaced typed pages (12-point font), including the Literature cited section. Like articles, notes describe an original contribution to fisheries science. They follow a format similar to that for articles: abstract, introduction, methods, results, and discussion, but the results and discussion sections may be combined and a conclusions section should not be included. They should include no more than 2 figures or tables (2 of each would be too many). They are distinguished from full articles in that they report a noteworthy new observation or discovery—such as the first report of a new species, a unique finding, condition, or event that expands our knowledge of fisheries science, engineering, or economics—and do not require a lengthy discussion. Manuscripts on range extensions will not be considered.

Companion articles should be submitted together and are published together as a scientific contribution. Both articles should address a closely related topic and may be articles that result from a workshop or conference.

Review articles of exceptional quality may be considered occasionally for publication on a case-by-case basis. They address a timely topic that is relevant to aspects of fisheries science. They should include an abstract, but the format of the article, per se, will be up to the author. Please contact the scientific editor to discuss your ideas regarding a potential review article before embarking on such a project.

Perspective essays generally are less than 5 double-spaced typed pages (12-point font) and provide clarification of misused terms or misunderstood topics in fisheries science. Essays are accepted at the discretion of the scientific editor. Opinion pieces on policy will not be considered. They should include an abstract and a list of the literature cited, but no other sections should divide the article. Please contact the scientific editor to discuss your idea before making a submission.

Preparation of manuscript

Title page should include authors' full names, affiliations, mailing addresses, and the senior author's email address.

Abstract should be limited to 200 words (one-half typed page), state the main scope of the research, and emphasize the authors' conclusions and relevant findings. Do not review the methods of the study or list the contents of the paper. Because abstracts are circulated by abstracting agencies, it is important that they represent the research clearly and concisely.

General text must be typed in 12-point Times New Roman font throughout. A brief introduction should convey the broad significance of the paper; the remainder of the paper should be divided into the following sections: Materials and methods, Results, Discussion, Conclusions, and Acknowledgments. Headings within each section must be short, reflect a logical sequence, and follow the rules of subdivision (i.e., there can be no subdivision without at least 2 subheadings). The entire text should be intelligible to interdisciplinary readers; therefore, all acronyms, abbreviations, and technical terms should be written out in full and defined the first time they are mentioned. Abbreviations should be used sparingly because they are not carried over to indexing databases and slow readability for those readers outside a discipline. They should never be used for the main subject (e.g., species or method) of a paper.

For general style, follow the U.S. Government Publishing Office *Style Manual* (2016, available at website) and *Scientific Style and Format: the CSE Manual for Authors, Editors, and Publishers* (2014, 8th ed.) published by the Council of Science Editors. For scientific nomenclature, use the current edition of the American Fisheries Society's (AFS) *Common and Scientific Names of Fishes from the United States, Canada, and Mexico* and its companion volumes (*Crustaceans, Mollusks, Cnidaria and Ctenophora*, and *World Fishes Important to North Americans*). For species not found in the previously mentioned AFS publications and for more recent changes in nomenclature, use the Integrated Taxonomic Information System (ITIS, available at website), or, secondarily, the California Academy of Sciences *Catalog of Fishes* (available at website) for species names not included in ITIS. Common (vernacular) names of species should be lowercase. Citations must be given for the identification of specimens. For example, "Fish species were identified according to Collette and Klein-MacPhee (2002); sponges were identified according to Stone et al. (2011)."

Dates should be written as follows: 11 November 2018. Measurements should be expressed in metric units, for example, "58 metric tons (t);" if other units of measurement are used, please make this fact explicit to the reader. Use numerals, not words, to express whole and decimal numbers in the general text, tables, and figure captions (except at the beginning of a sentence). For example, "We considered 3 hypotheses. We collected 7 samples in this location." Use American spelling. Refrain from using the shorthand slash (/), an ambiguous symbol, in the general text.

Cite all software, special equipment, and chemical solutions used in the study within parentheses in the general text, including the version number, company name, and the city and state (or nation) of the company headquarters, for example, "SAS, vers. 9.4 (SAS Institute Inc., Cary, NC)."

Word usage and grammar that may be useful are the following:

- *Aging*
  For our journal, the word *aging* is used to mean both age determination and the aging process (senescence). Authors should make clear which meaning is intended where ambiguity may arise.

- *Fish and fishes*
  The plural of the word fish (a collective noun that implies individuals without regard to species) is *fish*.
  Example: The *fish* were collected by trawl net.
  Example: The numbers of *fish* collected that season were less than the numbers from previous years.

  The plural for *fish species* is *fishes* (a contrived plural used by taxonomists to mean several or more *fish species*) or one can use *fish species* (which is preferred in this journal for clarity across disciplines).
  Example: The *fishes* of Puget Sound [biodiversity is implied] or
  Example: The *fish species* of Puget Sound [preferred plural for clarity across disciplines].

- *Crab and crabs, squid and squids, etc.*
  The plural of the word *crab* (i.e., many individuals without regard to species) is *crab*.
  Example: The crab were sorted by weight.
  Example: Many red king *crab* were dying [Many individuals of one species of crab.]

  The plural of *crab species* is *crabs* (a word used by taxonomists) or *crab species* (the latter is preferred in this journal for clarity).
  Example: These *crabs* were selected for treatment. [Different crab species are implied.]
  Example: These *crab species* were selected for treatment. [Preferred word choice for clarity.]
  Example: Snow *crabs* are found throughout the North Pacific Ocean and Bering Sea. [There are 2 species of snow crab; therefore the word *crabs* can be used here.]
  Example: *Two species* of snow *crab* are found throughout the North Pacific Ocean and Bering Sea. [Preferred usage for clarity.]
  Example: Three crabs were selected for treatment. [3 species of crab are implied.]
  Example: Three crab species were selected for treatment. [Preferred word choice for clarity.]

- We use *fisherman* and *fishermen*, not *fisher* and *fishers*, in this journal. One can always use crew member, vessel operator, and angler (the latter for recreational fishing).

- *The definite article with common names of species*
  When the singular common name of a species represents the entire class or group to which it belongs, use the definite article.
  Example: Only one species of the genus *Salmo* is found in the Atlantic Ocean—*the* Atlantic salmon (*Salmo salar*).
  Example: The sonic emissions of *the* bottlenose dolphin are complex.

  For plural common names, this rule does not apply.
  Example: Chinook salmon are found throughout the Pacific Ocean.
  Example: Bottlenose dolphins are found in temperate and tropical waters.

- *Sex*
  For the meaning of male and female, use the word *sex*, not *gender*. Do not write, "fish were sexed." Write, "sex was determined."

- *Participles*
  As adjectives, participles must modify a specific noun or pronoun.
  Example: Using mark-recapture methods, these scientists determined the size of the population. [Correct. The participle *using* modifies the word *scientists*.]

Example: These scientists, based on the collected data, concluded that the mortality rate of these fish had increased. [Incorrect. The scientists were not based on the collected data.]

Example: These scientists concluded, on the basis of collected data, that the mortality rate of these fish had increased. [Correct. The offending participle has been eliminated and an adverbial phrase modifies the verb *concluded*.]

Equations and mathematical symbols should be set from a standard mathematical program (MathType or Equation Editor). Equations formatted in LaTex are not acceptable. For mathematical symbols in the general text (α, χ^2, π, ±, etc.), use the symbols provided by the MS Word program and italicize all variables, except those variables represented by Greek letters and the superscript and subscript parts of variables and expressions. Do not use photo mode when creating these symbols in the general text, and do not cut and paste equations, letters, or symbols from a different software program.

Number equations (if there are more than one) for future reference by scientists; place the number within parentheses at the end of the first line of the equation.

Literature cited section comprises published works and those accepted for publication (in press) in peer-reviewed journals. Follow the name and year system for citation format in this section (i.e., citations should be listed alphabetically by the authors' last names, and then by year if there is more than one citation by the same author. A list of abbreviations for citing journal titles can be found on our website.

Authors are responsible for the accuracy and completeness of all citations. Avoid the use of multiple citations when a single citation sufficiently supports a statement; cite the work that first reported the information that supports a statement, not all of the subsequent works. Literature citation format: Authors (last name, followed by initials for first name and, if given, middle name of first author; then list names of additional authors with initials before last names). Year. Title of article. Abbreviated title of the journal in which it was published. Always include either the range of page numbers (for a journal article) or a total number of pages (for a book or other type of publication). List a sequence of citations in the general text chronologically, for example, "(Smith, 1932; Green, 1998; Smith and Jones, 2015)."

Acknowledgments should be no more than 6 lines of text. Only those who have contributed in an outstanding way should be acknowledged by name. For recognition of other persons or groups, use a general term, such as *crew*, *observers*, or *research coordinators*, and do not include names with these terms.

Digital object identifier (doi) code ensures that a publication has a permanent location online. A doi link (which may include a doi code) should be included at the end of citations of published literature. Authors are responsible for submitting accurate doi links. Faulty links will be deleted at the page-proof stage.

Footnotes are used for all documents that have not been formally peer reviewed and for observations and personal communications, but these types of references should be cited sparingly in manuscripts submitted to the journal.

All reference documents, administrative reports, internal reports, progress reports, project reports, contract reports, personal observations, personal communications, unpublished data, manuscripts in review, and council meeting notes are footnoted in 10-point font and placed at the bottom of the page on which they are first cited. Footnote format is the same as that for formal literature citations. A link to the online source (e.g., [Available from http://www..., accessed July 2017.]), or the mailing address of the agency or department holding the document, should be provided so that readers may obtain a copy of the document.

Tables are often overused in scientific papers; it is seldom necessary to present all the data associated with a study. Tables should not be excessive in size and must be cited in numerical order in the text. Headings should be short but ample enough to allow the table to be intelligible on its own.

All abbreviations and unusual symbols must be explained in the table legend. Other incidental comments may be footnoted with numeral footnote markers. Use asterisks only to indicate significance in statistical data. Do not put a table legend on a page separate from the table; place the legend above the table. *Do not submit tables in photo mode.*

- Note probability with a capital, italic *P*.
- Provide a zero before all decimal points for values less than one (e.g., 0.07).
- Round all values to 2 decimal points.
- Use a comma in numbers of 5 digits or more (e.g., 13,000 but 3000).

Figures must be cited in numerical order in the text. Graphics should aid in the comprehension of the text, but they should be limited to presenting patterns rather than raw data. The number of figures should not exceed 1 figure for every 4 pages of text.

Figure legends should explain all symbols and abbreviations seen in the figure and should be double spaced on a separate page at the end of the manuscript.

Line art and halftone figures should be saved at resolutions >600 dots per inch (dpi) and >300 dpi, respectively. Color is allowed in figures to show morphological differences among species (for species identification), to show stain reactions, to show gradations (such as those of temperature and salinity within maps), and to distinguish between numerous lines and symbols in graphs. Figures approved for color should be saved in CMYK format.

All figures must be submitted as PDF, TIFF, or EPS files.

- Capitalize only the first letter of the first word and proper nouns in all labels within figures.
- Do not use overly large font sizes for labels in maps and for axis labels in graphs.
- Use the same point size for all labels, except for panel labels (e.g., **A**), which should be slightly larger than other labels (e.g., 11 point versus 8 point).
- Use a sans serif font for all labels. Panel labels (e.g., **A**), however, should be in Times New Roman font.
- Do not use bold fonts or bold lines in figures. Do not use italic fonts. Exceptions include use of italic fonts for labels of bodies of water in maps and a bold font for panel labels (e.g., **A**).
- Do not place outline rules around graphs.
- Do not include vertical and horizontal lines in the background of graphs. Ticks for values on the x-axis and y-axis will suffice.
- Place a north arrow and label degrees latitude and longitude (e.g., 170°E) in all maps. If scale of map requires more than degrees, use degrees minutes, not decimal degrees.
- Place panel labels (e.g., **A**, **B**, **C**) within the upper-left area of each graph or photo in a multi-panel figure, from left to right, then top to bottom. If the letter is not visible against a dark background, put a white box behind it. Do not use white labels.
- Avoid placing labels vertically or diagonally. Y-axis labels can be vertical. Words in horizontal labels can be stacked vertically to fit.
- Use symbols, shading, or patterns (not clip art) in maps and graphs.
- For scale bars in maps, use kilometers. Use the label *km* or *kilometers* (lowercased).

Supplementary materials that are considered essential, but are too large or impractical for inclusion in a paper (e.g., metadata, figures, tables, videos, and websites), may be provided at the end of an article. These materials are subject to the editorial standards of the journal. A URL to the supplementary material and a brief explanation for including such material should be sent at the time of initial submission of the paper to the journal.

- **Metadata, figures, and tables** should be submitted in standard digital format (MS Word or PDF file) and should be cited in the general text, for example, as "... was determined (Suppl. Table 3, Suppl. Fig. 1)."
- **Websites** should be cited with a URL in the general text.
- **Videos** must not be larger than 30 MB to allow a swift technical response for viewing the video. Authors should consider whether a short video uniquely captures what text alone cannot capture for the understanding of a process or behavior under examination in the article. Supply an online link to the location of the video.

Copyright law does not apply to *Fishery Bulletin*, which falls within the public domain. However, if an author reproduces any part of an article from *Fishery Bulletin*, reference to source is considered correct form (e.g., Source: Fish. Bull. 117:105).

Failure to follow these guidelines and failure to correspond with editors in a timely manner will delay publication of a manuscript.

Submission of manuscript

Submit a manuscript online at the ScholarOne Manuscripts website for *Fishery Bulletin*. Commerce Department authors must provide proof of internal clearance of their manuscripts with either a completed and signed NOAA Form 25-700 or a copy of the clearance email from the Research Publication Tracking System. For further details on electronic submission, please contact the associate editor, Cara Mayo, at

cara.mayo@noaa.gov.

When requested, the text and tables should be submitted in MS Word format. Each figure should be sent as a separate PDF, TIFF, or EPS file. Send a copy of a figure in the original software if conversion to any of these formats yields a degraded version of the figure.

Questions? If you have questions regarding these guidelines, please contact the managing editor, Kathryn Dennis, at

kathryn.dennis@noaa.gov.

Questions regarding manuscripts under review should be addressed to Associate Editor Cara Mayo.

Fishery Bulletin

Subscription form

Superintendent of Documents **Publications** Order Form

*5178

☐ YES, please send me the following publications:

____ Subscriptions to *Fishery Bulletin*
for $32.00 per year ($44.80 foreign)

The total cost of my order is $ ________ . Prices include regular domestic postage and handling and are subject to change.

(Company or Personal Name) (Please type or print)

(Additional address/attention line)

(Street address)

(City, State, ZIP Code)

(Daytime phone including area code)

(Purchase Order No.)

Charge your order.
IT'S EASY!

VISA

MasterCard

Please Choose Method of Payment:

☐ Check payable to the Superintendent of Documents

☐ GPO Deposit Account ☐☐☐☐☐☐☐–☐

☐ VISA or MasterCard Account

☐☐☐☐☐☐☐☐☐☐☐☐☐☐☐☐☐☐☐☐

☐☐☐☐ (Credit card expiration date)

To fax your orders (202) 512-2104

(Authorizing Signature)

Mail to: Superintendent of Documents
P.O. Box 979050, St. Louis, Missouri 63197
Tel. no. (U.S. callers): 866-512-1800
Tel. no. (International callers): 1-202-512-1800

Thank you for your order!

Also available online at
https://bookstore.gpo.gov/products/fishery-bulletin
email: ContactCenter@gpo.gov

SMITHSONIAN LIBRARIES
3 9088 02039 7592